CTC-INF-952

COMPUTING TECHNOLOGY CENTER

DEVELOPMENT OF TWO-DIMENSIONAL DISCRETE ORDINATES TRANSPORT THEORY FOR RADIATION SHIELDING

by

F. R. Mynatt
F. J. Muckenthaler
P. N. Stevens

NOTICE

THIS WORK SUPPORTED BY
OAK RIDGE NATIONAL LABORATORY
UNDER THE
REACTOR AND WEAPONS RADIATION SHIELDING PROGRAMS
AEC CONTRACT W 7405 ENG 76
DASA SUBTASK RRP-5074

UNION CARBIDE CORPORATION
NUCLEAR DIVISION

Operating the

UNION CARBIDE

OAK RIDGE GASEOUS DIFFUSION PLANT • OAK RIDGE NATIONAL LABORATORY
OAK RIDGE Y-12 PLANT • PADUCAH GASEOUS DIFFUSION PLANT

For the Atomic Energy Commission Under U.S. Government Contract W7405 eng 26

Date of Issue: August 11, 1969

Report Number: CTC-INF-952

Subject Category: Mathematics
and
Computers

DEVELOPMENT OF TWO-DIMENSIONAL DISCRETE ORDINATES TRANSPORT THEORY FOR RADIATION SHIELDING[a]

by

F. R. Mynatt
F. J. Muckenthaler[b]
P. N. Stevens[c]

Computing Technology Center

NOTICE

This work supported by
Oak Ridge National Laboratory
Under the
Reactor and Weapons Radiation Shielding Programs
AEC Contract W 7405 Eng 76
DASA Subtask RRP-5074

[a]Submitted to the University of Tennessee by F. R. Mynatt as a doctoral dissertation in the Department of Nuclear Engineering.

[b]Oak Ridge National Laboratory, Oak Ridge, Tennessee.

[c]University of Tennessee, Knoxville, Tennessee.

UNION CARBIDE CORPORATION
NUCLEAR DIVISION
Oak Ridge, Tennessee

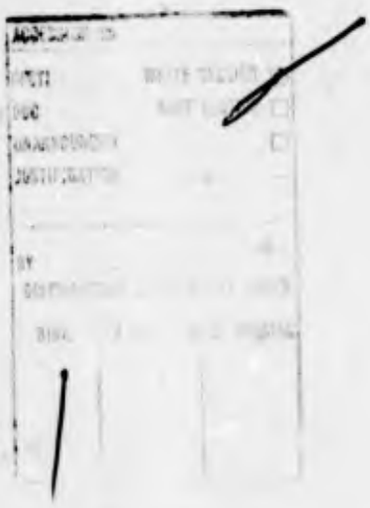

ACKNOWLEDGMENTS

The authors are indebted to the staff at the Oak Ridge National Laboratory Tower Shielding Facility for their capable execution of the experiment, and to Mr. C. E. Clifford, Mr. W. W. Engle, Jr., Dr. E. A. Straker, Dr. V. R. Cain, and Mr. R. J. Rodgers for their assistance and many helpful suggestions and comments.

ABSTRACT

The discrete ordinates (S_n) method, which is also known as the second version of the S_n method, was first introduced by B. G. Carlson. The two-dimensional discrete ordinates method has until recently been successful only for relatively easy problems such as criticality calculations for highly enriched uranium cylinders. The purpose of this study is to extend the capabilities of the two-dimensional discrete ordinates method in order to provide accurate calculations for deep-penetration radiation transport problems. The basic method is generalized and improved, a complete technique for application is developed, and a comprehensive comparison with experiment is performed.

The generalized discrete ordinates difference equation is derived by applying an integral operator to each term of the transport equation in a consistent manner. In the convection term the coefficients for ray-to-ray streaming in cylindrical geometry are obtained directly in contrast with older derivations where they are defined due to flow balance conservation only. In the total collision term a transformation is performed such that an assumption of flux separability is not required. In the scattering integral the angle dependence of the scattering cross section is approximated by a Legendre polynomial series, the addition theorem is used to transform from the collision coordinate system to the laboratory coordinate system, and the final difference form is given by straightforward application of the integral operator. The instability which is inherent in the diamond-difference technique when steep flux gradients occur is removed by a combination of the diamond-difference and step-difference techniques.

An example of the effect of mesh size on problem stability is shown.

The inner-iteration procedure is examined from both a physical and analytical viewpoint. Power iteration and normalized power iteration are discussed and two convergence acceleration techniques, the Chebyshev method and a space-dependent normalized power iteration, are developed. The problem of determining a convergence criteria is discussed and a zone-of-interest criteria is proposed for two-dimensional calculations. Two test problems are studied and it is shown that the Chebyshev method can reduce the number of iterations by one half and the space-dependent scaling can reduce the number of iterations by one seventh. These improvements in the inner-iteration procedure make it possible to obtain converged solutions to deep-penetration problems within reasonable computational times.

Three additional improvements in the method are developed. An analytic first collision source is developed for use in point source problems which may have "ray effects" and for problems with mono-directional beam sources in which the collided and uncollided components must be separated. The question of preferred quadrature sets is examined, and a method for using tailored quadratures is developed. The problem of calculating the flux at arbitrary points external to the system is considered. Three techniques are developed, two of which involve a surface integration of the angular flux, and the third, a last flight response based on an adjoint solution.

In order to provide an unequivocal test of the methods, a clean-geometry experiment was designed and executed, and the results are compared with calculations. The experiment comprises of large slab

shields exposed to a collimated reactor beam source. The emergent angle-dependent spectra were measured with the NE-213 liquid organic scintillator - FERDOR spectra unfolding system which gives spectra in the energy range from 0.8 to 15.0 MeV. Fast neutron dose measurements were also made, including dose profiles at the exit faces of the slabs. Lead, polyethylene, laminated lead and polyethylene, and depleted uranium slabs were included in the study. A large number of calculations were performed and many comparisons are shown.

TABLE OF CONTENTS

LIST OF TABLES

LIST OF FIGURES

BLANK PAGE

CHAPTER I

INTRODUCTION

In the area of nuclear engineering called "shielding," which encompasses all radiation penetration problems, there has traditionally been a lack of calculational methods which are accurate and yet readily applicable to many problems. This is largely due to the fact that in penetration problems it is usually the unusual particle which is of interest. It is equivalent to say that the least populous portions of phase space are usually of most importance. To illustrate this, consider a shield system which has an attenuation factor of 10^{-10}. For this case it is approximately true that only one particle leaves the shield for every 10^{10} particles introduced at the source.

This aspect of penetration problems, that of placing prime importance on the unusual particle, makes it very difficult to obtain good calculations and experiments. In the measurement of total cross sections, it is the minima of the cross section which are of greatest importance. In the spectra of neutrons and gamma rays from fission, the high energy portions of the curves, which are less intense and not well known, are most important. Thus, for certain penetration problems even the most fundamental data are often grossly inaccurate.

In order to calculate accurately the particle distribution in the least populous portions of phase space, a rigorous calculational technique is required. Since exact, analytic solutions to general transport theory problems do not exist, a rigorous method is here defined as one which gives a numerical solution of the Boltzmann

transport equation and in which the inherent approximations are adjustable such that the approximations do not materially affect the desired solution.

Before 1960, the principal calculational tools for shielding problems were the kernel, moments, diffusion, removal diffusion, and spherical harmonic methods. The kernel method assumes that all important radiation transport is in the line of sight from the sources. The total attenuation along the line of sight paths is calculated and scattering effects are approximated by infinite media build-up factors or modification of the total cross section. The kernel method is not rigorous, and, although usually used for three-dimensional geometries, effects due to scattering angle changes are completely ignored. The moments method can rigorously treat radiation transport in infinite homogeneous media. This method has been used extensively for the calculation of infinite media build-up factors for use in gamma-ray kernel calculations. More recently moments-method calculations are being performed for the study of the sensitivity of the infinite media flux distribution to changes in the cross sections. The geometry limitation, however, precludes its use for most practical problems. The diffusion theory method, either single-group or multigroup, is not very successful when applied to penetration problems because of the assumptions of isotropic scattering and nearly isotropic flux. The removal-diffusion method employs a combination of the kernel method using removal cross sections and the diffisuion method. This method is an improvement over either the kernel or diffusion methods taken separately. The technique is not rigorous and suffers from many

limiting assumptions. The difficulties due to the line-of-sight kernel method and the diffusion restrictions are only partly mitigated. The spherical harmonics method is a rigorous technique which has successfully been used for one-dimensional problems. The method suffers from several difficulties, including a rapidly increasing amount of computational effort required as the size of the problem and order of anisotropy are increased as is often required in shielding problems. The method has of yet not been extended to geometries having two space dimensions.

The Monte Carlo method has long been considered the ultimate calculational tool for radiation transport. This is especially true for complex geometries and complicated multiple particle transport for which the Monte Carlo calculation, when viewed as a physical analog, can incorporate any describable transport phenomenon. Unfortunately, the difficulty of preparing a Monte Carlo procedure for a problem is proportional to the complexity of the problem, and most successful problem solutions to date have been greatly simplified. Also, the Monte Carlo analogy method has only limited application to deep penetration problems since most of the computational time would be spent tracking the average particle which does not contribute to the answer. Only recently, methods have been developed which provide for importance biasing based on calculated value functions. This is an important improvement since previously importance biasing was based on artful ingenuity or, in rare cases, on analytic value functions. Much work is currently in progress to incorporate biasing of the scattering angle such that problems in three-dimensional

geometry can be solved efficiently. Important development areas include the need for improved statistical analysis of the biased histories and simplified problem preparation so that the method will become more widely used by engineering analysts.

The purpose of this study is to develop a technique based on the multigroup discrete ordinates (S_n) method that can accurately solve steady-state radiation penetration problems in two space dimensions. Although the discrete ordinates method has been used for many years as a tool for the analysis of highly enriched critical systems, attempted applications to penetration problems have not been successful. In order to extend the existing method for use in penetration problems it was necessary to:

1. develop a general treatment of anisotropic scattering so that the scattering approximation can be arbitrarily adjusted for the specific problem;
2. generalize the use of quadratures and provide flexible data-handling techniques so that very large and diverse problems could be solved;
3. remove or circumvent the instability known as "diamond difference breakdown," which gives oscillatory flux distributions in problems having severe flux gradients;
4. analyze and improve the convergence of the inner-iterations;
5. develop techniques for some of the special difficulties often encountered in shielding applications; and

6. develop, execute, and analyze a comprehensive and detailed experiment for determining the accuracy and versatility of the method.

This study is limited to neutron transport in cylindrical r-z geometry as this is one of the most difficult and useful areas of radiation transport. The technique as developed is applicable to cylindrical r-θ and slab x-y geometries and several types of radiation transport. In particular, coupled neutron and gamma-ray transport problems can be handled and the solutions are quite useful.

CHAPTER II

DISCRETE ORDINATES DIFFERENCE EQUATIONS

This chapter on the difference equations is intended to serve three purposes. First, a brief history is presented in order to assist the reader who is unfamiliar with the technology in determining the relevancy of this work. A detailed derivation of the discrete ordinates difference equation for steady state radiation transport in two-dimensional cylindrical r-z geometry is then developed. This derivation establishes a formalism for the development of the difference equation which helps in relating the final difference terms with the original analytic transport equation, introduces generalized anisotropic scattering in two-dimensional geometries, and identifies the approximations inherent in the application of the difference equation. Finally, the development of step- and diamond-difference equations and the application to penetration problems are discussed.

I. CHRONOLOGY OF DEVELOPMENTS

The original method of discrete ordinates is attributed to Wick (1)* and Chandrasekhar (2). The early work was limited primarily to simple problems such as the transport of monoenergetic neutrons in one-dimensional slabs with isotropic scattering. The fundamental assumption in the method is that the integral term in the Boltzmann transport equation may be approximated by a Gauss quadrature formula.

---

*Numbers appearing in parentheses, except for those giving identity to an equation, refer to the corresponding numbers in the Bibliography.

For example, for the simple problem described above, the transport equation is

$$\mu \frac{\partial \phi(x,\mu)}{\partial x} + \Sigma\, \phi(x,\mu) = \frac{1}{2}\, \Sigma_s \int_{-1}^{+1} \phi(x,\mu)\, d\mu. \qquad (2.1)$$

If the integral in (2.1) is replaced by a Gauss quadrature formula

$$\int_{-1}^{+1} \phi(x,\mu)\, d\mu = \sum_{d'=1}^{NOA} \phi(x,\mu_{d'})\omega_{d'}\,, \qquad (2.2)$$

where NOA is the total number of points, and μ_d and ω_d are the ordinates and weights for the Gaussian quadrature. If Equation (2.2) is introduced into (2.1), the right side depends only on the flux values $\phi(x,\mu_d)$ evaluated at discrete angles, μ_d. It is thus sufficient to evaluate the entire transport equation only at the discrete angles,

$$\mu_d \frac{\partial \phi(x,\mu_d)}{\partial x} + \Sigma\, \phi(x,\mu_d) = \frac{1}{2}\, \Sigma_s \sum_{d'=1}^{NOA} \phi(x,\mu_{d'})\omega_{d'}. \qquad (2.3)$$

Equation (2.3) represents a set of NOA coupled equations for the discrete angle fluxes, $\phi(x,\mu_d)$, which have been reduced effectively to functions of one variable. The coupled equations may be solved either numerically or analytically. Although the technique can be extended to include anisotropic scattering, it is limited to slab geometry.

The first S_n method was developed principally by B. G. Carlson as an improvement of some of the concepts in the Serber-Wilson method (3). In the first S_n method, S_2, the angular flux, $\phi(x,\mu)$, was approximated by two connected line segments on the μ intervals (-1,0) and (0,+1) of the form

$$\phi(x,\mu) = \phi(x,-1) + (\mu+1)\,[\phi(x,0) - \phi(x,-1)] \qquad (2.4)$$

$$\phi(x,\mu) = \phi(x,0) + \mu[\phi(x,+1) - \phi(x,0)]. \qquad (2.5)$$

The S_2 equations are given by first evaluating the transport equation, (2.1), at $\mu = -1$, and then alternatively substituting Equations (2.4) and (2.5) into (2.1) and integrating over the μ intervals (-1,0) and (0,+1), respectively. The result of these operations is a set of three coupled equations for the flux at $\mu = -1$, 0, and +1. These equations may then be solved either numerically or analytically.

The original S_2 method was generalized to S_n by performing the previously described operations for n equal intervals in the μ interval (-1,+1). This method in both monoenergetic and multigroup formulations was used for several years. The primary advantage over Wick's method was that the technique was applicable to spherical geometry. The technique was regarded to be quite accurate; however, flux aberrations were observed particularly near the center of spheres. Later a linear transformation of the original S_n equations to equivalent discrete ordinates equations showed that the directions, μ_d, in the equivalent set were not symmetrically located about $\mu = 0$. The flux aberrations were found to be caused by the unsymmetric quadrature (4). This difficulty, plus the inability to extend the original S_n

technique to higher dimension geometries, discouraged further development. All forms of this method were limited to isotropic scattering.

The second S_n method, otherwise known as the "discrete S_n" or "generalized discrete ordinates" method, was then developed (5). This method is both a simplification and generalization of the earlier versions. The difference equations were stated as a macroscopic flow balance in a manner nearly equivalent to the method of deriving the Boltzmann transport equation as a microscopic flow balance. As an example, the flow balance for a one-dimensional sphere is stated as,

$$\mu_D(A_{i+1}\,\phi_{i+1,D} - A_i\,\phi_{i,D}) + (\gamma_{d+1}\,\phi_{I,d+1} - \gamma_d\,\phi_{I,d})$$

$$+ V_I\,\Sigma\,\phi_{I,D} = V_I\,\Sigma_{s_{D'=1}}^{NOA}\,\phi_{I,D'}\omega_{D'} + V_I\,S_{I,D}\,, \qquad (2.6)$$

where

$A_i = 4\pi r_i^2$,

μ_D = cosine of a direction vector $\bar{\Omega}_D$ with respect to the radius,

$V_I = 4/3\,\pi\,(r_{i+1}^3 - r_i^3)$,

$\omega_D = \Delta\mu_D/2$,

$\phi_{I,D}$ = average flux in volume, V_I, and cosine interval, ω_D,

$\phi_{i,D}$ = average flux on surface, A_i, in cosine interval, ω_D,

$\phi_{I,d}$ = average flux on "surface," γ_d, in volume, V_I,

γ_d = undefined at present,

and Σ, Σ_s, and $S_{I,D}$ are total reaction cross section, scattering

cross section, and fixed source, respectively. Hence, for the space-angle cell, $V_I \omega_D$, the first term in Equation (2.6) represents net convective loss through the surfaces, A_i, the second term represents a similar convective loss through the surfaces, γ_i, the third term represents removal from $V_I \omega_D$ by collision, the fourth term represents scattering into $V_I \omega_D$, and the fifth term represents the source into $V_I \omega_D$. Thus, Equation (2.6) is quite simple and has a simple physical interpretation. The most important part of this development is the treatment of the angle-to-angle void streaming in curvilinear geometries. The undefined curvature coefficients, γ_d, are established by considering the special case of an infinite isotropic media for which removals equals scattering plus fixed source, and the angular flux is the same everywhere. Equation (2.6) then reduces to

$$\mu_D(A_{i+1} - A_i) + (\gamma_{d+1} - \gamma_d) = 0. \qquad (2.7)$$

Furthermore, at $\mu = \pm 1$, the associated γ coefficient must be zero since the flow is directly along the radius. Therefore, the recursion

$$\gamma_{d+1} = \gamma_d - \mu_D(A_{i+1} - A_i) \; ; \; \gamma_1 = 0.0, \qquad (2.8)$$

defines all the γ_d.

The first and second versions of the S_n method certainly involve much more than the contents of the preceding paragraphs indicate; however, the comments presented give the aspects of the method which are unique and set it apart from other techniques.

The work presented in this paper represents, in one form or another, an extension, generalization, optimization, and verification of the discrete S_n method and succeeding developments. Previous work has included extension to multigroup and to two-dimensional geometry (6), development of better quadrature (7,8), and extension to generalized anisotropic scattering in one-dimensional geometry (9-12).

II. DERIVATION OF DIFFERENCE EQUATIONS FOR CYLINDRICAL R-Z GEOMETRY

Although a general time-dependent discrete ordinates difference equation for one-, two-, or three-dimensional geometry may be derived by the following technique, the development here, although including general anisotropic scattering, is limited to the time-independent equation for two-dimensional r-z geometry. This is done because the experimental work, which is described subsequently, was performed in r-z geometry and the stationary condition. In the derivation which follows, the difference equations are derived in a term-wise consistent manner directly from the analytic form of the transport equation.

A drawing of the coordinate system for cylindrical geometry is shown in Figure 1. The transport equation is

$$\frac{d\phi(r,z,\theta,\eta,\psi,E)}{ds} + \Sigma^T(r,z,\theta,E)\,\phi(r,z,\theta,\eta,\psi,E) = S(r,z,\theta,\eta,\psi,E)$$
$$+ \int_{-1}^{+1}\int_{0}^{2\pi}\int_{0}^{\infty} \Sigma^S(r,z,\theta;E',\bar{\Omega}'\rightarrow E,\bar{\Omega})\phi(r,z,\theta,\eta',\psi',E')dE'd\psi'd\eta'. \qquad (2.9)$$

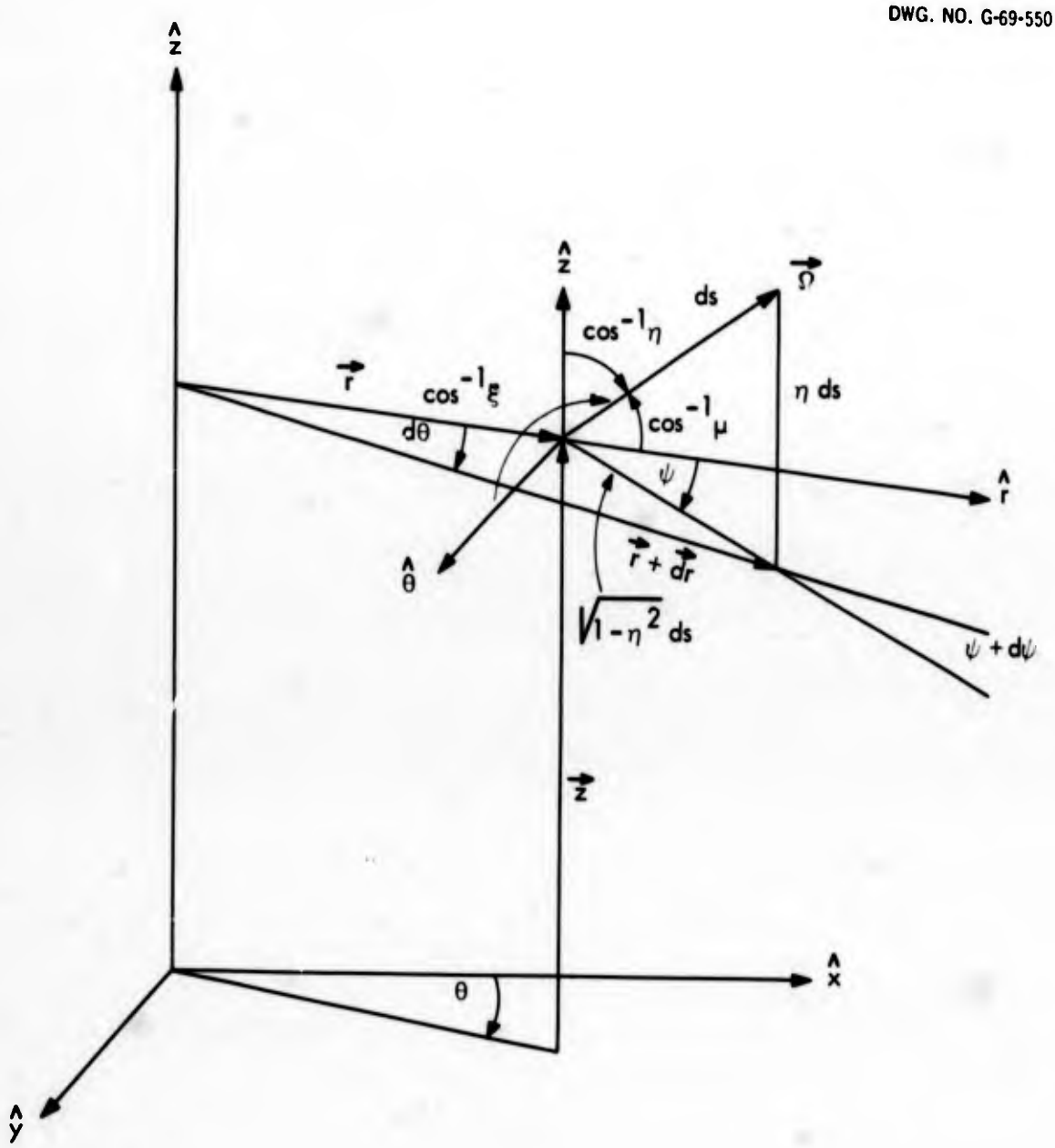

Figure 1. The coordinate system for cylindrical geometry.

The first term in Equation (2.9) may be rewritten as

$$\frac{d\phi}{ds} = \frac{\partial\phi}{\partial r}\frac{dr}{ds} + \frac{\partial\phi}{\partial z}\frac{dz}{ds} + \frac{\partial\phi}{\partial\theta}\frac{d\theta}{ds} + \frac{\partial\phi}{\partial\eta}\frac{d\eta}{ds} + \frac{\partial\phi}{\partial\psi}\frac{d\psi}{ds} \; . \tag{2.10}$$

From Figure 1 one can determine that

$$\frac{dr}{ds} = \mu \quad , \quad \frac{dz}{ds} = \eta \quad ,$$

$$\frac{d\theta}{ds} = \frac{\xi}{r} \quad , \text{ and } \frac{d\eta}{ds} = 0. \tag{2.11}$$

In order to determine the derivative, $d\psi/ds$, one first observes in Figure 1 that

$$\psi + d\psi = \psi - d\theta, \tag{2.12}$$

which gives

$$d\psi = -d\theta \tag{2.13}$$

and

$$\frac{d\psi}{d\theta} = -1 \; . \tag{2.14}$$

Equations (2.14) and (2.11) are then combined to give

$$\frac{d\psi}{ds} = \frac{d\psi}{d\theta}\frac{d\theta}{ds} = -\frac{\xi}{r} \; . \tag{2.15}$$

The combination of Equations (2.11), (2.15), and (2.10) with the transport equation (2.9), gives

$$\begin{aligned} &\mu\frac{\partial\phi(P)}{\partial r} + \eta\frac{\partial\phi(P)}{\partial z} + \frac{\xi}{r}\frac{\partial\phi(P)}{\partial\theta} - \frac{\xi}{r}\frac{\partial\phi(P)}{\partial\psi} \\ &+ \Sigma^T(r,z,\theta,E)\,\phi(P) = S(P) \\ &+ \int_{-1}^{+1}\int_{0}^{2\pi}\int_{0}^{\infty} \Sigma^s(r,z,\theta;E'\bar{\Omega}'\rightarrow E,\bar{\Omega})\,\phi(P')\,dE'd\psi'd\eta' \end{aligned} \tag{2.16}$$

where

$$\phi(P) = \phi(r,z,\theta,\eta,\psi,E)$$

and (2.17)

$$\phi(P') = \phi(r,z,\theta,\eta',\psi',E')$$

For two-dimensional r-z geometry, the material composition and geometry are invariant with respect to θ; therefore, the form of interest for the transport equation is

$$\mu\frac{\partial\phi(P)}{\partial r} + \eta\frac{\partial\phi(P)}{\partial z} - \frac{\xi}{r}\frac{\partial\phi(P)}{\partial\psi} + \Sigma^T(r,z,E)\,\phi(P) = S(P) \tag{2.18}$$

$$+ \int_{-1}^{+1}\int_{0}^{2\pi}\int_{0}^{\infty}\Sigma^S(r,z;E',\bar{\Omega}'\rightarrow E,\bar{\Omega})\,\phi(P')dE'd\psi'd\eta'.$$

The phase space P for Equation (2.18) is defined by the radius, r, axial displacement, z, polar direction cosine, η, azimuthal angle, ψ, and energy, E. The differential phase space cell, dP, is given by

$$dP = 2\pi r dr dz d\eta d\psi dE \tag{2.19}$$

The finite difference phase space cell, ΔP, is given by integrating Equation (2.19) over a five-dimensional finite cell defined in terms of the phase space variables.

Hence,

$$\Delta P = \int_{r_i}^{r_{i+1}}\int_{z_j}^{z_{j+1}}\int_{\eta_k}^{\eta_{k+1}}\int_{\psi_{n+1}}^{\psi_n}\int_{E_g}^{E_{g+1}} 2\pi r dr dz d\eta d\psi dE, \tag{2.20}$$

where the ψ_n mesh is constructed such that n increases as ψ decreases, and which gives

$$\Delta P = \pi(r_{i+1}^2 - r_i)\,(z_{j+1} - z_j)\,(\eta_{k+1} - \eta_k)$$

$$\times\,(\psi_n - \psi_{n+1})\,(E_{g+1} - E_g)\,, \tag{2.21}$$

or

$$\Delta P = V_{I,J}\Delta\eta_K\Delta\psi_N\Delta E_G\,. \tag{2.22}$$

The subscript convention is that lower case subscripts, i, j, k, n, g, refer to a quantity evaluated at a surface of the finite phase space cell and upper case subscripts, I, J, K, N, G, refer to quantities defined for the cell as a whole or having been averaged or integrated over the cell.

The discrete ordinates finite difference transport equation is derived by integrating the analytic transport equation (2.18) over the finite difference cell, as defined by Equation (2.20). It is noted that integration of Equation (2.18) over the finite phase space cell would involve integrands which contain products of a derivative and a coefficient containing the variable of integration. In order to place Equation (2.18) in the most convenient form for this integration, one then notes that

$$\frac{\partial[(\sin\psi)\,\phi(P)]}{\partial\psi} = (\cos\psi)\,\phi(P) + \sin\psi\,\frac{\partial\phi(P)}{\partial\psi} \tag{2.23}$$

and

$$\frac{\partial r\phi(P)}{\partial r} = \phi(P) + r\,\frac{\partial\phi(P)}{\partial r} \tag{2.24}$$

Hence,

$$\sin\psi\,\frac{\partial\phi(P)}{\partial r} = (\cos\psi)\,r\,\frac{\partial\phi(P)}{\partial r} + \frac{(\sin\psi)\phi(P)}{\partial\psi} - \cos\psi\,\frac{\partial r\phi(P)}{\partial r} \quad (2.25)$$

or

$$\frac{\xi}{r}\frac{\partial\phi(P)}{\partial\xi} = \mu\frac{\partial\phi(P)}{\partial r} + \frac{1}{r}\frac{\partial\xi\phi(P)}{\partial\psi} - \frac{\mu}{r}\frac{\partial r\phi(P)}{\partial\psi} \quad (2.26)$$

Substituting Equation (2.26) into (2.18) gives the desired form,

$$\frac{\mu}{r}\frac{\partial r\phi(P)}{\partial r} + \eta\frac{\partial\phi(P)}{\partial z} - \frac{1}{r}\frac{\partial\xi\phi(P)}{\partial\psi} + \Sigma^{T}(r,z,E)\phi(P) = S(P)$$
$$+ \int_{-1}^{+1}\int_{0}^{2\pi}\int_{0}^{\infty}\Sigma^{s}(r,z;E',\bar{\Omega}'\rightarrow E,\bar{\Omega})\phi(P')dE'd\psi'd\eta' \quad (2.27)$$

The integration of Equation (2.27) over the finite phase space cell is accomplished by applying the integral operator,

$$0 = \int_{r_i}^{r_{i+1}}\int_{z_j}^{z_{j+1}}\int_{\eta_k}^{\eta_{k+1}}\int_{\psi_{n+1}}^{\psi_n}\int_{E_g}^{E_{g+1}} 2\pi r dr dz d\eta d\psi dE \,, \quad (2.28)$$

in a consistent manner to each term. The first term becomes

$$T_1 = \int_{\Delta r_I}\int_{\Delta z_J}\int_{\Delta\eta_K}\int_{\Delta\psi_N}\int_{\Delta E_G}\frac{\mu}{r}\frac{\partial}{\partial r}\,r\phi(r,z,\eta,\psi,E)2\pi r dr dz d\eta d\psi dE, \quad (2.29)$$

where the symbols under the integral signs are simplifications representing the original limits in Equation (2.28). If the multigroup flux is defined by

$$\phi_G(r,z,\eta,\psi) = \int_{\Delta E_G}\phi(r,z,\eta,\psi,E)dE \,, \quad (2.30)$$

the first term, after rearrangement, becomes

$$T_1 = 2\pi \int_{\Delta z_J} \int_{\Delta \eta_K} \int_{\Delta \psi_N} \mu \left(\int_{\Delta r_I} \frac{\partial}{\partial r} r\phi_G(r,z,\eta,\psi)dr \right) d\psi d\eta dz \quad . \tag{2.31}$$

Since Equation (2.31) is integrated independently with respect to each variable,

$$\int_{\Delta r_I} \frac{\partial}{\partial r} r\phi_G(r,z,\eta,\psi)dr = [r_{i+1}\phi_{G,i+1}(z,\eta,\psi) - r_i\phi_{G,i}(z,\eta,\psi)] \quad . \tag{2.32}$$

where, by the subscript convention,

$$\phi_{G,i}(z,\eta,\psi) = \phi_G(r_i,z,\eta,\psi) \quad . \tag{2.33}$$

The first term then becomes

$$T_1 = 2\pi \int_{\Delta z_J} \int_{\Delta \eta_K} \int_{\Delta \psi_N} \mu[r_{i+1}\phi_{G,i+1}(z,\eta,\psi) - r_i\phi_{G,i}(z,\eta,\psi)]d\psi d\eta dz \quad . \tag{2.34}$$

From the mean value theorem (13) it follows that any integral can be approximated by

$$\int_{x_1}^{x_2} xf(x)dx \tilde{=} \bar{x}f(\bar{x})\Delta x \quad ,$$

for $x_1 < \bar{x} < x_2$, $\Delta x = x_2 - x_1$,

where $\bar{x}$ may be adjusted to give the equality; for well behaved functions, the closer $\bar{x}$ is to the real mean, the better the approximation.

Applying the mean value approximation to the z integral in Equation (2.34) gives

$$T_1 = 2\pi\ \Delta z_J \int_{\Delta\eta_K} \int_{\Delta\psi_N} \mu[r_{i+1}\phi_{G,i+1,J}(\eta,\psi) - r_i\phi_{G,i,J}(\eta,\psi)]d\psi d\eta\ , \qquad (2.36)$$

where

$$\phi_{G,i+1,J}(\eta,\psi) = \phi_{G,i+1}(\bar{z}_J,\eta,\psi)\ .$$

Integrals over solid angle, $d\psi d\eta$, are to be represented by a single summation over NOA (number of angles) points and weights where each is identified by an upper-case subscript, D. The weights are normalized so that the sum is unity instead of 4π. Hence,

$$\int_{\Delta\eta_K} \int_{\Delta\psi_N} \phi(\eta,\psi)d\psi d\eta \tilde{=} \phi_D\ \omega_D \qquad (2.37)$$

where

$$\phi_D = 4\pi\ \phi(\bar{\eta}_D,\bar{\psi}_D),$$

and

$$\int_{\Delta\eta_K} \int_{\Delta\psi_N} d\psi d\eta = 4\pi\omega_D\ .$$

Application of the approximation given by Equation (2.37) to Equation (2.36) gives the final form for T_1,

$$T_1 = 2\pi\ \bar{\mu}_D[r_{i+1}\phi_{G,i+1,J,D} - r_i\phi_{G,i,J,D}]\Delta z_J\omega_D\ . \qquad (2.38)$$

The integral operator is next applied to the second term of Equation (2.27) giving

$$T_2 = \int_{\Delta r_I} \int_{\Delta z_J} \int_{\Delta\eta_K} \int_{\Delta\psi_N} \int_{\Delta E_G} \eta\ \frac{\partial}{\partial z}\ \phi(r,z,\eta,\psi,E)\ 2\pi r dr dz d\eta d\psi dE. \qquad (2.39)$$

Using the definition of the multigroup flux, Equation (2.39) becomes

$$T_2 = 2\pi \int_{\Delta r_I} \int_{\Delta \eta_K} \int_{\Delta \psi_N} \eta \int_{\Delta z_J} \frac{\partial}{\partial z} \phi_G(r,z,\eta,\psi)\, dz r dr d\eta d\psi. \tag{2.40}$$

Integration over Δz_J gives

$$T_2 = 2\pi \int_{\Delta r_I} \int_{\Delta \eta_K} \int_{\Delta \psi_N} \eta[\phi_{G,j+1}(r,\eta,\psi) - \phi_{G,j}(r,\eta,\psi)] r dr d\eta d\psi, \tag{2.41}$$

where

$$\phi_{G,j}(r,\eta,\psi) = \phi_G(r,z_j,\eta,\psi)$$

The remaining integrals are evaluated by the mean value approximation giving the final form for T_2,

$$T_2 = 2\pi \bar{r}_I \bar{\eta}_D [\phi_{G,j+1,I,D} - \phi_{G,j,I,D}] \Delta r_I \omega_D, \tag{2.42}$$

where

$$\phi_{G,j,I,D} = \phi_G(\bar{r}_J, z_j, \bar{\eta}_D, \bar{\psi}_D) .$$

The third term of Equation (2.27) when integrated over the finite difference cell gives

$$T_3 = \int_{\Delta r_I} \int_{\Delta z_J} \int_{\Delta \eta_K} \int_{\Delta \psi_N} \int_{\Delta E_G} -\frac{1}{r} \frac{\partial}{\partial \psi} \xi\, \phi(r,z,\eta,\psi,E) 2\pi r dr dz d\eta d\psi dE. \tag{2.43}$$

The multigroup flux is defined as before giving

$$T_3 = 2\pi \int_{\Delta r_I} \int_{\Delta z_J} \int_{\Delta \eta_K} \int_{\psi_{n+1}}^{\psi_n} - \frac{\partial}{\partial \psi} \xi \, \phi_G(r,z,\eta,\psi) d\psi dr dz d\eta. \qquad (2.44)$$

The integral over $\Delta\psi$ is next evaluated,

$$T_3 = \frac{1}{2} \int_{\Delta r_I} \int_{\Delta z_J} \int_{\Delta \eta_K} - [\xi_n \phi_{G,n}(r,z,\eta) - \xi_{n+1} \phi_{G,n+1}(r,z,\eta)] r dr dz d\eta, \qquad (2.45)$$

where

$$\phi_{G,n}(r,z,\eta) = 4\pi \phi_G(r,z,\eta,\psi_n).$$

After evaluating the remaining integrals by the mean value approximation, the third term becomes

$$T_3 = \frac{1}{2}[\xi_{n+1} \phi_{G,n+1,I,J,K} - \xi_n \phi_{G,n,I,J,K}] \Delta r_I \Delta z_J \Delta \eta_K \, . \qquad (2.46)$$

T_3 is then rewritten,

$$T_3 = \Delta z_J (\gamma_{n+1} \phi_{G,n+1,I,J,K} - \gamma_n \phi_{G,n,I,G,K}) \qquad (2.47)$$

where the curvature coefficients, γ_n, are defined by

$$\gamma_n \equiv \frac{1}{2} \Delta r_I \Delta \eta_K \, \xi_n = \frac{1}{2} \Delta r_I \Delta \eta_K \sqrt{1-\eta_K^2} \, \sin \psi_n \qquad (2.48)$$

Two adjacent curvature coefficients are related by

$$\gamma_{n+1} - \gamma_n = \frac{1}{2} \Delta r_I \Delta \eta_K \sqrt{1-\eta_K^2} (\sin \psi_{n+1} - \sin \psi_n) \, . \qquad (2.49)$$

One notes that

$$\Delta\eta_K = \frac{4\pi\omega_D}{\Delta\psi_N} \tag{2.50}$$

and

$$(\sin\psi_{n+1} - \sin\psi_n) \tilde{=} -\cos\psi_N\Delta\psi_N \ . \tag{2.51}$$

Equation (2.49) can then be rewritten as

$$\gamma_{n+1} - \gamma_n = -2\pi\Delta r_I\omega_D\sqrt{1 - \eta_K^2}\cos\psi_N \tag{2.52}$$

or

$$\gamma_{n+1} = \gamma_n - 2\pi\Delta r_I\omega_D\bar{\mu}_D \tag{2.53}$$

where

$$\bar{\mu}_D = \sqrt{1 - \eta_K^2}\cos\psi_N$$

Since the term, T_3, which represents curvature flow is zero when $\psi = 0.0$ or $\psi = \pi$, it is necessary that $\gamma_1 = 0.0$ and $\gamma_{LAST} = 0.0$, which requires that

$$\sum_{n=1}^{LAST} \omega_D\bar{\mu}_D = 0.0, \tag{2.54}$$

where the summation represents an integration over $\Delta\psi_N$ for a fixed $\Delta\eta_K$. Using Equation (2.57) for the curvature coefficients, the sum of the first three terms, T_1 [Equation (2.42)], T_2 [Equation (2.46), and T_3 [Equation (2.51)], for an isotropic, flat flux (all fluxes equal) is

$$T_1 + T_2 + T_3 = 2\pi\ \bar{\mu}_D(r_{i+1} - r_i)\ \Delta z_J\omega_D + 0 + \Delta z_J(-2\pi\Delta r_I\omega_D\bar{\mu}_D),$$

or

$$T_1 + T_2 + T_3 = 0.0, \tag{2.55}$$

thus indicating no flow, which is correct for this case. It follows from this observation that an exact particle balance is maintained in the application of the finite difference form of the convection terms. In previous discussions of the S_n transport equation (11), the flat flux balance condition was used to determine the curvature coefficients.

The inscatter integral of Equation (2.27) upon integration over the finite phase space cell becomes

$$T_6 = \int_{\Delta r_I} \int_{\Delta z_J} \int_{\Delta \eta_K} \int_{\Delta \psi_N} \int_{\Delta E_G} \int_{-1}^{+1} \int_{0}^{2\pi} \int_{0}^{\infty} \phi(r,z,\eta',\psi',E') \times \Sigma^s(r,z;E',\Omega' \rightarrow E,\Omega) dE' d\psi' d\eta' dE d\psi d\eta dz 2\pi r dr. \tag{2.56}$$

Assuming that the cross sections are constant over individual spatial cells gives

$$T_6 = V_{I,J} \int_{\Delta \eta_K} \int_{\Delta \psi_N} \int_{\Delta E_G} \int_{-1}^{+1} \int_{0}^{2\pi} \int_{0}^{\infty} \phi_{I,J}(\eta',\psi',E') \times \Sigma^s_{I,J}(E',\bar{\Omega}' \rightarrow E,\bar{\Omega}) dE' d\psi' d\eta' dE d\psi d\eta \ . \tag{2.57}$$

From Figure 2, which gives the geometry for the scattering process, one notes that the scattering cross section may be written as a function of the cosine, μ_o, of the scattering angle, θ_o, and subsequently expanded as an ordinary Legendre polynomial series.

DWG. NO. G-69-551

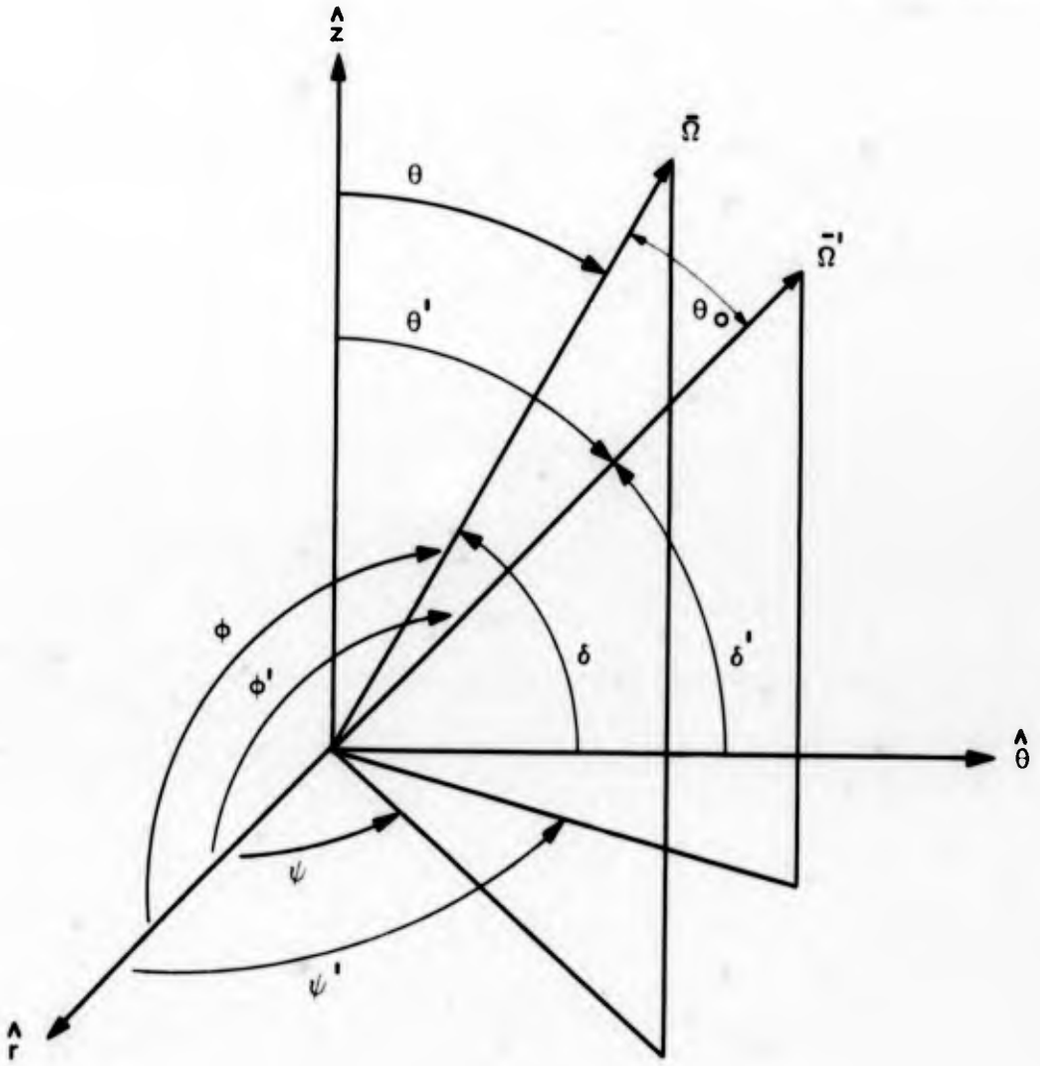

$\mu_o = \cos\theta_o \qquad d\Omega = \sin\theta\, d\theta\, d\psi$

$\eta = \cos\theta \qquad d\Omega = -d\eta d\psi$

$\eta' = \cos\theta'$

$\mu = \cos\phi = \sin\theta \cos\psi$

$\mu' = \cos\phi' = \sin\theta' \cos\psi'$

$\xi = \cos\delta = \sin\theta \sin\psi$

$\xi' = \cos\delta' = \sin\theta' \sin\psi'$

Figure 2. The coordinate system for particle scattering in cylindrical geometry.

$$\Sigma^{s}_{I,J}(E',\bar{\Omega}'\rightarrow E,\bar{\Omega}) = \frac{1}{4\pi}\sum_{\ell=0}^{\infty} S_\ell(E,E')P_\ell(\mu_o) \ . \qquad (2.58)$$

The Legendre series coefficients are then given by

$$S_\ell(E,E') = 4\pi\,\frac{2\ell+1}{2}\int_{-1}^{+1}\Sigma^{s}_{I,J}(E',\bar{\Omega}'\rightarrow E,\bar{\Omega})P_\ell(\mu_o)d\mu_o \ . \qquad (2.59)$$

Substitution of the Legendre expansion, Equation (2.58), into the scattering integral, Equation (2.56), gives

$$T_6 = \frac{V_{I,J}}{4\pi}\int_{\Delta\eta_K}\int_{\Delta\psi_N}\int_{\Delta E_G}\int_{-1}^{1}\int_{0}^{2\pi}\int_{0}^{\infty}\sum_{\ell=0}^{\infty}\phi_{I,J}(\eta',\psi',E')S_\ell(E,E') \qquad (2.60)$$

$$\times\, P_\ell(\mu_o)dE'd\psi'd\eta'dEd\psi d\eta \ .$$

Evaluation of the integrals in Equation (2.60) requires that the scattering cross section be described in the fixed coordinate system variables, η, η', ψ, and ψ', rather than μ_o, which is in the neutron coordinate system. From the addition theorem for Legendre polynomials (14),

$$P_\ell(\mu_o) = P_\ell(\eta)P_\ell(\eta') + 2\sum_{m=1}^{\ell}\frac{(\ell-m)!}{(\ell+m)!}P^m_\ell(\eta)P^m_\ell(\eta')\cos m(\psi-\psi') \ . \qquad (2.61)$$

The cosine term may be expanded giving the revised form,

$$P_\ell(\mu_o) = P_\ell(\eta)P_\ell(\eta') + 2\sum_{m=1}^{\ell}\frac{(\ell-m)!}{(\ell+m)!}P^m_\ell(\eta)P^m(\eta') \qquad (2.62)$$

$$\times\,(\cos m\psi\cos m\psi' + \sin m\psi\sin m\psi').$$

The scattering integral, Equation (2.64), may then be rewritten

$$T_6 = \frac{V_{I,J}}{4\pi} \int_{\Delta\eta_K} \int_{\Delta\psi_N} \int_{\Delta E_G} \int_{-1}^{+1} \int_{0}^{\infty} \sum_{\ell=0}^{\infty} \phi_{I,J}(\eta',\psi',E') S_\ell(E,E')$$

$$\times \left[P_\ell(\eta)P_\ell(\eta') + 2 \sum_{m=1}^{\ell} P_\ell^m(\eta)P_\ell^m(\eta')(\cos m\psi \cos m\psi' \right. \qquad (2.63)$$

$$\left. + \sin m\psi \sin m\psi')\right] dE'd\psi'd\eta'dEd\psi d\eta.$$

Due to the symmetry of cylindrical r-z geometry, the flux is an even function of ψ'; therefore, since $\sin m\psi'$ is an odd function of ψ', all terms involving $\sin m\psi'$ vanish under integration over ψ'. Equation (2.63) may then be rewritten as

$$T_6 = \frac{V_{I,J}}{4\pi} \int_{\Delta\eta_K} \int_{\Delta\psi_N} \int_{\Delta E_G} \int_{0}^{\infty} \sum_{\ell=0}^{\infty} \sum_{m=0}^{\ell} S_\ell(E,E')A_\ell^m(\eta)\cos m\psi \, d\psi d\eta$$

$$\times \int_{-1}^{+1} \int_{0}^{2\pi} \phi_{I,J}(\eta',\psi',E')A_\ell^m(\eta')\cos m\psi' \, d\psi'd\eta'dE', \qquad (2.64)$$

where $A_\ell^m(\eta) \cos m\psi = P_\ell(\eta)$

when $m = 0$ (2.65)

and $A_\ell^m(\eta) \cos m\psi = \left[2\frac{(\ell-m)!}{(\ell+m)!}\right]^{1/2} P_\ell^m(\eta) \cos m\psi$

when $m \neq 0$.

After replacing the energy integral in Equation (2.64) by a sum of group integrals,

$$\int_0^\infty dE' = \sum_{G'=1}^{G} \int_{\Delta E_{G'}} dE, \tag{2.66}$$

the multigroup scattering transfer polynomial coefficient is defined as

$$S^{\ell,m}_{I,J,G,G'} \equiv \frac{\int_{\Delta E_G} \int_{\Delta E_{G'}} S_\ell(E,E') j^{\ell,m}_{I,J}(E') dE' dE}{\int_{\Delta E_{G'}} j^{\ell,m}_{I,J}(E') dE'} \tag{2.67}$$

where

$$j^{\ell,m}_{I,J}(E') \equiv \int_{-1}^{+1} \int_0^{2\pi} \phi_{I,J}(\eta',\psi',E') A^m_\ell(\eta') \cos m\psi' \, d\psi' d\eta' dE'. \tag{2.68}$$

The assimilation of Equations (2.66), (2.67), and (2.68) into the scattering integral, Equation (2.64), gives the form

$$T_6 = \frac{V_{I,J}}{4\pi} \sum_{G'=1}^{NOG} \sum_{\ell=0}^{\infty} \sum_{m=0}^{\ell} \int_{\Delta\eta_K} \int_{\Delta\psi_N} S^{\ell,m}_{I,J,G,G'} A^m_\ell(\eta) \times \cos m\psi \, d\psi d\eta \, j^{\ell,m}_{I,J,G'} , \tag{2.69}$$

where $j^{\ell,m}_{I,J,G'}$ is the denominator of Equation (2.67). When the mean value approximation is used for the solid angle integration and the summations are rearranged, Equation (2.69) becomes

$$T_5 = V_{I,J}\omega_D \sum_{\ell=0}^{\infty} \sum_{m=0}^{\ell} A_D^{\ell,m} \sum_{G'=1}^{G} S_{I,J,G,G'}^{\ell,m} j_{I,J,G'}^{\ell,m} \tag{2.70}$$

where $A_D^{\ell,m} = P_\ell(\bar{\eta}_D)$

when $m = 0$,

and $A_D^{\ell,m} = \left[2\frac{(\ell-m)!}{(\ell+m)!}\right]^{1/2} P_\ell^m(\bar{\eta}_D) \cos m\bar{\psi}_D$

when $m \neq 0$.

Also, the angular flux coefficients are given by

$$j_{I,J,G'}^{\ell,m} = \sum_{D'=1}^{NOA} A_{D'}^{\ell,m} \phi_{I,J,G',D'}\omega_{D'}. \tag{2.71}$$

In practice, the Legendre expansion is truncated to $\ell = LMAX$, and the space dependence of S is treated by zone rather than by space point. The final form for the scattering integral is then,

$$T_6 = V_{I,J}\omega_D \sum_{\ell=0}^{LMAX} \sum_{m=0}^{\ell} A_D^{\ell,m} \sum_{G'=1}^{G} S_{G,G'}^{\ell,m} \sum_{D'=1}^{NOA} A_{D'}^{\ell,m} \phi_{I,J,G',D'}\omega_{D'}. \tag{2.72}$$

The application of the integral operator to the removal term, T_4, of Equation (2.27) gives

$$T_4 = \int_{\Delta r_I} \int_{\Delta z_J} \int_{\Delta \eta_K} \int_{\Delta \psi_N} \int_{\Delta E_G} \Sigma^T(r,z,E)\phi(r,z,\eta,\psi,E) 2\pi r dr dz d\eta d\psi dE. \tag{2.73}$$

In the construction of the removal term for the difference equations, it is desirable to avoid assuming separability of the angular flux in space, angle, and energy; however, it is desired that the multigroup total cross section be independent of angle. As the first step in deriving such a term, the energy integral in Equation (2.73) is

written as

$$T_4^E = \int_{\Delta E_G} \Sigma^T(r,z,E)\phi(r,z,\eta,\psi,E)dE = \Sigma_G^T(r,z)\phi_G(r,z,\eta,\psi) - R, \quad (2.74)$$

where R is a correction factor yet to be determined, and $\Sigma_G^T(r,z)$ is a scalar flux weighted total cross section for group G defined by

$$\Sigma_G^T(r,z) \equiv \frac{\int_{\Delta E_G} \Sigma^T(r,z,E)j^{oo}(r,z,E)dE}{\int_{\Delta E_G} j^{oo}(r,z,E)dE} \quad (2.75)$$

Rearrangement of Equation (2.74) provides an expression for R;

$$R = \Sigma_G^T(r,z)\phi_G(r,z,\eta,\psi) - \int_{\Delta E_G} \Sigma^T(r,z,E)\phi(r,z,\eta,\psi,E)dE, \quad (2.76)$$

where R should be small depending on the relative separability of ϕ. If ϕ is then expanded as a spherical harmonic,

$$\phi(r,z,\eta,\psi,E) = \sum_{\ell=0}^{LMAX} \sum_{m=0}^{\ell} N_\ell^m j^{\ell m}(r,z,E)P_\ell^m(\eta) \cos m\psi \ , \quad (2.77)$$

where $N_\ell^m = \frac{2\ell+1}{2}$

if $m = 0$,

or $N_\ell^m = \frac{2\ell+1}{\sqrt{2}}\left[\frac{(\ell-m)!}{(\ell+m)!}\right]3/2$

if $m \neq 0$,

Equation (2.76) becomes

$$R = \Sigma_G^T(r,z) \sum_{\ell=0}^{LMAX} \sum_{m=0}^{\ell} N_\ell^m j_G^{\ell m}(r,z) P_\ell^m(\eta) \cos m\psi$$

$$- \int_{\Delta E_G} \Sigma^T(r,z,E) \sum_{\ell=0}^{LMAX} \sum_{m=0}^{\ell} N_\ell^m j^{\ell m}(r,z) P_\ell^m(\eta) \cos m\psi dE. \tag{2.78}$$

Equation (2.78) can be reduced to

$$R = \sum_{\ell=0}^{LMAX} \sum_{m=0}^{\ell} N_\ell^m [\Sigma_G^T(r,z) - \Sigma_G^{T\ell m}(r,z)] j_G^{\ell m}(r,z) P_\ell^m(\eta) \cos m\psi \ , \tag{2.79}$$

where

$$j_G^{\ell m} = \int_{\Delta E_G} j^{\ell m}(r,z,E) dE \tag{2.80}$$

and

$$\Sigma_G^{T\ell m}(r,z) = \frac{\int_{\Delta E_G} \Sigma^T(r,z,E) j^{\ell m}(r,z,E) dE}{j_G^{\ell m}(r,z)} \ . \tag{2.81}$$

The energy integral part of the removal term is then

$$T_4^E = \Sigma_G^T(r,z)\phi_G(r,z,\eta,\psi) - \sum_{\ell=0}^{LMAX} \sum_{m=0}^{\ell} N_\ell^m [\Sigma_G^T(r,z)$$

$$- \Sigma_G^{T\ell m}(r,z)] j_G^{\ell m}(r,z) P_\ell^m(\eta) \cos m\psi \ . \tag{2.82}$$

Using Equation (2.82) in Equation (2.73) and evaluating all remaining integrals by the mean value approximation gives,

$$T_4 = V_{I,J}\omega_D\left\{\Sigma^T_{I,J,G}\phi_{I,J,D,G} - \sum_{\ell=0}^{LMAX}\sum_{m=0}^{\ell} N_\ell^m[\Sigma^T_{I,J,G} - \Sigma^{T\ell m}_{I,J,G}]j^{\ell m}_{I,J,G}P_\ell^m(\bar{\eta}_D)\cos m\bar{\psi}_D\right\}. \tag{2.83}$$

The series in Equation (2.83) is very similar in form to the inscattering integral term, Equation (2.72), and may be included there by replacing $S^{\ell m}_{J,G'}$ with

$$S^{\ell m(MOD)}_{G,G'} = S^{\ell m}_{G,G'} + \frac{N_\ell^m}{\left[2\frac{(\ell-m)!}{(\ell+m)!}\right]^{1/2}}[\Sigma^T_G - \Sigma^{T\ell m}_G]\delta_{G\,G'}, \tag{2.84}$$

where the space dependence is by zone and $\delta_{GG'} = 1$ if $G' = G$ and $= 0$ if $G' \neq G$. The modified removal term then has the desired form,

$$T_4 = V_{I,J}\omega_D\,\Sigma^T_G\phi_{I,J,D,G}. \tag{2.85}$$

Application of the integral operator to the source term, T_5, of Equation (2.27) is straightforward since, with the exception of defining multigroup constants, the mean value approximation is used to evaluate all integrals. For a simple fixed source,

$$T_5 = V_I\omega_D S_{I,J,D,G}. \tag{2.86}$$

If multiplication is present (eigenvalue problem),

$$S(r,z,\eta,\psi,E) = \frac{1}{k_{eff}}\chi(E)\int_0^\infty \nu\Sigma_f(r,z,E')j^{oo}(r,z,E')dE' \tag{2.87}$$

which gives

$$T_5 = V_{I,J}\omega_D \frac{\chi_G}{k_{eff}} \sum_{G'=1}^{NOG} \nu\Sigma^f_{G',J} j^{oo}_{I,J,G'} \quad , \tag{2.88}$$

where

k_{eff} = effective multiplication constant of the medium,

$\Sigma_f(E')$ = macroscopic fission cross section at energy E' for the material in the zone containing the space point I,J,

$\nu(E')$ = number of neutrons produced per fission by a neutron at energy E',

$\chi(E)$ = fission spectrum,

and

$$\chi_G = \int_{\Delta E_G} \chi(E)dE \quad , \tag{2.89}$$

$$\nu\Sigma^f_{G'} = \frac{\int_{\Delta E_{G'}} \nu\Sigma_f(E')j^{oo}_{I,J}(E')dE'}{\int_{\Delta E_{G'}} j^{oo}_{I,J}(E')dE'} \quad . \tag{2.90}$$

The discrete ordinates difference equation for cylindrical r-z geometry is obtained by substituting the derived expressions for each of the six terms into Equation (2.27) and dividing through by ω_D. The result is

$$2\pi\Delta z_J \bar{\mu}_D (r_{i+1}\phi_{G,i+1,J,D} - r_i \phi_{G,i,J,D}) + 2\pi \bar{r}_I \Delta r_I \bar{\eta}_D$$

$$(\phi_{G,I,j+1,D} - \phi_{G,I,j,D}) + \frac{\Delta z_J}{\omega_D}(\gamma_{n+1}\phi_{G,I,J,n+1,K}$$

$$- \gamma_n \phi_{G,I,J,n,K}) + V_{I,J}\Sigma^T_G \phi_{G,I,J,D} = V_{I,J} S_{G,I,J,D} \qquad (2.91)$$

$$+ V_{I,J} \sum_{\ell=0}^{LMAX} \sum_{m=0}^{\ell} A_D^{\ell,m} \sum_{G'=1}^{G} S^{\ell,m}_{G,G'} \sum_{D'=1}^{NOA} A^{\ell,m}_{D'} \phi_{G',I,J,D'} \omega_{D'} .$$

The relationships between the mean angles denoted by subscript, D, and the angle end points, n,K, and, n+1,K, will be clarified further in the discussion of the space-angle mesh sweep in the next section.

III. SUPPLEMENTARY DIFFERENCE EQUATIONS

Equation (2.91), although an accurate representation of the macroscopic flow for the phase space cell, is not sufficient to determine a solution for the flux. For each mesh cell, assuming the incoming fluxes on three of the faces are known from calculations of previous cells or boundary conditions, there are four unknowns, the outgoing fluxes on the other three faces and the centered flux which is averaged over all variables. In order to obtain a solution, it is necessary to define additional equations which relate the centered flux with each pair of associated cell face fluxes. Many such relationships have been proposed and implemented. There are two essential requirements: First, the equation relating the centered flux and two end-point fluxes should provide a good approximation

to the true variation of the flux in the neighborhood of the cell. Second, these equations, when combined with Equation (2.91), must produce a final set of equations which may be easily and quickly solved on the computer. Hence, an exponential variation which well suits the first requirement is, at present, prohibited by the second requirement.

A possible set of additional difference equations is given by the following:

$$\phi_{G,I,J,D} = a\phi_{G,i+1,J,D} + (1-a)\phi_{G,i,J,D} \quad , \quad \mu > o \tag{2.92}$$

$$\phi_{G,I,J,D} = (1-a)\phi_{G,i+1,D} + a\,\phi_{G,i,J,D} \quad , \quad \mu < o \tag{2.93}$$

$$\phi_{G,I,J,D} = b\,\phi_{G,I,j+1,D} + (1-b)\,\phi_{G,I,j,D} \quad , \quad \eta > o \tag{2.94}$$

$$\phi_{G,I,J,D} = (1-b)\,\phi_{G,I,j+1,D} + b\,\phi_{G,I,j,D} \quad , \quad \eta < o \tag{2.95}$$

$$\phi_{G,I,J,D} = c\,\phi_{G,I,J,n+1,K} + (1-c)\phi_{G,I,J,n,K} \quad , \tag{2.96}$$

where a, b, and c are constants on the interval (1/2,1) and may be adjusted on an interval by interval basis. Although it is conceptually possible to estimate the optimum values for the constants by an iterative procedure, the additional complication introduced is beyond the scope of this study.

Two special cases of Equations (2.92) through (2.96) are of interest. These are for a = b = c = 1/2, called the "diamond-difference method," (15), and a = b = c = 1, called the "step-function method" (16). If the diamond-difference equations are combined

with the transport difference equation (2.91), and one solves for the centered flux, the result is

$$\phi_{G,I,J,D} = \left(|\bar{\mu}_D| 2\pi \bar{r}_I \Delta z_J \begin{pmatrix} \phi_{G,i+1,J,D} \\ \text{or} \\ \phi_{G,i,J,D} \end{pmatrix} + |\bar{\eta}_D| 2\pi \bar{r}_I \Delta r_I \right.$$

$$\left. \begin{pmatrix} \phi_{G,I,j+1,D} \\ \text{or} \\ \phi_{G,I,j,D} \end{pmatrix} + \frac{\Delta z_J}{\omega_D} \bar{\gamma}_N \phi_{G,I,J,n,K} + 1/2\ V_{I,J} S'_{G,I,J,D} \right) / \qquad (2.97)$$

$$\left(|\bar{\mu}_D| \Delta z_J 2\pi \bar{r}_I + |\bar{\eta}_D| 2\pi \bar{r}_I \Delta r_I + \frac{\Delta z_J}{\omega_D} \bar{\gamma}_N + 1/2\ V_{I,J} \Sigma_G^T \right) ,$$

where

$$\bar{\gamma}_N = \frac{1}{2} (\gamma_{n+1} + \gamma_n), \qquad (2.98)$$

$S'_{G,I,J,D}$ includes the fixed source and all scattering sources which one assumes to have been computed with previous fluxes, and the choice of flux terms in the brackets depends on the direction cosines, i.e., the upper term in the first bracket for $\bar{\mu}_D < 0$ and the upper term in the second bracket for $\bar{\eta}_D < 0$ and vice versa. After solving Equation (2.97) for the centered flux, the undetermined end point fluxes are given by

$$\begin{pmatrix} \phi_{G,i,J,D} \\ \phi_{G,i+1,J,D} \end{pmatrix} = 2\phi_{G,I,J,D} - \begin{pmatrix} \phi_{G,i+1,J,D} \\ \phi_{G,i,J,D} \end{pmatrix} , \qquad (2.99)$$

$$\begin{pmatrix} \phi_{G,I,J,D} \\ \phi_{G,I,j+1,D} \end{pmatrix} = 2\phi_{G,I,J,D} - \begin{pmatrix} \phi_{G,I,j+1,D} \\ \phi_{G,I,j,D} \end{pmatrix} , \qquad (2.100)$$

and

$$\phi_{G,I,J,n+1,K} = 2\phi_{G,I,J,D} - \phi_{G,I,J,n,K} \ , \qquad (2.101)$$

where the same convention is used with respect to the terms in brackets.

The sweep over the I and J indices is initiated by boundary conditions at the exterior surfaces of the problem. In a similar manner, the sweep over the azimuthal angle index, n, must be initiated for every polar angle index, K, and space point, I,J. This is accomplished by solving Equation (2.91) for the angular fluxes, $\phi_{G,I,J,n,K}$, having an azimuthal angle of $\psi = \pi$, (n=0), direction cosines, $\bar{\eta}_D = \bar{\eta}_K$ and $\bar{\mu}_D = -\sqrt{1 - \bar{\eta}_K^2}$, and weight $\omega_D = 0.0$. For these directions, which are included in the general set having index D, the angle derivative term, T_3, approaches zero, and the equation for the centered flux using diamond difference is

$$\phi_{G,I,J,D} = \left(|\bar{\mu}_D| 2\pi \bar{r}_I \Delta z_J \phi_{G,i+1,J,D} + |\bar{\eta}_D| 2\pi \bar{r}_I \Delta r_I \right.$$

$$\left. \times \begin{pmatrix} \phi_{G,I,j+1,D} \\ \phi_{G,I,j,D} \end{pmatrix} + \frac{1}{2} V_{I,J} S'_{G,I,J,D} \right) / \left(|\bar{\mu}_D| \Delta z_J 2\pi \bar{r}_I \right. \qquad (2.102)$$

$$\left. + |\bar{\eta}_D| 2\pi \bar{r}_I \Delta r_I + \frac{1}{2} V_{I,J} \Sigma_G^T \right) .$$

where $\bar{\mu}_D < 0$ for all angles with $\psi = \pi$. The undetermined end point fluxes are given by Equation (2.99) using the upper bracket terms only and by Equation (2.100) using both terms.

For a given source, $S'_{G,I,J,D}$, the complete flux array can be determined using Equations (2.97) through (2.102). The order of calculation, which is called the mesh sweep, is determined primarily by the sequence of direction cosines, $\bar{\mu}_D$ and $\bar{\eta}_D$. The requirements, with regard to the sequence, are the following:

1. The directions must be grouped into levels within which all the angles have the same $\bar{\eta}$.
2. Each level must have an initial angle with $\bar{\mu}_D = -\sqrt{1-\bar{\eta}_K^2}$ and $\omega_D = 0.0$.
3. Within each level the sequence must begin with the initial angle and proceed with increasing $\bar{\mu}_D$ (decreasing $\bar{\psi}_D$).
4. All levels having $\bar{\eta}$'s of like sign must be grouped together.

If the negative $\bar{\eta}$ levels are first, the sweep begins at the top boundary condition and proceeds with decreasing J. For each J, the angles in the negative $\bar{\eta}$ levels are sequenced in order of increasing D. For each angle, D, the I index is sequenced in order of decreasing I for angles having negative $\bar{\mu}_D$ and in increasing I for angles having positive $\bar{\mu}_D$. The left or right boundary conditions are used at the beginning of each I sweep. When the bottom of the system, J = 1, is completed the sweep for positive $\bar{\eta}$ levels begins with the bottom boundary condition and proceeds with increasing J in the same manner as before.

From Equations (2.99), (2.100), and (2.101), one notes that if the flux is decreasing rapidly such that the centered flux is less than half the magnitude of the previous end point flux, the extrapolated end point flux will be negative, a phenomenon called

"diamond-difference breakdown." If this situation exists throughout the system, then the space-angle mesh is inadequate and must be refined. However, in all but the most well behaved problems, there will be a few points in the space-angle grid where an over-enthusiastic extrapolation will occur. Unfortunately, in penetration problems the negative end point flux has been most often observed to cause the subsequent fluxes to diverge in positive-negative oscillations until the entire problem collapses into a sea of meaningless negative fluxes, which are usually of absolute magnitude much greater than the true fluxes. It is thus desirable to invoke some alternate procedure in the event of a negative flux due to diamond-difference breakdown.

The most attractice method for "negative flux fix-up" from the standpoint of giving a positive, non-zero answer with the best accuracy for the least effort is that obtained using the step function (a = b = c = 1.0) option in Equations (2.92) through (2.96). It is, of course, possible to use the step option for only the single constant, a, b, or c, which led to the observed negative flux. This may, however, when the final difference equation is reconstructed and re-solved, lead to a negative flux in one of the other extrapolations. The number of possible checks and re-calculations is sufficiently great that the best alternative is to use a = b = c = 1.0, for which the final difference equation for the centered flux is

$$\phi_{G,I,J,D} = \left(|\bar{\mu}_D| 2\pi\Delta z_J \begin{vmatrix} r_{i+1}\phi_{G,i+1,J,D} \\ r_i \phi_{G,i,J,D} \end{vmatrix} + |\bar{\eta}_D| 2\pi \bar{r}_I \Delta r_I \begin{vmatrix} \phi_{G,I,j+1,D} \\ \phi_{G,I,J,D} \end{vmatrix}\right.$$

$$+ \frac{\Delta z_J}{\omega_D} \gamma_n \phi_{G,I,J,n,K} + V_{I,J} S'_{G,I,J,D})/(|\bar{\mu}_D| 2\pi \Delta z_J \begin{bmatrix} r_i \\ r_{i+1} \end{bmatrix}$$

$$+ |\bar{\eta}_D| 2\pi \bar{r}_I \Delta r_I + \frac{\Delta z_J}{\omega_D} \gamma_{n+1} + V_{I,J} \Sigma_G^T), \tag{2.103}$$

where the convention with respect to the bracket terms is the same as that previously used in Equations (2.97) and (2.102). The new end point fluxes are given by

$$\begin{bmatrix} \phi_{G,i,J,D} \\ \phi_{G,i+1,J,D} \end{bmatrix} = \phi_{G,I,J,D} , \tag{2.104}$$

$$\begin{bmatrix} \phi_{G,I,j,D} \\ \phi_{G,I,j+1,D} \end{bmatrix} = \phi_{G,I,J,D} , \tag{2.105}$$

and

$$\phi_{G,I,J,n+1,K} = \phi_{G,I,J,D} . \tag{2.106}$$

The initial flux for the step option is given by

$$\phi_{G,I,J,D} = (|\bar{\mu}_D| 2\pi r_{i+1} \Delta z_J \phi_{G,i+1,J,D} + |\bar{\eta}_D| 2\pi \bar{r}_I \Delta r_I$$

$$\begin{bmatrix} \phi_{G,I,j+1,D} \\ \phi_{G,I,j,D} \end{bmatrix} + V_{I,J} S'_{G,I,J,D})/(|\bar{\mu}_D| 2\pi r_{i+1} \Delta z_J \tag{2.107}$$

$$+ |\bar{\eta}_D| 2\pi \bar{r}_I \Delta r_I + V_{I,J} \Sigma_G^T) ,$$

where the new end point fluxes are given by Equation (2.104) using the upper bracket term only and Equation (2.105) using both terms.

In the sweep of the space-angle mesh, the difference equations based on "diamond difference," (2.97), (2.99), (2.100), (2.101), and (2.102), are used as standard procedure. If, in the extrapolation equations, (2.99), (2.100), (2.101), a negative end point flux is generated for any point, all the fluxes for that cell defined by I, J, D, are immediately recalculated using the "step" equations, (2.103), (2.104), (2.105), (2.106), and (2.107), which always give positive fluxes when the incoming fluxes and the source are positive. The use of this technique is valid for problems where the space-angle mesh is, for the most part, adequate or more than adequate for accurate calculations using "diamond difference." In the circumstance that a negative flux occurs, the recalculation with the step function equations gives a fairly reasonable, physically possible result which prevents the cascade of negative fluxes.

In order to demonstrate the mixed-mode, linear-step, difference technique, the simple problem of neutron transport in a water slab exposed to an isotropic fission surface source is solved for various space mesh intervals. The solution of the problem employs a S_{16} Gaussian quadrature and a P_3 scattering approximation using GAM-II (17) cross sections. Figure 3 shows the fast neutron dose as a function of penetration depth. The result for a 0.5-cm. interval size is calculated for the reference curve. Using linear diamond difference, the same curve is obtained for up to 2.0-cm. intervals. At 3.0-cm. interval size, some oscillation is observed in the lower energy groups for the linear model. At a mesh size of 5.0 cm. the fast dose, as shown in Figure 1, is oscillatory in a slightly divergent manner. At a mesh

DWG. NO. G-69-552

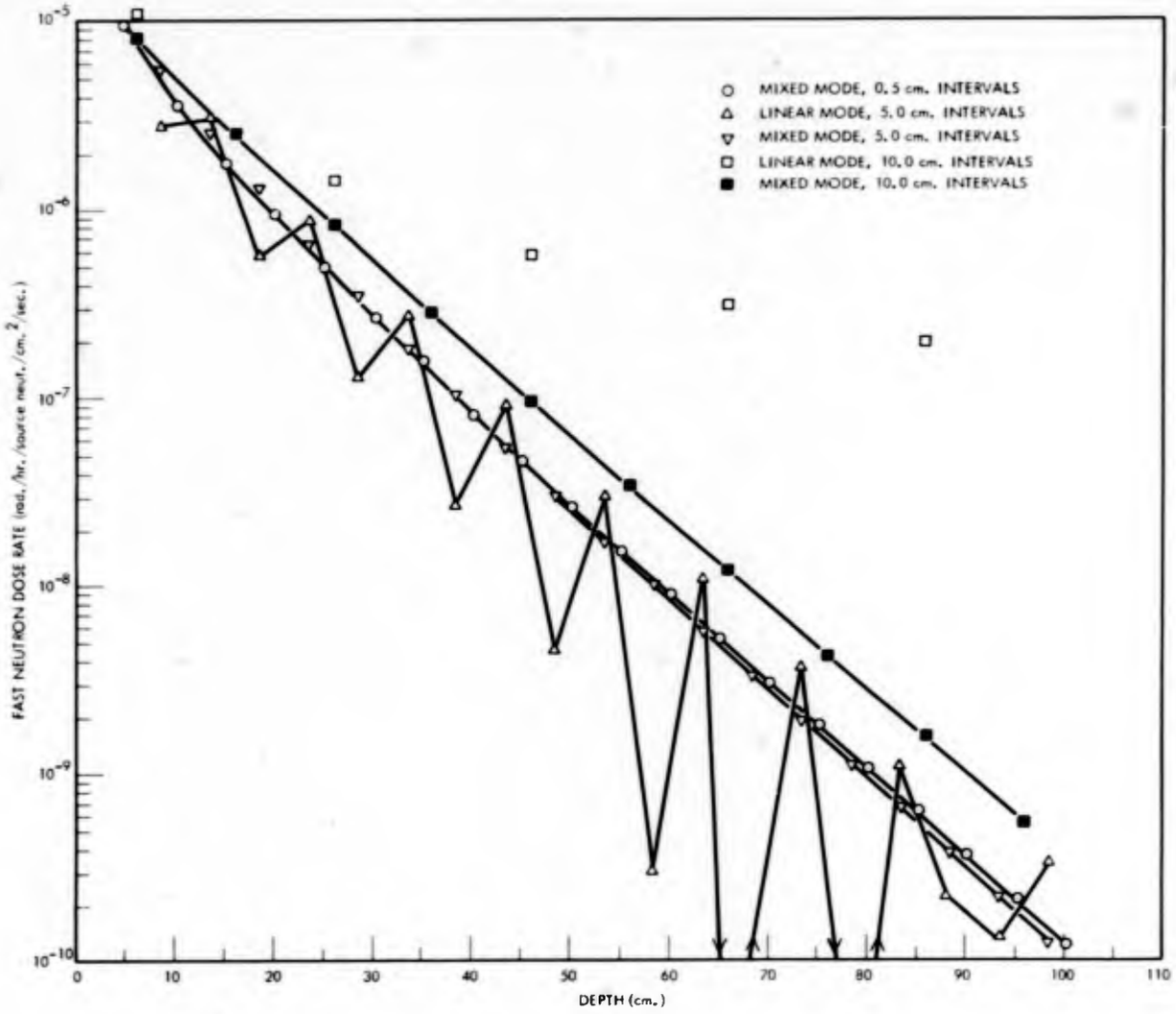

Figure 3. The effects of mesh spacing and difference model on the calculated fast neutron dose distribution in a water slab.

size of 10.0 cm., the linear difference method gives a divergent solution with every other mesh interval having a negative dose.

The mixed-mode calculations using the step function equations give exactly the same solutions as the linear method for very fine mesh intervals since no negative fluxes are calculated. The mixed-mode calculation for a 5.0-cm. mesh is stable and agrees fairly well with the best calculation. For a 10.0-cm. mesh the mixed-mode calculation is high by a factor of three at 90.0 cm. penetration, but it is stable. The mixed-mode calculation is always as good or better than the pure linear method. The primary benefit is obtained for mesh sizes where the linear model is still being used for the most important angles, and the step model prevents an over-enthusiastic linear extrapolation in an unimportant angle from causing an oscillation.

The major ingredients of the anisotropic, two-dimensional discrete ordinates transport method have been presented in this chapter. Except for the higher order anisotropic scattering which is of particular interest in penetration problems, the material in this chapter is of interest and has application in all problems involving neutron and gamma-ray transport. The remaining chapters will be concerned more with the particular ingredients of special interest in penetration problems and the experimental verification of the overall method.

CHAPTER III

THE INNER ITERATION PROCEDURE

In the derivation of the difference equations for the angular flux, Equations (2.97), (2.102), etc., it was assumed that the source, $S'_{G,I,J,D}$, includes the fixed component and scattering sources computed using previously calculated fluxes. In most neutron and all gamma-ray transport problems one may assume that particles undergoing scattering always degrade in energy. Thus, if one begins the flux solution with the highest energy group and proceeds downward in energy (increasing G), the downscatter source for any particular group,

$$S_G(\text{DOWN}) = V_{I,J}\omega_D \sum_{\ell=0}^{\text{LMAX}} \sum_{m=0}^{\ell} A_D^{\ell,m} \sum_{G'=1}^{G-1} S_{I,J,G,G'}^{\ell,m} j_{I,J,G'}^{\ell,m} , \qquad (3.1)$$

is completely determined and may be treated as a fixed component in the source for group G. The within-group scattering for group G,

$$S_G(\text{INGROUP}) = V_{I,J}\omega_D \sum_{\ell=0}^{\text{LMAX}} \sum_{m=0}^{\ell} A_D^{\ell,m} S_{I,J,G,G}^{\ell,m} j_{I,J,G}^{\ell,m} , \qquad (3.2)$$

involves fluxes yet to be determined for group G. The most straightforward method for determining the within-group scattering source is to iterate using the difference equations, (2.102), (2.104), (2.105), etc., and Equation (3.2). The equations for any particular group may be represented symbolically in the form

$$\phi_G = T_G(S_G + \Sigma_G^S \phi_G) . \qquad (3.3)$$

where ϕ_G is the complete flux vector, S_G is the fixed source including downscatter, T_G is the transport operator which determines the flux for a given source, and Σ_G^S is the within-group scattering operator. The iterative procedure may be more easily discussed using the symbolic form.

I. POWER ITERATION

Ordinary Gaussian iteration, or "power iteration," is the most simple method for solving iterative problems. The procedure is begun by assuming a flux guess, ϕ_G^o, which determines an initial scattering source which then leads to the first iterate flux,

$$\phi_G^1 = T_G(S_G + \Sigma_G^S \phi_G^o) \ . \tag{3.4}$$

The first iterate flux then becomes the next guess and the procedure is repeated,

$$\begin{aligned} \phi_G^2 &= T_G(S_G + \Sigma_G^S \phi_G^1) \\ &\vdots \\ \phi_G^n &= T_G(S_G + \Sigma_G^S \phi_G^{n-1}) \ . \end{aligned} \tag{3.5}$$

By successive substitutions, the equation for the n^{th} iterate of the flux may be rewritten as

$$\begin{aligned} \phi_G^n = T_G(S_G + \Sigma_G^S(T_G(S_G + \Sigma_G^S(T_G(S_G + \ \ldots \\ + \Sigma_G^S(T_G(S_G + \Sigma_G^S \phi_G^o) \ \ldots \ ) \end{aligned} \tag{3.6}$$

or

$$\phi_G^n = \sum_{i=0}^{i=n-1} (T_G \Sigma_G^S)^i \, T_G S_G + (T_G \Sigma_G^S)^{n-1} \, \Sigma_G^S \phi_G^o \, . \qquad (3.7)$$

If the initial flux guess is the null vector (as is usually the case), the n^{th} iterate flux is

$$\phi_G^n = \sum_{i=0}^{i=n-1} (T_G \Sigma_G^S)^i \, T_G S_G \, . \qquad (3.8)$$

The first term in the series in Equation (3.8) is identified as the uncollided flux for group G,

$$\phi_G^u = T_G S_G \, , \qquad (3.9)$$

where the source includes downscatters from the higher energy groups. The second term is the flux due to particles which have suffered one collision,

$$\phi_G^{u+1} = T_G \Sigma_G^S T_G S_G = T_G \Sigma_G^S \phi_G^u \, . \qquad (3.10)$$

The n^{th} iterate flux may thus be interpreted as the sum of the uncollided flux plus the flux due to one collision, plus the flux due to two collisions, ..., and finally plus the flux due to n-1 collisions. The number of iterations required for convergence is thus physically related to the number of collisions which contribute to the flux.

Although a direct analysis of the iteration process in the discrete ordinates method has not been done, some insight can be gained

by considering the behavior of the matrix problem

$$\phi_G = T_G \Sigma_G^S \phi_G + T_G S_G \ , \tag{3.11}$$

where one assumes that the eigenvalues, $\{\lambda_i\}_{i=1}^{i=n}$, of the nxn square matrix $T_G \Sigma_G$ are ordered such that

$$|\lambda_n| \leq |\lambda_{n-1}| \leq \text{---} \leq |\lambda_2| < \lambda_1 < 1,$$

and that the corresponding set of eigenvectors span the associated vector space. The iterative process is represented by

$$\phi_G^i = T_G \Sigma_G^S \phi_G^{i-1} + T_G S_G \ . \tag{3.12}$$

If the error vector is defined by

$$E_G^i \equiv \phi_G - \phi_G^i \ , \tag{3.13}$$

where ϕ_G is given by Equation (3.11) and ϕ_G^i by Equation (3.12), it then follows that

$$E_G^i = T \Sigma_G^S E_G^{i-1} \ , \tag{3.14}$$

and, by successive substitutions,

$$E_G^i = (T_G \Sigma_G^S)^i \ E_G^o \ . \tag{3.15}$$

If E_G^o is expanded in terms of the eigenvectors of $T_G \Sigma_G^S$

$$E_G^o = \sum_k C_k^o \psi_G^k \ , \tag{3.16}$$

where

$$T_G \Sigma_G^S \psi_G^k = \lambda_k \psi_G^k , \tag{3.17}$$

then

$$E_G^i = (T_G \Sigma_G^S)^i \left[\sum_k C_k^o \psi_G^k\right] = \sum_k (\lambda_k)^i C_k^o \psi_k . \tag{3.18}$$

where each error component, $C_k^o \psi_k$, is multiplied by the associated eigenvalue raised to the i^{th} power. For many iterations, $i >> 1$, then

$$E_G^i \tilde{=} (\lambda_1)^i C_1^o \psi_1 = (\lambda_1)^i E_G^o = \lambda_1 E_G^{i-1} , \tag{3.19}$$

and the most slowly decaying component of the error is multiplied by the modulus, λ_1, which is called the dominance ratio (18). It is frequently convenient to speak in terms of the convergence rate, R, which is defined by

$$R \equiv -\ell n\ \lambda \quad \text{or} \quad \lambda^{1/R} = e^{-1} . \tag{3.20}$$

From Equations (3.20) and (3.19) one may note that 1/R is approximately the number of iterations required to reduce the error by a factor of e.

An expression for λ_k is given by multiplying Equation (3.17) by the total cross section and integrating over all phase space

$$\int \Sigma_G^T T_G \Sigma_G^S \psi_G^k d\bar{\rho} = \lambda_k \int \Sigma_G^T \psi_G^k d\bar{\rho} \tag{3.21}$$

giving

$$\lambda_k = \frac{\int \Sigma_G^T T_G \Sigma_G^S \psi_G^k d\bar{\rho}}{\int \Sigma_G^T \psi_G^k d\bar{\rho}} \tag{3.22}$$

An estimate of the dominance ratio, λ_1, may be obtained by setting k=1 and approximating ψ_G^1 by ϕ_G, which gives

$$\lambda_1 \tilde{=} \frac{\int \Sigma_G^T T_G \Sigma_G^S \phi_G d\bar{\rho}}{\int \Sigma_G^T \phi_G d\bar{\rho}} \tag{3.23}$$

or

$$\lambda_1 = \frac{\text{number of collisions in the } (i+1)^{th} \text{ scattering generation}}{\text{number of collisions in the } i^{th} \text{ scattering generation}} .$$

The number of collisions in the $(i+1)^{th}$ scattering generation is equal to the number of collisions in the i^{th} generation less the removal and leakage. Hence,

$$\lambda_1 \tilde{=} \frac{\int \left(\Sigma_G^T \phi_G - \Sigma_G^R \phi_G - L_G \right) d\bar{\rho}}{\int \Sigma_G^T \phi_G d\bar{\rho}} = \frac{\int \left(\Sigma_G^S \phi_G - L_G \right) d\bar{\rho}}{\int \Sigma_G^T \phi_G d\bar{\rho}} . \tag{3.24}$$

If the leakage is small (which is true for most penetration problems) and the flux weighting is ignored, an approximation for λ_1 is

$$\lambda_1 \tilde{=} \frac{\Sigma_G^S}{\Sigma_G^T} . \tag{3.25}$$

Table I shows the effect of the ratio of the within-group scattering cross section, Σ_G^S, to the total cross section, Σ_G^T, on the number of iterations required to reduce the initial error by a factor of 10^{-3} as derived from Equations (3.25) and (3.20). The number of required iterations rises rapidly as λ_o approaches 1.0. For a typical multigroup structure having 20 or more groups, the dominance ratio for an average energy group for hydrogenous media is usually near 0.5, requiring about 10 iterations for convergence, but the dominance ratio for graphite or a metal such as lead in the same group structure may be 0.95 or greater, requiring many more iterations. Although this analysis is very simplified and the number of iterations is influenced by leakage and other characteristics such as the depth of penetration, the observed number of iterations can usually be explained on this basis.

II. NORMALIZED POWER ITERATION

A simple procedure which is used to accelerate the convergence of the inner iterations is a space-independent normalization (19). In power iteration, as suggested by Equation (3.5), the total number of losses per iteration is not constant since

$$(L_G + \Sigma_G^R)\phi_G^i = (L_G + \Sigma_G^R)(TS + \Sigma_G^S\phi_G^{i-1}) \neq (L_G + \Sigma_G^R)\phi_G^{i-1}, \qquad (3.26)$$

TABLE I

THE EFFECT OF THE DOMINANCE RATIO ON THE NUMBER OF ITERATIONS REQUIRED FOR AN IDEALIZED PROBLEM

$\lambda_1 \simeq \frac{\Sigma_S}{\Sigma_T}$	$R = -\ln \lambda_1$	Number of Iterations for 10^{-3} Error Reduction
.1	2.30	3
.3	1.21	6
.5	0.692	10
.8	0.224	31
.9	0.106	66
.95	0.0514	134
.97	0.0304	227
.99	0.0101	687

where L_G is the leakage operator and Σ_G^R the removal operator such that $(L_G + \Sigma_G^R)\phi_G^i$ gives the total loss from group G at iterate i. Another symbolic form of the transport equation is

$$(L_G + \Sigma_G^R + \Sigma_G^S)\phi_G^i = S_G + \Sigma_G^S \phi_G^{i-1} , \tag{3.27}$$

where each term represents the application of the operator and integral over space and angle. A scale factor, f, may be determined such that the total loss equals the total source,

$$(L_G + \Sigma_G^R) f\ \phi_G^i = S_G \tag{3.28}$$

then

$$f(S_G + \Sigma_G^S \phi_G^{i-1} - \Sigma_G^S \phi_G^i) = S_G , \tag{3.29}$$

or

$$f = \frac{S_G}{S_G + \Sigma_G^S(\phi_G^{i-1} - \phi_G^i)} . \tag{3.30}$$

If the fluxes are multiplied by the scale factor which is computed after each iteration, the number of particles in the system is conserved and the convergence rate is increased. Integral normalization always improves the convergence rate but the amount of improvement is dependent on the problem. The number of iterations for a problem with uniform sources and a very high dominance ratio may be reduced by a factor of 10 or more.

Honeck (19) asserts that the error vector decays as the i^{th} power of the second eigenvalue, $(\lambda_2)^i$, of the operator $T_G \Sigma_G^S$, but

this is difficult to verify. In a penetration problem, which is characterized by a localized source and large system in which the flux decreases by orders of magnitude, the normalization process is ineffective. This is deduced from Equations (3.8) through (3.10) which show that the flux converges most rapidly near the source where particles suffering few collisions contribute most of the flux. Also, since the flux near the source is orders of magnitude greater than that in the usual areas of interest, the integral within group scattering rate in Equation (3.30) is dominated by these fluxes which converge relatively soon. Thus, after a few iterations the normalization factor is unity and has no further driving effect on the iteration. A driving effect which is position dependent is thus desired.

III. CHEBYSHEV ITERATION

The Chebyshev polynomial method of iteration (19,20) can be readily adapted to improve the inner-iteration procedure. Furthermore, the physical interpretation of power iteration as successive scatterings can be used to obtain estimates of parameters required in the Chebyshev method. The within-group iteration process is represented as before by the matrix equation,

$$\phi_G = T_G \Sigma_G^S \phi_G + T_G S_G \,, \tag{3.31}$$

where the eigenvalues, $\{\lambda_i\}_{i=1}^{i=n}$, of the nxn square matrix, $T_G \Sigma_G^S$, are ordered such that

$$|\lambda_n| \leq |\lambda_{n-1}| \leq \ldots \leq |\lambda_2| < \lambda_1 < 1 .$$

To solve Equation (3.31) one can use the iterative procedure given by Varga (21),

$$\phi_G^{i+1} = \omega_{i+1}(T_G \Sigma_G^S \phi_G^i + T_G S_G - \phi_G^{i-1}) + \phi_G^{i-1} . \tag{3.32}$$

The sequence, ω_{i+1}, is given by $\omega_1 = 1$, and

$$\omega_{i+1} = 2C_i(1/\lambda_1)/\lambda_1 C_{i+1}(1/\lambda_1) \text{ for } i \geq 1 , \tag{3.33}$$

where $C_i(1/\lambda_1)$ is the Chebyshev polynomial of degree i in $(1/\lambda_1)$. Varga (21) has shown that the error vector E_G^i, Equation (3.13), after i Chebyshev iterations is given by

$$E_G^i = P_i(T_G \Sigma_G^S) E_G^o , \tag{3.34}$$

where

$$P_i(T_G \Sigma_G^S) \equiv C_i(T_G \Sigma_G^S/\lambda_1)/C_i(1/\lambda_1) . \tag{3.35}$$

The expansion of E_G^o gives

$$E_G^i = P_i(T_G \Sigma_G) \left(\sum_k C_k^o \psi_G^k \right) = \sum_k P_i(\lambda_k) C_k^o \psi_G^k , \tag{3.36}$$

where the operator polynomial $P_i(T_G \Sigma_G^S)$ operates term by term on the error components such that in the final result each error component is multiplied by an i^{th} order polynomial in the eigenvalue, λ_k. Thus, after many iterations the most slowly decaying contribution to the initial error decays as $P_i(\lambda_1)$ and

$$E_G^i \tilde{=} P_i(\lambda_1) E_G^o . \tag{3.37}$$

In typical applications of the Chebyshev method to matrix iterative problems, the most difficult problem is the estimation of the dominance ratio, λ_1, and hence the acceleration factor, ω_i. For example, the method developed by Hageman (18) involves first the application of ordinary power iterations. After several iterations one calculates the ratio of the norms of the residual vectors,

$$Q(i) = \frac{|| R(i) ||}{|| R(i-1) ||} \tag{3.38}$$

where

$$R(i) = (\phi_G^{i+1} - \phi_G^i),$$

and for the power iteration method one observes that

$$\lim_{i \to \infty} Q(i) = \lambda_1 . \tag{3.39}$$

Hence, when successive residual vector ratios converge within an arbitrary criteria, the final value of Q(i) is used as the value of λ_1 for the Chebyshev iteration. The full implementation of Hageman's method involves re-estimation of λ_1 and the start of a new Chebyshev iteration at each new determination of λ_1. Unfortunately, many iterations are often required to converge the residual vector ratios.

For the inner iteration problem the physical interpretation for λ_1 given by Equation (3.24) may be used for the Chebyshev iteration. The scheme which is used involves the calculation of λ_1 for each iteration of the normalized power iteration method. When successive values of λ_1 converge within an arbitrary criteria, the Chebyshev

iteration is started. After several iterations the numerator and denominator of Equation (3.33) grow quite large and may cause overflow in the finite digital computer word. However, the values of ω_i are observed to converge after several Chebyshev iterations such that recalculation of Equation (3.33) is discontinued and the converged value of ω is used in succeeding iterations.

As will be shown in the comparisons at the end of this chapter, the Chebyshev method of inner iteration is a significant improvement over the normalized power iteration. The convergence acceleration, however, is spacially dependent only due to the relative flux change since the driving factor ω is spacially independent.

IV. SPACE-DEPENDENT NORMALIZED POWER ITERATION

A space-dependent driving function can be obtained by generalizing the normalized power iteration to include a space-dependent normalization factor (22). In a manner similar to that used in Equation (3.27), a symbolic form of the transport equation for a particular space interval is

$$\begin{aligned} &LI^{i}_{I-1,J} + LI^{i}_{I+1,J} + LI^{i}_{I,J-1} + LI^{i}_{I,J+1} \\ &+ LO^{i}_{I,J} + \Sigma^{R}\phi^{i} + \Sigma^{S}\phi^{i} = S + \Sigma^{S}\phi^{i-1}, \end{aligned} \tag{3.40}$$

where each term represents an integral over angle to give a scalar balance, and the convection terms have been separated into incoming leakage, LI, and outgoing leakage, LO, terms. The combinations of

indices on the incoming leakage terms indicate that these are computed with fluxes belonging to adjoining intervals. If the fluxes are multiplied by scale factors that are functions of space interval in order to equate losses with sources, the result is

$$f_{I-1,J}LI^{i}_{I-1,J} + f_{I+1,J}LI^{i}_{I+1,J} + f_{I,J-1}LI^{i}_{I,J-1} + f_{I,J+1}LI^{i}_{I,J+1} + f_{I,J}(LO^{i} + \Sigma^{R}\phi^{i}) = S \ , \tag{3.41}$$

which is a five point difference equation in terms of the scale factors $f_{I,J}$ similar to the two-dimensional diffusion equation. For the one-dimensional discrete ordinates equation, the J indices would not be present and Equation (3.41) becomes

$$f_{I-1}LI^{i}_{I-1} + f_{I+1,J}LI^{i}_{I+1} + f_{I}(LO^{i} + \Sigma^{R}\phi^{i}) = S \ , \tag{3.42}$$

a tri-diagonal matrix equation which can be solved by Gaussian reduction.

Several methods can be used to obtain solutions for Equation (3.41). One possible technique involves the integration of Equation (3.41) over the I mesh and J mesh separately to give two one-dimensional equations having the form of Equation (3.42). A better method depends on an iterative solution. One first assumes that $f_{I,J} = 1.0$ for all I and J. The equation for iteration is

$$f^{n}_{I-1,J}LI^{i}_{I-1,J} + f^{n}_{I+1,J}LI^{i}_{I+1,J} + f^{n}_{I,J}(LO^{i} + \Sigma^{R}\phi^{i}) = S - f^{n-1}_{I,J-1}LI^{i}_{I,J-1} - f^{n-1}_{I,J+1}LI^{i}_{I,J+1} \ , \tag{3.43}$$

where i designates the i^{th} inner iteration and n designates the n^{th} iteration on the scale factors. For a given iteration, n, the right-hand side of Equation (3.43) is determined since it contains the previous iteration scale factors, and the equation can be solved by reduction in the same manner as for Equation (3.42). The iteration on scale factors continues until

$$\max \frac{| f^{n}_{I,J} - f^{n-1}_{I,J} |}{f^{n}_{I,J}} \leq 0.001, \text{ all } I,J \ . \qquad (3.44)$$

In the implementation of space-dependent normalization in the one-dimensional code, ANISN, (22), it was determined that the scaling should be performed on every third iteration due to instabilities which occurred in some problems.

V. CONVERGENCE CRITERIA

The companion problem to the acceleration of the rate of convergence which was discussed in the previous sections is the specification of a criteria which determines when the inner iterations are sufficiently converged. Earlier discrete ordinates codes which were used primarily for the analysis of fast critical assemblies considered the inner iterations to be converged if

$$\frac{\int \Sigma^{S}(\phi^{i} - \phi^{i-1})dv}{\int \Sigma^{S} \phi^{i} dv} \leq EPS \ , \qquad (3.45)$$

where the integration is performed over the volume of the entire system, and EPS is usually equal to .001. Although this criteria is usually

sufficient for critical assemblies where the flux does not vary much in magnitude, it is not suitable for penetration problems. The integral is dominated by the flux near the source which has the greatest magnitude and converges most rapidly.

The convergence criteria now commonly used in the anisotropic one-dimensional codes (11,12) is based on the maximum pointwise error,

$$\max \frac{| \phi_I^i - \phi_I^{i-1} |}{\phi_I^i} < \text{EPS} \quad \text{all I} . \tag{3.46}$$

This criteria may be over-sensitive depending on the requirements of the problem. One-dimensional problems are usually sufficiently simple such that the maximum pointwise error is the best choice.

Two-dimensional problems are sufficiently complex that there is usually some point which will not satisfy the pointwise criteria. These points are usually in some obscure corner or unimportant location. One must, in two-dimensional calculations, consider the errors in terms of their importance to the problem. A generalized test might be

$$\sum_{\text{all } I,J} |\phi_{I,J,G}^i - \phi_{I,J,G}^{i-1}| \; I_{I,J,G} = \Delta ANS_G \leq \varepsilon ANS_G , \tag{3.47}$$

where ANS_G is the portion of the desired answer in group G, and $I_{I,J,G}$ is the contribution to the answer ANS_G due to the flux at point I,J. If the desired answer is the dose at point I',J', then $I_{I,J,G}$ is equal to the dose factor at point I',J', and is zero elsewhere. The error test thus reduces to a special case of the pointwise error.

If, however, one considers a dose response including an analytic last flight then one has

$$I_{I,J,G} = \Sigma^{S}(\Omega' \rightarrow \Omega, G \rightarrow G) e^{-\Sigma_G^T |\vec{r}_{I,J} - \vec{r}_{I',J'}|} DF_{I',J'} , \qquad (3.48)$$

which is the probability of scattering into the proper angle, arriving uncollided at I',J', and contributing to the dose.

Although the criteria given using Equation (3.48) would be accurate and not sensitive to the localized fluctuations which affect the pointwise criteria, it appears to be too difficult to use. An approximation which is simple to apply yet suitably sensitive is to assume that $I_{I,J,G}$ is constant over some small zone around the point of interest and zero elsewhere. With this zone-of-interest approximation, the criteria is

$$\sum_{\text{all } I,J \text{ in ZOI}} \frac{|\phi^{i}_{I,J,G} - \phi^{i-1}_{I,J,G}|}{\phi^{i}_{I,J,G}} V_{I,J} \leq \text{EPS} \sum_{\text{ZOI}} V_{I,J}, \qquad (3.49)$$

where the summation is only for points within the zone of interest. All of the convergence criteria which have been discussed are available in DOT, but that given by Equation (3.49) is recommended.

VI. COMPARISON OF METHODS

A study and demonstration of the effects of the three methods of inner iteration which have been discussed can be done with almost any applied transport problem. It is more emphatic to pick a problem which is difficult to converge, although the effects on the "easy" problems are also of interest. In most multigroup problems some

energy groups are relatively easy to converge while others may be quite difficult. Thus, by looking at two energy groups in the same problem both an "easy" and a "difficult" example may be obtained. A demonstration of the effects of normalized power iteration, Chebyshev iteration, and point-scaled iteration as implemented in the one-dimensional code, ANISN, was performed using a multigroup adjoint calculation of a very large sphere of air with a surface source (22). This problem was unusually difficult since the low energy groups which are typically the most difficult to converge are computed first in an adjoint calculation, and the overall results are much more sensitive to a possible lack of convergence of these groups.

In order to study the effects of the methods of iteration and the zone-of-interest method of convergence, as implemented in the two-dimensional code, DOT, one of the problems to be considered in the experimental comparisons in Chapters V and VI is considered. The selected problem is that of a cylinder of lead approximately five feet in diameter and eleven inches thick. A monodirectional neutron beam source, approximately 4.25 inches in diameter, is incident on one face. In a multigroup calculation of neutron transport in lead the energy groups are much wider than the average energy loss due to elastic scattering. Since inelastic scattering is relatively unimportant, each group acts essentially independent of the others. Two groups from the 38-group structure given in Chapter VI are considered. Group 10, extending from 2.47 MeV. to 2.02 MeV., has a total cross section of 0.2045 $cm.^{-1}$ and a within-group scattering cross section of 0.1743 $cm.^{-1}$, giving an approximate dominance ratio of 0.85. Group 25, extending from 0.1228 MeV. to 0.0865 MeV., has a total cross section

of 0.3433 cm.$^{-1}$ and a within-group scattering cross section of 0.3337 cm.$^{-1}$, giving an approximate dominance ratio of 0.97. Calculations were performed for each group using each of the three iteration methods and two zones of interest for convergence, giving 12 calculations. The first zone of interest is a small cylindrical portion of the slab directly opposite the source. The second zone of interest is an annular band around the slab and near the exit surface.

Figure 4 shows the zone-of-interest convergence indicator as defined by Equation (3.49) as a function of iteration number for the three iteration methods and the first zone of interest. The regular normalized power iteration method reaches the prescribed criteria of EPS = 10^{-3} in 50 iterations. The Chebyshev iteration, which began at the sixth iteration with a converged λ_{eff} of 0.9 satisfies the convergence criteria at iteration 26. The point-scaled method satisfies the convergence criteria at iteration 16. The errors for each third iteration include the effect of scaling and are not included in the data. It is also interesting to consider the flux behavior corresponding to the convergence indications. Figure 5 shows the flux behavior for a point, I = 6, J = 2, in the convergence zone. The regular method converges very smoothly with only a slight "overshoot." Once the Chebyshev iteration starts, the flux rises very rapidly, overshoots the answer fairly strongly, and then converges. The flux for the point-scaled iteration varies more erratically but converges more quickly. The Chebyshev method takes about one-half the iterations required of the regular method, and the point-scaled method takes about one-third.

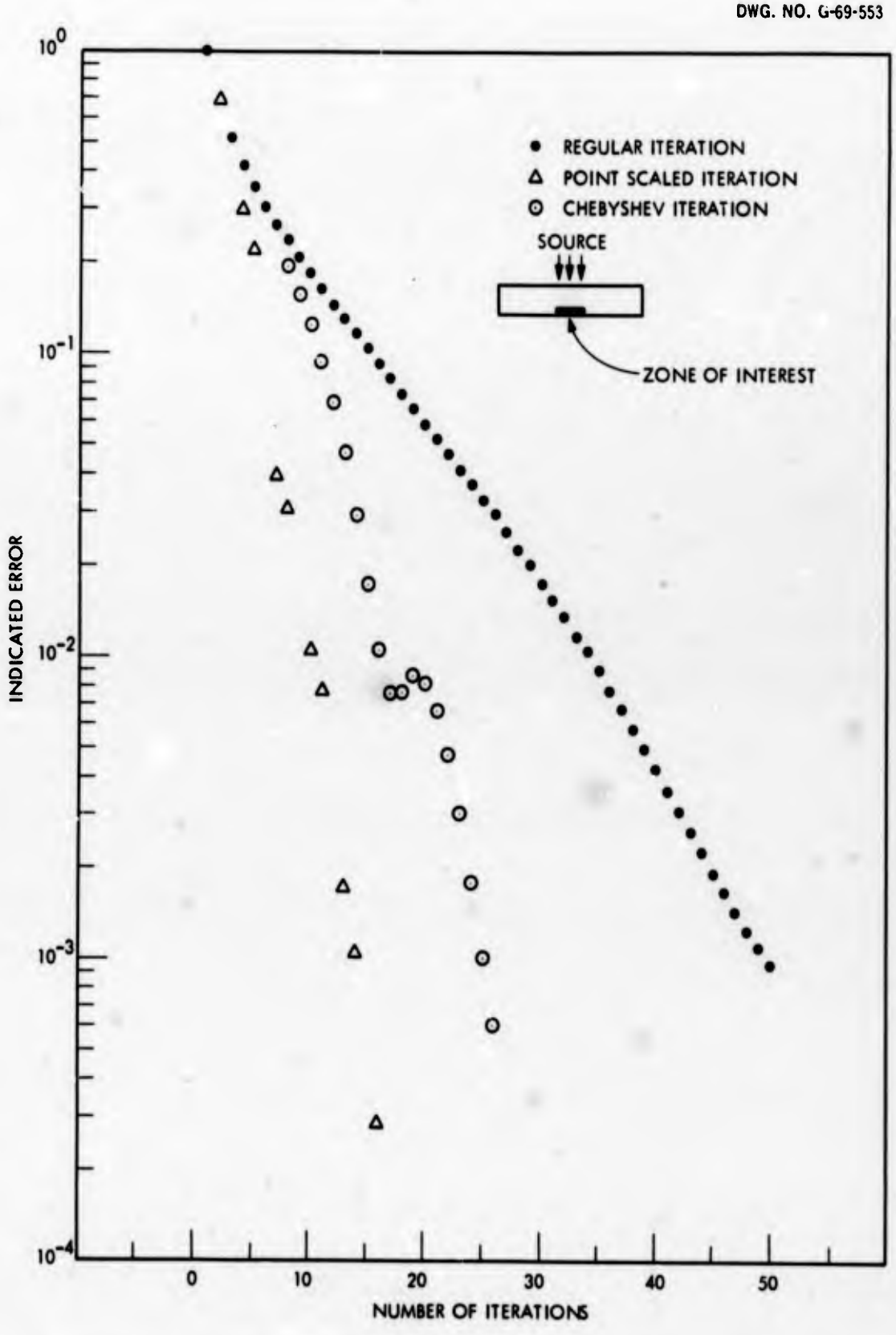

Figure 4. A comparison of three iteration methods for group 25 of the lead slab problem with the first zone of interest.

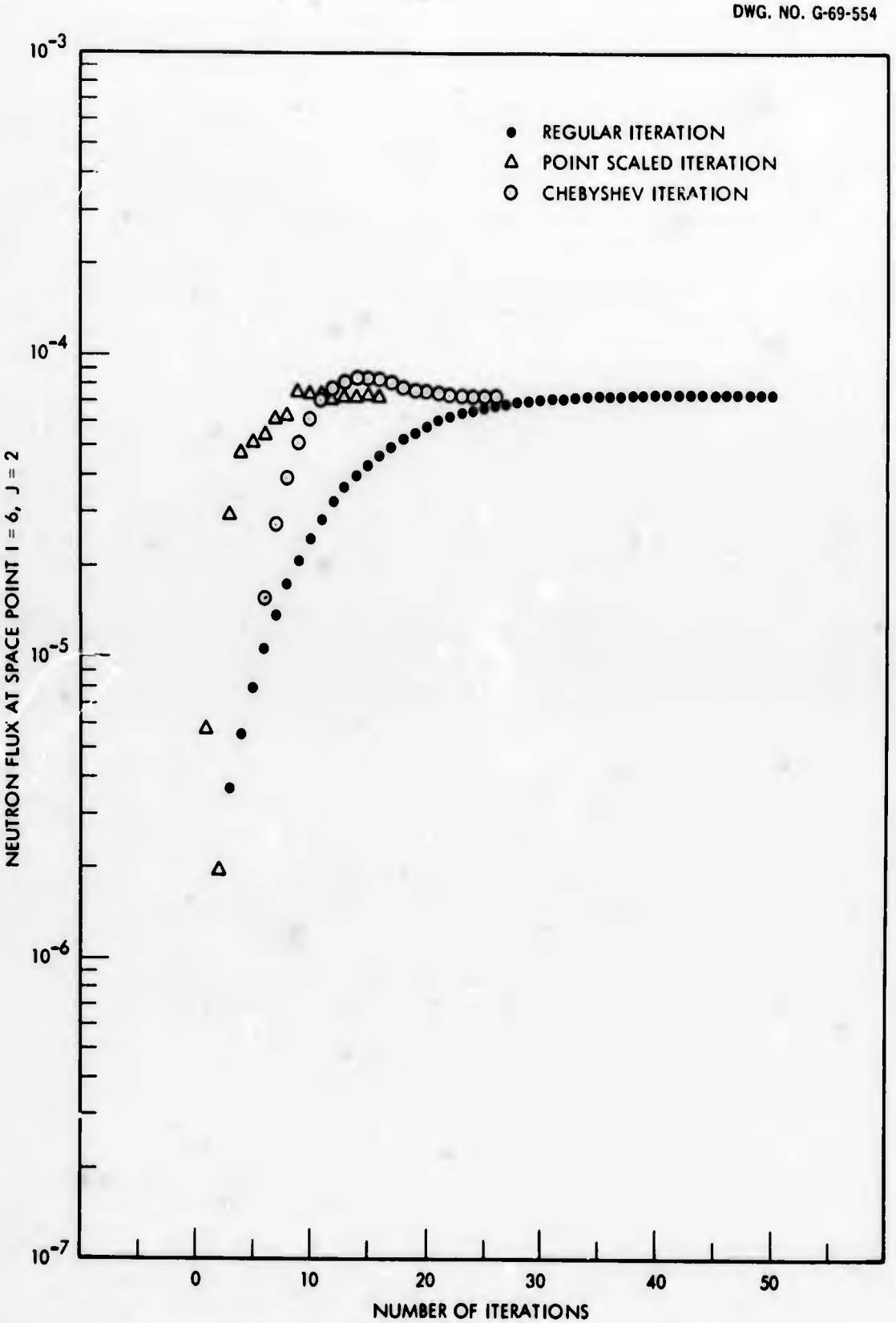

Figure 5. A comparison of the flux behavior at the space point, I=6, J=2, for group 25.

Figure 6 shows a similar comparison of convergence indicators for group 25 with the second zone of interest. This criteria is more difficult since the important particles must be transported over 25 mean free paths in a direction at right angles to the source. The regular method does not converge by 50 iterations, and it is estimated that 140 iterations would be required. The Chebyshev method does much better, indicating convergence at 48 iterations, and the point-scaled method appears best by indicating convergence at 23 iterations. The flux behavior for this problem is shown in Figure 7. At the point I = 44, J = 6, the flux with the regular method is still rising and is about a factor of three low at 50 iterations. The Chebyshev method gives a smooth behavior with no overshoot in this case. The flux with the point-scaled iteration overshoots, but then is essentially converged at 15 iterations.

Figure 8 shows the behavior of the convergence indicator for the three methods of iteration for energy group 10 with the second zone of interest. This problem is somewhat easier to converge than those for group 25. The regular method requires 37 iterations for convergence, the Chebyshev method requires 26 iterations, and the point-scaled method requires 16 iterations. The behavior for the flux at I = 44, J = 6, is shown in Figure 9. Figure 10 shows the convergence indicator as a function of iteration for group 10 with the second zone of interest. This is the easiest problem of the group, and the advantage of the point-scaled method over the regular method is reduced. The Chebyshev method surprisingly takes two more iterations than the regular method. Since this problem

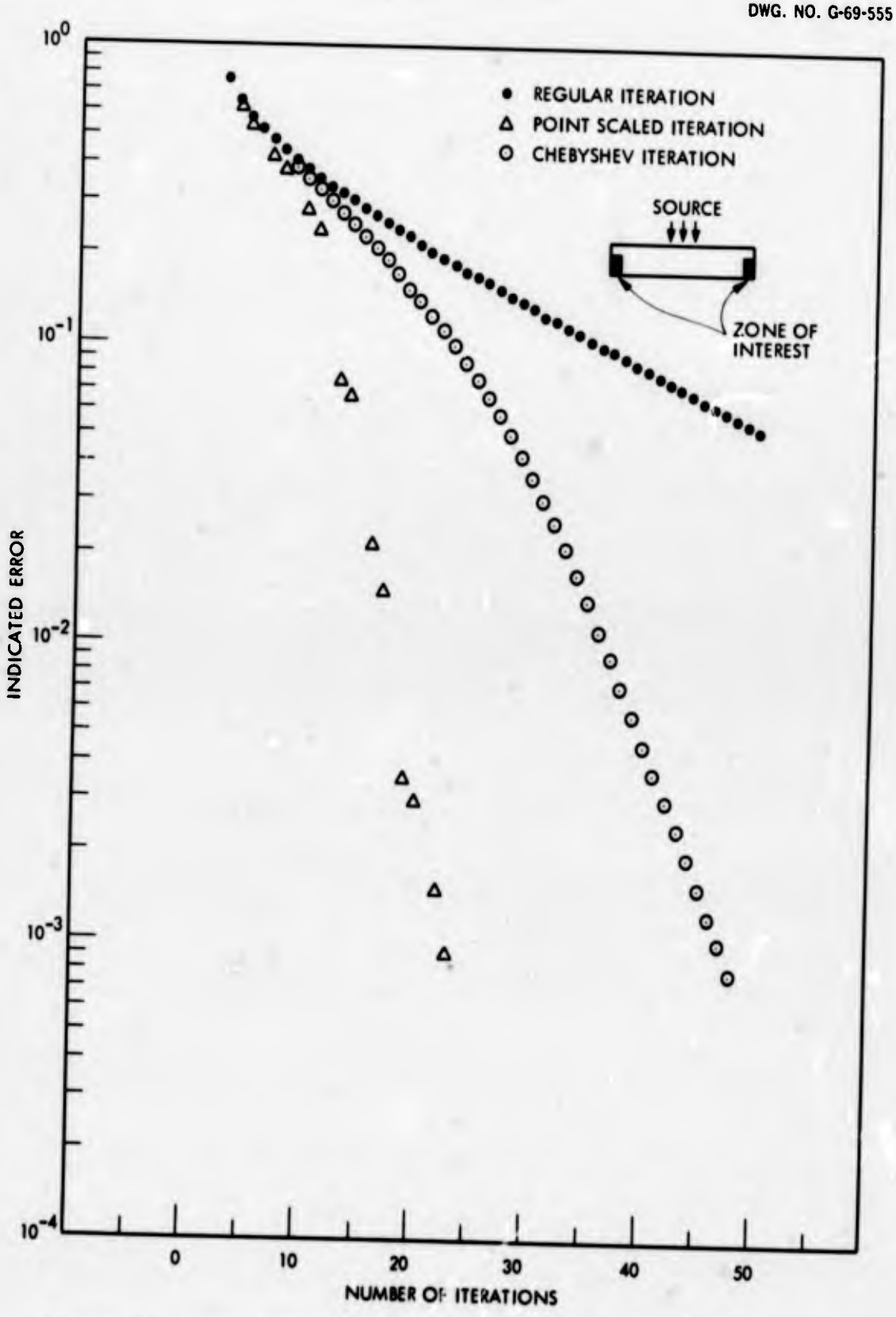

Figure 6. A comparison of three iteration methods for group 25 of the lead slab problem with the second zone of interest.

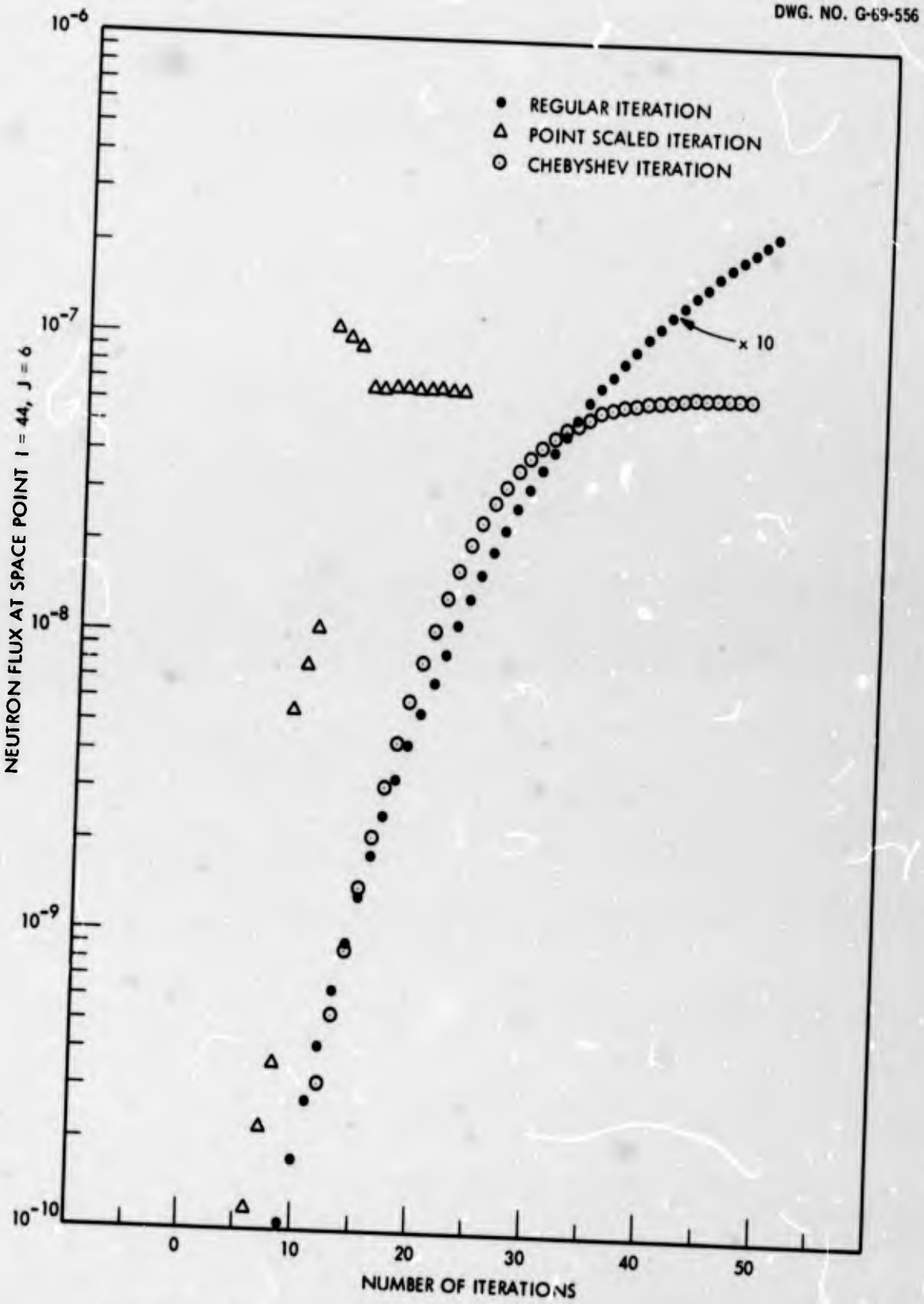

Figure 7. A comparison of the flux behavior at the space point, I=44, J=6, for group 25.

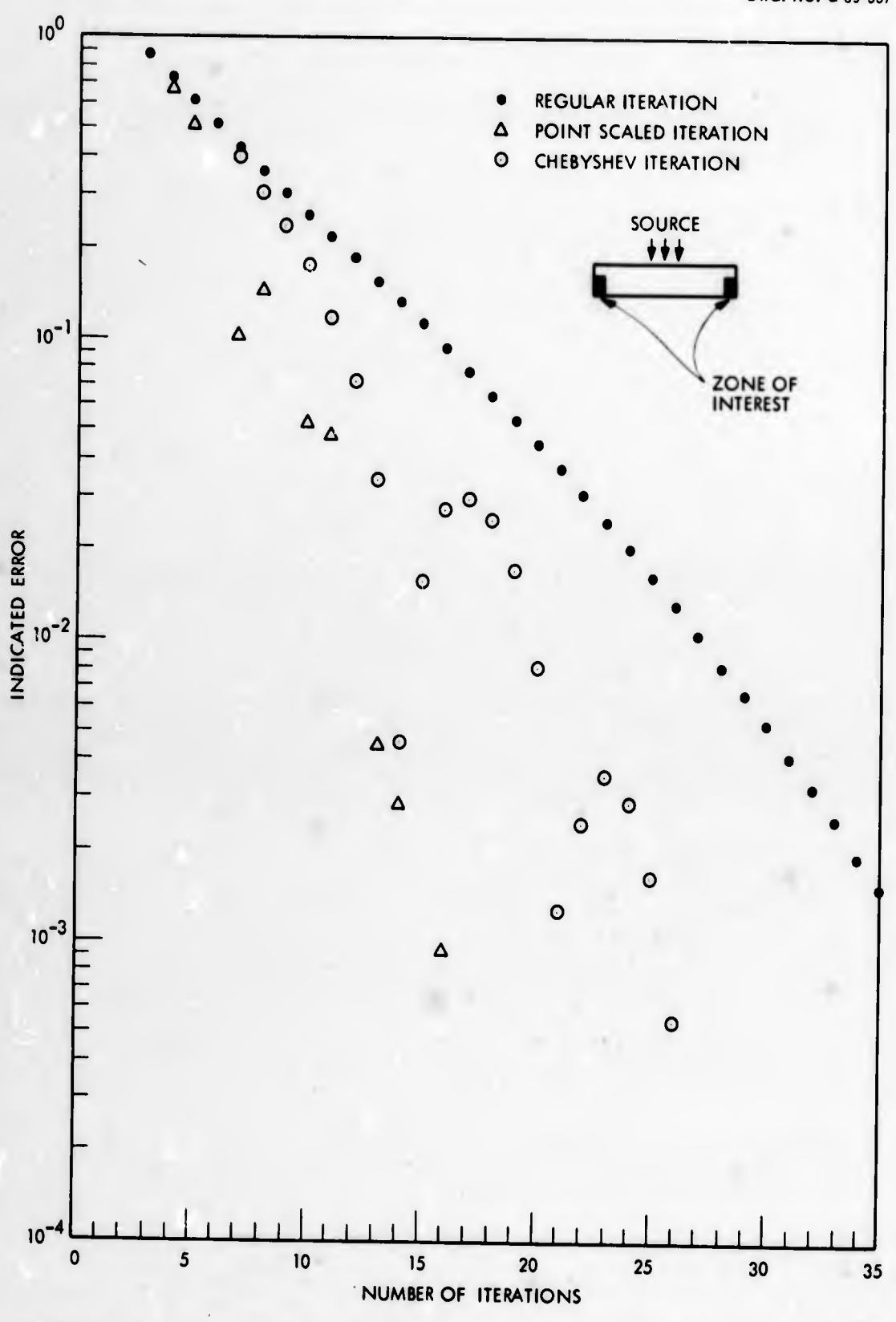

Figure 8. A comparison of three iteration methods for group 10 of the lead slab problem with the second zone of interest.

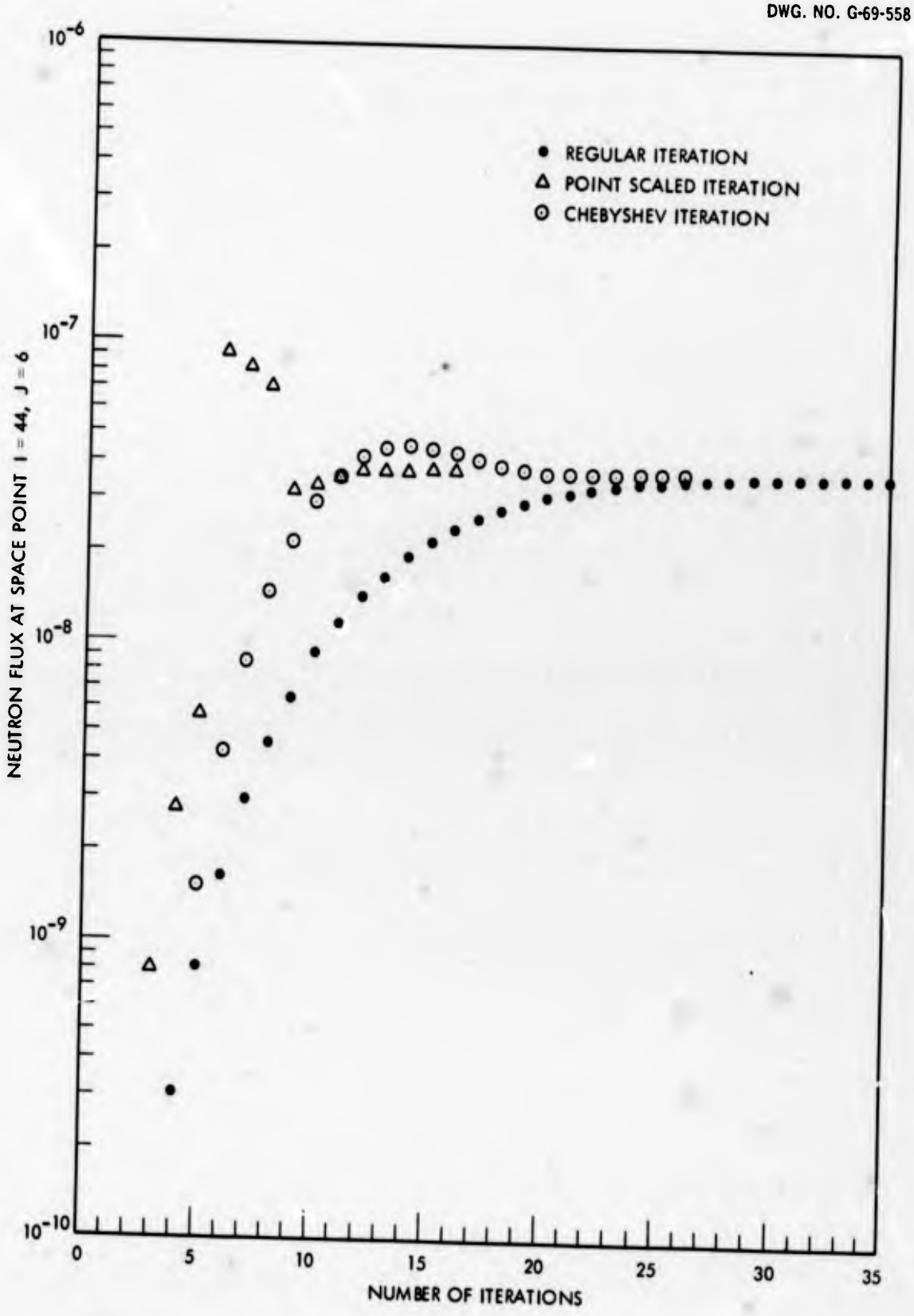

Figure 9. A comparison of the flux behavior at the space point, I=44, J=6, for group 10.

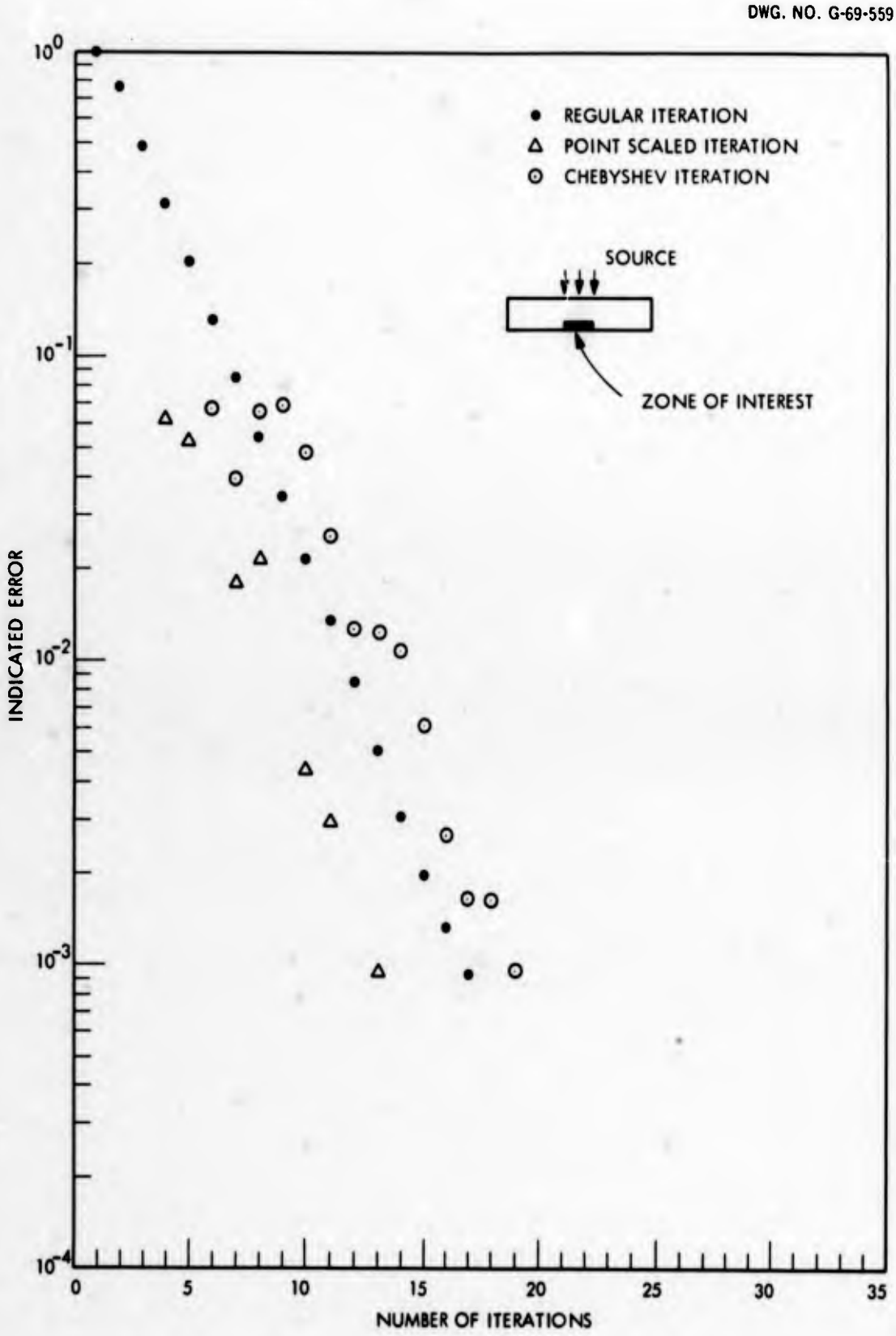

Figure 10. A comparison of three iteration methods for group 10 of the lead slab problem with the first zone of interest.

is the same as the latter, except for the zone of interest, this merely indicates that, while the Chebyshev method is considerably beneficial to the hard part of the problem, it is slightly detrimental to the easy part. The flux behavior shown in Figure 11 further illustrates this problem.

The results of this study on iterations are most important for the application of the two-dimensional discrete ordinates method to large penetration problems. The factor of ten advantage of the point-scaled method in difficult problems makes many problems which were previously intractable now feasible. The zone-of-interest convergence criteria makes it possible to have a good indication of the convergence in the important part of the geometry. These two methods together provide the transport code with the efficiency necessary in the calculation of large shielding problems.

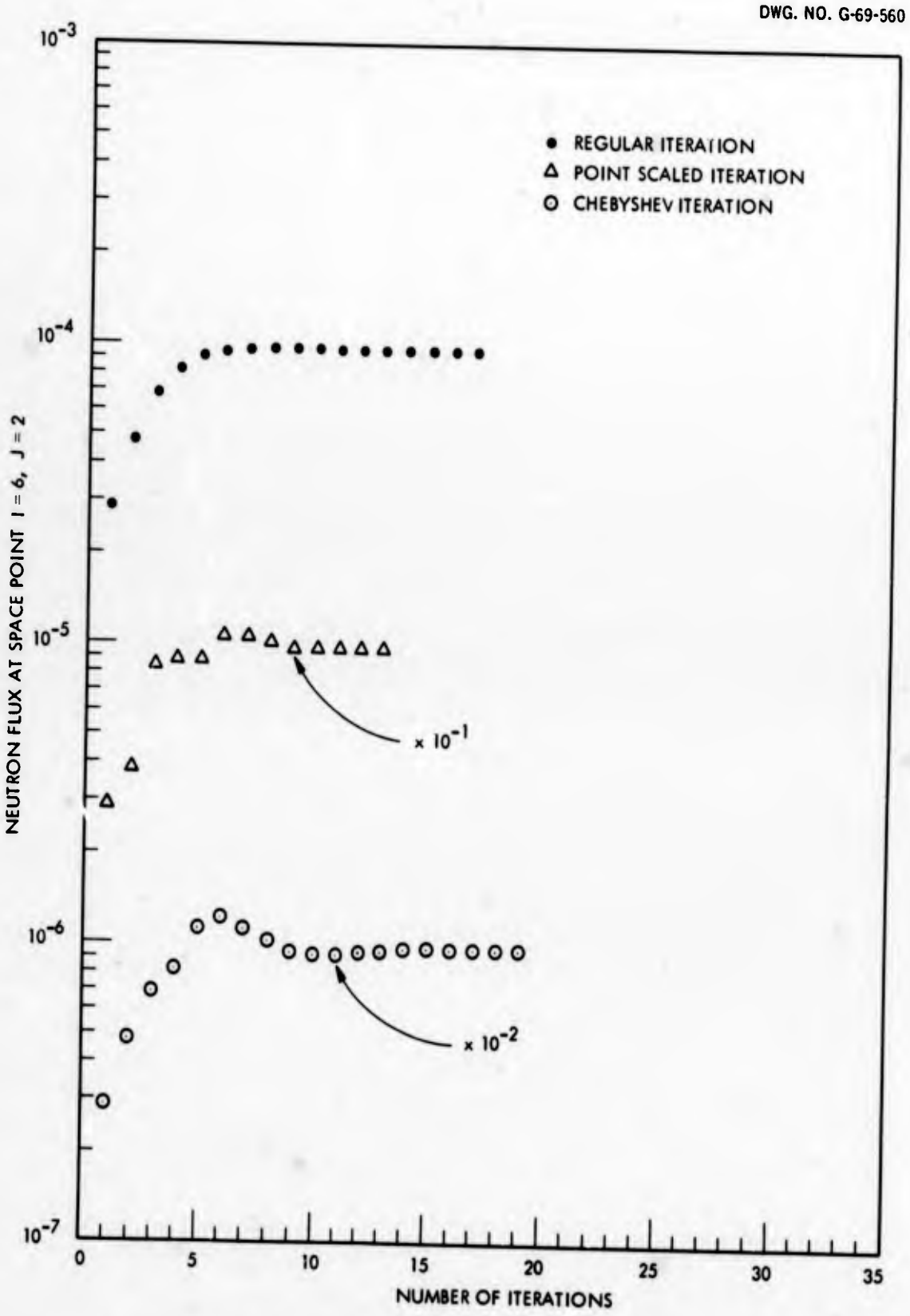

Figure 11. A comparison of the flux behavior at the space point, I=6, J=2, for group 10.

CHAPTER IV

ADDITIONAL IMPROVEMENTS

In the previous chapters a general method has been developed which is inherently capable of solving most two-dimensional neutron and gamma-ray transport problems, including deep penetration. The approximations are not limiting since, at least in principle, the number of energy groups, solid angle segments and space intervals, and the order of expansion of the differential scattering cross sections may be increased as necessary to obtain the desired solution. However, the problems which can be solved in practice are limited by the finite computer speed and memory size. In order to extend the capabilities, a combination of efficient programming and analytical "tricks" are used. The programming techniques involve methods for efficient and flexible allocation of the main computer memory, handling of large blocks of data on external storage devices, and the concentration of the innermost loops into a single, small subroutine which is programmed in machine language. These change as existing machines are modified or as new machines become available. The analytical techniques principally involve methods which take advantage of simplifications to certain problems. Three techniques, the analytic first collision source, biased quadrature sets, and the determination of the flux in an external void, are discussed in this chapter.

I. ANALYTIC FIRST COLLISION SOURCE

In two-dimensional r-z cylindrical geometry, the finite number of angles may result in an anomaly called the "ray effect." The problems in which ray effects are noticed are characterized by sources and detectors which are small compared to the total geometry, and a scattering mean free path which is long compared to the space mesh. Hence, if a problem such as a point source and point detector in a highly absorbing medium is approximated by the equations given in Chapter II, the fluxes along a spherical surface centered about the source are observed to rise and fall in a wave-like pattern instead of being constant. Furthermore, the peaks in the distribution are observed to fall along rays following the polar angles of the quadrature centered at the source.

In the discrete ordinates solution of the two-dimensional cylindrical transport equation, the angles in the quadrature are arranged in levels which comprise of directions having the same polar direction cosine, η. Within these levels particles change angles due to the curvature derivative [term 3, Equation (2.51)], as well as scattering [term 6, Equation (2.76)]. However, transfers from a direction in one η level to one in another level occur only through scattering. Particles that start out in an η level tend to stay in the same level until scattered. Since there are only a finite number of η levels, particles tend to appear only at space intervals which are oriented with the source along a discrete η level. If the source region is distributed or if scattering is

dominant, no ray effects appear; however, if the source is localized and spacial convection is dominant, ray effects may be significant.

An obvious way to mitigate ray effects would be to increase the number of η levels. However, this approach is uneconomical and usually only slightly effective. Another technique is to employ an analytic first collision source. This method essentially removes ray effects since the source is now distributed continuously in angle. For points within a mean free path or so of the source the analytic uncollided flux dominates. For intermediate points a few mean free paths from the source the flux is dominated by the source from first collisions which, although emitted into the discrete mesh, is distributed smoothly in space due to the analytic uncollided flux. For points many mean free paths from the source the flux is due to particles which have suffered many collisions, a situation in which ray effects would not normally appear.

Unfortunately, the technical problems involved in implementing the analytic first collision source in the general problem are prohibitive. For an arbitrary source distribution the contribution to each space point from each source interval must be calculated. Furthermore, the cylindrical symmetry in r-z geometry must be accounted for by an azimuthal integration for each source interval. For example, a problem with 3000 space points and only 10 azimuthal intervals would require up to 9×10^7 calculations to determine the uncollided flux. The point source on the cylindrical axis problem which produces the worst ray effects involves only 3000 calculations for the same problem. Problems which have a co-axial parallel beam

source may also be treated. Although these problems do not normally show severe ray effects, the source is usually input in the directions nearest the axis, which are usually 13° or more from the axis. This causes a slightly incorrect uncollided flux and also makes it difficult to determine the collided flux in the near axis angles.

An analytic first collision source technique has been developed for the two-dimensional code, DOT, for the simple sources described above. The procedure is described in the following:

1. The geometry is described with the same space mesh and material zones as for the DOT problem.
2. The uncollided flux (magnitude and angle) is calculated for each space point and energy group.
3. The first collision source, S, a function of radial interval, I, axial interval, J, angular moment, L, and group, G, is calculated with the expression,

$$S(I,J,L,G) = \sum_{G'=1}^{G} \Sigma^{\ell}(G'\rightarrow G)\phi_u(I,J,G')P_{\ell}^{m}(\mu)\sqrt{2} \times \left[\frac{(\ell-m)!}{(\ell+m)!}\right]^{1/2}\cos(m\psi) , \tag{4.1}$$

where $\Sigma^{\ell}(G'\rightarrow G)$ is the ℓ^{th} Legendre coefficient of the scattering cross section from group G' to G, ϕ_u is the magnitude of the uncollided flux, μ is the direction cosine of the flux, ϕ_u, with the radius vector, cos $(m\psi)$ is -1 for downward angles and +1 for upward angles, and L corresponds to a particular pair of indices ℓ and m.

4. The source array, S, and the scalar uncollided flux are written on magnetic tape.
5. DOT has been modified to use, as option, the anisotropic source array, S, as the fixed source. The result of such a calculation is the collided flux $\phi_c(I,J,G,D)$ where the arguments are as before except that D, for angle, is added. At the end of the calculation the scalar uncollided flux is added to the scalar collided flux such that the total flux is printed in the DOT output.

II. NEW QUADRATURE SETS

The effect of a given type and/or order of quadrature on the solutions obtained from the discrete ordinates method for practical problems is not well known. Several types of quadrature have been used and the changes or improvements have sometimes been made for obscure reasons. Much of the difficulty in understanding is due to the dual role which is played by the quadrature set. First of all, it acts like a classical quadrature in the calculation of the integral terms in Equation (2.96) and must be able to integrate Legendre polynomials; however, in the convection terms of Equation (2.96) the discrete directions define the mean values for the direction cosines such as $\bar{\mu}_D$ and $\bar{\eta}_D$, and the associated weights define the solid angle segments.

One method used to study the effect of quadrature is to pick a problem and vary the type and order of quadrature in such a manner as to increase accuracy and note the conditions at which selected

answers cease to vary rapidly. In other cases, particularly for comparisons with experiments measuring angular flux, the limiting factor is the angular resolution necessary for a meaningful comparison, or perhaps a high resolution is desired in order to determine the flux at points in the space beyond the calculated system. For these problems it is desirable to have a technique which will produce a tailored direction set which is also capable of integrating low order Legendre polynomials exactly and hence conserve balance.

The first quadrature method for two-dimensional discrete ordinates which was used with the TDC code (5) was based on equal solid angles. The direction set is symmetric by octant such that the description of the quadrature for a single octant determines the entire quadrature. For a specified n order of quadrature, the octant is first divided by n/2 latitude bands. Starting with the latitude nearest the z axis, the latitude bands are divided into 1, 2, 3, ..., n/2 longitudinal sections. The requirement of equal solid angles completely determines the latitudes and longitudes. The discrete angles associated with the solid angles are adjustable within the requirement that they lie within their respective solid angles. The determination of angles to match various moment conditions has been considered (23).

It was later observed that the quadratures formed by intersections of longitudes and latitudes were not rotationally symmetric (7). That is, the new quadrature which is formed by a rotational change of axes is different from the original. It was also observed that a problem in x-y geometry did not give the same answer when the axes were

interchanged. C. E. Lee developed a rather complex method based on areas formed by intersections of great circles which produced rotationally symmetric quadrature (7). His method has the advantage of always giving positive weights, but it lacks much, if not all, of the flexibility which is desired.

Carlson and Lathrop (8,24), in a study of the equivalence of certain moments equations and discrete ordinates equations, suggest that quadratures be developed on this basis. The requirement is simply that the quadrature be able to integrate polynomials in the direction cosines. For a two-dimensional quadrature this is

$$\sum_{k=1}^{K} \mu_k^{\ell} \eta_k^{m} \omega_k = \frac{2}{\pi} \int_0^{\pi/2} \int_0^{1} \mu^{\ell} \eta^{m} d\mu d\psi \ . \tag{4.2}$$

The integral on the right of Equation (4.2) is integrated analytically to give

$$\sum_{k=1}^{K} \mu_k^{\ell} \eta_k^{m} \omega_k = \frac{1}{2} \frac{\Gamma\left(\frac{\ell+1}{2}\right) \Gamma\left(\frac{m+1}{2}\right)}{\Gamma\left(\frac{1}{2}\right) \Gamma\left(\frac{\ell+m+3}{2}\right)} \ . \tag{4.3}$$

The author has developed a computer program which solves Equation (4.3). Given input values of μ_k and η_k, a sufficient number of moments, ℓ and m, are picked such that a solution for ω_k is possible.

It appears at first that this approach should provide all the flexibility desired. However, for arbitrary angles the solution of Equation (4.3) will as often as not give some negative weights. When completely symmetric angles are used positive weights are obtained up through S_{12} (84 angles with non-zero weight). When μ_k and η_k are

picked from the set of zeroes of a Legendre polynomial the resultant quadrature is half symmetric inasmuch as the third direction cosine, ξ_k, cannot be from the same set of numbers. For these quadratures positive weights are obtained up through S_{10}. This quadrature is interesting since the level weights for μ and η levels are found to be the Gaussian quadrature weights. Table II gives, for illustration, a comparison of collision probabilities calculated for infinite cylinders with several quadratures and by the analytic chord method (25).

Comparisons of quadratures made on the basis of simple analytic problems are only partially informative. The reason, of course, is that the applications of interest are for real problems which have, as yet, no analytic solutions. In fact, comparisons with analytic solutions can often lead to erroneous conclusions since these problems represent extreme cases. For real problems one is left with judgments made on qualitative comparisons of results of various quadratures.

As mentioned previously, there is a class of problems which requires a higher order of quadrature than is actually necessary for the transport. This is observed when the order of quadrature is increased and the spatial distributions of the angular moments of the flux do not change, yet the quadrature is not adequate for the angular resolution desired. In these problems additional directions may be added, so long as the basic integration abilities of the quadrature are not reduced. One technique which is employed in the experiment comparisons in Chapter VI in order to increase the resolution in the polar direction cosine, η, is to add segments of a higher order Gaussian quadrature to the basic quadrature. In this case, the basic

TABLE II

COLLISION PROBABILITIES FOR PURELY ABSORBING CYLINDERS

$\Sigma a \cdot R$	Quadrature	Calculated Answer	Analytic Answer	% Error
0.02	Lee's - S_8[a]	.02435	.02561	4.92
0.02	Level Moment - S_8[b]	.02468	.02561	3.64
0.02	Full Moment - S_8[c]	.02472	.02561	3.48
0.02	Full Moment - S_{10}[c]	.02484	.02561	3.00
0.02	Half Symmetric - S_8[d]	.02520	.02561	1.60
0.02	Half Symmetric - S_{10}[d]	.02539	.02561	0.86
0.02	Level Moment - S_{16}[b]	.02515	.02561	1.78
0.5	Lee's - S_8	.4019	.4041	0.54
0.5	Level Moment - S_8	.4038	.4041	0.07
0.5	Full Moment - S_8	.4038	.4041	0.07
0.5	Full Moment - S_{10}	.4039	.4041	0.05
0.5	Half Symmetric - S_8	.4050	.4041	0.22
0.5	Half Symmetric - S_{10}	.4052	.4041	0.27
0.5	Level Moment - S_{16}	.4042	.4041	0.04
1.0	Lee's - S_8	.5909	.5929	0.33
1.0	Level Moment - S_8	.5922	.5929	0.11
1.0	Full Moment - S_8	.5922	.5929	0.11
1.0	Full Moment - S_{10}	.5924	.5929	0.08
1.0	Half Symmetric - S_8	.5928	.5929	0.01
1.0	Half Symmetric - S_{10}	.5933	.5929	0.07
1.0	Level Moment - S_{16}	.5928	.5929	0.01

[a] See reference 7.

[b] See reference 8.

[c] From Equation (4.3) with symmetric directions from reference 7.

[d] From Equation (4.3) with μ and η determined by zeroes of a Legendre polynomial.

quadrature is an S_{10} Gaussian with a forward angle resolution of about 21°. The angular resolution desired is on the order of 1° which is characteristic of S_{96}. It was observed that the total solid angle represented by the first eleven levels of the S_{96} quadrature was nearly equal to that of the first level of the S_{10}. The eleven S_{96} weights and directions were then substituted for the first S_{10} weight and direction and the weights were renormalized to correct for the slight discrepancy introduced. The DOT code is constructed such that the quadrature need not be symmetric in η such that the additional directions may be added in the negative η directions and the regular set used for positive η directions. This quadrature will be discussed further in the description of the calculations in Chapter VI.

III. DETERMINATION OF THE FLUX IN AN EXTERNAL VOID

In many shielding situations the final answer desired is the spectrum or dose at some point or collection of points in the space outside the shield. For example, a space reactor power system is usually located at some distance from the point of the design dose. The shield analyst, after calculating the flux distribution within the reactor and shield, is then faced with the problem of calculating the dose at the design points at distances of 100 feet or more from the reactor.

A similar situation exists in the calculation of experimentally measured spectra transmitted through shielding materials. Even if the scintillation crystal is placed directly adjacent to the test

shield the void containing the detector must be included in the transport calculations because of the difference in areas viewed at forward or oblique angles. The detector is often located in heavily shielded housings and views the shield surface through a collimator at a reasonable distance from the shield because of the desire for low background and a well defined response surface with even intensity.

The problems described in the preceding paragraphs present some difficulty to users of the discrete ordinates methods. The large space up to and including the detector system cannot be reasonably included in the discrete ordinates solution since ray effects are most severe in particle transport through a void. If the point of interest is sufficiently far from the calculated system such that the distance from the surface is not significantly different from the distance from which the average particle scattered last, the following method is reasonable.

The angular flux at the surface is known as a result of the discrete ordinates solution. The number of particles emitted per unit steradian about the direction $\bar{\Omega}$, per unit time, from an element of surface area, dA_s, is given by the product,

$$\phi(\bar{r}_s,E,\bar{\Omega})\bar{\Omega} \cdot \bar{n}\, dA_s \ , \qquad (4.4)$$

where $\phi(\bar{r}_s,E,\bar{\Omega})$ is the angular flux at the position on the surface given by $\bar{r}_s$, $\bar{\Omega}$ is the unit direction vector, and $\bar{n}$ is the normal to the surface. If each element of surface area is represented as an anisotropic point source emitting $\phi(\bar{r}_s,E,\bar{\Omega})\bar{\Omega} \cdot \bar{n}\, dA_s$ particles per

steradian about the direction $\bar{\Omega}$, per unit time, then the flux at an arbitrary point in space, $\bar{r}_d$, is given by

$$\phi(\bar{r}_d,E) = \int_{SURFACE} \frac{\phi(\bar{r}_s,E,\bar{\Omega})\bar{\Omega} \cdot \bar{n}}{|\bar{r} - \bar{r}_s|^2} dA_s \, . \qquad (4.5)$$

For a two-dimensional r-z cylinder one has the flux at the flat end surface, $\phi(r,Z_s,E,\bar{\Omega})$, and the curved cylindrical surface, $\phi(R_s,z,E,\bar{\Omega})$. Of course, only one end surface can be viewed at a time so both are not represented. In order to perform a surface integration for a two-dimensional cylinder an azimuthal angle, α, must be introduced. The angle α is measured about the $\bar{Z}$ axis and from the plane containing the detector point, $\bar{r}_d$, and the $\bar{Z}$ axis. The flux at the detector is then given by

$$\phi(\bar{r}_d,E) = \int_0^H \int_0^{2\pi} \frac{\phi(R_s,z,E,\bar{\Omega})\bar{\Omega}\cdot\bar{R}}{\rho^2} R_s \, d\alpha dz + \int_0^R \int_0^{2\pi} \frac{\phi(r,Z_s,E,\bar{\Omega})\bar{\Omega}\cdot\bar{Z}}{\rho^2} r dr d\alpha \, , \qquad (4.6)$$

where ρ represents the distance from the surface points to the detector and the curved surface integration is restricted to $\bar{\Omega} \cdot \bar{R} \geq 0$.

In the DOT calculation the flux is given in terms of a finite space grid and finite solid angle segments with representative mean directions. The azimuthal integration is performed by summing over a grid of finite intervals. Figure 12 shows a pictorial representation of the grid and detector geometry. The numerical form of Equation (4.6) is

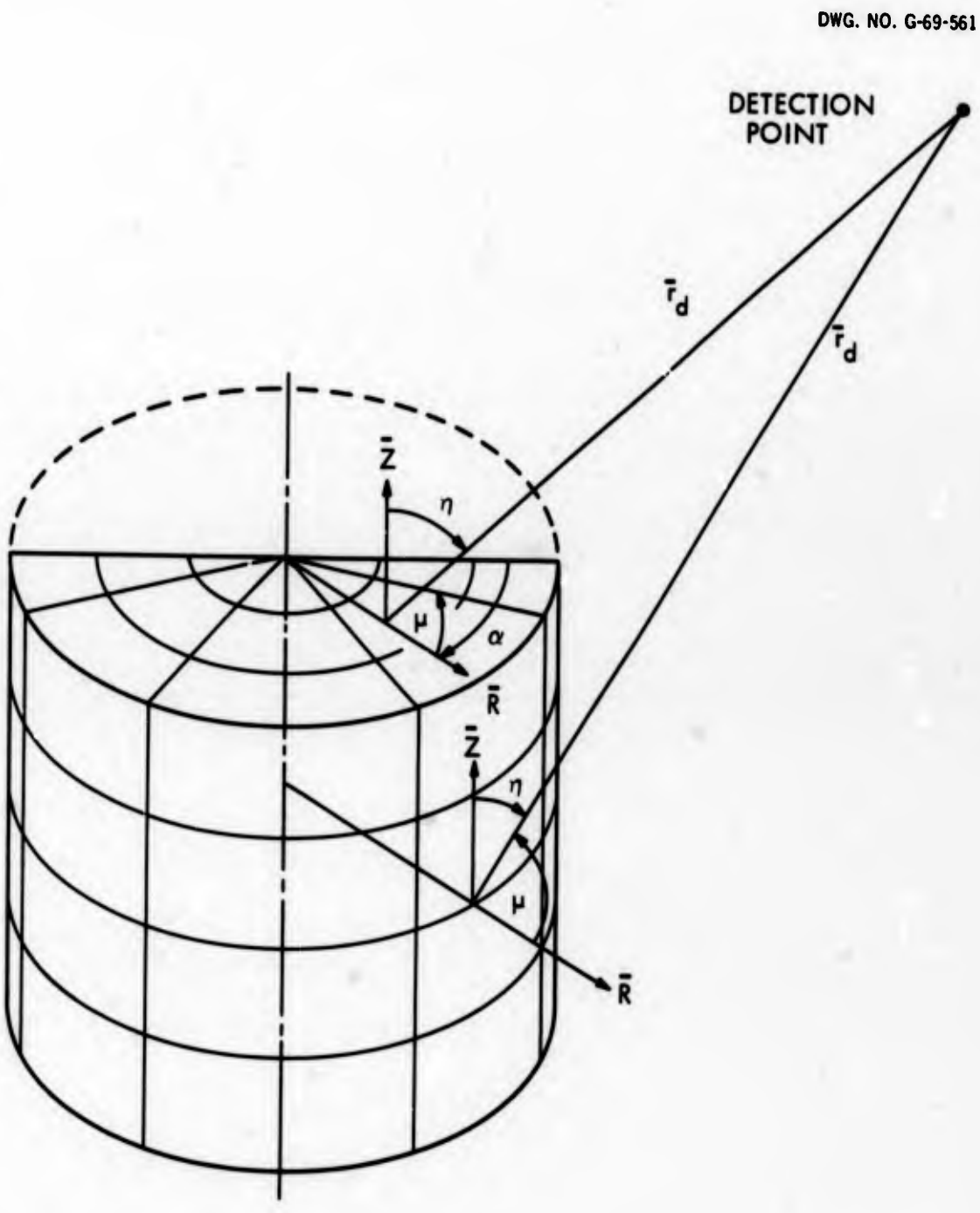

Figure 12. The surface mesh and detector geometry for SPACETRAN surface integration.

$$\phi_G(\bar{r}_d) = 2 \sum_{J=1}^{JM} \sum_{\ell=1}^{N\alpha} \frac{\phi_{I,J,G,D'} \mu_d}{4\pi \rho_d^2} R_s \Delta\alpha_\ell \Delta Z_J + 2 \sum_{I=1}^{IM} \sum_{\ell=1}^{N\alpha} \frac{\phi_{I,J,G,D'} |\eta_d|}{4\pi \rho_d^2} r_I \Delta r_I \Delta\alpha_\ell \ , \tag{4.7}$$

where $|\mu_d|$ and $|\eta_d|$ are the direction cosines with respect to the $\bar{R}$ axis and $\bar{Z}$ axis, respectively, and are determined geometrically for each surface integration point. The mean direction index, D', is chosen for each surface point by searching the quadrature direction for the one having the maximum dot product with the vector from the surface point to the detector.

For detector points which are very far from the calculated system, the polar angle, η, and distance, ρ, remain effectively constant during the α integration. In this case the α integration may be handled separately giving for the top

$$\phi_T(r,Z_s,E,\eta) = 2 \int_0^{\pi} \phi(\bar{\Omega}) d\alpha \ , \tag{4.8}$$

and, for the side,

$$\phi_s(R_s,z,E,\eta) = 2 \int_0^{\alpha max} \phi(\bar{\Omega}) d\alpha \ . \tag{4.9}$$

The flux at a point in space exposed to both the top and side is

$$\phi(E) = \int_0^H \frac{\phi_s(R_s,z,E,\eta)}{\rho^2} R_s dz + \int_0^R \frac{\phi_T(r,Z_s,E,\eta)}{\rho^2} r dr \ , \tag{4.10}$$

where η is the polar direction cosine from some representative surface point to the detector and is assumed constant during the integration. This simplification reduces the computational effort since most of the time required to integrate Equation (4.7) is spent determining the proper angle, $\bar{\Omega}_d$, for each surface interval and detector point. Instead of assuming that the flux for a given direction cosine, η, is equal to that for the nearest discrete η_i, one may easily use an interpolation based on a Legendre series expansion,

$$\phi(\eta) = \sum_{\ell=0}^{L} \frac{2\ell+1}{2} P_\ell(\eta) \sum_{i=1}^{I} P_\ell(\eta_i)\phi(\eta_i)\Delta\eta_i \ , \qquad (4.11)$$

where L is arbitrary and I is the number of discrete cosines.

Although the preceding methods work well when the detectors are relatively far from the systems, both fail for points close to the system. The points may be included in the discrete ordinates calculation by extending the space mesh into the void, or, if this is impractical, by a complex method employing a last flight importance function.

In order to establish a general understanding of the importance function as referred to here, the transport equation is written for the flux at a phase space point, (r,E,Ω), due to a unit source at (r_o,E_o,Ω_o),

$$\bar{\Omega}\cdot\nabla\phi(\bar{r},E,\bar{\Omega};\bar{r}_o,E_o,\bar{\Omega}_o) + \sigma_T(\bar{r},E)\phi(\bar{r},E,\bar{\Omega};\bar{r}_o,E_o,\bar{\Omega}_o) = \delta(\bar{r}-\bar{r}_o)$$

$$\times \delta(\bar{\Omega}\cdot\bar{\Omega}_o)\delta(E-E_o) + \chi(E)\int_0^\infty\int_0^{4\pi} dE'd\bar{\Omega}' \ \phi(\bar{r},E',\bar{\Omega}';\bar{r}_o,E_o,\bar{\Omega}_o)\nu\sigma_f(\bar{r},E')$$

$$+ \int_0^\infty \int_0^{4\pi} dE'd\bar{\Omega}' \ \phi(\bar{r},E,\bar{\Omega}';r_o,E_o,\bar{\Omega}_o')\sigma(E'\to E,\bar{\Omega}'\to\bar{\Omega}), \qquad (4.12)$$

and the equation for the adjoint flux at $(\bar{r},E,\bar{\Omega})$ due to a unit source at $(\bar{r}_1,E_1,\bar{\Omega}_1)$,

$$\begin{aligned} &-\bar{\Omega}\cdot\nabla\phi^+(\bar{r},E,\bar{\Omega};\bar{r}_1,E_1,\bar{\Omega}_1) + \sigma_T(\bar{r},E)\ \phi(\bar{r},E,\bar{\Omega};\bar{r}_1,E_1,\bar{\Omega}_1) \\ &= \delta(\bar{r}-\bar{r}_1)\ \delta_2(\bar{\Omega}\cdot\bar{\Omega}_1)\ \delta(E-E_1) + \nu\sigma_f(E) \int_0^\infty \int_0^{4\pi} dE'd\Omega' \\ &\times \phi^+(\bar{r},E',\bar{\Omega}';\bar{r}_1,E_1,\bar{\Omega}_1)\chi(E') + \int_0^\infty \int_0^{4\pi} dE'd\bar{\Omega}' \ \phi^+(\bar{r},E',\bar{\Omega}'; \\ &r_1,E_1,\bar{\Omega}_1)\sigma(E\to E',\bar{\Omega}\to\bar{\Omega}'). \end{aligned} \qquad (4.13)$$

Equation (4.12) is multiplied by ϕ^+ and Equation (4.13) by ϕ. The resulting equations are subtracted and integrated over the system volume. It is noted that

$$\int_V (\phi^+\bar{\Omega}\cdot\nabla\phi + \phi\bar{\Omega}\cdot\nabla\phi^+)dv = \int_V \bar{\Omega}\cdot\nabla\phi\phi^+dv = \int_S \bar{n}\cdot\bar{\Omega}\phi\phi^+ds = 0 \qquad (4.14)$$

since $\phi(r_s,E,\bar{\Omega}) = 0$ for $\bar{\Omega}\cdot\bar{n} < 0$

and $\phi^+(r_s,E,\bar{\Omega}) = 0$ for $\bar{\Omega}\cdot\bar{n} > 0$.

The resulting equation is

$$\begin{aligned} &\int_0^\infty \int_0^{4\pi} \int_V dvd\bar{\Omega}dE \ \phi^+(\bar{r},E,\bar{\Omega};\bar{r}_1,E_1,\bar{\Omega}_1)\delta(\bar{r}-\bar{r}_o)\delta_2(\bar{\Omega}\cdot\Omega_o)\delta(E-E_o) \\ &= \int_0^\infty \int_0^{4\pi} \int_V dvd\bar{\Omega}dE \ \phi(\bar{r},E,\bar{\Omega};\bar{r}_o,E_o,\bar{\Omega}_o)\delta(\bar{r}-\bar{r}_1)\delta_2(\bar{\Omega}\cdot\Omega_1)\delta(E-E_1) \end{aligned}$$

$$- \int_V \int_0^\infty \int_0^{4\pi} \int_0^\infty \int_0^{4\pi} d\bar{\Omega}' dE' d\bar{\Omega} dE dv [\phi^+(\bar{r},E,\bar{\Omega};\bar{r}_1,E_1,\bar{\Omega}_1)\chi(E)$$

$$\times \phi(\bar{r},E',\bar{\Omega}';\bar{r}_o,E_o,\bar{\Omega}_o)\nu\sigma_f(E') - \phi(\bar{r},E,\bar{\Omega};\bar{r}_o,E_o,\bar{\Omega}_o)\nu\sigma_f(E)$$

$$\times \phi^+(\bar{r},E',\bar{\Omega}';\bar{r}_1,E_1,\bar{\Omega}_1)\chi(E')] - \int_V \int_0^\infty \int_0^{4\pi} \int_0^\infty \int_0^{4\pi} d\bar{\Omega}' dE' d\bar{\Omega} dE dv \qquad (4.15)$$

$$\times [\phi^+(\bar{r},E,\bar{\Omega};\bar{r}_1,E_1,\bar{\Omega}_1)\sigma(E'\to E,\Omega'\to\Omega)\phi(\bar{r},E',\bar{\Omega}';r_o E_o,\Omega_o)$$

$$- \phi(\bar{r},E,\bar{\Omega};\bar{r}_o,E_o,\bar{\Omega}_o)\sigma(E\to E',\Omega\to\Omega')\phi^+(\bar{r},E',\bar{\Omega}';\bar{r}_1,E_1,\Omega_1)] \ .$$

The last two integrals in Equation (4.15) are zero and the result is

$$\phi(\bar{r}_1,E_1,\bar{\Omega}_1;\bar{r}_o E_o,\bar{\Omega}_o) = \phi^+(\bar{r}_o,E_o,\bar{\Omega}_o;\bar{r}_1,E_1,\bar{\Omega}_1) \ . \qquad (4.16)$$

The terms in Equation (4.16) may be interpreted physically in the following manner:

$$\phi(\bar{r}_1,E_1,\bar{\Omega}_1;\bar{r}_o,E_o,\bar{\Omega}_o)dP_1 = \begin{array}{l} \text{flux at } \bar{r}_1,E_1,\bar{\Omega}_1 \text{ due to a} \\ \text{unit source at } \bar{r}_o,E_o,\bar{\Omega}_o \ = \\ \text{probability that a neutron emitted} \\ \text{at } \bar{r}_o,E_o,\bar{\Omega}_o \text{ will contribute to the} \\ \text{flux at } \bar{r}_1,E_1,\bar{\Omega}_1 \ , \end{array}$$

hence,

$$\phi^+(\bar{r}_o,E_o,\bar{\Omega}_o;\bar{r}_1,E_1,\bar{\Omega}_1)dP_1 = \begin{array}{l} \text{probability that a neutron emitted} \\ \text{at } \bar{r}_o,E_o,\bar{\Omega}_o \text{ will contribute to the} \\ \text{flux at } \bar{r}_1,E_1,\bar{\Omega}_1 \ . \end{array} \qquad (4.17)$$

Using the general reciprocity equation, (4.16), a transport problem may be solved using either the forward or adjoint formulations of the transport equation. For example, the dose at a given point may

be determined by calculating the flux due to the specified source and then integrating the product of the flux and dose response at the point. The same answer is determined by calculating the adjoint flux due to a "source" which is the dose response function at the point in question, and then integrating the product of the adjoint flux and the true particle source over all space.

A special case of the adjoint formulation is used for the problem of determining the flux at a specific point in the space outside a system which has been calculated with discrete ordinates. The uncollided adjoint flux, $\phi_u^+(\bar{r}_o,E_o,\bar{\Omega}_o;\bar{r}_1,E_1,\bar{\Omega}_1)$ is the probability that a particle emitted at $\bar{r}_o,E_o,\bar{\Omega}_o$ will contribute to the flux at $\bar{r}_1,E_1,\bar{\Omega}_1$ without suffering a further collision. The spectrum at a point $\bar{r}_1$ in space is then obtained by calculating the uncollided adjoint flux in each group due to a unit isotropic source at $\bar{r}_1$ and then integrating the product of the total source distribution (including scattering) and the adjoint uncollided flux over the entire system,

$$\phi(\bar{r}_1,E) = \int_V \phi_u^+(\bar{r},E,\bar{\Omega};\bar{r}_1)S(\bar{r},E,\bar{\Omega})dv \qquad (4.18)$$

The uncollided adjoint flux may be calculated analytically for simple problems by the same program which calculates the analytic first collision source. For more complex problems the uncollided adjoint flux can be calculated with the discrete ordinates code, starting with the adjoint flux on the surface as boundary condition. Although this is the most accurate method for calculating the spectrum at

points beyond the calculated system, the methods described previously are usually sufficient.

CHAPTER V

THE SLAB EXPERIMENT

The development of a major transport code such as DOT is an interesting and perhaps enjoyable task. However, when a working version of the code is finished one is faced with the problems of determining if the code is accurate, both in method and in programming, and evaluating the sensitivity of the solution to the choices made in the various free parameters. For a code based on a simple method with few options this procedure may be relatively easy. However, for a complex transport code, the process of exploring its accuracy and usefulness may require considerably more effort than the original development. In this study the problem is further complicated since the anisotropic two-dimensional discrete ordinates method in principle can be applied to any neutron and gamma-ray transport problem in two dimensions and is perhaps more powerful than any other two-dimensional method for deep penetration problems.

After the DOT code was first made operable the usual test problems traditional to discrete ordinates codes were calculated to check basic operations. These test problems comprise criticality calculations for highly enriched systems and, at best, only test those features found in the older codes. As a first test of the extended capabilities of DOT, calculations of fast neutron transport in water in the ORNL Lid Tank geometry were performed. This system consisted of a semi-infinite body of water adjacent to

a 71.2-cm.-diameter circular fission source plate and, through geometric transformations, can be calculated in one-dimensional plane and spherical geometry (26), as well as two-dimensional cylindrical geometry. The one-dimensional fast neutron dose in the Lid Tank was calculated with the ANISN code using spherical geometry with a point fission source and plane geometry with a plane, isotropic, fission source (26). The dose distributions in these calculations were then transformed to the actual geometry. This approach assumes that the fission rate is constant over the source and that no neutrons enter the tank after scattering behind the source plate. The final results of the one-dimensional comparisons are shown in Figure 13. A comparison with moments method and Monte Carlo calculations had been reported by Trubey (27).

In the two-dimensional DOT calculation the Lid Tank was represented by a cylinder of water 171.12 cm. in diameter and 150 cm. long and the source plate by a boundary condition on the inward-directed surface angular fluxes. For convenience the source was assumed constant over the plate, a fission spectrum was used, and the neutrons entering the system due to scattering behind the source plate were omitted. The cross sections were from GAM-II (17) using 27 energy groups and a P_2 expansion of the angle dependence of the scattering cross sections. The fast neutron dose distribution was calculated from the fluxes using Henderson single collision dose factors (28).

Although off-centerline dose measurements were made at the Lid Tank Facility (29), these data were never published and are considered more questionable than the centerline data. In order to have a basis

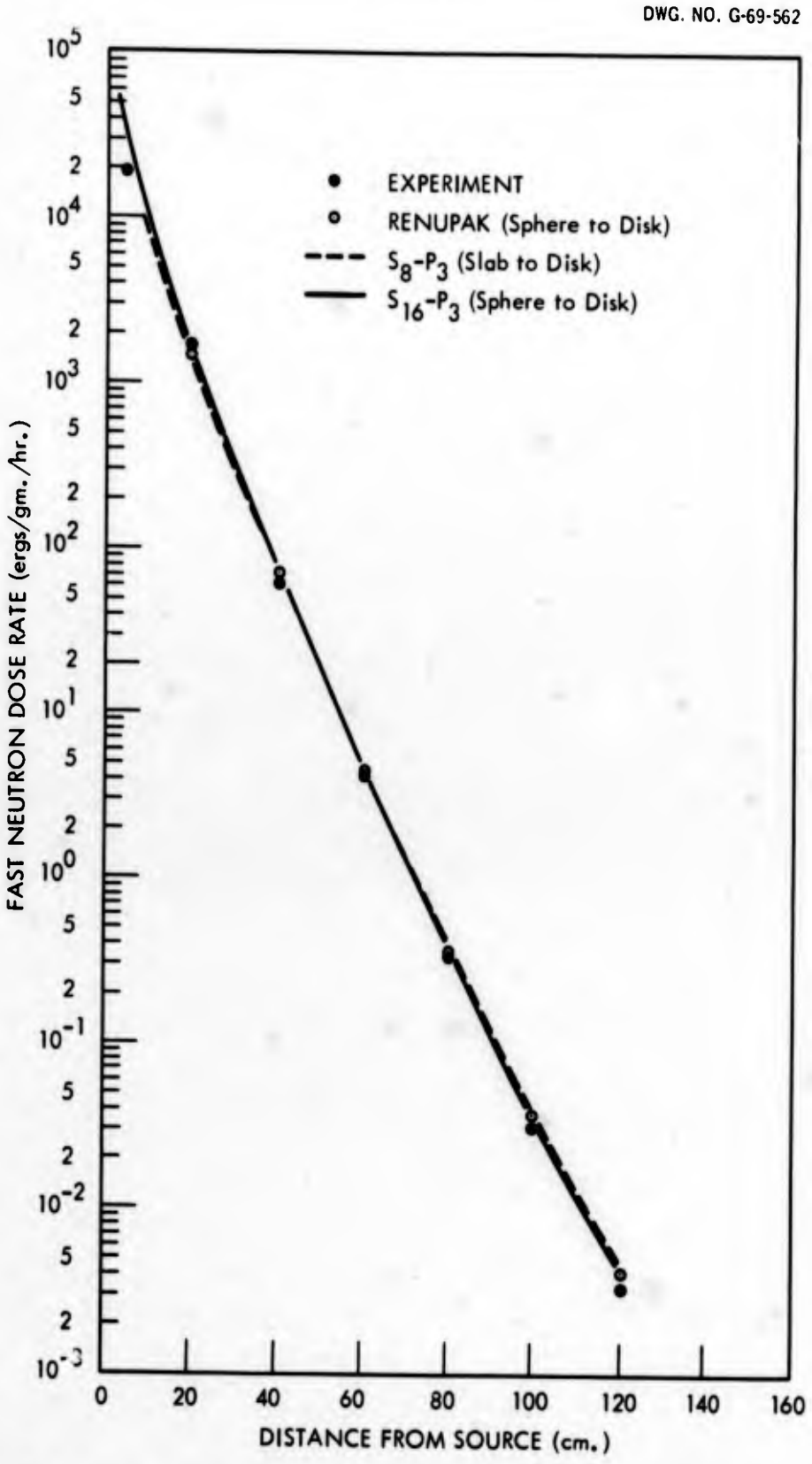

Figure 13. Comparison of calculations and measurements of fast neutron dose in the ORNL Lid Tank.

of comparison for the two-dimensional calculation, the off-centerline dose is calculated by the kernel equation,

$$D(R,Z) = S \int_0^{2\pi} \int_0^{R} G(\rho) r dr d\alpha \ , \qquad (5.1)$$

where ρ = distance from (r,α) to (R,Z),

and $G(\rho)$ is the dose at a distance ρ from a point fission source. The dose kernel $G(\rho)$ is taken from the ANISN calculation of the point fission source in water. The comparison should be exact except for error in the numerical integration of Equation (5.1) and errors in the two-dimensional calculation. Comparison with experiment is inferred by the previous comparison of the ANISN kernel with the centerline dose as shown in Figure 13.

The comparison of the results of the DOT calculation and the kernel integration is shown in Figure 14. The agreement for the most part is very good with discrepancies of less than 5% except for some points with Z's of 5 and 11 cm., and R's greater than 50 cm. These points view the source far to the side at very wide angles, giving rise to very steep flux gradients such that it is not surprising that the calculation would have difficulty with them.

The agreement in this comparison indicates that the code contains no basic errors, and that the treatment of the general anisotropic inscatter integral is probably correct. The calculation is, after all, a relatively difficult penetration problem involving an overall dose attenuation of 10^{-8}. Such a comparison, however, is not entirely satisfying. First, the comparison with experiment is

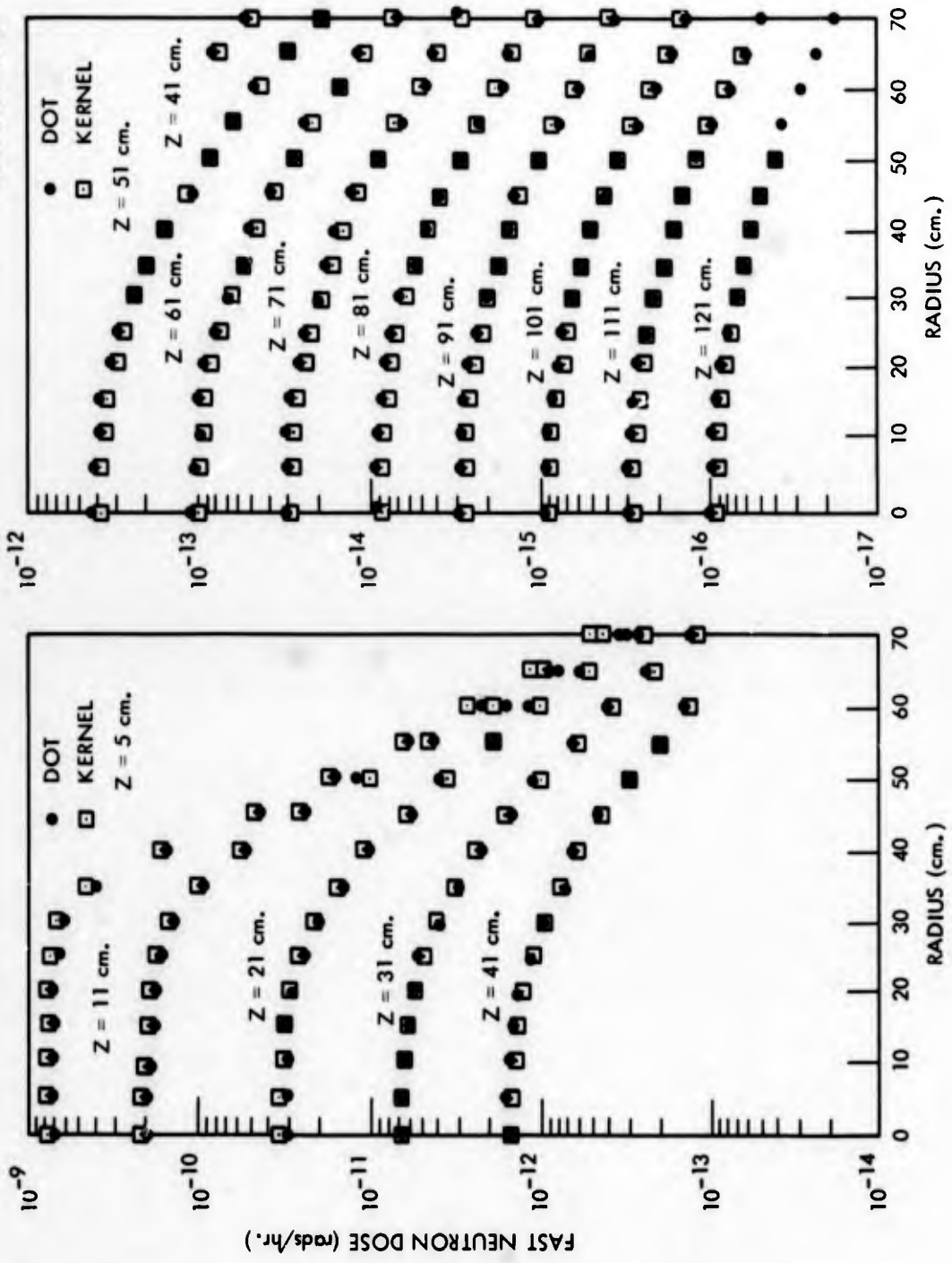

Figure 14. Calculated two-dimensional dose profiles in the ORNL Lid Tank.

indirect and not thorough by any means. Dose comparisons also do not reveal errors in the spectrum or the angular distribution of the flux. Furthermore, as will be discussed in greater detail later, the instrument dose response is not known well enough to permit accurate comparisons of dose in a soft spectrum.

I. THE DESIGN OF THE TSF SLAB EXPERIMENT

In order to gain insight into the effects of cross-section representation, quadrature, space mesh, source representation, and an overall check on the capability of the method, an experiment providing accurate measurements of the angle-dependent fast neutron spectra emerging from optically thick shield materials is desired. Such an experiment was constructed using equipment and instrumentation which were available at the Oak Ridge National Laboratory Tower Shielding Facility. The foremost objective of the experiment was to significantly extend the available data which forms the basis for evaluation of radiation transport calculation methods. The best of these methods, such as Monte Carlo and discrete ordinates, may be intercompared in considerable detail. However, such comparisons suffer from a lack of reality and, of course, give no indication of the applicability of the cross-section data. On the other hand, a good experiment will give an indication of the true answer and will provide a basis of comparison for other calculations.

The shielding experiments performed in the past are generally not usable for such comparisons. In most cases the experiments were designed to provide data for engineering designs and as such the

geometries were too complex for clean comparisons. In virtually all cases quantities such as tissue equivalent dose were measured. These integral quantities do not provide sufficient detail for evaluation of the calculations, and the dose response functions are not well known. Also, in most experiments the exact source intensity, space, and angle-dependent spectra were not measured. For a rigorous comparison of experiment and calculations, the source must be well known.

A drawing of the TSF slab experiment configuration is shown in Figure 15. The TSR-II reactor (30) is a spherical assembly containing spherical highly-enriched plate-type fuel elements and is cooled and moderated by water. The reactor is surrounded by a two-zone, spherical, permanent shield. The first zone is approximately 25 inches thick and is composed of 50% by volume lead shot and 50% water. The second zone is 23 inches thick and is composed of water. The reactor and shield assembly were placed in a concrete blockhouse which is 32 inches thick at the forward wall and 16 inches thick on the sides.

The source beam was extracted with a collimator extending from the reactor primary containment vessel through the shields and blockhouse forward wall. The collimator design is the result of Monte Carlo calculations by E. A. Straker (31) and features convergent entrance and divergent exit sections which serve to reduce collimator scattering effects. The collimator was formed by four water-filled aluminum tanks and has a cylindrical throat with an inside diameter of 4.25 inches.

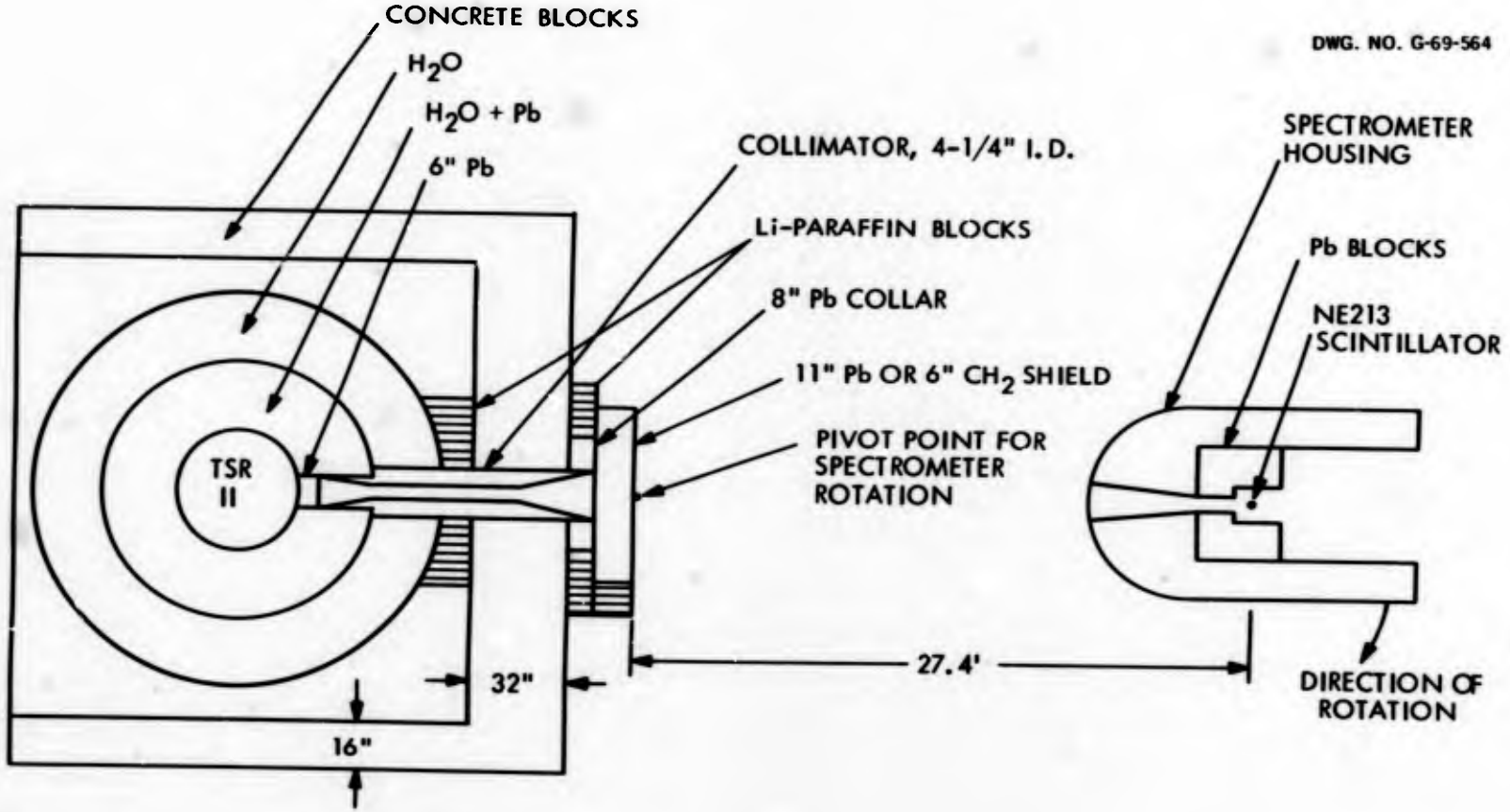

Figure 15. Configuration of slab experiment at the ORNL Tower Shielding Facility.

The shield slab materials consisted of lead, polyethylene, and depleted uranium. The individual slabs were usually about one inch thick and were square nominally five feet wide. These slabs were placed on a steel support frame, perpendicular to the beam, and flush with the exit of the collimator. An eight-inch-thick lead collar was positioned between the slabs and the blockhouse wall so that media behind the slab could be included in the calculation. A six-inch-thick lead insert covered the entrance of the collimator to reduce the gamma-ray intensity. Lithium-impregnated paraffin blocks were stacked between the reactor housing and the inner blockhouse wall and behind and around the shield slabs to prevent neutron streaming around the slabs.

The spectrometer housing consisted of an aluminum tank filled with borated water. A NE-213 liquid organic scintillator (32) was located on the centerline of the housing. The collimator in the spectrometer housing was tapered such that the entire surface of the scintillator was uniformly illuminated by the entire surface of the shield slabs. The spectrometer housing was supported by wheels and was attached by a tongue to a pivot point directly in front of the slabs. The spectrometer could rotate about the pivot point and remain oriented such that the collimator was directed at the center of the slab.

II. INSTRUMENTATION

The instrumentation used in the slab experiment was chosen from that available at the Tower Shielding Facility. The techniques used

for measurement of neutron dose and spectra are actually composed of both hardware, software (such as computer programs), and methodogy based on experience. These same measurement techniques have been used in other experiments and the experience gained has resulted in a completely dependable system of instrumentation.

The principal measurement technique required in the slab experiment was fast neutron spectrometry using the spectrometer system developed by W. R. Burrus, V. V. Verbinski, R. M. Freestone, and the staff at the Tower Shielding Facility (33). A schematic diagram of this system is shown in Figure 16. The 4.60-cm.-diameter by 4.65-cm.-long cylindrical NE-213 liquid organic proton recoil scintillator was used as a compromise between sensitivity and resolution and because of its relatively isotropic response. A 14-dynode photomultiplier tube is coupled to the scintillator by means of a 0.63-cm.-thick lucite light pipe. The signal is removed at the eleventh dynode, amplified by linear preamplifier and amplifier and routed to a 400-channel multichannel analyzer. A modified Forte pulse-shape discriminator circuit takes the signals from the fourteenth dynode and anode and produces a small positive or large negative pulse if the signal is due to a gamma ray and a large positive pulse if the signal is due to a neutron pulse. These pulses determine trigger and routing signals which are sent to the multichannel analyzer and result in the linear signal from the eleventh dynode being stored and identified as a gamma-ray pulse or neutron pulse.

The neutron pulse-height distribution is input into the computer code, FERDOR, which unfolds the neutron spectrum giving, as a function

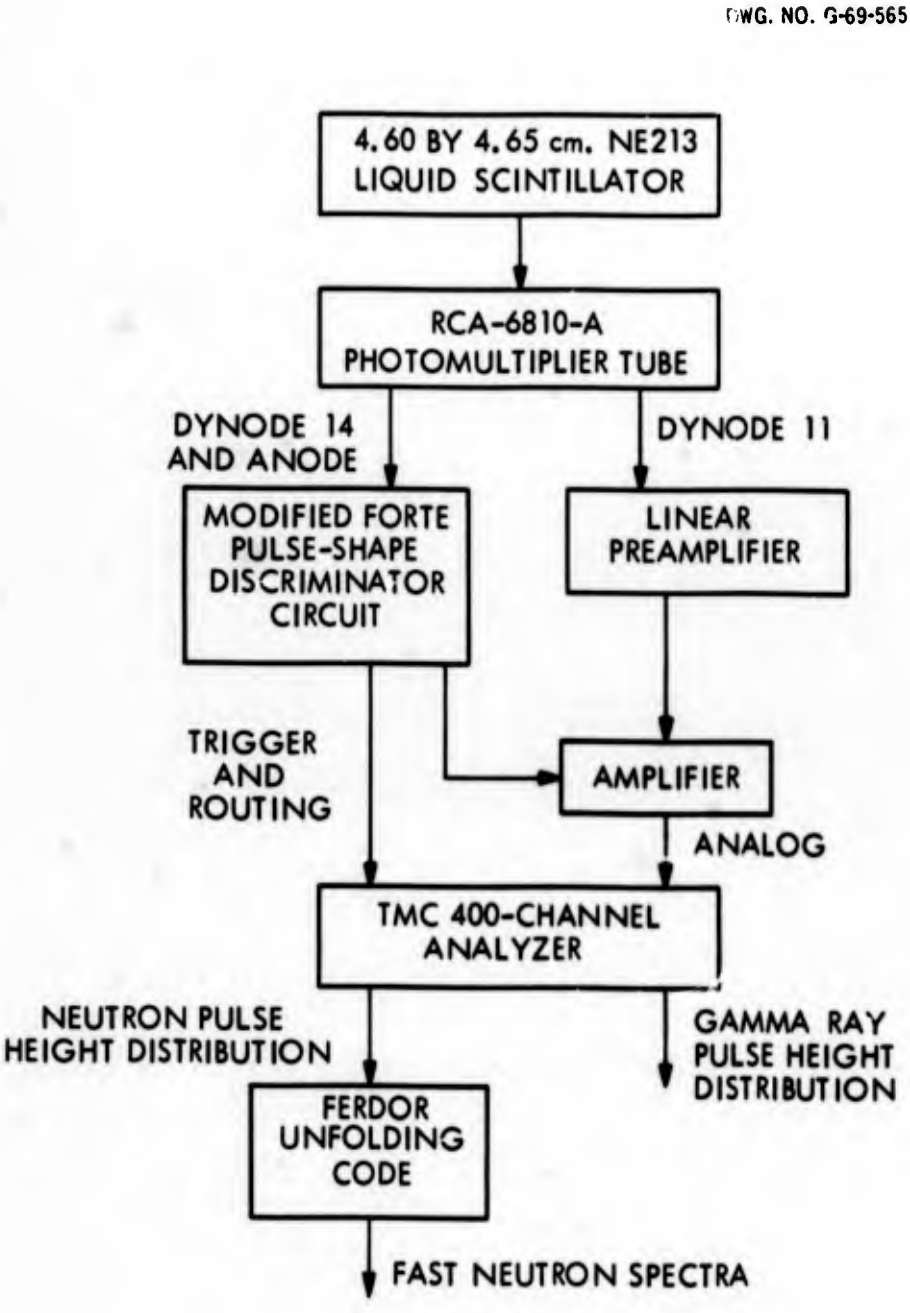

Figure 16. A schematic diagram of the neutron spectrometer system.

of energy, the upper and lower probable count rate which would be given by an ideal Gaussian response spectrometer. The probable error which is indicated represents counting statistics, errors in the numerical unfolding procedure, and errors in the response functions used in the unfolding. The complete spectrometer system has been extensively verified and used in several experiments such as the measurement of uncollided spectra transmitted by extremely thick samples (34).

Two fast neutron dosimeters were used for certain special measurements during the experiment. A diagram of the dosimeter instrumentation and logic is shown in Figure 17. The Hurst dosimeter (35) is a proton recoil device having a polyethylene-lined chamber filled with a hydrocarbon gas and is operated as a proportional counter. The Hornyak button (36) is a scintillator formed by zinc sulfide crystals dispersed in lucite plastic. The emitted light is detected by a photomultiplier tube, and the signals from the two detectors are similarly amplified. The output pulses from the amplifier are processed by an electronic integrating circuit, a pulse height selector circuit, PHS, and a multichannel analyzer.

The electronic integrating circuit converts the pulse height to a relative time constant. An electronic gate is opened such that a four-megacycle oscillator is operated for a time equivalent to the relative time constant. The total number of oscillations per second for a given counting period is assumed proportional to the neutron dose rate.

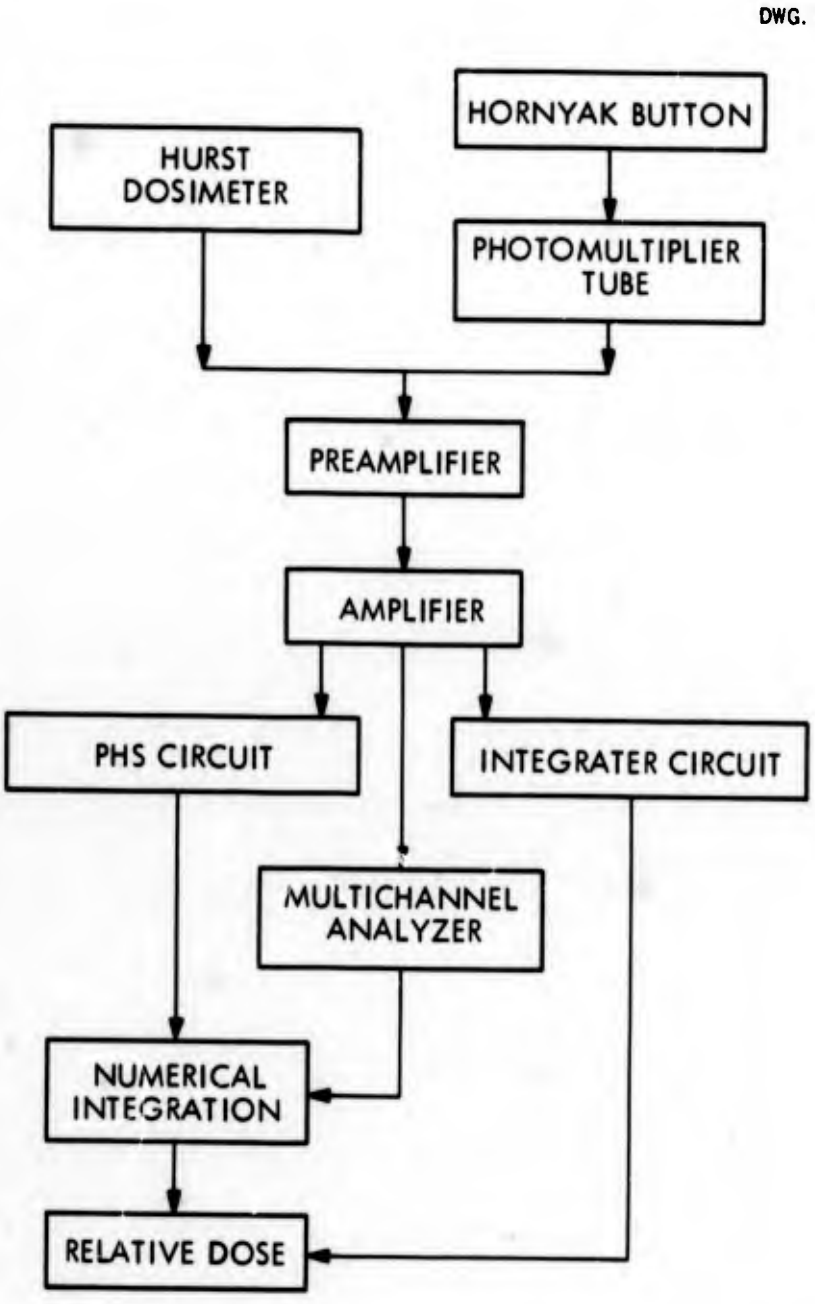

Figure 17. A schematic diagram of the fast neutron dosimeter system.

In the pulse height selector circuit the total number of pulses above a particular height are counted, and this is assumed to be proportional to the dose. For calibration and instrument checking the PHS reading is taken for several voltage settings and the curve formed by the collection of points is integrated numerically to give an approximation to the total energy being detected. The nominal PHS readings give a good approximation of the dose only when the neutron spectrum is the same as that used for the calibration.

The multichannel analyzer stores the count for an individual pulse into a channel corresponding to the energy of the pulse. The data in the analyzer is summed in either of two equivalent ways to get the total energy. The first method is to sum the product of the counts per channel and the channel,

$$E = \sum_{n=1}^{256} nc(n) , \tag{5.1}$$

where it is assumed that the channel number is proportional to the energy. The second method is to sum for each channel the counts in and above that channel,

$$K(m) = \sum_{n=m}^{256} c(n) , \tag{5.2}$$

and then numerically integrate the curve given by K(m). Although Simpson's rule integration is normally used, one may note that trapezoidal integration of K(m) is equivalent to Equation (5.1);

$$\sum_{m=1}^{256} \sum_{n=m}^{256} c(n) = \sum_{\ell=1}^{256} \ell c(\ell) \ . \qquad (5.3)$$

The function K(m) is similar to a PHS curve with many thresholds. The dose rate for a given run is given by the total energy divided by the counting time,

$$D \propto \frac{E}{T} \ . \qquad (5.4)$$

The dosimeter system is calibrated with a known Po-Be source which gives a specified dose at a fixed distance. All three techniques given above will thus give the same dose readings for neutron spectra similar to that of the Po-Be source. For spectra with a significant low energy component all three dosimeter analysis methods give erroneous readings due to the bias necessary to reject gamma-ray pulses which are similar to low energy neutron pulses. In the multichannel analyzer technique the low-energy pulse height distribution is given by extrapolating back from higher energies where the gamma rays do not contribute. The neutron dosimeter does not provide information concerning the energy dependence of the flux and gives questionable results when the flux spectra differs from that of the calibration. It should be used for measurements only when the spectrometer cannot be used.

Another instrument which was used to estimate the source spectrum below 1 MeV was the low energy spectrometer developed and operated by T. V. Blosser (37). This device consists of a BF_3 chamber in a B_4C housing with a cylindrical collimator. The count rate is measured with the collimator uncovered and then covered with several

thicknesses of B_4C. A foil measurement is made in order to normalize the BF_3 data. Given the count rate as a function of foil thickness, one assumes a spectra such as a Maxwellian and a 1/E shape connected with a transition region and folds the spectra with the response of the detector to determine the several count rates. These are compared with the measured count rates and adjustments are made in the assumed shape until the comparison is satisfactory. This is more of an art than a science and success depends upon considerable prior knowledge of the spectrum.

III. DISCUSSION OF MEASUREMENTS

During the course of the experiment, extensive data were taken using the instrumentation previously discussed. Some of this data will be presented later in this chapter and in the selected comparisons with calculations discussed in Chapter VI. A list of the NE-213 spectra measurements is given in Table III and the dose measurements in Table IV. Appendix I contains most of the unfolded spectra from the NE-213 measurements in tabular form. Appendix II contains selected portions of the dose data. Some of the dose measurements were for internal checks and adjustments such as locating the exact beam position and need not be reported.

The slabs used in the measurements do not represent real shielding configurations for specific engineering applications. For the purpose of establishing the accuracy of a calculational method it is sufficient to study arbitrary materials as long as the basic transport mechanisms are present. This study includes

TABLE III

FAST NEUTRON SPECTRA MEASUREMENTS

Material	Angle	TSF Run Number
Bare Beam	0°	22C - 22D
Bare Beam	4.16°	24A - 24B
Bare Beam	8.6°	23A - 23B
Bare Beam	0°	33A - 30C
Bare Beam	4.16°	33B - 29F
Bare Beam	8.6°	33C - 29E
Bare Beam	0°	50B - 50C
6 in. CH_2	0°	37A - 37B
6 in. CH_2	13°	70A - 71A
6 in. CH_2	30°	38B - 38C
6 in. CH_2	30°	51A - 51B
11 in. Pb	0°	19F - 19G
11 in. Pb	13°	19H - 19I
11 in. Pb	47°	20B - 20C
11 in. Pb	64°	20D - 20E
11 in. Pb	0°	39C - 39D
11 in. Pb	13°	46B - 47A
11 in. Pb	30°	39E - 40B
11 in. Pb	47°	40C - 40D
11 in. Pb	64°	45A - 45C
Lam. Pb-CH_2	0°	73A - 73B
Lam. Pb-CH_2	13°	74D - 74E
Lam. Pb-CH_2	30°	75E - 75F
Lam. Pb-CH_2	30°	82A - 82A8
Lam. Pb-CH_2	47°	76E - 76E8
Lam. Pb-CH_2	64°	76G - 76G8
5.5 in. U	0°	163C - 163C8
5.5 in. U	13°	164A - 160B
5.5 in. U	30°	163B - 159C
5.5 in. U	47°	157B - 161B
5.5 in. U	64°	158A - 161C

TABLE IV

DOSE MEASUREMENTS

Title	Detector
Horizontal traverse 1 in. from Pb collar	Hornyak Button
Linear traverse along beam centerline	Hornyak Button
Vertical traverse 4 ft. from Pb collar	Hornyak Button
Horizontal traverse 30 ft. from Pb collar	Hornyak Button
Horizontal traverse 30 ft. from Pb collar	Hurst Dosimeter
Vertical traverse 4 ft. from Pb collar	Hurst Dosimeter
Horizontal traverse 4 ft. from Pb collar	Hurst Dosimeter
Horizontal traverse 3-7/8 in. from Pb collar	Hurst Dosimeter
Vertical traverse 30 ft. from Pb collar	Hurst Dosimeter
Bare beam at radius of 18 ft. 10 in. and angles of 0, 4.16, and 8.6°	Hurst Dosimeter
Bare beam at radius of 27.4 ft. and angles of 0, 4.16, and 8.6°	Hurst Dosimeter
Pb slabs at radius of 27.4 ft. and angles of 0, 13, 30, 47, and 64°	Hurst Dosimeter
CH_2 slabs at radius of 27.4 ft. and angles of 0, 13, 30, 47, and 64°	Hurst Dosimeter
Lam. slabs at radius of 27.4 ft. and angles of 0, 13, 30, 47, and 64°	Hurst Dosimeter
Horizontal traverse 1-3/4 in. from Pb slab	Hornyak Button
Horizontal traverse 2 in. from CH_2 slab	Hornyak Button
Horizontal traverse 1-3/4 in. from Lam. slab	Hornyak Button
Horizontal traverse 1 in. from U slab	Hornyak Button

the two extremes, a light, hydrogenous material, CH_2, and heavy metals, Pb, and depleted uranium. A lamination of lead and polyethylene, 1-1/2 in. Pb - 1 in. CH_2 - 1-1/2 in. Pb - 1 in. CH_2 - 1-1/2 in. Pb - 1 in. CH_2 - 1-1/2 in. Pb, was also included. The thicknesses of the slabs, 6 in. CH_2, 11 in. Pb, 5.5 in. U, were determined by the availability of materials and the minimum intensity for reasonable measurements times. The intensity at a reactor power of 100 kilowatts is such that much larger slab thicknesses could be used at an angle of 0° but not at the larger angles and still get good counting statistics. Wide angle measurements for polyethylene were also prohibited by the high gamma to neutron ratio. For the heavy metals the reactor gammas were removed and large angle measurements could be made.

One objective of the experiment was to provide data which is sufficiently differential to demonstrate various transport effects and yet could be readily measured such that counting statistics were reasonable and comparisons with calculations straightforward. The most differential form for the leakage flux in a transport calculation is the surface angular flux, $\phi(r_s,E,\bar{\Omega})$, a function of position, r_s, energy, E, and angle, $\bar{\Omega}$. The angle-dependent spectra measurements effectively measure the surface integral of the angle-dependent current, and the dose traverse measurements made directly on the shield surface measure the radial dependence of a weighted integral of the flux. Although in the real case the flux is not separable, the geometry is such that the radial dependence of the flux is similar for each energy and angle. Thus, if the transport

calculations agree with the two different measurements, these taken together infer that the calculation of the angular flux is essentially correct. Of course, the comparisons taken separately allow precise comparisons and give good indications of the accuracy of the transport calculation.

Since the purpose of the experiment was to provide data for detailed comparisons with transport calculations, it was of utmost importance that the source term for the calculation be accurately determined. For this reason a large portion of the experimental effort was devoted to measurements relating to the determination of the source. It is assumed that the source is separable in space, energy, and angle. This is generally a good assumption for a well collimated source which may thus be described by a radial dependence, energy dependence, and angle dependence at the slab entrance,

$$S(r,E,\bar{\Omega}) = f(r)g(E)h(\bar{\Omega}) \ . \qquad (5.5)$$

The radial distribution, f(r), is determined from a Hornyak button traverse at a distance of one inch from the outer surface of the lead collar. A plot of this data is shown in Figure 18. The dose was essentially constant from the centerline of the collimator to a radius of slightly over two inches, which corresponds to the radius of the long cylindrical section of the collimator. The dose then drops rapidly with increasing radius. Although the shape was incorporated into the calculations, it is an excellent approximation to assume a flat distribution up to a radius of 2-1/8 inches and a value of zero elsewhere. The Hornyak button used for this traverse was 1/2 inch in diameter and 1/16 inch thick, which gave a reasonably

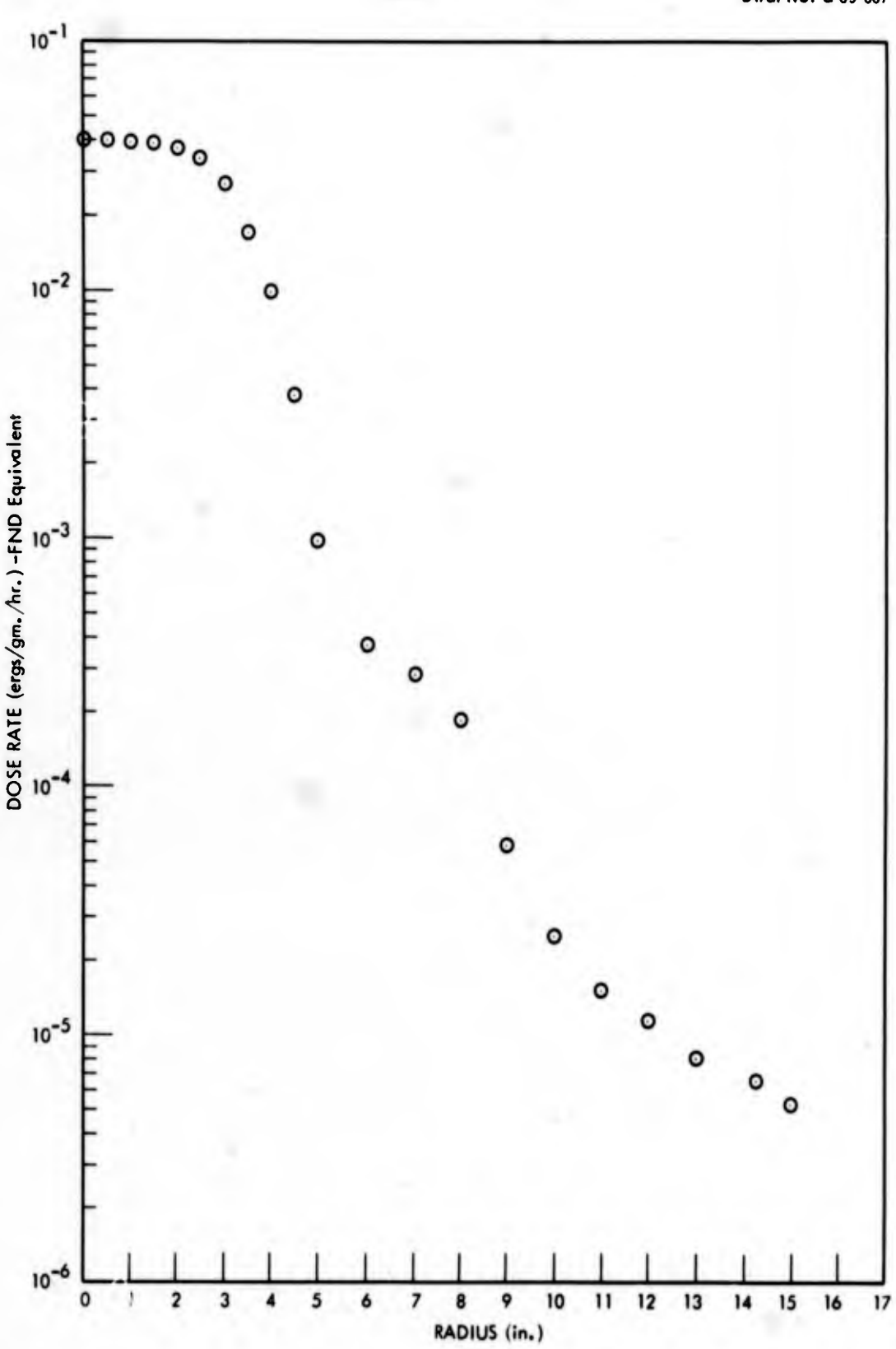

Figure 18. Horizontal traverse with Hornyak button one inch from the collimator exit.

good resolution of the shape. The Hurst dosimeter, which is two inches in diameter, is too large to resolve the shape, and the NE-213 scintillator is too sensitive to reactor gammas as well as being too large.

The angular distribution, $h(\bar{\Omega})$, is determined from three NE-213 measurements made at a radius of 27.4 feet and angles of 0, 4.16, and 8.6°. The unfolded spectra from these measurements are shown in Figure 19. The intensity falls very rapidly with increasing angle with an angle at half maximum of less than 4° and falling by two decades at an angle of 8.6°. The assumption that the source is separable in energy and angle is substantiated by these data since the spectrum is quite similar for the three angles. Although the angular distribution of the source could be incorporated into the calculations with considerable difficulty, the collimation is such that one can assume that the source is monodirectional at 0°. In a discrete ordinates calculation the source is input in the angle nearest 0°.

The energy distribution, g(E), of the source is determined from the unfolded NE-213 data at 0° such as that shown in Figure 19. As mentioned previously, the source below 1 MeV. was estimated from the B_4C filtered BF_3 spectrometer. The source spectrum in lethargy units is shown in Figure 20. The source below a lethargy of 2.6 is from the unfolded NE-213 data and the remaining data is from the BF_3 data. The two portions of the curve are given in their absolute intensities as measured and thus show excellent agreement in the

DWG. NO. G-69-568

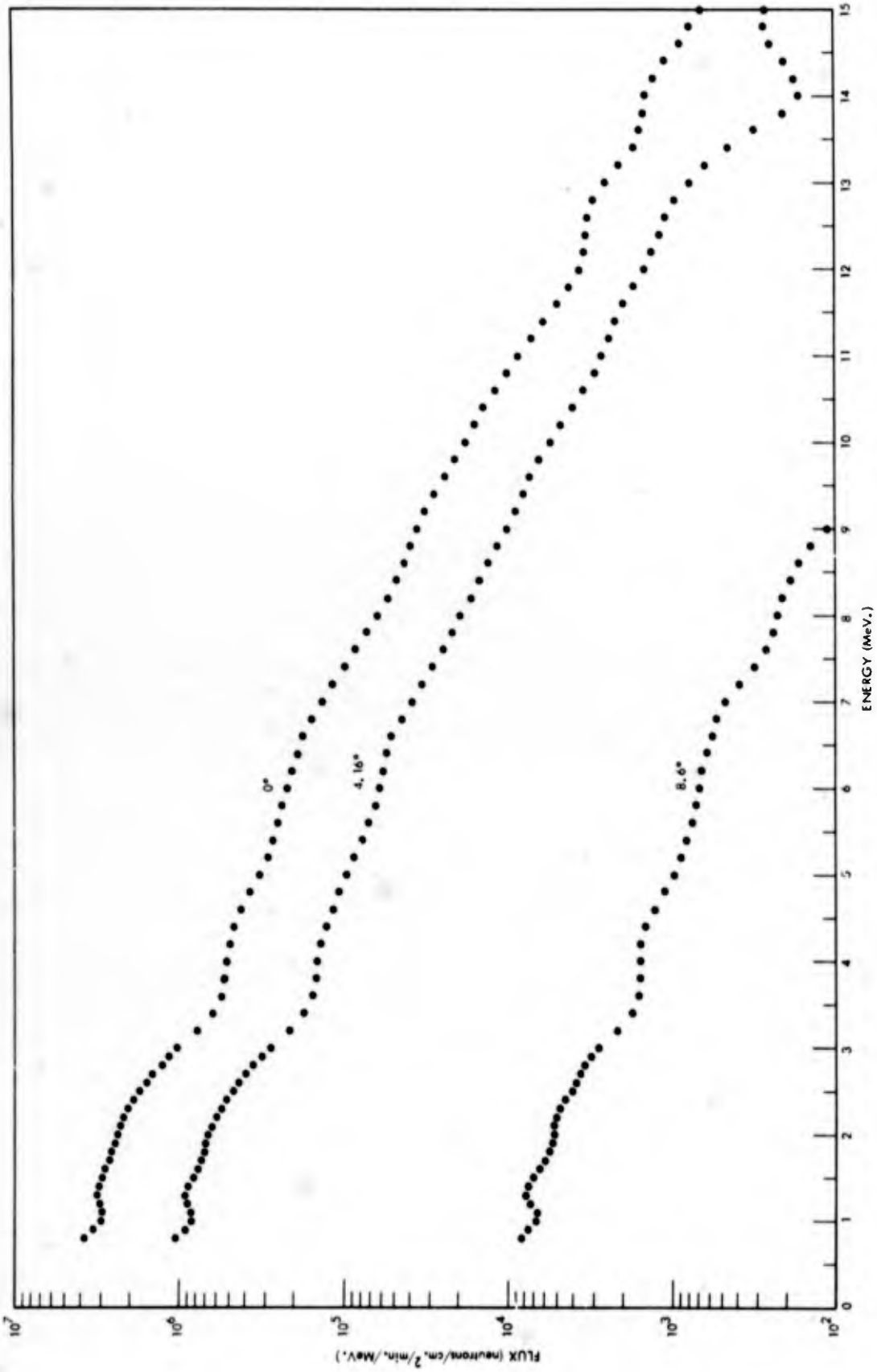

Figure 19. Bare beam measurements at three angles, 0, 4.16, and 8.6°.

DWG. NO. G-69-569

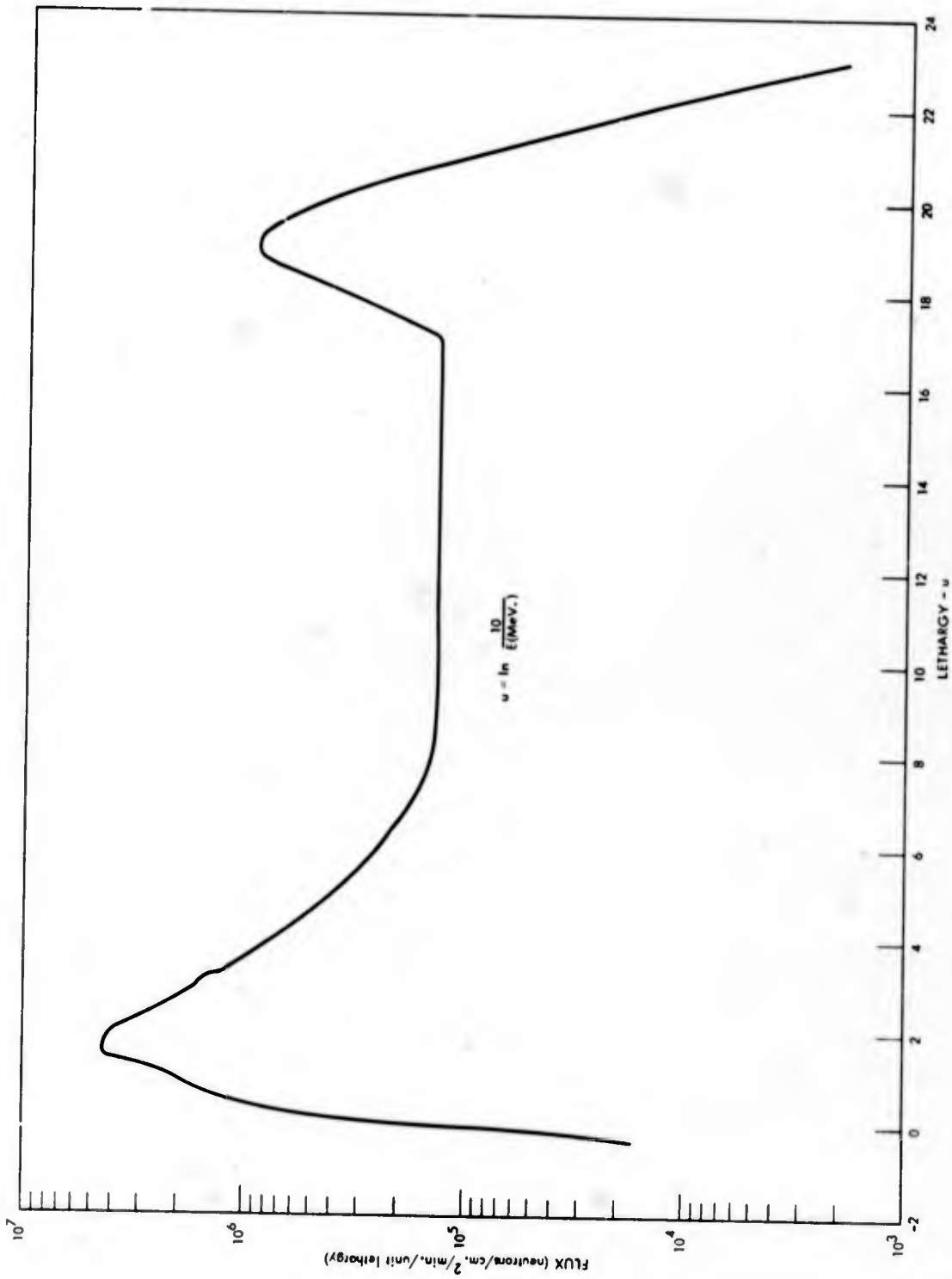

Figure 20. The combined source spectrum.

region of overlap. The low energy source data is used only for the calculations of relative dose shape and for the depleted uranium where fissions must be included.

The intensity of the source is based primarily on the unfolded NE-213 data at 27.4 feet radius and 0°. This gives the flux intensity in the flat portion of the horizontal traverse at a distance of 27.4 feet from the collar. This intensity was scaled to that for the location at the collimator exit by two Hornyak button measurements, one at the NE-213 location and one at the collimator exit. This gave the intensity in the flat portion of the horizontal traverse at the collar interface. The 0° energy distribution scaled to the intensity at the collimator exit is shown in Figure 21. In the calculation the source energy, space, and angle distribution was adjusted such that the flux spectrum in the center of the flat portion was that given in Figure 21. This adjustment was based on only one group such as the first energy group since the energy distribution was already incorporated. These calibrations indicate that at a reactor power of 100 kilowatts, 7.05×10^{10} neutrons per minute entered the slabs with energies greater than 0.8 MeV.

The reproducibility of the experiment, which is the ability to obtain the same data on different runs, depended on the calibrations of the reactor power and the detection instrumentation. The reactor power was monitored independently by several BF_3 chambers, and, although the actual power used for a given run depended on the intensity at the detector, all data was reported as scaled to a reactor power of 100 kilowatts. The Hurst dosimeter and the NE-213

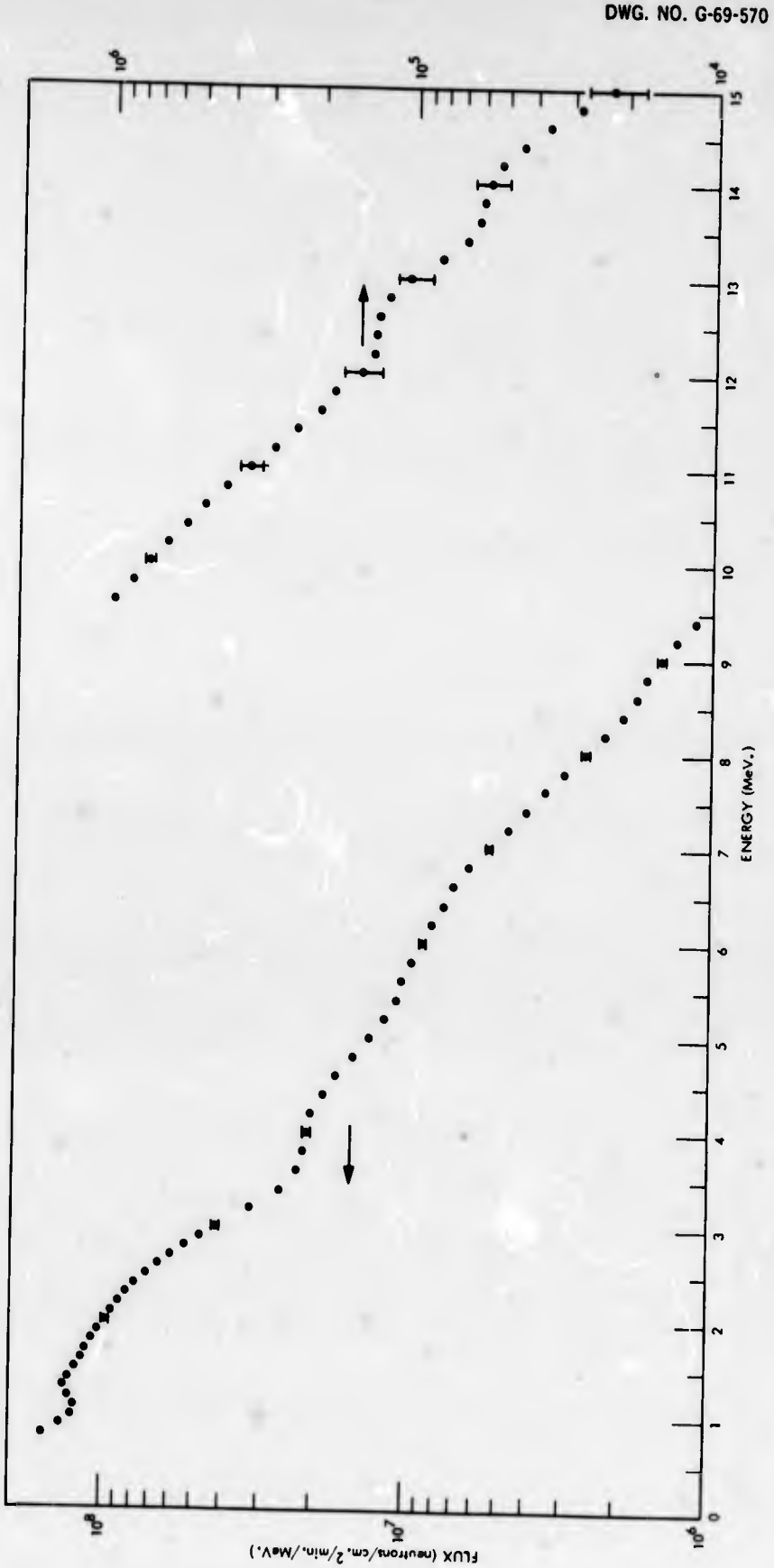

Figure 21. The source intensity at the slab entrance.

scintillator were calibrated with a known Po-Be source, and a known Co^{60} source was also used for the NE-213. The NE-213 pulse height distributions for the Po-Be source were taken at the beginning and end of each run and compared to detect possible changes. Periodically these pulse height distributions were unfolded to see if there were changes which could be detected in the unfolding.

As a test of the experimental reproducibility several of the NE-213 measurements were repeated over periods separated by several weeks. Figure 22 shows two bare beam measurements at 0°, runs 33A + 30C and 50B + 50C, and Figure 23 shows two measurements for the polyethylene slabs at 30°, runs 38B + 38C and 41A + 51B. In each case the two runs are plotted a factor of ten apart so that the two sets of data can be distinguished. As is demonstrated in these comparisons the reproducibility is excellent.

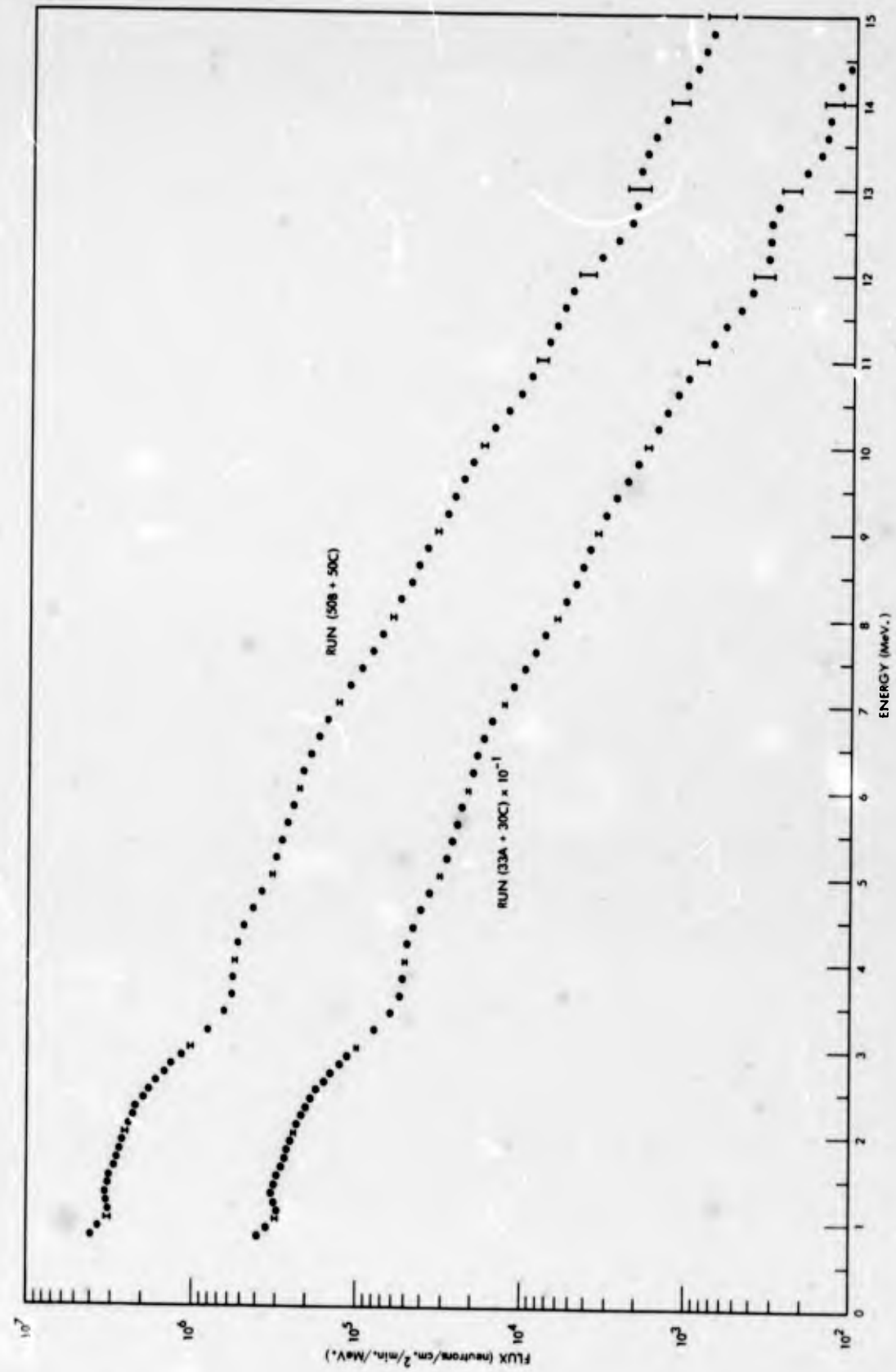

Figure 22. Reproducibility of 0° bare beam measurements.

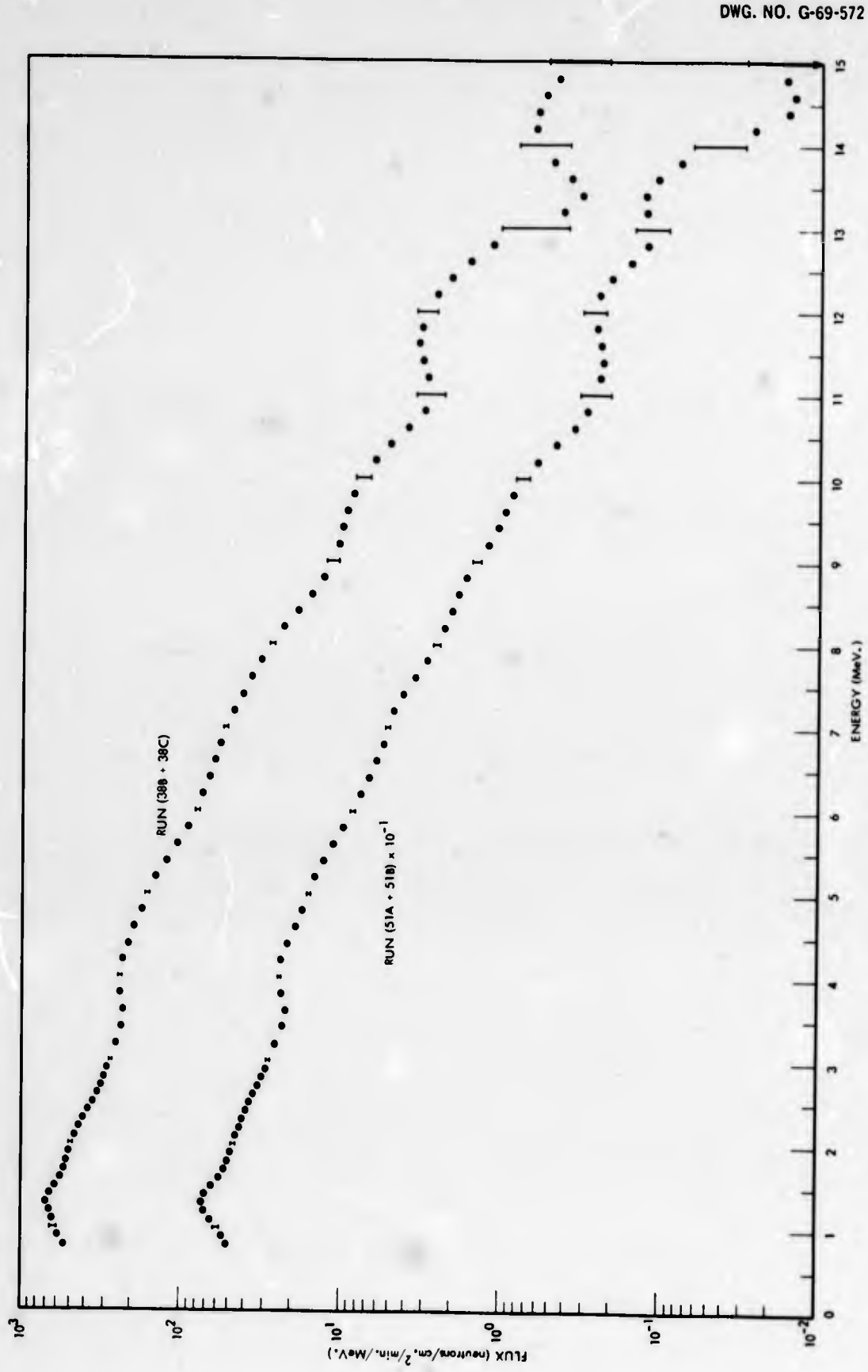

Figure 23. Reproducibility of 30° polyethylene slab measurements.

CHAPTER VI

COMPARISONS OF RESULTS OF DISCRETE ORDINATES CALCULATIONS WITH THE SLAB EXPERIMENT

The procedure followed during the development of the techniques described in Chapters II, III, and IV was to perform calculations of the experiments described in Chapter V for each improvement. Each calculation, at the time it was performed, represented the best calculation which could be done for the given experiment. The experiments provide a basis for determining the sensitivity of the calculations to the space-angle mesh, number of groups, anisotropic cross-section expansion, and cross-section weighting procedure. The main purpose in this chapter is to demonstrate the accuracy and versatility of the method.

In calculations for the determination of dose rate, heating, damage, or multiplication factor a broad group structure may usually be found which, through good cross-section weighting, gives an accurate answer economically. However, for spectra comparison the finest group structure that can be used is preferred since the objective is shape comparison. The group structure which was used for the spectra comparison calculations contains the first 30 fine groups of the 99-group GAM-II structure. The broader group structure which was used for dose calculations and for the depleted uranium, where fission iterations were done, is a 38-group structure extending from 15 MeV to thermal. The energy bounds for these two group structures are given in Table V along with the single collision dose factors for the 38-group structure. The dose response numbers

TABLE V

ENERGY GROUP STRUCTURES AND DOSE FACTORS

Group	Upper Energy Bounds of 30 Group Structure	Upper Energy Bounds of 38 Group Structure	Dose Factors[a] for 38 Group Structure
1	1.492×10^7 eV.	1.492×10^7 eV.	1.969×10^{-5}
2	1.350×10^7	1.221×10^7	1.869×10^{-5}
3	1.221×10^7	1.000×10^7	1.740×10^{-5}
4	1.105×10^7	8.187×10^6	1.691×10^{-5}
5	1.000×10^7	6.703×10^6	1.621×10^{-5}
6	9.048×10^6	5.488×10^6	1.561×10^{-5}
7	8.187×10^6	4.493×10^6	1.553×10^{-5}
8	7.408×10^6	3.679×10^6	1.421×10^{-5}
9	6.703×10^6	3.012×10^6	1.226×10^{-5}
10	6.065×10^6	2.466×10^6	1.131×10^{-5}
11	5.488×10^6	2.019×10^6	1.062×10^{-5}
12	4.966×10^6	1.653×10^6	9.680×10^{-6}
13	4.493×10^6	1.353×10^6	9.025×10^{-6}
14	4.066×10^6	1.108×10^6	8.444×10^{-6}
15	3.679×10^6	9.072×10^5	7.241×10^{-6}
16	3.329×10^6	7.427×10^5	6.532×10^{-6}
17	3.012×10^6	6.081×10^5	6.025×10^{-6}
18	2.725×10^6	4.979×10^5	5.527×10^{-6}
19	2.466×10^6	4.076×10^5	4.859×10^{-6}
20	2.231×10^6	3.337×10^5	4.069×10^{-6}
21	2.019×10^6	2.732×10^5	3.792×10^{-6}
22	1.827×10^6	2.237×10^5	3.592×10^{-6}
23	1.653×10^6	1.832×10^5	3.158×10^{-6}
24	1.496×10^6	1.500×10^5	2.748×10^{-6}
25	1.353×10^6	1.228×10^5	2.287×10^{-6}
26	1.225×10^6	8.652×10^4	1.289×10^{-6}
27	1.108×10^6	3.183×10^4	5.516×10^{-7}
28	1.003×10^6	1.171×10^4	7.260×10^{-8}
29	9.072×10^5	4.307×10^3	2.670×10^{-8}
30	8.209×10^5	1.585×10^3	9.830×10^{-9}
31	7.427×10^5	5.830×10^2	3.620×10^{-9}
32		2.145×10^2	1.040×10^{-9}
33		7.889×10^1	4.890×10^{-10}
34		2.902×10^1	1.800×10^{-10}
35		1.068×10^1	6.600×10^{-11}
36		3.928×10^0	2.430×10^{-11}
37		1.445×10^0	7.900×10^{-12}
38		thermal[b]	3.100×10^{-13}

[a] Dose response units are rads/hr./neutron/cm.^{2}/sec.

[b] Thermal group extends up to 0.414 eV.

for groups 1 through 26 are the single collision dose factors reported by Henderson (28) and are used for comparison with the Hurst dosimeter measurements. For comparison with the Hornyak button measurements, the dose response numbers are extended to thermal assuming that they are proportional to energy.

Two source representations were used. The first method used a space-angle-energy-dependent boundary condition which was incorporated into DOT. The energy and radial distributions were based on the source data provided in Chapter V. The neutrons were assumed to be normally incident on the slab and were input into the discrete directions nearest the axis. In calculations performed prior to the development of "tailored quadrature," the input of the source into the near 13° directions of the S_{10} quadrature which was then in use made it difficult to determine the collided flux at 13°. With the development of highly refined quadratures it was possible to use this source input for calculations for comparison with the 0 and 13° measurements. The second source representation also used the assumption of a monodirectional source, but the analytic first collision source technique discussed in Chapter IV was used. These DOT calculations, which included only the collided component of the flux, were most important for the 0 and 13° comparisons. The comparisons at larger angles and the 38-group dose calculations were fairly insensitive to the choice of source representation.

The space mesh (radial and axial intervals) was nearly the same for all problems which were calculated. All of the slabs were five feet square and were represented as cylinders 86.0 cm. in radius. The

radial mesh contained four equally spaced intervals from 0.0 to 5.398 cm. and 41 equally spaced intervals from 5.398 cm. to 86.0 cm. The lead, polyethylene, and uranium calculations contained 15 equally spaced axial intervals from 0.0 to 27.94, 15.24, and 13.97 cm., respectively. These calculations thus contained 675 space points. The laminated lead-polyethylene slab contained three equally spaced axial intervals in each of the four 3.81-cm.-thick lead slabs and two equally spaced intervals in each of the three 2.54-cm.-thick polyethylene slabs. Calculations performed for comparison of dose profiles near the back of the slabs contained three additional axial intervals in order to calculate the transport effects due to the small separation distance between the slab surface and the detector.

The following sections are concerned with the cross-section data and specific quadrature used for the specific slabs. The lead slabs have an atomic density of 3.3×10^{22} atoms/cm.^{3} The polyethylene has a composition of 7.729×10^{22} atoms/cm.^{3} of hydrogen and 3.865×10^{22} atoms/cm.^{3} of carbon. The uranium slab composition is 1.202×10^{20} atoms/cm.^{3} of uranium-235 and 4.721×10^{22} atoms/cm.^{3} of uranium-238. These data, along with the source description, energy group structure, and space mesh, completely describe the transport calculations which were performed with DOT. The neutron spectra at the spectrometer location were calculated both with the SPACETRAN method described in Chapter IV and the simplified method given in Equation (4.10). These methods give essentially the same answer since the detector is sufficiently far away that the distance from any point on the slab surface to the detector is essentially constant.

The transport calculations in these slabs are rather severe two-dimensional problems. The radial gradients, which are due to the source, are steep and change rapidly with penetration into the slab. The axial gradients, which are due to penetration, are significant and of course vary rapidly with radius. The comparisons provide a good test of the transport code since both penetration and lateral spreading of the flux distribution due to scattering are important effects.

Since the spectrometer views the entire surface of the slab at such a distance that the angle to any point on the slab is essentially constant, calculations of the spectra may be performed to a good approximation with a one-dimensional code. In order to do this, the source is input on the surface of the one-dimensional slab as an infinite parallel beam. If the source is normalized to the total intensity of the source, the angular current at the exit face, divided by the square of the distance to the detector, gives the absolute intensity at the detector. Several one-dimensional ANISN calculations were performed for the experiment, and they agreed well with the DOT results.

I. THE LEAD SLAB

A large proportion of the effort was devoted to the lead slab measurements. This was due to the fact that during the early calculations the disagreements were more severe in the comparisons with lead than in those for polyethylene and the laminated slab. This was primarily attributed to the very high degree of anisotropy for

elastic scattering of high energy neutrons in lead. Early calculations were performed with 30-group GAM-II (17) cross sections with the maximum available P_3 expansion of the scattering cross section. Since the disagreements were probably due to the scattering anisotropy, it was deemed necessary to obtain cross sections of a higher cross-section expansion. Elastic scattering data from the Aldermaston data file (38) were processed for the 30-group structure using the CSP code (39), which was based on the elastic scattering routine, TRANSFER (40). The multigroup inelastic scattering data from GAM-II were merged with the multigroup elastic data from CSP to form the complete set of transfer tables necessary for the discrete ordinates calculations.

Figure 24 shows comparisons of calculations and experiment for the 0° measurement for lead. These calculations required the use of the analytic first collision source routine, AFCS, in order to separate the collided and uncollided components. The uncollided flux, using the AWRE data, was obtained by taking the multigroup values for the bare beam spectra at the detector location and multiplying by exponential attenuation factors using the multigroup total cross sections. Two collided flux calculations are shown, both using the AWRE data with a P_8 scattering expansion. In one calculation an S_{10} quadrature resulting from a solution of Equation (4.2) with P_{10} Legendre zeroes for μ_k and η_k was used for the iterations. This was followed by a one-iteration calculation with a quadrature denoted by the symbol S_{130}, which was composed of the original S_{10} quadrature with the first level replaced by 11 levels having level weights and polar cosines given by

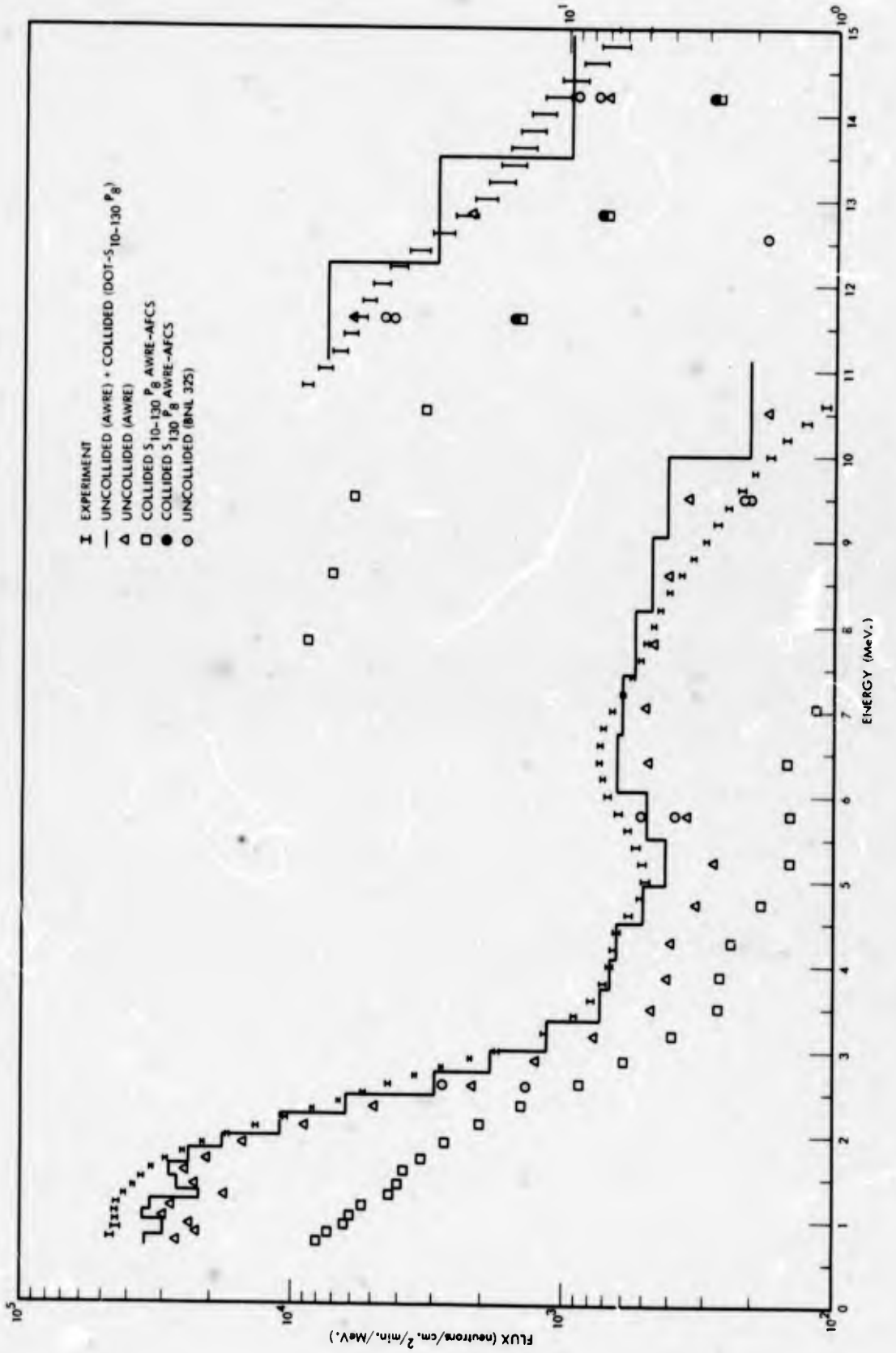

Figure 24. Comparison of calculations with the 0° measurement for the lead slab.

an order-96 Gaussian quadrature with azimuthal angles from the original S_{10} quadrature. This quadrature thus has 11 levels with three angles each, followed by the regular S_{10} quadrature progression, omitting the first level. This modification gives a resolution of about 1° in the polar angle nearest the axis. The method is based on the assumption that the transport within the slab is adequately calculated with the S_{10} quadrature, and the high resolution quadrature is necessary only to define the angular flux as seen by the detector. At the end of the S_{10} calculation, all of the spherical harmonic coefficients describing the scattering source were saved and then input into the S_{130} calculation. In the S_{130} calculation the convection terms of the discrete ordinates difference equation used the new quadrature, while the scattering source was defined by the S_{10} results. This is similar in concept to using a last flight estimator to obtain the results at the detector. A check was performed by using the S_{130} quadrature throughout the iterations. The results for this calculation are shown for the first three groups below which the collided calculations give exactly the same answers.

The sum of the uncollided and collided components is shown as a histogram. The other points actually represent the midpoints of histogram levels. The sum curve agrees very well with the experimental values. In an attempt to determine the effect of total cross-section uncertainty on the results, a few points were calculated using point data from BNL-325 (41). Since point data were used, the results for a group are given as two numbers. The upper number was obtained using the minimum cross section in the group energy range,

and the lower value was obtained using the maximum cross section. The average value for the group must thus fall between these two points. At 11.6, 9.5, and 5.8 MeV., the uncollided flux obtained with the AWRE data lies outside the range given by the BNL data. In these cases the indicated uncertainty is comparable to or greater than the disagreement between the calculation and the experiment. Although the BNL data appears to give much better results, particularly at 9.5 MeV., a transport calculation cannot be performed with these data since only the total cross sections are given.

Figures 25 through 28 show comparisons for the lead slab at 13, 30, 47, and 64°. For the 13° comparison only calculations using the analytic first collision source can be used since this is the angle into which the boundary source was introduced. The calculation using GAM-II data gave a spectrum which is consistently low. This effect is largely due to the P_3 scattering approximation as is demonstrated by the results of the calculation with the AWRE data using the P_3 approximation. At this angle, the S_{10}-P_8, S_{10-130}-P_8, and S_{130}-P_8 calculations all agree with each other.

In the 30° comparison the effect of source description, as well as cross-section type, and P_n expansion are shown. The S_{10}-P_8 calculation with the analytic first collision source gave negative fluxes for the first three groups at this angle and gave a much lower spectrum than the S_{10}-P_8 calculation with boundary source for the next few groups. These two calculations agree better as the energy decreases and have identical answers below 6.5 MeV. The effect of P_n is demonstrated by the S_{10}-P_3 and S_{10}-P_8 calculations using AWRE

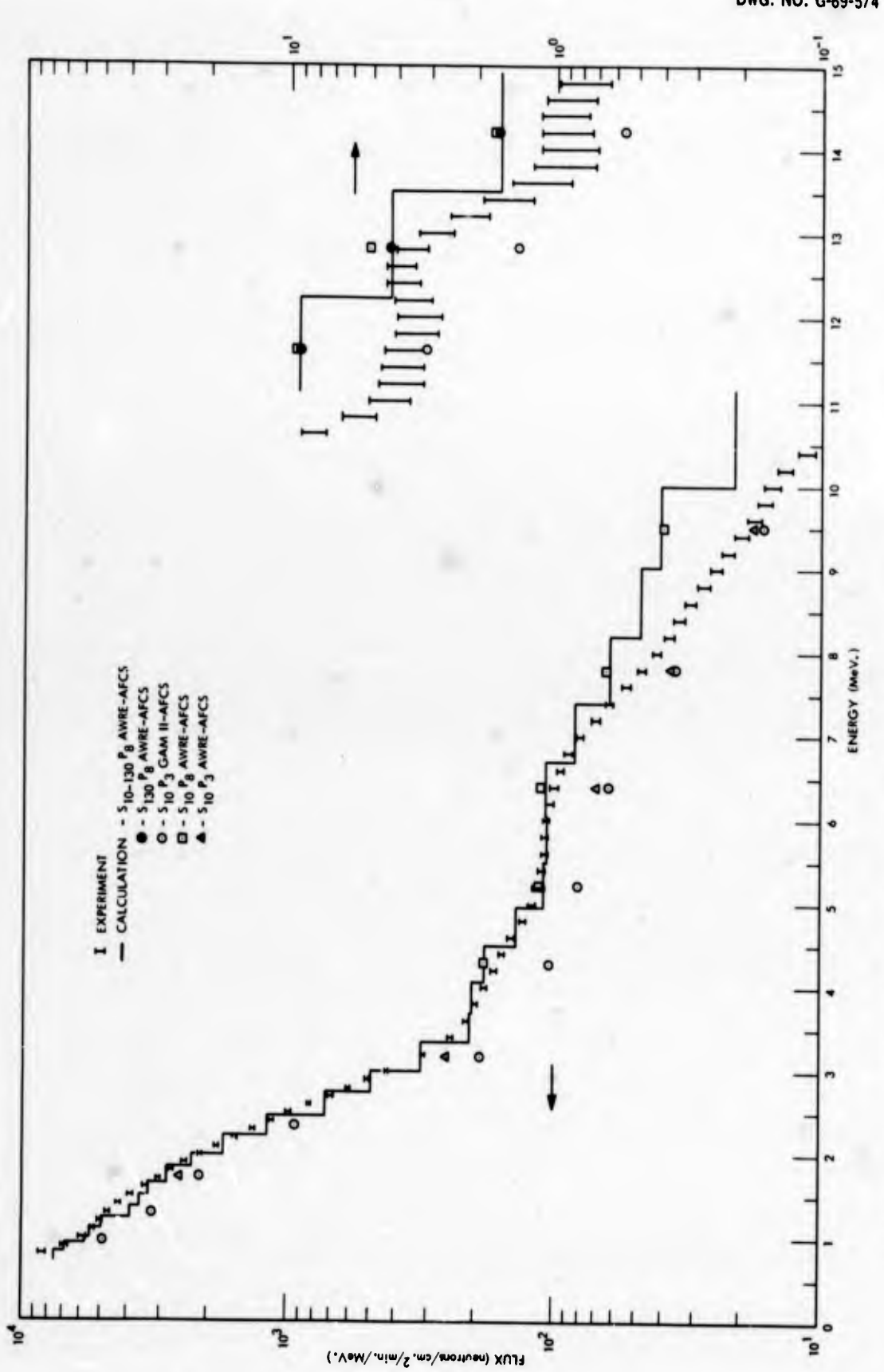

Figure 25. Comparison of calculations with the 13° measurement for the lead slab.

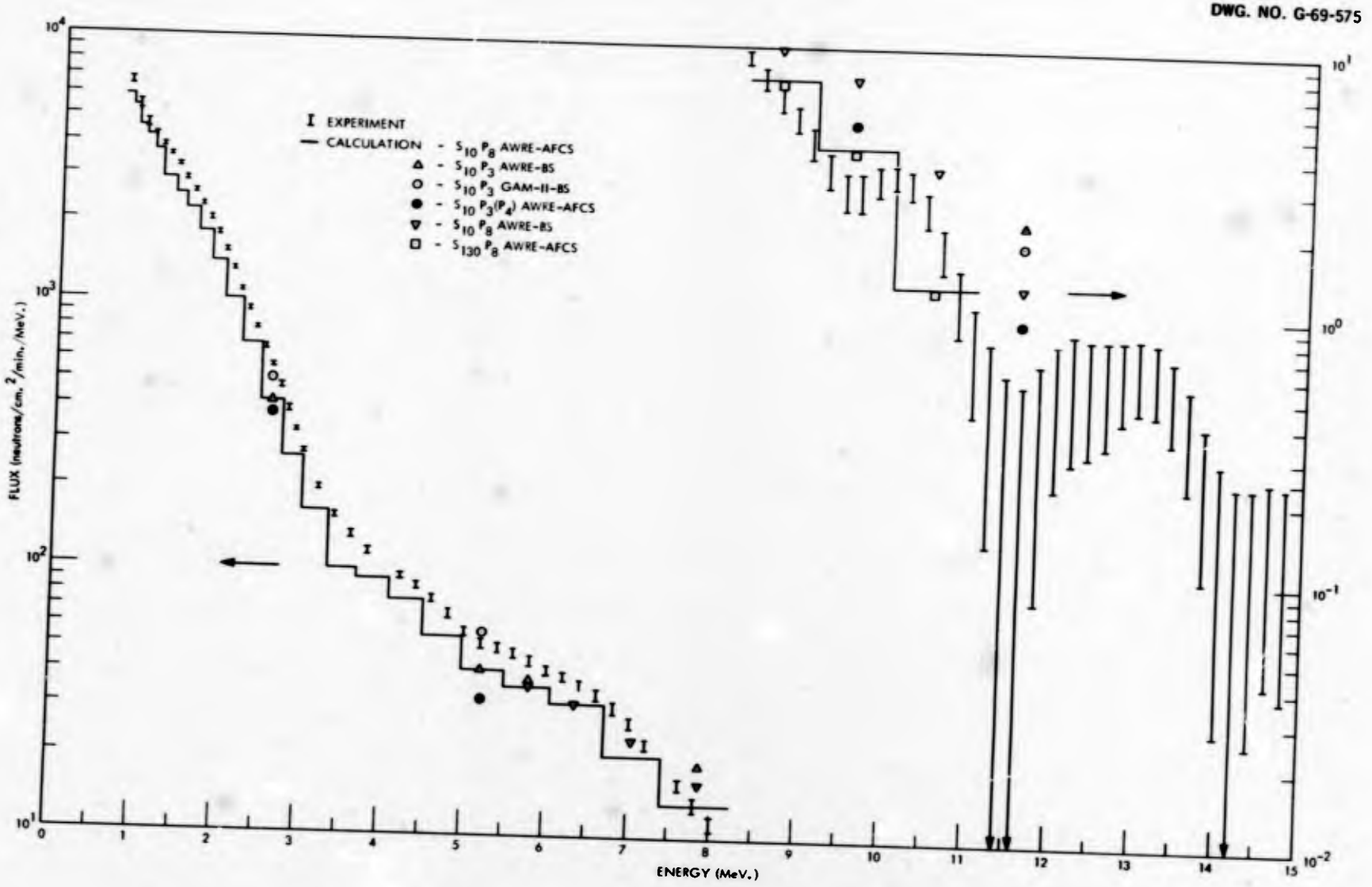

Figure 26. Comparison of calculations with the 30° measurement for the lead slab.

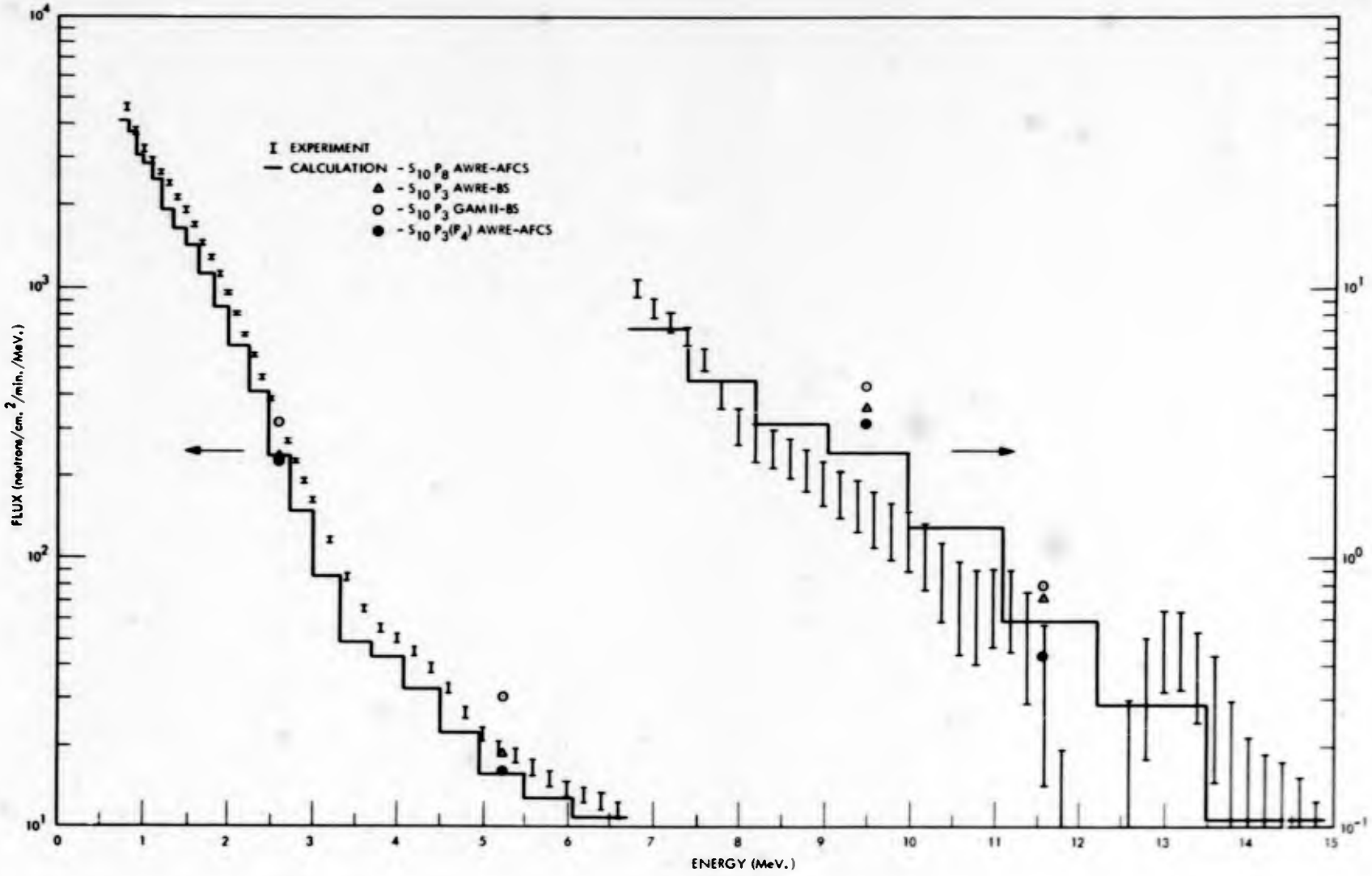

Figure 27. Comparison of calculations with the 47° measurement for the lead slab.

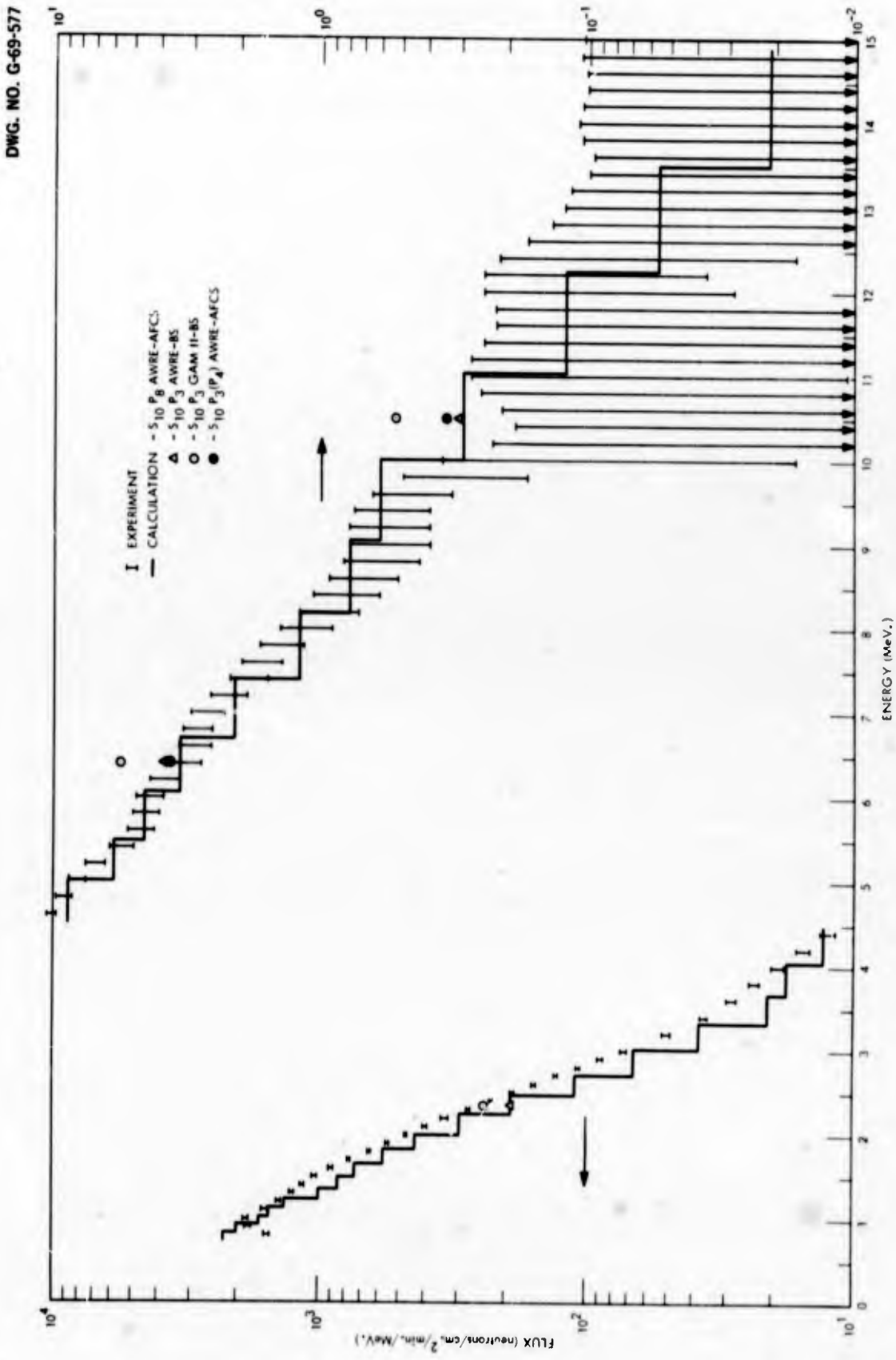

Figure 28. Comparison of calculations with the 64° measurement for the lead slab.

data and boundary sources. At 11.6 MeV. the P_3 result is almost a factor of two higher than the P_8 result, at 9.5 MeV. the P_3 result is about 25 percent higher, and below 5.78 MeV. the results are virtually identical. The results of the S_{10}-P_3 calculation using GAM-II cross sections are higher than the other calculations and appear to agree with experiment better at energies below 6 MeV.

The calculations denoted by the symbol S_{10}-$P_3(P_4)$ used cross sections with a forward scattering delta function approximation for within-group scattering. In this approximation the P_4 within-group scattering angular distribution, which is given by a five-term Legendre series,

$$f(\mu) = \frac{1}{2} \sum_{\ell=0}^{4} (2\ell+1) f_\ell P_\ell(\mu) \ , \qquad (6.1)$$

is replaced by a four-term Legendre series, plus a delta function,

$$f'(\mu) = \frac{1}{2} \sum_{\ell=0}^{3} (2\ell+1) f'_\ell P_\ell(\mu) + C\ \delta(\mu-1). \qquad (6.2)$$

The coefficients, f' and C, are determined by equating the expressions in Equations (6.1) and (6.2), multiplying through by a Legendre polynomial, $P_n(\mu)$, when n varies from zero to four, and then integrating over μ. Since it is true that

$$\sum_{\ell=0}^{4} \int_{-1}^{+1} (2\ell+1) f_\ell P_\ell(\mu) P_n(\mu) d\mu \begin{cases} = 2f_n & \text{for } n \leq 4 \\ = 0 & \text{for } n > 4 \end{cases} , \qquad (6.3)$$

and

$$\int_{-1}^{+1} C\ \delta(\mu-1)P_n(\mu)d\mu = C\ , \tag{6.4}$$

then the results of the above operations are

$$f_{\ell}' = f_{\ell} - C \quad \text{for } \ell \leq 4$$

and $$f_4 = C\ . \tag{6.5}$$

Since the actual multigroup transfer coefficients contain the $(2\ell+1)$ factors, the coefficients are modified by

$$\Sigma_{\ell}' = \Sigma_{\ell} - \frac{2\ell+1}{2(4)+1}\Sigma_4 \quad \text{for } \ell \leq 4. \tag{6.6}$$

The modified four-term Legendre series coefficients are used in the scattering integral and the delta function is accounted for by subtracting f_4 from the total cross section. This has the effect of replacing a straight-ahead scattering by no scattering at all. The results of calculations with this modification were contradictory in that agreement with experiment is better than that with the P_3 approximation at some energies and angles and worse at others.

The lead comparisons at 47 and 64° show the same tendencies as the 30° comparison. The ability of the method to accurately calculate the changes of the spectrum with angle appears to be good.

Figure 29 shows the comparison of the calculated and measured dose profile for the lead slab. The detector was a Hornyak button 1/2 inch in diameter and 1/16 inch thick. The center of the detector

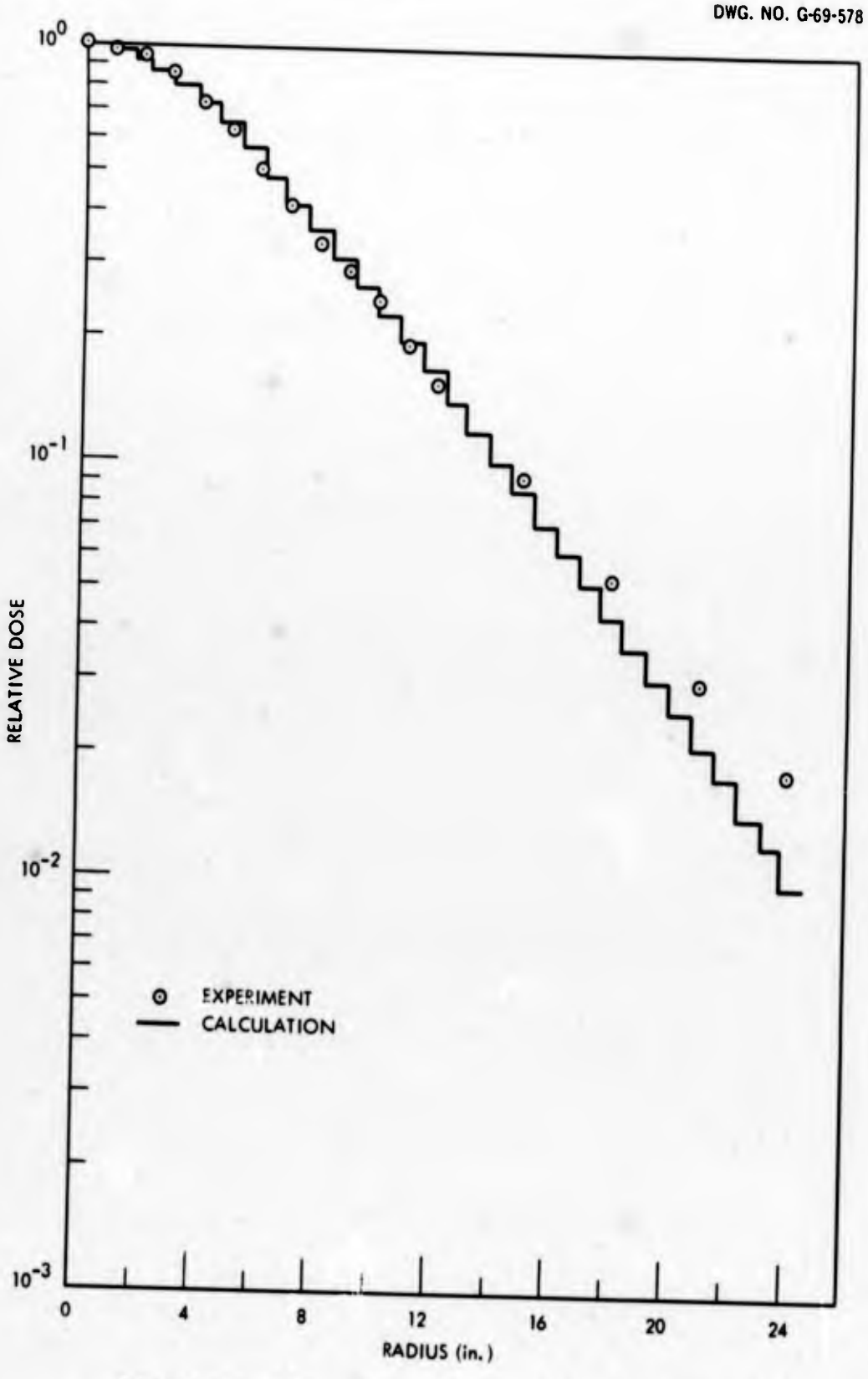

Figure 29. Comparison of calculated and measured dose profiles for the lead slab.

was located 1-3/4 inches from the face of the slab during the traverse. This was accounted for by the three additional axial intervals in the void beyond the slab. The dose profile was calculated in the third interval which was 1/16 inch thick and centered 1-3/4 inches from the slab. The comparison of the dose shape with experiment is very good out to a radius of 14 inches. The disagreement beyond this point may be due to background, to the lack of knowledge of the low energy response of the Hornyak button, or to a lack of convergence.

II. THE POLYETHYLENE SLAB

Figure 30 shows the comparison of experiment and uncollided flux calculation for the polyethylene slab at 0°. This calculation was performed by hand using the multigroup total cross sections in the same manner as for lead at 0°. The collided flux for this case is not significant in comparison with the uncollided flux and is therefore not included. The agreement of the uncollided flux with experiment is excellent except for the groups at 7.8 MeV., 2.87 MeV., and below 1.0 MeV. The cross sections are from the ENDF-B (42) data file and were reduced to multigroup-multitable form by the CSP code (39). The results of an uncollided calculation using GAM-II data is also shown.

Figure 31 shows the comparison of calculated and experimental results for the polyethylene slab at 13°. The S_{10}-P_3 calculation using GAM-II cross sections agrees well with experiment from 1.5 to 4.0 MeV., but is as much as a factor of two or three low at higher energies. The S_{10}-P_3 calculation using ENDF data shows similar

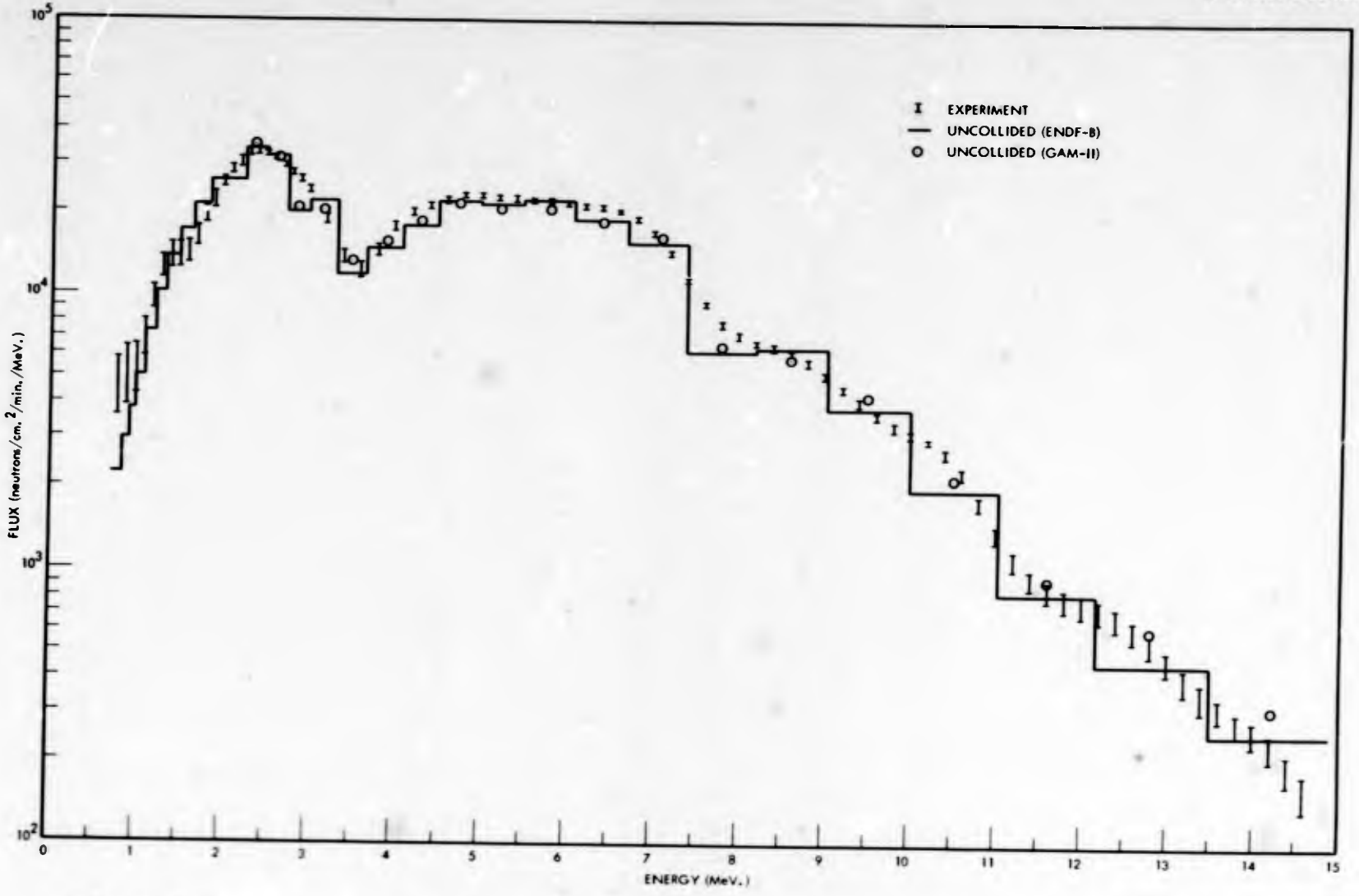

Figure 30. Comparison of calculations with the 0° measurement for the polyethylene slab.

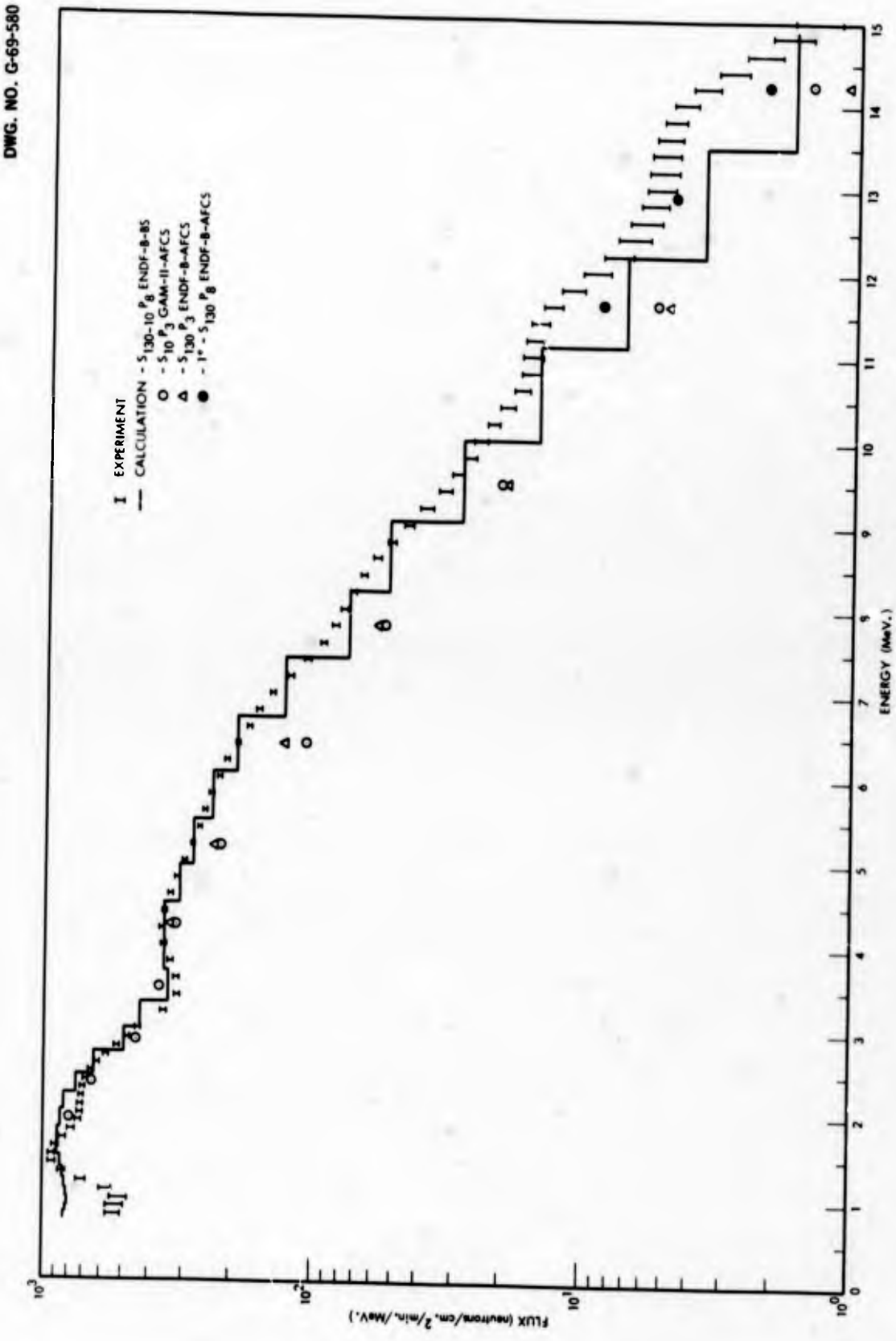

Figure 31. Comparison of calculations with the 13° measurement for the polyethylene slab.

results. The S_{130}-P_8 calculation using ENDF data agrees much better but is as much as 50% low at high energies. It is interesting to note that the collided flux at 1° from the S_{130}-P_8 calculation is still 25% low at high energies. This indicates that either the basic scattering angular distributions are wrong or that P_8 is not a sufficient approximation for an exact comparison.

Figure 32 shows the comparisons for the polyethylene slab at 30°. The agreement of the S_{10}-P_8 calculation with the experiment is excellent. The effect of using a P_3 approximation is less than 20% at the highest energies and is insignificant below 7 MeV. The use of an S_{130} quadrature instead of S_{10} also is a small effect. The rapid dropoff of the experiment below 1.25 MeV. in both this and the 13° measurement is not understood and may be due to errors in the unfolding.

The comparison of the radial dose profile for the polyethylene slab is shown in Figure 33. For this measurement the detector centerline was located two inches from the surface of the slab due to the uneven or wavy surface. During the traverse the location of the detector was measured from the surface of the lead collimator collar so that at a given location the distance from the polyethylene surface may be more or less than two inches. Nevertheless, the calculated and measured profiles agree quite well.

III. THE LAMINATED SLAB

The laminated slab experiment was performed to answer the obvious question as to whether the transport method could calculate laminated

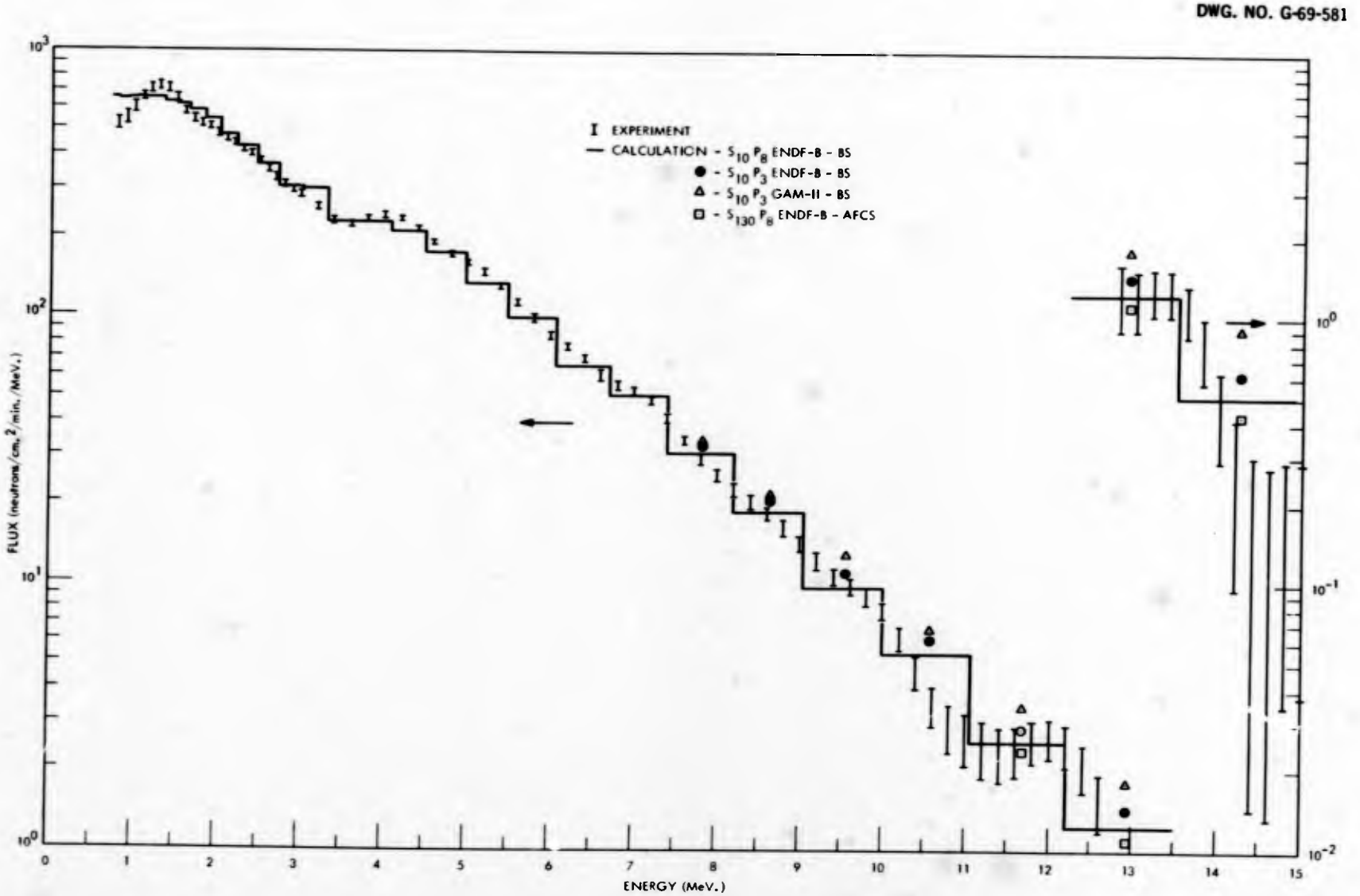

Figure 32. Comparison of calculations with the 30° measurement for the polyethylene slab.

DWG. NO. G-69-582

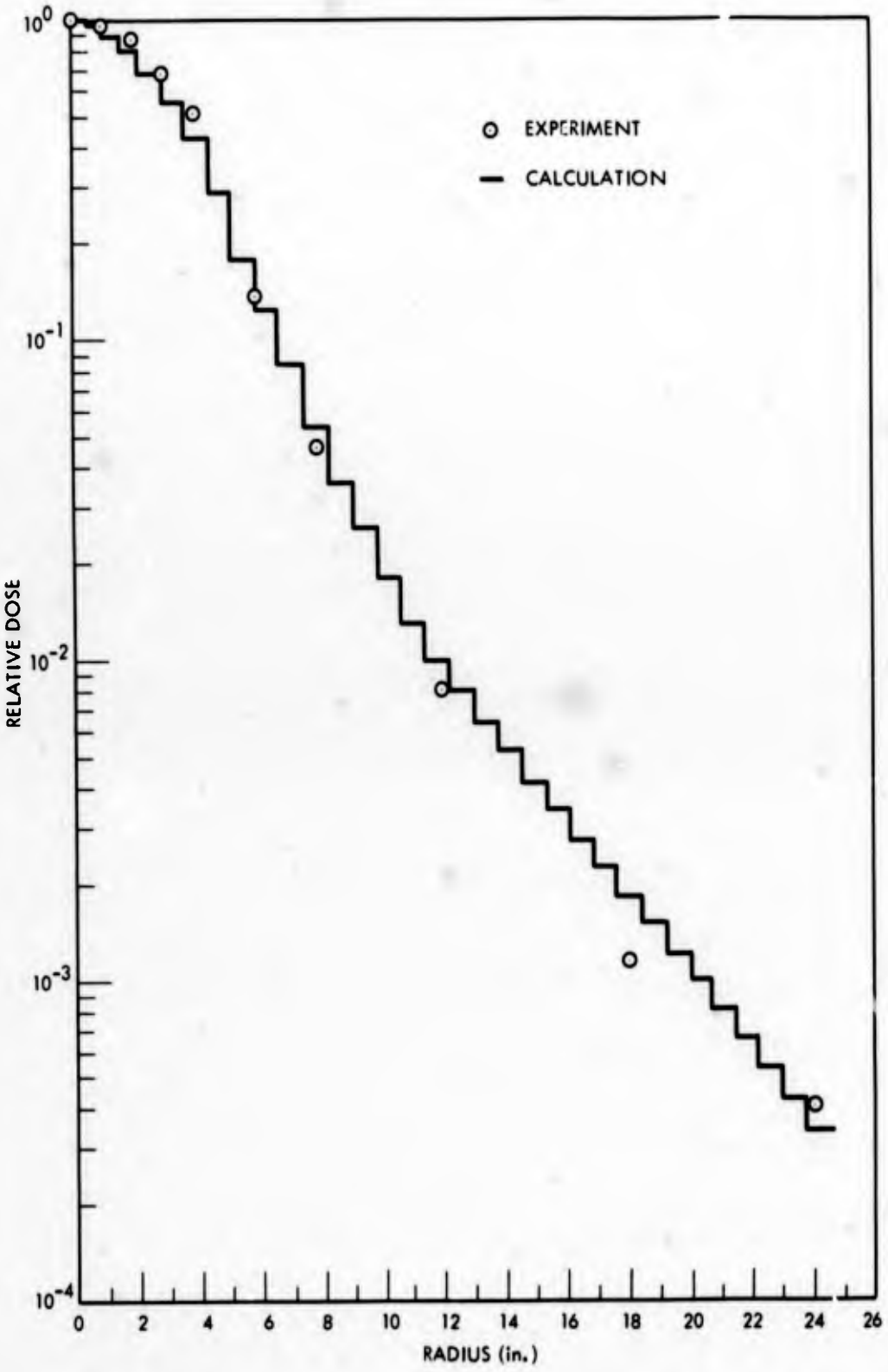

Figure 33. Comparison of calculated and measured dose profiles for the polyethylene slab.

systems. The slab was composed of four 1-1/2-inch lead slabs and three one-inch polyethylene slabs. From an analytical point of view there is no reason to suspect that the discrete ordinates transport method would be limited to homogeneous systems. Thus, the ability to calculate good results for lead and polyethylene separately implies the ability to calculate the laminated slab. For this reason, and due also to the considerable effort involved, the laminated slab was not studied as completely as were the individual lead and polyethylene cases.

Figure 34 shows a comparison of the results of calculations and the experiment for the laminated slab at 30°. The spectrum shows some similarity with both the lead and polyethylene spectra. The agreement of the calculation with the experiment is also similar to that for lead. The results of the S_{10}-P_3 calculation with GAM-II data agrees well up to 6.5 MeV. and then is quite high at the upper energies. The S_{130-10}-P_8 calculation using AWRE and ENDF-B data shows better agreement. The comparison of calculated and measured dose profiles is shown in Figure 35. The shape of the dose traverse also shows the effects of both media in that it is steeper than that for lead but not as steep as that for polyethylene. The disagreement at large radii is similar to that observed for lead and is not considered a significant difficulty because of the low intensity along with the possibility of background effects.

DWG. NO. G-69-583

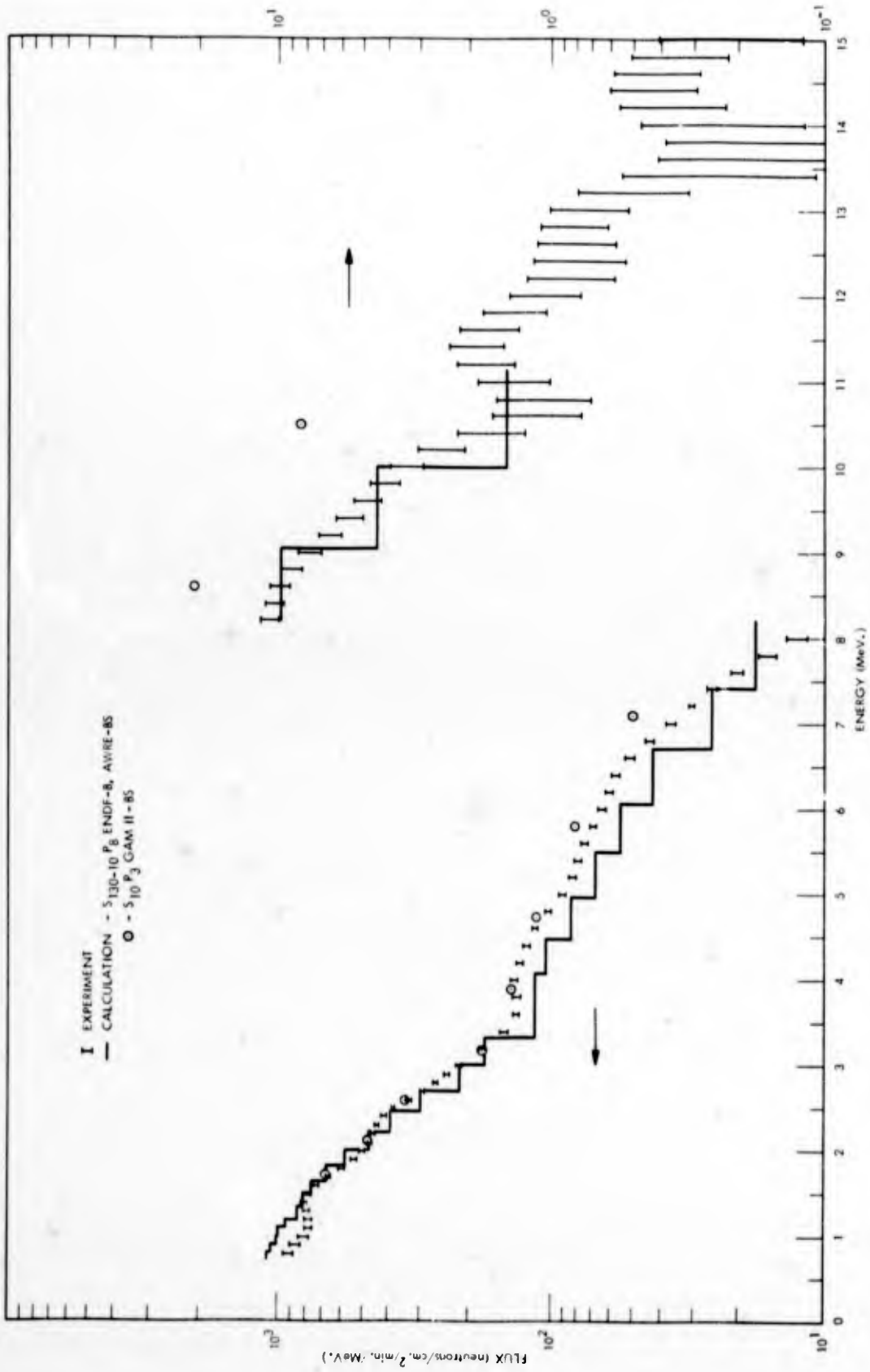

Figure 34. Comparison of calculations with the 30° measurement for the laminated slab.

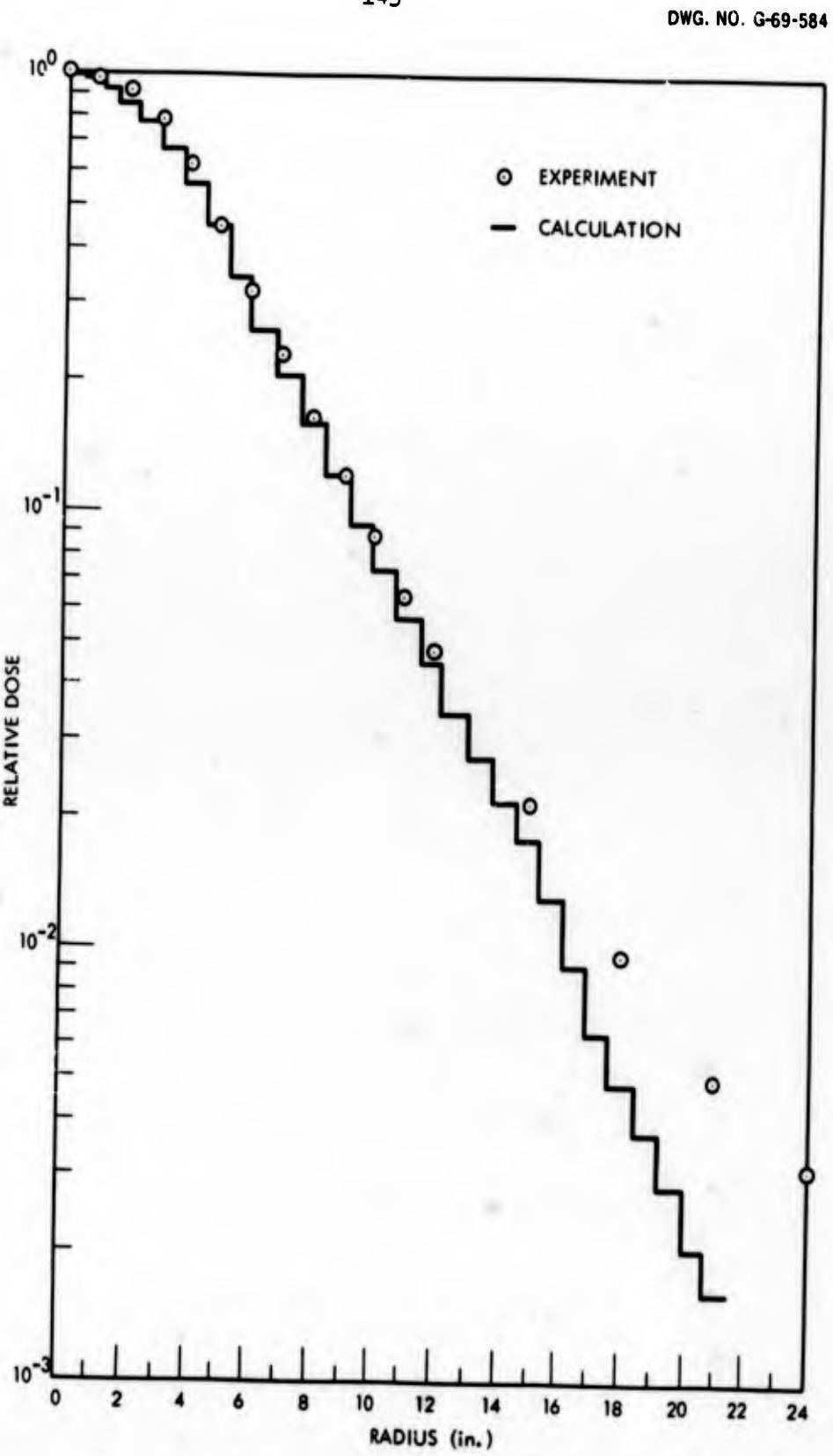

Figure 35. Comparison of calculated and measured dose profiles for the laminated slab.

IV. THE URANIUM SLAB

The depleted uranium slab received even less attention in the analysis effort than the laminated slab. Originally the uranium slab was included in the study because of the disagreements shown by lead slab calculations (with GAM-II cross sections) and experiment at high energies. It was thus desirable to obtain experimental data for another heavy metal which has highly anisotropic elastic scattering. The depleted uranium was available and the cross sections were considered well known. When the AWRE data were made available for the lead calculations and the cross-section effects were identified, the necessity for studying another heavy metal became less urgent.

Figure 36 shows the comparison of calculated and measured spectra for the uranium slab at 30°. The first calculations performed for uranium were similar to those for the other slabs. The GAM-II cross sections with 30 fast groups were used along with the boundary source description. For the uranium comparison the high energy groups agreed fairly well but for the lower energies the calculation was low by a factor of two or more. It was then found that the fissioning of the uranium in the slab was important. A calculation using GAM-II cross sections in the 38-group structure was then performed such that both the fixed boundary source and the fissioning of the slab were included. Of course, this required power or outer iterations in order to compute the distribution of fissions within the slab. It was found that for every neutron incident on the slab

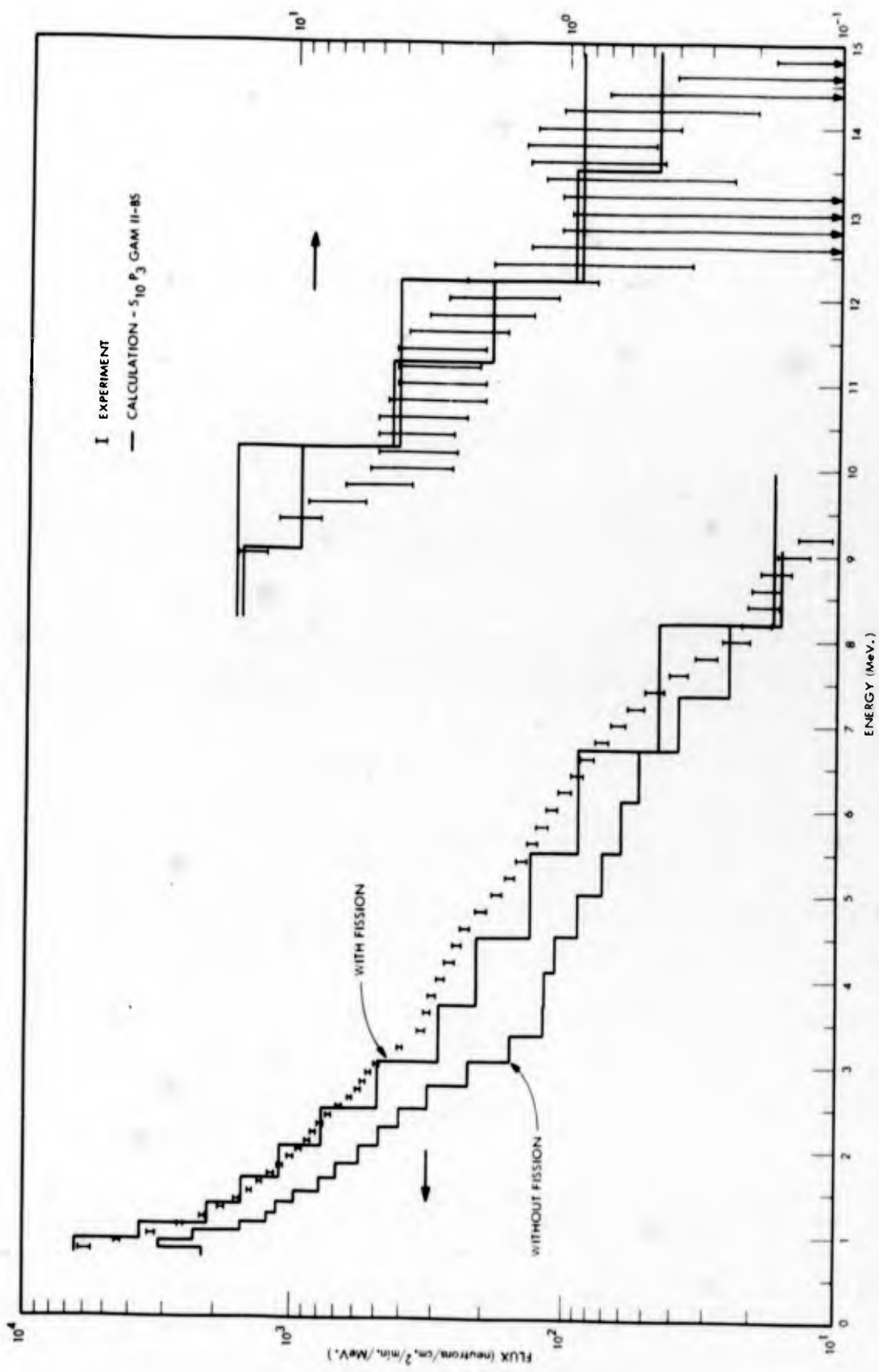

Figure 36. Comparison of calculations with the 30° measurement for the depleted uranium slab.

from the beam, 0.338 neutrons were produced from fission. For this calculation the spectrum above 0.8 MeV given by the first 15 groups of the 38-group structure is shown in Figure 36. The agreement of this calculation with experiment is much better. An extensive study of the uranium data using different cross-section sets and higher order cross-section expansions would require the ability in the code of simultaneously including a fixed boundary source and a fixed space-dependent volumetric source due to fission. Otherwise, each calculation would have to include the energy range down to thermal and compute the power distribution iteratively.

The complete set of experimental data for the depleted uranium slab, including the dose profile, is given in the Appendices. Thus, the data is available for possible further study in the future.

The comparisons of calculations and experimental data presented in this chapter demonstrate the accuracy of the two-dimensional discrete ordinates method in calculating the absolute intensity of angle-dependent spectra and the shape of radial dose profiles. The effects of quadrature, cross-section data, and order of expansion of the scattering angular distribution were also shown. Since both heavy metal slabs with highly anisotropic elastic scattering, hydrogenous slabs with high moderating power, and laminated slabs were considered, the study provides a comprehensive verification of the calculational method.

CHAPTER VII

SUMMARY AND CONCLUSIONS

In this study the two-dimensional discrete ordinates transport method has been improved and extended such that deep-penetration transport problems can be accurately and efficiently calculated. The accuracy and versatility of the method were demonstrated by comparisons of calculations with the results of a clean-geometry experiment.

In Chapter II the discrete ordinates difference equation was derived from the analytic transport equation. A general treatment of anisotropic scattering was included and the method used to generate the difference terms was consistent throughout. The major approximations which were identified during the derivation are due to:

1. the finite size of the space and angle mesh,
2. the finite number of terms in the Legendre expansion of the angular distribution of the scattering transfer cross sections, and
3. the approximation introduced in the multigroup constants due to assumed weighting functions.

The error introduced by these approximations can be estimated by systematically increasing the number of space points, order of Legendre expansion, and number of groups. Thus, in principle, the accuracy of the calculation may be arbitrarily improved within the available capacity.

The phenomenon of "diamond-difference breakdown" was solved by implementing a mixed-mode calculation. In this method the linear model is used whenever possible. A negative flux due to over extrapolation is recalculated with a step model which always gives positive fluxes for positive sources. It was shown that with this mixed-mode model a mesh size of 5 cm. gave good results for neutron transport in water, and even a mesh size of 10 cm. gave a stable result. The effect of this is that the more complex calculations are now quite insensitive to mesh choices, and any reasonable guess for the mesh size will usually be sufficient.

In Chapter III the inner-iteration procedure was discussed from both an analytic and physical basis. It was first shown that, for power iteration, the number of iterations required is related to the number of within-group collisions which can contribute to the answer and is thus a function of the depth of penetration as well as the scattering properties of the media. Integral normalized power iteration was discussed and was shown to be relatively inefficient in deep penetration problems.

Two advanced iteration schemes were incorporated in the method. The semi-iterative method based on Chebyshev polynomials was implemented using an extension of the work of Hageman and Varga. For difficult problems this technique gave convergence in less than one half the number of iterations required by the normalized power iteration method. An extension of the normalized iteration was made such that a separate normalization factor is calculated for each space point. This space-dependent scaling method was shown to give

convergence in as little as one-seventh the number of iterations required by the regular method. This improvement obviously makes the method much more efficient. It is perhaps more important that the point-scaled iteration makes the calculation much less sensitive to the depth of penetration. Thus, one need not be greatly concerned with this effect when preparing a calculation. The zone-of-interest convergence criteria was shown to give a good indication of convergence and was capable of meeting the varied requirements of different problems.

In Chapter IV three improvements which are problem dependent were considered. First, the "ray effect" was described. An analytic first collision source procedure was developed which considerably mitigates this effect. The analytic source procedure is also useful for separating the uncollided flux from the forward collided flux for geometries having monodirectional beam sources.

The problem of the effects of quadrature sets was discussed briefly. The need for flexible quadratures and special tailored quadratures was discussed. A tailored quadrature suitable for high resolution angle-dependent spectra measurements was developed. The procedures for efficiently using the tailored quadratures were also developed.

The problem of calculating the flux at points in space beyond the calculated system was considered. Two approximate methods based on surface integration were developed. An exact method based on an adjoint last flight response function was developed but not fully implemented. A general reciprocity relationship was developed in

order to describe this method.

In Chapter V the need for comparisons with experiment was discussed. Comparisons of calculated and measured fast neutron dose profiles in the ORNL Lid Tank Facility were presented, and the need for detailed angular spectra comparisons was discussed. An experiment to meet these requirements was constructed using the available material and equipment at the ORNL Tower Shielding Facility. Angle-dependent fast neutron spectra and fast neutron dose profiles were obtained for slabs of lead, polyethylene, depleted uranium, and a laminated slab of lead and polyethylene. The instrumentation, experimental technique, and the reliability of the measurements were presented. It was shown that the measurements of the same spectra performed on two different occasions agreed within the indicated experimental uncertainty. The description of the experiment includes considerable detail concerning the source so that other investigators can perform good comparison calculations using other methods.

In Chapter VI calculations using the two-dimensional discrete ordinates method are compared with experiment. For the lead slab the absolute comparisons of angle-dependent spectra give good agreement which is shown to be within the uncertainty due to different cross-section sets. For polyethylene the agreement between calculation and experiment is excellent. For the laminated and depleted uranium slabs the agreement is comparable to that for lead. The comparisons of calculated and measured fast neutron dose profiles show generally good agreement.

In summary, the two-dimensional discrete ordinates method has been developed into a useful and accurate tool for the calculation of radiation transport problems. The previous major difficulties which were instability in the difference solution and the lack of general anisotropic scattering were removed. The development of space-dependent normalized inner iterations and zone-of-interest convergence criteria make it possible to obtain good results for very deep penetration problems. The development of the analytic first collision source technique, flexible quadrature techniques, and special techniques for obtaining the flux in the space beyond the system, are useful and necessary in many problems. Finally, the accurate calculations shown in comparison with the detailed, clean-geometry experiment establishes the accuracy and utility of the method.

Future work should include the obvious extension to transport of other particles and other energy ranges. Work is already in progress for neutron transport from 400 MeV. to 0.001 eV., for gamma rays, x-rays, light, and electrons. Such extensions require thorough investigation, including detailed comparison with experiment in order to establish accuracy and utility.

Extensions of the discrete ordinates methods to include time dependence and other geometries are under consideration. The current work is very preliminary and many investigations will be required in order to determine the most efficient procedures. Extensions to two-dimensional spherical r-θ geometry, the orthogonal three-dimensional geometries, and non-orthogonal geometries should

be investigated to determine practicality.

The present method could be made much more efficient if the space-angle-energy mesh and the Legendre expansion for scattering were variable during problem execution and were adjusted automatically to meet the minimum requirements of the various portions of the problem. For example, a reactor or shield calculation may require a broad space grid, fine angle grid, and high order of scattering expansion at high neutron energies, and a fine space grid, broad angle grid, and low order of scattering expansion at low neutron energies. The methods which could be developed to predict this dependence must be accurate and highly efficient in order to obtain the possible gain.

BIBLIOGRAPHY

BIBLIOGRAPHY

1. Weinberg, A. M., and Eugene P. Wigner, The Physical Theory of Neutron Chain Reactors, pp. 268-271 (The University of Chicago Press, Chicago, 1958).

2. Davison, B., and J. B. Sykes, Neutron Transport Theory, pp. 174-182 (Oxford at the Clarendon Press, London, 1957).

3. Carlson, B. G., Development of the Sn Discrete Ordinates, "A Review of the Discrete Ordinates Sn Method for Radiation Transport Calculations," pp. 1-24, USAEC Report ORNL-RSIC-19, March 1968.

4. Carlson, B. G., and K. D. Lathrop, "Transport Theory, The Method of Discrete Ordinates," USAEC Report LA-3251-MS.

5. Carlson, B. G., and G. I. Bell, Solution of the Transport Equation by the Sn Method, "Proceedings of the Second United Nations International Conference on the Peaceful Uses of Atomic Energy, Geneva, 1956," p. 2386, International Atomic Energy Agency, Geneva, 1958.

6. Carlson, B. G., C. Lee, and J. Worlton, "The DSN and TDC Neutron Transport Codes," USAEC Report LAMS-2346, February 1960.

7. Lee, C. E., "The Discrete Sn Approximation to Transport Theory," USAEC Report LA-2595, March 1962.

8. Lathrop, K. D., and B. G. Carlson, "Discrete Ordinates Angular Quadrature of the Neutron Transport Equation," USAEC Report LA-3186, February 1965.

9. Alexander, J. H., G. W. Hinman, and J. R. Triplett, "GAPLSN - A Modified DSN Program for the Solution of the One-Dimensional Anisotropic Transport Equation," USAEC Report GA-4972, 1964.

10. Craven, C. W., Jr., "Inscatter Approximations in Discrete Variable Transport Theory," USAEC Report ORNL-3966 (to be issued).

11. Lathrop, K. D., "DTF-IV, A Fortran IV Program for Solving the Multigroup Transport Equation with Anisotropic Scattering," USAEC Report LA-3373, 1965.

12. Engle, W. W., Jr., "A User's Manual for ANISN, A One-Dimensional Discrete Ordinates Transport Code with Anisotropic Scattering," USAEC Report K-1693, 1967.

13. Taylor, A. E., Advanced Calculus, p. 52 (Ginn and Company, Boston, 1955).

14. Jahnke, E., and F. Ende, Tables of Functions, p. 115 (Dover Publications, New York, 1945).

15. Carlson, B. G., "Numerical Solution of Transient and Steady-State Neutron Transport Problems," USAEC Report LA-2260, October 1959.

16. Carlson, B. G., Numerical Solution of Neutron Transport Problems, "Proceedings of Symposium in Applied Mathematics, Volume XI," American Mathematics Society, 1961.

17. Joanou, G. D., and J. S. Dudek, "GAM-II: A B_3 Code for the Calculation of Fast Neutron Spectra and Associated Multigroup Constants," USAEC Report GA-4265, 1963.

18. Hageman, L. A., "The Chebyshev Polynomial Method of Iteration," USAEC Report WAPD-TM-537, January 1967.

19. Honeck, H. C., "THERMOS, A Thermalization Theory Code for Reactor Lattice Calculations," USAEC Report BNL-5826.

20. Wachspress, E. L., Iterative Solution of Elliptic Systems (Prentice Hall, New Jersey, 1966).

21. Varga, R. S., Matrix Iterative Analysis (Prentice Hall, New Jersey, 1966).

22. Engle, W. W., Jr., and F. R. Mynatt, "A Comparison of Two Methods of Inner Iteration Convergence Acceleration in Discrete Ordinates Codes," Transactions of the American Nuclear Society, Volume II, No. 1, American Nuclear Society, June 1968.

23. Askew, J. R., and R. J. Brissenden, "Some Improvements with Discrete Ordinates Method of B. G. Carlson for Solving the Neutron Transport Equation," UKAEA Report AEEW-R161, August 1963.

24. Carlson, B. G., "A Method of Moments for Solving the Neutron Transport Equation," USAEC Report LA-3060, February 1965.

25. Case, K. M., F. de Hoffmann, and G. Placzek, Introduction to the Theory of Neutron Diffusion, U. S. Government Printing Office, Washington, D. C., 1953.

26. Mynatt, F. R., N. M. Greene, and W. W. Engle, Jr., "On the Application of Discrete Ordinates Transport Theory to Deep-Penetration Fast Neutron Dose Calculations in Water," Transactions of the American Nuclear Society, Volume IX, No. 2, American Nuclear Society, October, 1966.

27. Trubey, D. K., and M. B. Emmett, "A Comparison of First and Last Flight Expectation Values Used in an 05R Monte Carlo Calculation of Neutron Distributions in Water," USAEC Report ORNL-RSIC-3 1965.

28. Henderson, B. J., "Conversion of Neutron or Gamma-Ray Flux to Absorbed Dose Rate," USAEC Report XDC 58-8-179, August 1959.

29. Clifford, C. E., private communication.

30. Clifford, C. E., and L. B. Holland, "Design for a Spherical Tower Shielding Reactor (TSR-II)," USAEC Report ORNL-2389, Chapter 3.1, October 1957.

31. Straker, E. A., "Fast-Neutron Collimator Studies in the Design of the TSF-SNAP Core Mapping Collimator," Oak Ridge National Laboratory Report ORNL-TM-2299, August 1968.

32. Verbinski, V. V., et al., "Calibration of an Organic Scintillator for Neutron Spectrometry," Oak Ridge National Laboratory Report ORNL-TM-2183, June 1968.

33. Burrus, W. R., and V. V. Verbinski, "Fast-Neutron Spectroscopy with Thick Organic Scintillator" (unpublished report).

34. Clifford, C. E., et al., "Measurements of the Spectra of Uncollided Fission Neutrons Transmitted Through Thick Samples of Nitrogen, Oxygen, Carbon and Lead: Investigation of the Minima in Total Cross Sections," Oak Ridge National Laboratory Report ORNL-TM-1656, March 1967.

35. Hurst, G. S., "Fast Neutron Dosimetry," Chapter IVG in Fast Neutron Physics, J. L. Fowler and J. Marion, Editors (Interscience Press, New York, 1960).

36. Muckenthaler, F. J., "Development of the Hornyak Button as a Fast-Neutron Dosimeter," USAEC Report ORNL-2389, October 1957 (Chapter 10.6).

37. Muckenthaler, F. J., and R. M. Freestone, private communication.

38. Buckingham, B. R. S., K. Parker, and E. D. Pendlebury, "Neutron Cross Sections of Selected Elements and Isotopes for Use in Neutronics Calculations in the Energy Range 0.025 eV. - 15 MeV.," UKAEA Report AWRE 0-28/60, March 1961.

39. Yost, K. J., and N. M. Greene, "CSP-I: A Neutron Cross-Section Averaging Package for Use with the 05R Data Tape," USAEC Report ORNL-4130, December 1967.

40. Craven, C. W., Jr., and J. L. Lucius, "TRANSFER: A Program to Calculate Pn Multigroup Scattering Matrices," USAEC Report ORNL-TM-1537, May 1966.

41. Stehn, J. R., et al., "Neutron Cross Sections, Volume II-C, Z = 61-87," USAEC Report BNL-325, Second Edition, August 1966.

42. ENDF-B Nuclear Data File, Tapes 114 and 115.

APPENDICES

APPENDIX A

FAST NEUTRON SPECTRA

Tables VI through XXXVI contain the bulk of the spectra taken during the experiment. The title of each table indicates the run number, the sample, and the angle. The data in the tables are the outputs of the FERDOR unfolding code. For each energy point the upper and lower limits define the one standard deviation error bounds for the spectra. All spectra are normalized to a reactor power of 100 kilowatts and have units of neutrons/cm.^{2}/min./MeV.

TABLE VI

RUN 22C+22D BARE BEAM AT 0 DEG.

ENERGY	UPPER LIMIT	LOWER LIMIT	ENERGY	UPPER LIMIT	LOWER LIMIT
8.00E 05	3.971E 06	3.708E 06	7.00E 06	1.379E 05	1.319E 05
9.00E 05	3.529E 06	3.237E 06	7.20E 06	1.175E 05	1.119E 05
1.00E 06	3.173E 06	2.938E 06	7.40E 06	1.021E 05	9.694E 04
1.10E 06	3.074E 06	2.888E 06	7.60E 06	8.993E 04	8.506E 04
1.20E 06	3.137E 06	2.975E 06	7.80E 06	7.944E 04	7.485E 04
1.30E 06	3.200E 06	3.050E 06	8.00E 06	6.995E 04	6.566E 04
1.40E 06	3.147E 06	2.993E 06	8.20E 06	6.108E 04	5.708E 04
1.50E 06	2.990E 06	2.839E 06	8.40E 06	5.290E 04	4.904E 04
1.60E 06	2.824E 06	2.686E 06	8.60E 06	4.572E 04	4.205E 04
1.70E 06	2.702E 06	2.577E 06	8.80E 06	4.000E 04	3.656E 04
1.80E 06	2.606E 06	2.490E 06	9.00E 06	3.619E 04	3.296E 04
1.90E 06	2.508E 06	2.406E 06	9.20E 06	3.394E 04	3.088E 04
2.00E 06	2.397E 06	2.308E 06	9.40E 06	3.178E 04	2.883E 04
2.10E 06	2.283E 06	2.204E 06	9.60E 06	2.842E 04	2.558E 04
2.20E 06	2.177E 06	2.107E 06	9.80E 06	2.388E 04	2.121E 04
2.30E 06	2.067E 06	2.007E 06	1.00E 07	1.901E 04	1.652E 04
2.40E 06	1.936E 06	1.882E 06	1.02E 07	1.460E 04	1.222E 04
2.50E 06	1.779E 06	1.732E 06	1.04E 07	1.124E 04	8.947E 03
2.60E 06	1.614E 06	1.574E 06	1.06E 07	9.286E 03	6.979E 03
2.70E 06	1.461E 06	1.424E 06	1.08E 07	8.423E 03	5.949E 03
2.80E 06	1.325E 06	1.290E 06	1.10E 07	7.871E 03	5.248E 03
2.90E 06	1.199E 06	1.166E 06	1.12E 07	7.153E 03	4.610E 03
3.00E 06	1.073E 06	1.043E 06	1.14E 07	6.455E 03	4.152E 03
3.20E 06	8.233E 05	7.991E 05	1.16E 07	6.175E 03	4.047E 03
3.40E 06	6.422E 05	6.203E 05	1.18E 07	6.361E 03	4.272E 03
3.60E 06	5.612E 05	5.399E 05	1.20E 07	6.593E 03	4.458E 03
3.80E 06	5.394E 05	5.197E 05	1.22E 07	6.477E 03	4.286E 03
4.00E 06	5.332E 05	5.155E 05	1.24E 07	5.891E 03	3.734E 03
4.20E 06	5.121E 05	4.970E 05	1.26E 07	5.055E 03	3.086E 03
4.40E 06	4.723E 05	4.588E 05	1.28E 07	4.380E 03	2.656E 03
4.60E 06	4.225E 05	4.105E 05	1.30E 07	4.139E 03	2.537E 03
4.80E 06	3.743E 05	3.637E 05	1.32E 07	4.225E 03	2.637E 03
5.00E 06	3.329E 05	3.229E 05	1.34E 07	4.332E 03	2.798E 03
5.20E 06	2.997E 05	2.900E 05	1.36E 07	4.291E 03	2.866E 03
5.40E 06	2.778E 05	2.684E 05	1.38E 07	4.113E 03	2.803E 03
5.60E 06	2.628E 05	2.538E 05	1.40E 07	3.896E 03	2.687E 03
5.80E 06	2.475E 05	2.388E 05	1.42E 07	3.728E 03	2.610E 03
6.00E 06	2.306E 05	2.225E 05	1.44E 07	3.628E 03	2.595E 03
6.20E 06	2.155E 05	2.079E 05	1.46E 07	3.556E 03	2.581E 03
6.40E 06	2.017E 05	1.945E 05	1.48E 07	3.451E 03	2.510E 03
6.60E 06	1.845E 05	1.776E 05	1.50E 07	3.290E 03	2.383E 03
6.80E 06	1.618E 05	1.554E 05			

TABLE VII

RUN 24A+24B BARE BEAM AT 4.16 DEG.

ENERGY	UPPER LIMIT	LOWER LIMIT	ENERGY	UPPER LIMIT	LOWER LIMIT
8.00E 05	1.149E 06	1.072E 06	7.00E 06	4.625E 04	4.376E 04
9.00E 05	1.014E 06	9.272E 05	7.20E 06	3.936E 04	3.700E 04
1.00E 06	9.160E 05	8.463E 05	7.40E 06	3.377E 04	3.160E 04
1.10E 06	9.037E 05	8.480E 05	7.60E 06	2.965E 04	2.763E 04
1.20E 06	9.346E 05	8.863E 05	7.80E 06	2.617E 04	2.426E 04
1.30E 06	9.384E 05	8.931E 05	8.00E 06	2.283E 04	2.104E 04
1.40E 06	9.102E 05	8.638E 05	8.20E 06	1.972E 04	1.807E 04
1.50E 06	8.708E 05	8.252E 05	8.40E 06	1.700E 04	1.539E 04
1.60E 06	8.325E 05	7.908E 05	8.60E 06	1.468E 04	1.313E 04
1.70E 06	8.068E 05	7.688E 05	8.80E 06	1.292E 04	1.148E 04
1.80E 06	7.883E 05	7.530E 05	9.00E 06	1.176E 04	1.041E 04
1.90E 06	7.625E 05	7.315E 05	9.20E 06	1.093E 04	9.608E 03
2.00E 06	7.289E 05	7.018E 05	9.40E 06	1.006E 04	8.790E 03
2.10E 06	6.918E 05	6.677E 05	9.60E 06	9.015E 03	7.809E 03
2.20E 06	6.535E 05	6.321E 05	9.80E 06	7.829E 03	6.679E 03
2.30E 06	6.146E 05	5.962E 05	1.00E 07	6.602E 03	5.514E 03
2.40E 06	5.742E 05	5.578E 05	1.02E 07	5.432E 03	4.400E 03
2.50E 06	5.294E 05	5.151E 05	1.04E 07	4.340E 03	3.333E 03
2.60E 06	4.816E 05	4.692E 05	1.06E 07	3.339E 03	2.294E 03
2.70E 06	4.350E 05	4.234E 05	1.08E 07	2.514E 03	1.383E 03
2.80E 06	3.922E 05	3.811E 05	1.10E 07	1.950E 03	7.579E 02
2.90E 06	3.533E 05	3.430E 05	1.12E 07	1.605E 03	4.426E 02
3.00E 06	3.170E 05	3.074E 05	1.14E 07	1.351E 03	2.708E 02
3.20E 06	2.519E 05	2.443E 05	1.16E 07	1.154E 03	1.199E 02
3.40E 06	2.058E 05	1.987E 05	1.18E 07	1.137E 03	9.418E 01
3.60E 06	1.822E 05	1.753E 05	1.20E 07	1.404E 03	3.274E 02
3.80E 06	1.726E 05	1.661E 05	1.22E 07	1.858E 03	7.627E 02
4.00E 06	1.677E 05	1.617E 05	1.24E 07	2.222E 03	1.148E 03
4.20E 06	1.588E 05	1.535E 05	1.26E 07	2.272E 03	1.264E 03
4.40E 06	1.458E 05	1.408E 05	1.28E 07	2.069E 03	1.140E 03
4.60E 06	1.331E 05	1.284E 05	1.30E 07	1.876E 03	9.970E 02
4.80E 06	1.223E 05	1.180E 05	1.32E 07	1.855E 03	1.011E 03
5.00E 06	1.124E 05	1.083E 05	1.34E 07	1.973E 03	1.169E 03
5.20E 06	1.023E 05	9.825E 04	1.36E 07	2.110E 03	1.352E 03
5.40E 06	9.139E 04	8.751E 04	1.38E 07	2.176E 03	1.475E 03
5.60E 06	8.227E 04	7.857E 04	1.40E 07	2.154E 03	1.507E 03
5.80E 06	7.675E 04	7.316E 04	1.42E 07	2.062E 03	1.453E 03
6.00E 06	7.320E 04	6.984E 04	1.44E 07	1.924E 03	1.341E 03
6.20E 06	6.899E 04	6.581E 04	1.46E 07	1.768E 03	1.210E 03
6.40E 06	6.388E 04	6.088E 04	1.48E 07	1.638E 03	1.106E 03
6.60E 06	5.873E 04	5.585E 04	1.50E 07	1.575E 03	1.074E 03
6.80E 06	5.299E 04	5.033E 04			

TABLE VIII

RUN 23A+23B BARE BEAM AT 8.6 DEG.

ENERGY	UPPER LIMIT	LOWER LIMIT	ENERGY	UPPER LIMIT	LOWER LIMIT
8.00E 05	9.733E 03	9.047E 03	7.00E 06	5.103E 02	4.716E 02
9.00E 05	9.271E 03	8.517E 03	7.20E 06	4.437E 02	4.065E 02
1.00E 06	8.276E 03	7.679E 03	7.40E 06	3.742E 02	3.392E 02
1.10E 06	7.602E 03	7.125E 03	7.60E 06	3.106E 02	2.774E 02
1.20E 06	7.783E 03	7.369E 03	7.80E 06	2.541E 02	2.226E 02
1.30E 06	8.092E 03	7.708E 03	8.00E 06	2.040E 02	1.738E 02
1.40E 06	7.995E 03	7.601E 03	8.20E 06	1.625E 02	1.334E 02
1.50E 06	7.479E 03	7.097E 03	8.40E 06	1.327E 02	1.034E 02
1.60E 06	6.793E 03	6.443E 03	8.60E 06	1.138E 02	8.454E 01
1.70E 06	6.225E 03	5.899E 03	8.80E 06	1.070E 02	7.814E 01
1.80E 06	5.917E 03	5.606E 03	9.00E 06	1.153E 02	8.694E 01
1.90E 06	5.763E 03	5.487E 03	9.20E 06	1.324E 02	1.041E 02
2.00E 06	5.611E 03	5.367E 03	9.40E 06	1.399E 02	1.103E 02
2.10E 06	5.399E 03	5.183E 03	9.60E 06	1.229E 02	9.067E 01
2.20E 06	5.150E 03	4.952E 03	9.80E 06	8.096E 01	4.679E 01
2.30E 06	4.903E 03	4.723E 03	1.00E 07	2.205E 01	-1.304E 01
2.40E 06	4.680E 03	4.515E 03	1.02E 07	-5.125E 01	-8.701E 01
2.50E 06	4.449E 03	4.307E 03	1.04E 07	-1.408E 02	-1.797E 02
2.60E 06	4.167E 03	4.045E 03	1.06E 07	-2.432E 02	-2.898E 02
2.70E 06	3.845E 03	3.723E 03	1.08E 07	-3.428E 02	-4.004E 02
2.80E 06	3.502E 03	3.377E 03	1.10E 07	-4.175E 02	-4.832E 02
2.90E 06	3.177E 03	3.057E 03	1.12E 07	-4.497E 02	-5.161E 02
3.00E 06	2.878E 03	2.767E 03	1.14E 07	-4.333E 02	-4.969E 02
3.20E 06	2.328E 03	2.237E 03	1.16E 07	-3.709E 02	-4.344E 02
3.40E 06	1.905E 03	1.818E 03	1.18E 07	-2.683E 02	-3.349E 02
3.60E 06	1.709E 03	1.621E 03	1.20E 07	-1.441E 02	-2.149E 02
3.80E 06	1.657E 03	1.568E 03	1.22E 07	-1.919E 01	-9.331E 01
4.00E 06	1.651E 03	1.566E 03	1.24E 07	9.634E 01	2.261E 01
4.20E 06	1.636E 03	1.559E 03	1.26E 07	2.103E 02	1.424E 02
4.40E 06	1.572E 03	1.497E 03	1.28E 07	3.363E 02	2.758E 02
4.60E 06	1.432E 03	1.361E 03	1.30E 07	4.751E 02	4.180E 02
4.80E 06	1.262E 03	1.198E 03	1.32E 07	6.091E 02	5.533E 02
5.00E 06	1.130E 03	1.070E 03	1.34E 07	7.146E 02	6.625E 02
5.20E 06	1.028E 03	9.674E 02	1.36E 07	7.745E 02	7.278E 02
5.40E 06	9.246E 02	8.656E 02	1.38E 07	7.812E 02	7.401E 02
5.60E 06	8.275E 02	7.707E 02	1.40E 07	7.373E 02	7.012E 02
5.80E 06	7.567E 02	7.015E 02	1.42E 07	6.545E 02	6.224E 02
6.00E 06	7.235E 02	6.730E 02	1.44E 07	5.498E 02	5.214E 02
6.20E 06	7.026E 02	6.551E 02	1.46E 07	4.404E 02	4.157E 02
6.40E 06	6.654E 02	6.199E 02	1.48E 07	3.399E 02	3.188E 02
6.60E 06	6.162E 02	5.721E 02	1.50E 07	2.555E 02	2.377E 02
6.80E 06	5.661E 02	5.252E 02			

TABLE IX

RUN 33A+30C BARE BEAM AT 0 DEG.

ENERGY	UPPER LIMIT	LOWER LIMIT	ENERGY	UPPER LIMIT	LOWER LIMIT
8.00E 05	3.961E 06	3.693E 06	7.00E 06	1.357E 05	1.314E 05
9.00E 05	3.524E 06	3.227E 06	7.20E 06	1.165E 05	1.124E 05
1.00E 06	3.150E 06	2.912E 06	7.40E 06	1.005E 05	9.676E 04
1.10E 06	3.072E 06	2.884E 06	7.60E 06	8.712E 04	8.364E 04
1.20E 06	3.200E 06	3.037E 06	7.80E 06	7.518E 04	7.189E 04
1.30E 06	3.269E 06	3.118E 06	8.00E 06	6.454E 04	6.147E 04
1.40E 06	3.190E 06	3.037E 06	8.20E 06	5.599E 04	5.313E 04
1.50E 06	3.032E 06	2.881E 06	8.40E 06	4.965E 04	4.690E 04
1.60E 06	2.875E 06	2.738E 06	8.60E 06	4.494E 04	4.234E 04
1.70E 06	2.753E 06	2.629E 06	8.80E 06	4.101E 04	3.861E 04
1.80E 06	2.646E 06	2.531E 06	9.00E 06	3.710E 04	3.482E 04
1.90E 06	2.533E 06	2.433E 06	9.20E 06	3.284E 04	3.066E 04
2.00E 06	2.414E 06	2.327E 06	9.40E 06	2.850E 04	2.646E 04
2.10E 06	2.292E 06	2.214E 06	9.60E 06	2.462E 04	2.270E 04
2.20E 06	2.170E 06	2.101E 06	9.80E 06	2.142E 04	1.962E 04
2.30E 06	2.044E 06	1.985E 06	1.00E 07	1.881E 04	1.713E 04
2.40E 06	1.908E 06	1.856E 06	1.02E 07	1.653E 04	1.498E 04
2.50E 06	1.759E 06	1.714E 06	1.04E 07	1.443E 04	1.297E 04
2.60E 06	1.604E 06	1.565E 06	1.06E 07	1.250E 04	1.108E 04
2.70E 06	1.450E 06	1.414E 06	1.08E 07	1.072E 04	9.328E 03
2.80E 06	1.302E 06	1.267E 06	1.10E 07	9.112E 03	7.737E 03
2.90E 06	1.160E 06	1.128E 06	1.12E 07	7.672E 03	6.373E 03
3.00E 06	1.026E 06	9.964E 05	1.14E 07	6.446E 03	5.260E 03
3.20E 06	7.969E 05	7.732E 05	1.16E 07	5.449E 03	4.356E 03
3.40E 06	6.398E 05	6.183E 05	1.18E 07	4.683E 03	3.647E 03
3.60E 06	5.622E 05	5.414E 05	1.20E 07	4.143E 03	3.139E 03
3.80E 06	5.365E 05	5.174E 05	1.22E 07	3.842E 03	2.870E 03
4.00E 06	5.232E 05	5.058E 05	1.24E 07	3.716E 03	2.820E 03
4.20E 06	4.986E 05	4.840E 05	1.26E 07	3.587E 03	2.814E 03
4.40E 06	4.632E 05	4.504E 05	1.28E 07	3.300E 03	2.607E 03
4.60E 06	4.179E 05	4.068E 05	1.30E 07	2.844E 03	2.160E 03
4.80E 06	3.675E 05	3.580E 05	1.32E 07	2.336E 03	1.688E 03
5.00E 06	3.230E 05	3.146E 05	1.34E 07	1.949E 03	1.386E 03
5.20E 06	2.917E 05	2.836E 05	1.36E 07	1.752E 03	1.274E 03
5.40E 06	2.711E 05	2.637E 05	1.38E 07	1.675E 03	1.253E 03
5.60E 06	2.538E 05	2.470E 05	1.40E 07	1.602E 03	1.213E 03
5.80E 06	2.373E 05	2.304E 05	1.42E 07	1.465E 03	1.101E 03
6.00E 06	2.210E 05	2.145E 05	1.44E 07	1.263E 03	9.277E 02
6.20E 06	2.064E 05	2.006E 05	1.46E 07	1.036E 03	7.376E 02
6.40E 06	1.929E 05	1.876E 05	1.48E 07	8.268E 02	5.675E 02
6.60E 06	1.768E 05	1.718E 05	1.50E 07	6.621E 02	4.323E 02
6.80E 06	1.567E 05	1.521E 05			

TABLE X

RUN 33B+29F BARE BEAM AT 4.16 DEG.

ENERGY	UPPER LIMIT	LOWER LIMIT	ENERGY	UPPER LIMIT	LOWER LIMIT
8.00E 05	1.094E 06	1.012E 06	7.00E 06	3.950E 04	3.808E 04
9.00E 05	9.768E 05	8.925E 05	7.20E 06	3.387E 04	3.252E 04
1.00E 06	8.777E 05	8.108E 05	7.40E 06	2.894E 04	2.770E 04
1.10E 06	8.696E 05	8.170E 05	7.60E 06	2.509E 04	2.393E 04
1.20E 06	9.222E 05	8.769E 05	7.80E 06	2.221E 04	2.112E 04
1.30E 06	9.449E 05	9.029E 05	8.00E 06	1.979E 04	1.876E 04
1.40E 06	9.114E 05	8.688E 05	8.20E 06	1.748E 04	1.653E 04
1.50E 06	8.482E 05	8.066E 05	8.40E 06	1.534E 04	1.443E 04
1.60E 06	7.858E 05	7.479E 05	8.60E 06	1.343E 04	1.257E 04
1.70E 06	7.463E 05	7.120E 05	8.80E 06	1.175E 04	1.095E 04
1.80E 06	7.250E 05	6.932E 05	9.00E 06	1.033E 04	9.575E 03
1.90E 06	7.046E 05	6.769E 05	9.20E 06	9.210E 03	8.485E 03
2.00E 06	6.772E 05	6.530E 05	9.40E 06	8.294E 03	7.610E 03
2.10E 06	6.423E 05	6.208E 05	9.60E 06	7.435E 03	6.787E 03
2.20E 06	6.021E 05	5.832E 05	9.80E 06	6.554E 03	5.938E 03
2.30E 06	5.591E 05	5.428E 05	1.00E 07	5.690E 03	5.115E 03
2.40E 06	5.165E 05	5.021E 05	1.02E 07	4.913E 03	4.384E 03
2.50E 06	4.758E 05	4.632E 05	1.04E 07	4.230E 03	3.731E 03
2.60E 06	4.363E 05	4.254E 05	1.06E 07	3.621E 03	3.128E 03
2.70E 06	3.966E 05	3.864E 05	1.08E 07	3.114E 03	2.624E 03
2.80E 06	3.551E 05	3.455E 05	1.10E 07	2.765E 03	2.292E 03
2.90E 06	3.136E 05	3.046E 05	1.12E 07	2.555E 03	2.110E 03
3.00E 06	2.750E 05	2.666E 05	1.14E 07	2.374E 03	1.962E 03
3.20E 06	2.144E 05	2.077E 05	1.16E 07	2.137E 03	1.753E 03
3.40E 06	1.756E 05	1.695E 05	1.18E 07	1.857E 03	1.499E 03
3.60E 06	1.558E 05	1.499E 05	1.20E 07	1.617E 03	1.280E 03
3.80E 06	1.495E 05	1.441E 05	1.22E 07	1.454E 03	1.135E 03
4.00E 06	1.459E 05	1.410E 05	1.24E 07	1.340E 03	1.044E 03
4.20E 06	1.375E 05	1.333E 05	1.26E 07	1.222E 03	9.589E 02
4.40E 06	1.269E 05	1.232E 05	1.28E 07	1.072E 03	8.413E 02
4.60E 06	1.173E 05	1.141E 05	1.30E 07	8.961E 02	6.863E 02
4.80E 06	1.080E 05	1.052E 05	1.32E 07	7.117E 02	5.143E 02
5.00E 06	9.836E 04	9.583E 04	1.34E 07	5.347E 02	3.516E 02
5.20E 06	8.877E 04	8.635E 04	1.36E 07	3.851E 02	2.194E 02
5.40E 06	7.955E 04	7.731E 04	1.38E 07	2.817E 02	1.342E 02
5.60E 06	7.160E 04	6.946E 04	1.40E 07	2.336E 02	1.020E 02
5.80E 06	6.574E 04	6.361E 04	1.42E 07	2.344E 02	1.143E 02
6.00E 06	6.216E 04	6.019E 04	1.44E 07	2.639E 02	1.521E 02
6.20E 06	5.957E 04	5.774E 04	1.46E 07	2.971E 02	1.919E 02
6.40E 06	5.633E 04	5.462E 04	1.48E 07	3.146E 02	2.147E 02
6.60E 06	5.150E 04	4.985E 04	1.50E 07	3.079E 02	2.124E 02
6.80E 06	4.553E 04	4.401E 04			

TABLE XI

RUN 33C+29E BARE BEAM AT 8.6 DEG.

ENERGY	UPPER LIMIT	LOWER LIMIT	ENERGY	UPPER LIMIT	LOWER LIMIT
8.00E 05	8.461E 03	7.849E 03	7.00E 06	4.844E 02	4.477E 02
9.00E 05	7.853E 03	7.170E 03	7.20E 06	4.027E 02	3.674E 02
1.00E 06	7.071E 03	6.516E 03	7.40E 06	3.240E 02	2.913E 02
1.10E 06	6.985E 03	6.537E 03	7.60E 06	2.760E 02	2.456E 02
1.20E 06	7.593E 03	7.205E 03	7.80E 06	2.561E 02	2.272E 02
1.30E 06	7.951E 03	7.589E 03	8.00E 06	2.431E 02	2.154E 02
1.40E 06	7.679E 03	7.307E 03	8.20E 06	2.240E 02	1.980E 02
1.50E 06	7.054E 03	6.693E 03	8.40E 06	2.015E 02	1.765E 02
1.60E 06	6.470E 03	6.141E 03	8.60E 06	1.777E 02	1.540E 02
1.70E 06	6.019E 03	5.713E 03	8.80E 06	1.508E 02	1.284E 02
1.80E 06	5.655E 03	5.364E 03	9.00E 06	1.217E 02	9.997E 01
1.90E 06	5.415E 03	5.160E 03	9.20E 06	9.621E 01	7.489E 01
2.00E 06	5.305E 03	5.080E 03	9.40E 06	8.243E 01	6.177E 01
2.10E 06	5.234E 03	5.032E 03	9.60E 06	8.459E 01	6.519E 01
2.20E 06	5.088E 03	4.905E 03	9.80E 06	9.730E 01	7.920E 01
2.30E 06	4.815E 03	4.652E 03	1.00E 07	1.070E 02	8.963E 01
2.40E 06	4.477E 03	4.327E 03	1.02E 07	1.024E 02	8.562E 01
2.50E 06	4.131E 03	4.000E 03	1.04E 07	8.333E 01	6.713E 01
2.60E 06	3.835E 03	3.721E 03	1.06E 07	5.905E 01	4.324E 01
2.70E 06	3.592E 03	3.481E 03	1.08E 07	4.015E 01	2.475E 01
2.80E 06	3.373E 03	3.259E 03	1.10E 07	3.229E 01	1.744E 01
2.90E 06	3.131E 03	3.021E 03	1.12E 07	3.440E 01	2.017E 01
3.00E 06	2.852E 03	2.748E 03	1.14E 07	4.097E 01	2.765E 01
3.20E 06	2.233E 03	2.146E 03	1.16E 07	4.625E 01	3.381E 01
3.40E 06	1.803E 03	1.718E 03	1.18E 07	4.617E 01	3.417E 01
3.60E 06	1.641E 03	1.555E 03	1.20E 07	4.060E 01	2.894E 01
3.80E 06	1.601E 03	1.516E 03	1.22E 07	3.191E 01	2.065E 01
4.00E 06	1.602E 03	1.519E 03	1.24E 07	2.319E 01	1.264E 01
4.20E 06	1.583E 03	1.509E 03	1.26E 07	1.686E 01	7.488E 00
4.40E 06	1.489E 03	1.418E 03	1.28E 07	1.414E 01	5.917E 00
4.60E 06	1.317E 03	1.252E 03	1.30E 07	1.462E 01	6.911E 00
4.80E 06	1.143E 03	1.082E 03	1.32E 07	1.633E 01	8.933E 00
5.00E 06	1.011E 03	9.525E 02	1.34E 07	1.741E 01	1.045E 01
5.20E 06	9.140E 02	8.566E 02	1.36E 07	1.696E 01	1.068E 01
5.40E 06	8.365E 02	7.810E 02	1.38E 07	1.513E 01	9.600E 00
5.60E 06	7.806E 02	7.275E 02	1.40E 07	1.255E 01	7.631E 00
5.80E 06	7.465E 02	6.946E 02	1.42E 07	9.853E 00	5.375E 00
6.00E 06	7.141E 02	6.653E 02	1.44E 07	7.447E 00	3.374E 00
6.20E 06	6.732E 02	6.269E 02	1.46E 07	5.564E 00	1.869E 00
6.40E 06	6.292E 02	5.854E 02	1.48E 07	4.280E 00	8.297E-01
6.60E 06	5.895E 02	5.471E 02	1.50E 07	3.538E 00	1.584E-01
6.80E 06	5.458E 02	5.067E 02			

TABLE XII

RUN 50B+50C BARE BEAM AT 0 DEG.

ENERGY	UPPER LIMIT	LOWER LIMIT	ENERGY	UPPER LIMIT	LOWER LIMIT
8.00E 05	4.138E 06	3.859E 06	7.00E 06	1.368E 05	1.326E 05
9.00E 05	3.697E 06	3.389E 06	7.20E 06	1.168E 05	1.128E 05
1.00E 06	3.294E 06	3.047E 06	7.40E 06	9.903E 04	9.538E 04
1.10E 06	3.197E 06	3.001E 06	7.60E 06	8.533E 04	8.194E 04
1.20E 06	3.288E 06	3.118E 06	7.80E 06	7.462E 04	7.142E 04
1.30E 06	3.358E 06	3.200E 06	8.00E 06	6.517E 04	6.217E 04
1.40E 06	3.322E 06	3.161E 06	8.20E 06	5.691E 04	5.413E 04
1.50E 06	3.173E 06	3.015E 06	8.40E 06	5.030E 04	4.764E 04
1.60E 06	2.975E 06	2.832E 06	8.60E 06	4.489E 04	4.238E 04
1.70E 06	2.825E 06	2.695E 06	8.80E 06	3.988E 04	3.755E 04
1.80E 06	2.730E 06	2.610E 06	9.00E 06	3.505E 04	3.283E 04
1.90E 06	2.641E 06	2.535E 06	9.20E 06	3.078E 04	2.867E 04
2.00E 06	2.536E 06	2.443E 06	9.40E 06	2.738E 04	2.542E 04
2.10E 06	2.419E 06	2.338E 06	9.60E 06	2.458E 04	2.272E 04
2.20E 06	2.296E 06	2.224E 06	9.80E 06	2.181E 04	2.004E 04
2.30E 06	2.160E 06	2.098E 06	1.00E 07	1.890E 04	1.727E 04
2.40E 06	2.010E 06	1.955E 06	1.02E 07	1.608E 04	1.458E 04
2.50E 06	1.847E 06	1.799E 06	1.04E 07	1.356E 04	1.215E 04
2.60E 06	1.679E 06	1.638E 06	1.06E 07	1.149E 04	1.010E 04
2.70E 06	1.515E 06	1.477E 06	1.08E 07	9.895E 03	8.511E 03
2.80E 06	1.357E 06	1.321E 06	1.10E 07	8.707E 03	7.345E 03
2.90E 06	1.206E 06	1.173E 06	1.12E 07	7.777E 03	6.492E 03
3.00E 06	1.064E 06	1.033E 06	1.14E 07	6.991E 03	5.825E 03
3.20E 06	8.203E 05	7.953E 05	1.16E 07	6.281E 03	5.219E 03
3.40E 06	6.599E 05	6.371E 05	1.18E 07	5.559E 03	4.553E 03
3.60E 06	5.927E 05	5.708E 05	1.20E 07	4.752E 03	3.772E 03
3.80E 06	5.795E 05	5.594E 05	1.22E 07	3.900E 03	2.945E 03
4.00E 06	5.672E 05	5.491E 05	1.24E 07	3.161E 03	2.255E 03
4.20E 06	5.353E 05	5.201E 05	1.26E 07	2.675E 03	1.880E 03
4.40E 06	4.908E 05	4.775E 05	1.28E 07	2.463E 03	1.793E 03
4.60E 06	4.341E 05	4.227E 05	1.30E 07	2.410E 03	1.791E 03
4.80E 06	3.772E 05	3.675E 05	1.32E 07	2.337E 03	1.722E 03
5.00E 06	3.361E 05	3.275E 05	1.34E 07	2.153E 03	1.569E 03
5.20E 06	3.103E 05	3.019E 05	1.36E 07	1.900E 03	1.375E 03
5.40E 06	2.897E 05	2.821E 05	1.38E 07	1.648E 03	1.188E 03
5.60E 06	2.685E 05	2.615E 05	1.40E 07	1.432E 03	1.025E 03
5.80E 06	2.490E 05	2.421E 05	1.42E 07	1.252E 03	8.792E 02
6.00E 06	2.324E 05	2.259E 05	1.44E 07	1.102E 03	7.499E 02
6.20E 06	2.160E 05	2.101E 05	1.46E 07	9.781E 02	6.538E 02
6.40E 06	1.973E 05	1.920E 05	1.48E 07	8.817E 02	5.972E 02
6.60E 06	1.770E 05	1.721E 05	1.50E 07	8.098E 02	5.596E 02
6.80E 06	1.569E 05	1.524E 05			

TABLE XIII

RUN 37A+37B CH2 SLAB AT 0 DEG.

ENERGY	UPPER LIMIT	LOWER LIMIT	ENERGY	UPPER LIMIT	LOWER LIMIT
8.00E 05	5.863E 03	3.678E 03	7.00E 06	1.737E 04	1.689E 04
9.00E 05	6.476E 03	3.996E 03	7.20E 06	1.479E 04	1.434E 04
1.00E 06	6.607E 03	4.299E 03	7.40E 06	1.203E 04	1.161E 04
1.10E 06	8.092E 03	5.880E 03	7.60E 06	9.689E 03	9.295E 03
1.20E 06	1.093E 04	8.903E 03	7.80E 06	8.147E 03	7.773E 03
1.30E 06	1.390E 04	1.173E 04	8.00E 06	7.352E 03	6.997E 03
1.40E 06	1.537E 04	1.273E 04	8.20E 06	7.014E 03	6.677E 03
1.50E 06	1.531E 04	1.268E 04	8.40E 06	6.735E 03	6.405E 03
1.60E 06	1.564E 04	1.312E 04	8.60E 06	6.349E 03	6.034E 03
1.70E 06	1.770E 04	1.509E 04	8.80E 06	5.866E 03	5.571E 03
1.80E 06	2.081E 04	1.814E 04	9.00E 06	5.336E 03	5.054E 03
1.90E 06	2.384E 04	2.143E 04	9.20E 06	4.792E 03	4.520E 03
2.00E 06	2.665E 04	2.443E 04	9.40E 06	4.264E 03	4.006E 03
2.10E 06	2.938E 04	2.725E 04	9.60E 06	3.804E 03	3.558E 03
2.20E 06	3.184E 04	2.982E 04	9.80E 06	3.453E 03	3.229E 03
2.30E 06	3.352E 04	3.167E 04	1.00E 07	3.239E 03	3.022E 03
2.40E 06	3.418E 04	3.243E 04	1.02E 07	3.049E 03	2.849E 03
2.50E 06	3.353E 04	3.195E 04	1.04E 07	2.774E 03	2.584E 03
2.60E 06	3.204E 04	3.061E 04	1.06E 07	2.359E 03	2.169E 03
2.70E 06	3.037E 04	2.894E 04	1.08E 07	1.878E 03	1.687E 03
2.80E 06	2.874E 04	2.729E 04	1.10E 07	1.465E 03	1.280E 03
2.90E 06	2.706E 04	2.562E 04	1.12E 07	1.192E 03	1.019E 03
3.00E 06	2.510E 04	2.367E 04	1.14E 07	1.033E 03	8.738E 02
3.20E 06	1.966E 04	1.836E 04	1.16E 07	9.315E 02	7.839E 02
3.40E 06	1.461E 04	1.331E 04	1.18E 07	8.648E 02	7.235E 02
3.60E 06	1.311E 04	1.178E 04	1.20E 07	8.233E 02	6.849E 02
3.80E 06	1.523E 04	1.391E 04	1.22E 07	7.887E 02	6.538E 02
4.00E 06	1.849E 04	1.720E 04	1.24E 07	7.385E 02	6.104E 02
4.20E 06	2.074E 04	1.958E 04	1.26E 07	6.666E 02	5.524E 02
4.40E 06	2.199E 04	2.090E 04	1.28E 07	5.861E 02	4.889E 02
4.60E 06	2.302E 04	2.203E 04	1.30E 07	5.128E 02	4.227E 02
4.80E 06	2.369E 04	2.279E 04	1.32E 07	4.484E 02	3.585E 02
5.00E 06	2.348E 04	2.262E 04	1.34E 07	3.919E 02	3.069E 02
5.20E 06	2.313E 04	2.226E 04	1.36E 07	3.473E 02	2.739E 02
5.40E 06	2.309E 04	2.226E 04	1.38E 07	3.148E 02	2.533E 02
5.60E 06	2.295E 04	2.217E 04	1.40E 07	2.868E 02	2.318E 02
5.80E 06	2.255E 04	2.176E 04	1.42E 07	2.546E 02	2.020E 02
6.00E 06	2.205E 04	2.132E 04	1.44E 07	2.172E 02	1.675E 02
6.20E 06	2.173E 04	2.105E 04	1.46E 07	1.816E 02	1.369E 02
6.40E 06	2.141E 04	2.080E 04	1.48E 07	1.543E 02	1.154E 02
6.60E 06	2.073E 04	2.016E 04	1.50E 07	1.371E 02	1.017E 02
6.80E 06	1.938E 04	1.886E 04			

TABLE XIV

RUN 70A+71A CH2 SLAB AT 13 DEG.

ENERGY	UPPER LIMIT	LOWER LIMIT	ENERGY	UPPER LIMIT	LOWER LIMIT
8.00E 05	5.747E 02	5.030E 02	7.00E 06	1.475E 02	1.415E 02
9.00E 05	5.686E 02	4.917E 02	7.20E 06	1.285E 02	1.227E 02
1.00E 06	5.495E 02	4.781E 02	7.40E 06	1.102E 02	1.048E 02
1.10E 06	6.052E 02	5.420E 02	7.60E 06	9.685E 01	9.180E 01
1.20E 06	7.372E 02	6.806E 02	7.80E 06	8.841E 01	8.362E 01
1.30E 06	8.717E 02	8.166E 02	8.00E 06	8.219E 01	7.766E 01
1.40E 06	9.456E 02	8.862E 02	8.20E 06	7.581E 01	7.152E 01
1.50E 06	9.528E 02	8.942E 02	8.40E 06	6.867E 01	6.451E 01
1.60E 06	9.209E 02	8.669E 02	8.60E 06	6.124E 01	5.730E 01
1.70E 06	8.636E 02	8.118E 02	8.80E 06	5.382E 01	5.013E 01
1.80E 06	8.005E 02	7.503E 02	9.00E 06	4.652E 01	4.305E 01
1.90E 06	7.562E 02	7.118E 02	9.20E 06	4.016E 01	3.670E 01
2.00E 06	7.403E 02	7.005E 02	9.40E 06	3.509E 01	3.178E 01
2.10E 06	7.395E 02	7.029E 02	9.60E 06	3.151E 01	2.831E 01
2.20E 06	7.369E 02	7.030E 02	9.80E 06	2.886E 01	2.578E 01
2.30E 06	7.228E 02	6.925E 02	1.00E 07	2.648E 01	2.354E 01
2.40E 06	6.998E 02	6.716E 02	1.02E 07	2.387E 01	2.109E 01
2.50E 06	6.674E 02	6.421E 02	1.04E 07	2.114E 01	1.843E 01
2.60E 06	6.275E 02	6.051E 02	1.06E 07	1.888E 01	1.618E 01
2.70E 06	5.840E 02	5.617E 02	1.08E 07	1.765E 01	1.489E 01
2.80E 06	5.377E 02	5.153E 02	1.10E 07	1.730E 01	1.451E 01
2.90E 06	4.912E 02	4.693E 02	1.12E 07	1.705E 01	1.438E 01
3.00E 06	4.459E 02	4.246E 02	1.14E 07	1.618E 01	1.375E 01
3.20E 06	3.663E 02	3.479E 02	1.16E 07	1.454E 01	1.231E 01
3.40E 06	3.256E 02	3.079E 02	1.18E 07	1.246E 01	1.034E 01
3.60E 06	3.271E 02	3.093E 02	1.20E 07	1.049E 01	8.390E 00
3.80E 06	3.457E 02	3.286E 02	1.22E 07	8.946E 00	6.878E 00
4.00E 06	3.639E 02	3.482E 02	1.24E 07	7.874E 00	5.916E 00
4.20E 06	3.692E 02	3.555E 02	1.26E 07	7.109E 00	5.372E 00
4.40E 06	3.600E 02	3.476E 02	1.28E 07	6.546E 00	5.034E 00
4.60E 06	3.425E 02	3.313E 02	1.30E 07	6.204E 00	4.779E 00
4.80E 06	3.244E 02	3.143E 02	1.32E 07	6.029E 00	4.639E 00
5.00E 06	3.038E 02	2.944E 02	1.34E 07	5.902E 00	4.611E 00
5.20E 06	2.835E 02	2.743E 02	1.36E 07	5.716E 00	4.572E 00
5.40E 06	2.695E 02	2.607E 02	1.38E 07	5.379E 00	4.374E 00
5.60E 06	2.577E 02	2.492E 02	1.40E 07	4.847E 00	3.942E 00
5.80E 06	2.439E 02	2.355E 02	1.42E 07	4.147E 00	3.318E 00
6.00E 06	2.290E 02	2.212E 02	1.44E 07	3.382E 00	2.626E 00
6.20E 06	2.136E 02	2.063E 02	1.46E 07	2.684E 00	1.994E 00
6.40E 06	1.963E 02	1.892E 02	1.48E 07	2.147E 00	1.505E 00
6.60E 06	1.790E 02	1.722E 02	1.50E 07	1.794E 00	1.189E 00
6.80E 06	1.637E 02	1.574E 02			

TABLE XV

RUN 38B+38C CH2 SLAB AT 30 DEG.

ENERGY	UPPER LIMIT	LOWER LIMIT	ENERGY	UPPER LIMIT	LOWER LIMIT
8.00E 05	5.821E 02	5.215E 02	7.00E 06	5.586E 01	5.235E 01
9.00E 05	6.293E 02	5.635E 02	7.20E 06	5.042E 01	4.711E 01
1.00E 06	6.592E 02	6.056E 02	7.40E 06	4.424E 01	4.117E 01
1.10E 06	6.787E 02	6.351E 02	7.60E 06	3.851E 01	3.567E 01
1.20E 06	7.060E 02	6.681E 02	7.80E 06	3.355E 01	3.092E 01
1.30E 06	7.199E 02	6.844E 02	8.00E 06	2.885E 01	2.638E 01
1.40E 06	6.938E 02	6.567E 02	8.20E 06	2.421E 01	2.190E 01
1.50E 06	6.416E 02	6.054E 02	8.40E 06	1.999E 01	1.777E 01
1.60E 06	5.963E 02	5.631E 02	8.60E 06	1.651E 01	1.442E 01
1.70E 06	5.697E 02	5.383E 02	8.80E 06	1.398E 01	1.202E 01
1.80E 06	5.514E 02	5.213E 02	9.00E 06	1.241E 01	1.052E 01
1.90E 06	5.310E 02	5.045E 02	9.20E 06	1.153E 01	9.709E 00
2.00E 06	5.068E 02	4.833E 02	9.40E 06	1.095E 01	9.236E 00
2.10E 06	4.808E 02	4.593E 02	9.60E 06	1.034E 01	8.707E 00
2.20E 06	4.536E 02	4.338E 02	9.80E 06	9.478E 00	7.913E 00
2.30E 06	4.247E 02	4.069E 02	1.00E 07	8.362E 00	6.896E 00
2.40E 06	3.954E 02	3.789E 02	1.02E 07	7.083E 00	5.729E 00
2.50E 06	3.668E 02	3.519E 02	1.04E 07	5.742E 00	4.438E 00
2.60E 06	3.419E 02	3.287E 02	1.06E 07	4.529E 00	3.238E 00
2.70E 06	3.225E 02	3.094E 02	1.08E 07	3.726E 00	2.472E 00
2.80E 06	3.083E 02	2.951E 02	1.10E 07	3.460E 00	2.235E 00
2.90E 06	2.965E 02	2.837E 02	1.12E 07	3.547E 00	2.342E 00
3.00E 06	2.849E 02	2.725E 02	1.14E 07	3.722E 00	2.583E 00
3.20E 06	2.583E 02	2.479E 02	1.16E 07	3.836E 00	2.803E 00
3.40E 06	2.380E 02	2.282E 02	1.18E 07	3.771E 00	2.804E 00
3.60E 06	2.361E 02	2.264E 02	1.20E 07	3.466E 00	2.522E 00
3.80E 06	2.453E 02	2.359E 02	1.22E 07	2.972E 00	2.096E 00
4.00E 06	2.466E 02	2.378E 02	1.24E 07	2.431E 00	1.564E 00
4.20E 06	2.339E 02	2.261E 02	1.26E 07	1.924E 00	1.239E 00
4.40E 06	2.175E 02	2.102E 02	1.28E 07	1.448E 00	7.976E-01
4.60E 06	2.005E 02	1.937E 02	1.30E 07	1.025E 00	3.899E-01
4.80E 06	1.821E 02	1.758E 02	1.32E 07	7.248E-01	1.202E-01
5.00E 06	1.637E 02	1.578E 02	1.34E 07	5.975E-01	4.742E-02
5.20E 06	1.462E 02	1.405E 02	1.36E 07	6.240E-01	1.255E-01
5.40E 06	1.283E 02	1.229E 02	1.38E 07	7.236E-01	2.605E-01
5.60E 06	1.101E 02	1.050E 02	1.40E 07	8.144E-01	3.749E-01
5.80E 06	9.461E 01	8.960E 01	1.42E 07	8.516E-01	4.299E-01
6.00E 06	8.420E 01	7.954E 01	1.44E 07	8.257E-01	4.178E-01
6.20E 06	7.694E 01	7.252E 01	1.46E 07	7.469E-01	3.552E-01
6.40E 06	7.051E 01	6.630E 01	1.48E 07	6.390E-01	2.751E-01
6.60E 06	6.495E 01	6.089E 01	1.50E 07	5.346E-01	2.117E-01
6.80E 06	6.040E 01	5.664E 01			

TABLE XVI

RUN 51A+51B CH2 SLAB AT 30 DEG.

ENERGY	UPPER LIMIT	LOWER LIMIT	ENERGY	UPPER LIMIT	LOWER LIMIT
8.00E 05	5.409E 02	4.837E 02	7.00E 06	5.422E 01	5.079E 01
9.00E 05	5.781E 02	5.134E 02	7.20E 06	4.995E 01	4.666E 01
1.00E 06	6.257E 02	5.723E 02	7.40E 06	4.303E 01	3.998E 01
1.10E 06	6.809E 02	6.372E 02	7.60E 06	3.584E 01	3.301E 01
1.20E 06	7.304E 02	6.925E 02	7.80E 06	3.040E 01	2.775E 01
1.30E 06	7.518E 02	7.162E 02	8.00E 06	2.652E 01	2.403E 01
1.40E 06	7.273E 02	6.904E 02	8.20E 06	2.356E 01	2.123E 01
1.50E 06	6.630E 02	6.271E 02	8.40E 06	2.132E 01	1.909E 01
1.60E 06	5.961E 02	5.630E 02	8.60E 06	1.945E 01	1.734E 01
1.70E 06	5.569E 02	5.257E 02	8.80E 06	1.739E 01	1.543E 01
1.80E 06	5.344E 02	5.044E 02	9.00E 06	1.509E 01	1.323E 01
1.90E 06	5.123E 02	4.859E 02	9.20E 06	1.297E 01	1.120E 01
2.00E 06	4.884E 02	4.648E 02	9.40E 06	1.142E 01	9.768E 00
2.10E 06	4.651E 02	4.435E 02	9.60E 06	1.040E 01	8.842E 00
2.20E 06	4.438E 02	4.238E 02	9.80E 06	9.494E 00	8.014E 00
2.30E 06	4.235E 02	4.056E 02	1.00E 07	8.303E 00	6.907E 00
2.40E 06	4.033E 02	3.868E 02	1.02E 07	6.773E 00	5.447E 00
2.50E 06	3.815E 02	3.666E 02	1.04E 07	5.224E 00	3.974E 00
2.60E 06	3.583E 02	3.451E 02	1.06E 07	4.099E 00	2.911E 00
2.70E 06	3.364E 02	3.233E 02	1.08E 07	3.528E 00	2.351E 00
2.80E 06	3.176E 02	3.045E 02	1.10E 07	3.264E 00	2.066E 00
2.90E 06	3.025E 02	2.898E 02	1.12E 07	3.049E 00	1.868E 00
3.00E 06	2.898E 02	2.776E 02	1.14E 07	2.884E 00	1.784E 00
3.20E 06	2.626E 02	2.523E 02	1.16E 07	2.893E 00	1.885E 00
3.40E 06	2.351E 02	2.253E 02	1.18E 07	3.051E 00	2.097E 00
3.60E 06	2.271E 02	2.175E 02	1.20E 07	3.120E 00	2.210E 00
3.80E 06	2.382E 02	2.289E 02	1.22E 07	2.915E 00	2.059E 00
4.00E 06	2.475E 02	2.389E 02	1.24E 07	2.448E 00	1.640E 00
4.20E 06	2.394E 02	2.317E 02	1.26E 07	1.921E 00	1.172E 00
4.40E 06	2.176E 02	2.103E 02	1.28E 07	1.567E 00	9.164E-01
4.60E 06	1.933E 02	1.866E 02	1.30E 07	1.478E 00	9.238E-01
4.80E 06	1.746E 02	1.684E 02	1.32E 07	1.529E 00	1.030E 00
5.00E 06	1.614E 02	1.555E 02	1.34E 07	1.514E 00	1.034E 00
5.20E 06	1.486E 02	1.430E 02	1.36E 07	1.318E 00	8.613E-01
5.40E 06	1.319E 02	1.265E 02	1.38E 07	9.862E-01	5.754E-01
5.60E 06	1.147E 02	1.096E 02	1.40E 07	6.478E-01	2.912E-01
5.80E 06	1.007E 02	9.578E 01	1.42E 07	4.096E-01	9.590E-02
6.00E 06	8.916E 01	8.453E 01	1.44E 07	2.985E-01	1.455E-02
6.20E 06	7.934E 01	7.498E 01	1.46E 07	2.784E-01	1.337E-02
6.40E 06	7.093E 01	6.682E 01	1.48E 07	2.898E-01	3.573E-02
6.60E 06	6.326E 01	5.922E 01	1.50E 07	2.884E-01	3.861E-02
6.80E 06	5.766E 01	5.396E 01			

TABLE XVII

RUN 19F+19G PB SLAB AT 0 DEG.

ENERGY	UPPER LIMIT	LOWER LIMIT	ENERGY	UPPER LIMIT	LOWER LIMIT
8.00E 05	4.714E 04	4.382E 04	7.00E 06	6.945E 02	6.578E 02
9.00E 05	4.517E 04	4.190E 04	7.20E 06	6.712E 02	6.357E 02
1.00E 06	4.524E 04	4.277E 04	7.40E 06	6.359E 02	6.025E 02
1.10E 06	4.537E 04	4.360E 04	7.60E 06	5.837E 02	5.519E 02
1.20E 06	4.396E 04	4.254E 04	7.80E 06	5.288E 02	4.984E 02
1.30E 06	4.131E 04	4.011E 04	8.00E 06	4.872E 02	4.586E 02
1.40E 06	3.853E 04	3.748E 04	8.20E 06	4.604E 02	4.333E 02
1.50E 06	3.582E 04	3.486E 04	8.40E 06	4.357E 02	4.093E 02
1.60E 06	3.258E 04	3.176E 04	8.60E 06	4.049E 02	3.798E 02
1.70E 06	2.877E 04	2.814E 04	8.80E 06	3.677E 02	3.443E 02
1.80E 06	2.481E 04	2.431E 04	9.00E 06	3.285E 02	3.061E 02
1.90E 06	2.074E 04	2.034E 04	9.20E 06	2.907E 02	2.692E 02
2.00E 06	1.674E 04	1.642E 04	9.40E 06	2.558E 02	2.354E 02
2.10E 06	1.316E 04	1.291E 04	9.60E 06	2.244E 02	2.051E 02
2.20E 06	1.029E 04	1.010E 04	9.80E 06	1.974E 02	1.790E 02
2.30E 06	8.184E 03	8.034E 03	1.00E 07	1.754E 02	1.581E 02
2.40E 06	6.551E 03	6.429E 03	1.02E 07	1.585E 02	1.425E 02
2.50E 06	5.262E 03	5.163E 03	1.04E 07	1.453E 02	1.302E 02
2.60E 06	4.200E 03	4.118E 03	1.06E 07	1.333E 02	1.183E 02
2.70E 06	3.320E 03	3.246E 03	1.08E 07	1.200E 02	1.047E 02
2.80E 06	2.643E 03	2.574E 03	1.10E 07	1.045E 02	8.932E 01
2.90E 06	2.134E 03	2.069E 03	1.12E 07	8.788E 01	7.355E 01
3.00E 06	1.737E 03	1.677E 03	1.14E 07	7.228E 01	5.938E 01
3.20E 06	1.190E 03	1.139E 03	1.16E 07	5.993E 01	4.816E 01
3.40E 06	9.029E 02	8.536E 02	1.18E 07	5.171E 01	4.033E 01
3.60E 06	8.039E 02	7.533E 02	1.20E 07	4.644E 01	3.508E 01
3.80E 06	7.538E 02	7.022E 02	1.22E 07	4.286E 01	3.154E 01
4.00E 06	7.113E 02	6.605E 02	1.24E 07	3.971E 01	2.876E 01
4.20E 06	6.693E 02	6.216E 02	1.26E 07	3.618E 01	2.610E 01
4.40E 06	6.311E 02	5.841E 02	1.28E 07	3.203E 01	2.309E 01
4.60E 06	5.949E 02	5.493E 02	1.30E 07	2.761E 01	1.921E 01
4.80E 06	5.538E 02	5.094E 02	1.32E 07	2.331E 01	1.490E 01
5.00E 06	5.246E 02	4.803E 02	1.34E 07	1.974E 01	1.158E 01
5.20E 06	5.257E 02	4.807E 02	1.36E 07	1.769E 01	1.020E 01
5.40E 06	5.623E 02	5.175E 02	1.38E 07	1.727E 01	1.049E 01
5.60E 06	6.246E 02	5.804E 02	1.40E 07	1.757E 01	1.131E 01
5.80E 06	6.935E 02	6.492E 02	1.42E 07	1.742E 01	1.148E 01
6.00E 06	7.348E 02	6.919E 02	1.44E 07	1.619E 01	1.044E 01
6.20E 06	7.446E 02	7.028E 02	1.46E 07	1.399E 01	8.459E 00
6.40E 06	7.417E 02	7.011E 02	1.48E 07	1.139E 01	6.152E 00
6.60E 06	7.345E 02	6.938E 02	1.50E 07	9.058E 00	4.137E 00
6.80E 06	7.164E 02	6.780E 02			

TABLE XVIII

RUN 19H+19I PB SLAB AT 13 DEG.

ENERGY	UPPER LIMIT	LOWER LIMIT	ENERGY	UPPER LIMIT	LOWER LIMIT
8.00E 05	8.116E 03	7.739E 03	7.00E 06	8.788E 01	8.056E 01
9.00E 05	6.796E 03	6.389E 03	7.20E 06	7.887E 01	7.192E 01
1.00E 06	5.833E 03	5.535E 03	7.40E 06	7.082E 01	6.439E 01
1.10E 06	5.230E 03	5.020E 03	7.60E 06	6.275E 01	5.671E 01
1.20E 06	4.888E 03	4.719E 03	7.80E 06	5.343E 01	4.768E 01
1.30E 06	4.584E 03	4.439E 03	8.00E 06	4.403E 01	3.855E 01
1.40E 06	4.228E 03	4.096E 03	8.20E 06	3.765E 01	3.253E 01
1.50E 06	3.873E 03	3.749E 03	8.40E 06	3.557E 01	3.061E 01
1.60E 06	3.519E 03	3.413E 03	8.60E 06	3.534E 01	3.058E 01
1.70E 06	3.150E 03	3.062E 03	8.80E 06	3.375E 01	2.926E 01
1.80E 06	2.802E 03	2.727E 03	9.00E 06	2.982E 01	2.547E 01
1.90E 06	2.477E 03	2.414E 03	9.20E 06	2.503E 01	2.082E 01
2.00E 06	2.149E 03	2.097E 03	9.40E 06	2.152E 01	1.751E 01
2.10E 06	1.827E 03	1.783E 03	9.60E 06	2.011E 01	1.622E 01
2.20E 06	1.544E 03	1.506E 03	9.80E 06	2.002E 01	1.616E 01
2.30E 06	1.319E 03	1.288E 03	1.00E 07	2.034E 01	1.648E 01
2.40E 06	1.134E 03	1.107E 03	1.02E 07	2.090E 01	1.703E 01
2.50E 06	9.757E 02	9.530E 02	1.04E 07	2.173E 01	1.782E 01
2.60E 06	8.329E 02	8.136E 02	1.06E 07	2.230E 01	1.830E 01
2.70E 06	7.073E 02	6.884E 02	1.08E 07	2.177E 01	1.754E 01
2.80E 06	6.044E 02	5.852E 02	1.10E 07	1.965E 01	1.512E 01
2.90E 06	5.208E 02	5.025E 02	1.12E 07	1.614E 01	1.139E 01
3.00E 06	4.488E 02	4.316E 02	1.14E 07	1.199E 01	7.147E 00
3.20E 06	3.276E 02	3.133E 02	1.16E 07	8.157E 00	3.242E 00
3.40E 06	2.458E 02	2.319E 02	1.18E 07	5.484E 00	5.092E-01
3.60E 06	2.160E 02	2.018E 02	1.20E 07	4.298E 00	-8.018E-01
3.80E 06	2.157E 02	2.016E 02	1.22E 07	4.247E 00	-9.346E-01
4.00E 06	2.099E 02	1.962E 02	1.24E 07	4.338E 00	-7.634E-01
4.20E 06	1.868E 02	1.742E 02	1.26E 07	3.557E 00	-1.343E 00
4.40E 06	1.630E 02	1.509E 02	1.28E 07	1.556E 00	-3.156E 00
4.60E 06	1.471E 02	1.357E 02	1.30E 07	-1.340E 00	-5.894E 00
4.80E 06	1.360E 02	1.252E 02	1.32E 07	-4.559E 00	-8.947E 00
5.00E 06	1.263E 02	1.157E 02	1.34E 07	-7.578E 00	-1.176E 01
5.20E 06	1.195E 02	1.089E 02	1.36E 07	-9.824E 00	-1.377E 01
5.40E 06	1.181E 02	1.078E 02	1.38E 07	-1.070E 01	-1.439E 01
5.60E 06	1.197E 02	1.097E 02	1.40E 07	-9.892E 00	-1.335E 01
5.80E 06	1.211E 02	1.113E 02	1.42E 07	-7.737E 00	-1.099E 01
6.00E 06	1.195E 02	1.102E 02	1.44E 07	-5.023E 00	-8.079E 00
6.20E 06	1.151E 02	1.062E 02	1.46E 07	-2.486E 00	-5.362E 00
6.40E 06	1.098E 02	1.013E 02	1.48E 07	-4.398E-01	-3.159E 00
6.60E 06	1.043E 02	9.599E 01	1.50E 07	1.140E 00	-1.440E 00
6.80E 06	9.690E 01	8.914E 01			

TABLE XIX

RUN 20B+20C PB SLAB AT 47 DEG.

ENERGY	UPPER LIMIT	LOWER LIMIT	ENERGY	UPPER LIMIT	LOWER LIMIT
8.00E 05	4.657E 03	4.413E 03	7.00E 06	7.215E 00	5.033E 00
9.00E 05	3.826E 03	3.608E 03	7.20E 06	5.846E 00	3.809E 00
1.00E 06	3.301E 03	3.145E 03	7.40E 06	6.030E 00	4.145E 00
1.10E 06	2.937E 03	2.832E 03	7.60E 06	6.608E 00	4.869E 00
1.20E 06	2.657E 03	2.576E 03	7.80E 06	6.358E 00	4.679E 00
1.30E 06	2.414E 03	2.345E 03	8.00E 06	5.063E 00	3.431E 00
1.40E 06	2.169E 03	2.108E 03	8.20E 06	3.468E 00	1.968E 00
1.50E 06	1.924E 03	1.869E 03	8.40E 06	2.552E 00	1.189E 00
1.60E 06	1.691E 03	1.644E 03	8.60E 06	2.394E 00	1.053E 00
1.70E 06	1.488E 03	1.449E 03	8.80E 06	2.457E 00	1.097E 00
1.80E 06	1.307E 03	1.274E 03	9.00E 06	2.514E 00	1.181E 00
1.90E 06	1.128E 03	1.101E 03	9.20E 06	2.654E 00	1.362E 00
2.00E 06	9.575E 02	9.345E 02	9.40E 06	2.772E 00	1.528E 00
2.10E 06	8.095E 02	7.897E 02	9.60E 06	2.616E 00	1.371E 00
2.20E 06	6.871E 02	6.694E 02	9.80E 06	2.134E 00	7.837E-01
2.30E 06	5.830E 02	5.674E 02	1.00E 07	1.531E 00	5.941E-02
2.40E 06	4.893E 02	4.750E 02	1.02E 07	1.038E 00	-4.751E-01
2.50E 06	4.071E 02	3.946E 02	1.04E 07	7.052E-01	-8.318E-01
2.60E 06	3.386E 02	3.279E 02	1.06E 07	4.807E-01	-1.177E 00
2.70E 06	2.827E 02	2.723E 02	1.08E 07	4.194E-01	-1.429E 00
2.80E 06	2.387E 02	2.284E 02	1.10E 07	6.927E-01	-1.349E 00
2.90E 06	2.027E 02	1.931E 02	1.12E 07	1.301E 00	-9.473E-01
3.00E 06	1.718E 02	1.633E 02	1.14E 07	1.910E 00	-5.493E-01
3.20E 06	1.232E 02	1.165E 02	1.16E 07	2.191E 00	-4.356E-01
3.40E 06	9.022E 01	8.398E 01	1.18E 07	2.236E 00	-4.600E-01
3.60E 06	7.080E 01	6.458E 01	1.20E 07	2.574E 00	-2.487E-01
3.80E 06	6.007E 01	5.407E 01	1.22E 07	3.395E 00	3.503E-01
4.00E 06	5.360E 01	4.797E 01	1.24E 07	4.368E 00	1.147E 00
4.20E 06	4.657E 01	4.155E 01	1.26E 07	4.963E 00	1.693E 00
4.40E 06	3.779E 01	3.305E 01	1.28E 07	4.808E 00	1.538E 00
4.60E 06	3.044E 01	2.609E 01	1.30E 07	3.796E 00	5.456E-01
4.80E 06	2.768E 01	2.367E 01	1.32E 07	2.149E 00	-1.050E 00
5.00E 06	2.779E 01	2.405E 01	1.34E 07	3.784E-01	-2.778E 00
5.20E 06	2.626E 01	2.257E 01	1.36E 07	-9.456E-01	-4.107E 00
5.40E 06	2.153E 01	1.798E 01	1.38E 07	-1.466E 00	-4.603E 00
5.60E 06	1.792E 01	1.462E 01	1.40E 07	-1.106E 00	-4.136E 00
5.80E 06	1.711E 01	1.393E 01	1.42E 07	-3.510E-02	-2.927E 00
6.00E 06	1.695E 01	1.399E 01	1.44E 07	1.370E 00	-1.406E 00
6.20E 06	1.574E 01	1.294E 01	1.46E 07	2.640E 00	-4.700E-02
6.40E 06	1.388E 01	1.132E 01	1.48E 07	3.374E 00	7.793E-01
6.60E 06	1.202E 01	9.641E 00	1.50E 07	3.397E 00	9.005E-01
6.80E 06	9.677E 00	7.400E 00			

TABLE XX

RUN 20D+20E PB SLAB AT 64 DEG.

ENERGY	UPPER LIMIT	LOWER LIMIT	ENERGY	UPPER LIMIT	LOWER LIMIT
8.00E 05	5.718E 04	5.527E 04	7.00E 06	2.121E 00	1.527E 00
9.00E 05	4.374E 04	4.176E 04	7.20E 06	1.406E 00	7.956E-01
1.00E 06	3.623E 04	3.494E 04	7.40E 06	1.040E 00	4.518E-01
1.10E 06	3.024E 04	2.952E 04	7.60E 06	9.740E-01	4.341E-01
1.20E 06	2.508E 04	2.459E 04	7.80E 06	9.928E-01	4.851E-01
1.30E 06	2.045E 04	2.009E 04	8.00E 06	1.021E 00	5.202E-01
1.40E 06	1.608E 04	1.580E 04	8.20E 06	1.039E 00	5.504E-01
1.50E 06	1.205E 04	1.182E 04	8.40E 06	1.022E 00	5.451E-01
1.60E 06	8.694E 03	8.514E 03	8.60E 06	9.654E-01	5.089E-01
1.70E 06	6.234E 03	6.099E 03	8.80E 06	8.816E-01	4.556E-01
1.80E 06	4.415E 03	4.306E 03	9.00E 06	7.732E-01	3.555E-01
1.90E 06	3.006E 03	2.914E 03	9.20E 06	6.416E-01	2.013E-01
2.00E 06	1.937E 03	1.860E 03	9.40E 06	5.110E-01	4.043E-02
2.10E 06	1.206E 03	1.141E 03	9.60E 06	4.267E-01	-8.260E-02
2.20E 06	7.690E 02	7.129E 02	9.80E 06	4.079E-01	-1.456E-01
2.30E 06	5.533E 02	5.052E 02	1.00E 07	4.278E-01	-1.563E-01
2.40E 06	4.491E 02	4.067E 02	1.02E 07	4.598E-01	-1.683E-01
2.50E 06	4.032E 02	3.680E 02	1.04E 07	5.105E-01	-2.224E-01
2.60E 06	3.596E 02	3.304E 02	1.06E 07	5.748E-01	-2.698E-01
2.70E 06	2.993E 02	2.715E 02	1.08E 07	6.614E-01	-2.772E-01
2.80E 06	2.204E 02	1.954E 02	1.10E 07	7.796E-01	-2.702E-01
2.90E 06	1.432E 02	1.242E 02	1.12E 07	9.123E-01	-2.524E-01
3.00E 06	8.275E 01	7.044E 01	1.14E 07	1.061E 00	-2.129E-01
3.20E 06	2.982E 01	2.568E 01	1.16E 07	1.230E 00	-1.708E-01
3.40E 06	2.095E 01	1.875E 01	1.18E 07	1.339E 00	-1.565E-01
3.60E 06	1.921E 01	1.735E 01	1.20E 07	1.326E 00	-2.167E-01
3.80E 06	1.689E 01	1.514E 01	1.22E 07	1.219E 00	-3.643E-01
4.00E 06	1.472E 01	1.308E 01	1.24E 07	1.101E 00	-5.754E-01
4.20E 06	1.289E 01	1.146E 01	1.26E 07	9.907E-01	-7.582E-01
4.40E 06	1.093E 01	9.615E 00	1.28E 07	8.849E-01	-8.602E-01
4.60E 06	8.859E 00	7.661E 00	1.30E 07	7.975E-01	-9.339E-01
4.80E 06	7.104E 00	6.016E 00	1.32E 07	6.967E-01	-1.051E 00
5.00E 06	5.833E 00	4.816E 00	1.34E 07	5.378E-01	-1.200E 00
5.20E 06	4.950E 00	3.954E 00	1.36E 07	4.041E-01	-1.294E 00
5.40E 06	4.336E 00	3.391E 00	1.38E 07	4.613E-01	-1.216E 00
5.60E 06	3.759E 00	2.851E 00	1.40E 07	7.645E-01	-9.169E-01
5.80E 06	3.226E 00	2.334E 00	1.42E 07	1.171E 00	-5.067E-01
6.00E 06	2.990E 00	2.166E 00	1.44E 07	1.449E 00	-1.953E-01
6.20E 06	3.036E 00	2.258E 00	1.46E 07	1.457E 00	-1.297E-01
6.40E 06	3.169E 00	2.433E 00	1.48E 07	1.224E 00	-2.907E-01
6.60E 06	3.196E 00	2.479E 00	1.50E 07	8.924E-01	-5.535E-01
6.80E 06	2.841E 00	2.186E 00			

TABLE XXI

RUN 39C+39D PB SLAB AT 0 DEG.

ENERGY	UPPER LIMIT	LOWER LIMIT	ENERGY	UPPER LIMIT	LOWER LIMIT
8.00E 05	4.763E 04	4.461E 04	7.00E 06	6.764E 02	6.529E 02
9.00E 05	4.585E 04	4.254E 04	7.20E 06	6.189E 02	5.962E 02
1.00E 06	4.548E 04	4.299E 04	7.40E 06	5.689E 02	5.476E 02
1.10E 06	4.562E 04	4.382E 04	7.60E 06	5.328E 02	5.126E 02
1.20E 06	4.457E 04	4.311E 04	7.80E 06	5.044E 02	4.851E 02
1.30E 06	4.192E 04	4.070E 04	8.00E 06	4.764E 02	4.579E 02
1.40E 06	3.894E 04	3.786E 04	8.20E 06	4.456E 02	4.283E 02
1.50E 06	3.622E 04	3.523E 04	8.40E 06	4.118E 02	3.950E 02
1.60E 06	3.318E 04	3.234E 04	8.60E 06	3.752E 02	3.592E 02
1.70E 06	2.952E 04	2.887E 04	8.80E 06	3.391E 02	3.242E 02
1.80E 06	2.561E 04	2.509E 04	9.00E 06	3.074E 02	2.933E 02
1.90E 06	2.154E 04	2.113E 04	9.20E 06	2.801E 02	2.665E 02
2.00E 06	1.747E 04	1.714E 04	9.40E 06	2.543E 02	2.414E 02
2.10E 06	1.377E 04	1.351E 04	9.60E 06	2.286E 02	2.163E 02
2.20E 06	1.075E 04	1.054E 04	9.80E 06	2.035E 02	1.920E 02
2.30E 06	8.492E 03	8.337E 03	1.00E 07	1.799E 02	1.692E 02
2.40E 06	6.772E 03	6.647E 03	1.02E 07	1.570E 02	1.471E 02
2.50E 06	5.467E 03	5.366E 03	1.04E 07	1.344E 02	1.250E 02
2.60E 06	4.417E 03	4.335E 03	1.06E 07	1.132E 02	1.039E 02
2.70E 06	3.530E 03	3.457E 03	1.08E 07	9.570E 01	8.638E 01
2.80E 06	2.804E 03	2.737E 03	1.10E 07	8.280E 01	7.356E 01
2.90E 06	2.223E 03	2.162E 03	1.12E 07	7.351E 01	6.479E 01
3.00E 06	1.766E 03	1.709E 03	1.14E 07	6.658E 01	5.874E 01
3.20E 06	1.201E 03	1.154E 03	1.16E 07	6.138E 01	5.433E 01
3.40E 06	9.337E 02	8.893E 02	1.18E 07	5.692E 01	5.031E 01
3.60E 06	8.087E 02	7.638E 02	1.20E 07	5.169E 01	4.524E 01
3.80E 06	7.370E 02	6.933E 02	1.22E 07	4.517E 01	3.885E 01
4.00E 06	6.951E 02	6.537E 02	1.24E 07	3.806E 01	3.211E 01
4.20E 06	6.729E 02	6.356E 02	1.26E 07	3.144E 01	2.624E 01
4.40E 06	6.430E 02	6.077E 02	1.28E 07	2.612E 01	2.174E 01
4.60E 06	5.891E 02	5.562E 02	1.30E 07	2.234E 01	1.833E 01
4.80E 06	5.334E 02	5.024E 02	1.32E 07	1.976E 01	1.582E 01
5.00E 06	5.100E 02	4.790E 02	1.34E 07	1.787E 01	1.419E 01
5.20E 06	5.220E 02	4.889E 02	1.36E 07	1.640E 01	1.317E 01
5.40E 06	5.526E 02	5.199E 02	1.38E 07	1.510E 01	1.230E 01
5.60E 06	5.956E 02	5.636E 02	1.40E 07	1.374E 01	1.123E 01
5.80E 06	6.502E 02	6.169E 02	1.42E 07	1.220E 01	9.913E 00
6.00E 06	7.008E 02	6.689E 02	1.44E 07	1.056E 01	8.492E 00
6.20E 06	7.353E 02	7.052E 02	1.46E 07	8.994E 00	7.140E 00
6.40E 06	7.514E 02	7.232E 02	1.48E 07	7.626E 00	5.953E 00
6.60E 06	7.504E 02	7.233E 02	1.50E 07	6.479E 00	4.954E 00
6.80E 06	7.244E 02	6.995E 02			

TABLE XXII

RUN 46B+47A PB SLAB AT 13 DEG.

ENERGY	UPPER LIMIT	LOWER LIMIT	ENERGY	UPPER LIMIT	LOWER LIMIT
8.00E 05	8.671E 03	8.266E 03	7.00E 06	8.300E 01	7.862E 01
9.00E 05	7.083E 03	6.660E 03	7.20E 06	7.354E 01	6.936E 01
1.00E 06	6.073E 03	5.766E 03	7.40E 06	6.472E 01	6.086E 01
1.10E 06	5.510E 03	5.296E 03	7.60E 06	5.681E 01	5.318E 01
1.20E 06	5.152E 03	4.981E 03	7.80E 06	4.975E 01	4.629E 01
1.30E 06	4.801E 03	4.654E 03	8.00E 06	4.392E 01	4.067E 01
1.40E 06	4.384E 03	4.250E 03	8.20E 06	3.968E 01	3.666E 01
1.50E 06	3.927E 03	3.802E 03	8.40E 06	3.636E 01	3.343E 01
1.60E 06	3.486E 03	3.379E 03	8.60E 06	3.302E 01	3.022E 01
1.70E 06	3.110E 03	3.022E 03	8.80E 06	2.955E 01	2.694E 01
1.80E 06	2.789E 03	2.714E 03	9.00E 06	2.643E 01	2.397E 01
1.90E 06	2.482E 03	2.420E 03	9.20E 06	2.376E 01	2.140E 01
2.00E 06	2.171E 03	2.119E 03	9.40E 06	2.129E 01	1.902E 01
2.10E 06	1.868E 03	1.825E 03	9.60E 06	1.911E 01	1.697E 01
2.20E 06	1.594E 03	1.558E 03	9.80E 06	1.753E 01	1.555E 01
2.30E 06	1.361E 03	1.331E 03	1.00E 07	1.636E 01	1.452E 01
2.40E 06	1.159E 03	1.134E 03	1.02E 07	1.476E 01	1.303E 01
2.50E 06	9.863E 02	9.655E 02	1.04E 07	1.219E 01	1.052E 01
2.60E 06	8.398E 02	8.225E 02	1.06E 07	9.107E 00	7.469E 00
2.70E 06	7.151E 02	6.994E 02	1.08E 07	6.557E 00	4.971E 00
2.80E 06	6.100E 02	5.953E 02	1.10E 07	5.199E 00	3.636E 00
2.90E 06	5.184E 02	5.050E 02	1.12E 07	4.784E 00	3.257E 00
3.00E 06	4.376E 02	4.252E 02	1.14E 07	4.670E 00	3.245E 00
3.20E 06	3.183E 02	3.085E 02	1.16E 07	4.472E 00	3.131E 00
3.40E 06	2.496E 02	2.405E 02	1.18E 07	4.179E 00	2.869E 00
3.60E 06	2.195E 02	2.105E 02	1.20E 07	4.044E 00	2.778E 00
3.80E 06	2.044E 02	1.957E 02	1.22E 07	4.203E 00	3.020E 00
4.00E 06	1.882E 02	1.799E 02	1.24E 07	4.468E 00	3.385E 00
4.20E 06	1.731E 02	1.655E 02	1.26E 07	4.475E 00	3.490E 00
4.40E 06	1.622E 02	1.549E 02	1.28E 07	4.052E 00	3.157E 00
4.60E 06	1.499E 02	1.430E 02	1.30E 07	3.337E 00	2.511E 00
4.80E 06	1.356E 02	1.290E 02	1.32E 07	2.570E 00	1.817E 00
5.00E 06	1.258E 02	1.195E 02	1.34E 07	1.933E 00	1.253E 00
5.20E 06	1.200E 02	1.137E 02	1.36E 07	1.495E 00	8.886E-01
5.40E 06	1.148E 02	1.086E 02	1.38E 07	1.251E 00	7.261E-01
5.60E 06	1.119E 02	1.059E 02	1.40E 07	1.161E 00	7.064E-01
5.80E 06	1.115E 02	1.057E 02	1.42E 07	1.158E 00	7.413E-01
6.00E 06	1.104E 02	1.048E 02	1.44E 07	1.158E 00	7.620E-01
6.20E 06	1.073E 02	1.020E 02	1.46E 07	1.103E 00	7.314E-01
6.40E 06	1.030E 02	9.789E 01	1.48E 07	9.902E-01	6.415E-01
6.60E 06	9.809E 01	9.311E 01	1.50E 07	8.464E-01	5.199E-01
6.80E 06	9.154E 01	8.691E 01			

TABLE XXIII

RUN 39E+40B PB SLAB AT 30 DEG.

ENERGY	UPPER LIMIT	LOWER LIMIT	ENERGY	UPPER LIMIT	LOWER LIMIT
8.00E 05	6.850E 03	6.533E 03	7.00E 06	2.835E 01	2.608E 01
9.00E 05	5.649E 03	5.320E 03	7.20E 06	2.394E 01	2.182E 01
1.00E 06	4.837E 03	4.601E 03	7.40E 06	1.998E 01	1.809E 01
1.10E 06	4.322E 03	4.161E 03	7.60E 06	1.687E 01	1.511E 01
1.20E 06	3.978E 03	3.850E 03	7.80E 06	1.430E 01	1.266E 01
1.30E 06	3.670E 03	3.562E 03	8.00E 06	1.202E 01	1.052E 01
1.40E 06	3.321E 03	3.224E 03	8.20E 06	9.979E 00	8.597E 00
1.50E 06	2.961E 03	2.871E 03	8.40E 06	8.304E 00	6.989E 00
1.60E 06	2.634E 03	2.557E 03	8.60E 06	7.052E 00	5.841E 00
1.70E 06	2.344E 03	2.281E 03	8.80E 06	6.048E 00	4.927E 00
1.80E 06	2.080E 03	2.028E 03	9.00E 06	5.035E 00	3.943E 00
1.90E 06	1.833E 03	1.789E 03	9.20E 06	4.051E 00	2.997E 00
2.00E 06	1.589E 03	1.553E 03	9.40E 06	3.437E 00	2.454E 00
2.10E 06	1.351E 03	1.322E 03	9.60E 06	3.388E 00	2.473E 00
2.20E 06	1.136E 03	1.112E 03	9.80E 06	3.674E 00	2.811E 00
2.30E 06	9.585E 02	9.392E 02	1.00E 07	3.840E 00	3.016E 00
2.40E 06	8.115E 02	7.953E 02	1.02E 07	3.576E 00	2.794E 00
2.50E 06	6.891E 02	6.758E 02	1.04E 07	2.915E 00	2.183E 00
2.60E 06	5.830E 02	5.721E 02	1.06E 07	2.140E 00	1.446E 00
2.70E 06	4.895E 02	4.796E 02	1.08E 07	1.503E 00	8.395E-01
2.80E 06	4.102E 02	4.008E 02	1.10E 07	1.077E 00	4.253E-01
2.90E 06	3.439E 02	3.352E 02	1.12E 07	7.911E-01	1.381E-01
3.00E 06	2.884E 02	2.805E 02	1.14E 07	5.990E-01	-3.356E-02
3.20E 06	2.096E 02	2.034E 02	1.16E 07	5.508E-01	-4.657E-02
3.40E 06	1.637E 02	1.578E 02	1.18E 07	6.602E-01	8.433E-02
3.60E 06	1.391E 02	1.332E 02	1.20E 07	7.964E-01	2.235E-01
3.80E 06	1.216E 02	1.158E 02	1.22E 07	8.603E-01	2.884E-01
4.00E 06	1.067E 02	1.011E 02	1.24E 07	8.560E-01	3.047E-01
4.20E 06	9.770E 01	9.268E 01	1.26E 07	8.375E-01	3.459E-01
4.40E 06	9.088E 01	8.610E 01	1.28E 07	8.431E-01	4.175E-01
4.60E 06	8.204E 01	7.759E 01	1.30E 07	8.569E-01	4.609E-01
4.80E 06	7.158E 01	6.745E 01	1.32E 07	8.165E-01	4.429E-01
5.00E 06	6.190E 01	5.796E 01	1.34E 07	7.044E-01	3.565E-01
5.20E 06	5.571E 01	5.185E 01	1.36E 07	5.513E-01	2.270E-01
5.40E 06	5.309E 01	4.939E 01	1.38E 07	4.007E-01	1.039E-01
5.60E 06	5.072E 01	4.718E 01	1.40E 07	2.907E-01	2.841E-02
5.80E 06	4.735E 01	4.391E 01	1.42E 07	2.396E-01	9.975E-03
6.00E 06	4.401E 01	4.081E 01	1.44E 07	2.376E-01	2.585E-02
6.20E 06	4.137E 01	3.836E 01	1.46E 07	2.517E-01	4.241E-02
6.40E 06	3.881E 01	3.599E 01	1.48E 07	2.472E-01	3.827E-02
6.60E 06	3.588E 01	3.318E 01	1.50E 07	2.122E-01	1.072E-02
6.80E 06	3.241E 01	2.996E 01			

TABLE XXIV

RUN 40C+40D PB SLAB AT 47 DEG.

ENERGY	UPPER LIMIT	LOWER LIMIT	ENERGY	UPPER LIMIT	LOWER LIMIT
8.00E 05	4.743E 03	4.552E 03	7.00E 06	9.137E 00	7.804E 00
9.00E 05	3.874E 03	3.667E 03	7.20E 06	8.112E 00	6.877E 00
1.00E 06	3.319E 03	3.167E 03	7.40E 06	7.189E 00	6.043E 00
1.10E 06	2.958E 03	2.853E 03	7.60E 06	5.909E 00	4.841E 00
1.20E 06	2.689E 03	2.607E 03	7.80E 06	4.537E 00	3.533E 00
1.30E 06	2.438E 03	2.370E 03	8.00E 06	3.560E 00	2.632E 00
1.40E 06	2.185E 03	2.124E 03	8.20E 06	3.155E 00	2.286E 00
1.50E 06	1.946E 03	1.891E 03	8.40E 06	2.994E 00	2.141E 00
1.60E 06	1.717E 03	1.670E 03	8.60E 06	2.779E 00	1.968E 00
1.70E 06	1.497E 03	1.459E 03	8.80E 06	2.509E 00	1.741E 00
1.80E 06	1.304E 03	1.273E 03	9.00E 06	2.278E 00	1.544E 00
1.90E 06	1.134E 03	1.108E 03	9.20E 06	2.098E 00	1.397E 00
2.00E 06	9.709E 02	9.501E 02	9.40E 06	1.923E 00	1.245E 00
2.10E 06	8.180E 02	8.010E 02	9.60E 06	1.741E 00	1.092E 00
2.20E 06	6.830E 02	6.690E 02	9.80E 06	1.592E 00	9.825E-01
2.30E 06	5.695E 02	5.582E 02	1.00E 07	1.473E 00	8.996E-01
2.40E 06	4.728E 02	4.632E 02	1.02E 07	1.326E 00	7.736E-01
2.50E 06	3.926E 02	3.846E 02	1.04E 07	1.136E 00	5.896E-01
2.60E 06	3.272E 02	3.205E 02	1.06E 07	9.678E-01	4.371E-01
2.70E 06	2.738E 02	2.674E 02	1.08E 07	9.007E-01	4.070E-01
2.80E 06	2.315E 02	2.252E 02	1.10E 07	9.194E-01	4.627E-01
2.90E 06	1.961E 02	1.903E 02	1.12E 07	9.067E-01	4.509E-01
3.00E 06	1.653E 02	1.600E 02	1.14E 07	7.547E-01	2.779E-01
3.20E 06	1.178E 02	1.137E 02	1.16E 07	4.742E-01	1.432E-02
3.40E 06	8.706E 01	8.320E 01	1.18E 07	1.972E-01	-2.203E-01
3.60E 06	6.782E 01	6.399E 01	1.20E 07	3.807E-02	-3.791E-01
3.80E 06	5.791E 01	5.422E 01	1.22E 07	9.663E-03	-4.145E-01
4.00E 06	5.237E 01	4.886E 01	1.24E 07	1.034E-01	-2.923E-01
4.20E 06	4.669E 01	4.358E 01	1.26E 07	2.963E-01	-5.753E-02
4.40E 06	4.052E 01	3.762E 01	1.28E 07	5.107E-01	1.801E-01
4.60E 06	3.405E 01	3.139E 01	1.30E 07	6.416E-01	3.226E-01
4.80E 06	2.793E 01	2.547E 01	1.32E 07	6.421E-01	3.332E-01
5.00E 06	2.335E 01	2.101E 01	1.34E 07	5.422E-01	2.497E-01
5.20E 06	2.100E 01	1.875E 01	1.36E 07	4.037E-01	1.494E-01
5.40E 06	1.971E 01	1.755E 01	1.38E 07	2.846E-01	8.249E-02
5.60E 06	1.786E 01	1.578E 01	1.40E 07	2.150E-01	4.997E-02
5.80E 06	1.609E 01	1.410E 01	1.42E 07	1.879E-01	3.177E-02
6.00E 06	1.488E 01	1.301E 01	1.44E 07	1.740E-01	1.648E-02
6.20E 06	1.404E 01	1.227E 01	1.46E 07	1.530E-01	-1.777E-04
6.40E 06	1.336E 01	1.172E 01	1.48E 07	1.233E-01	-2.064E-02
6.60E 06	1.233E 01	1.076E 01	1.50E 07	9.179E-02	-4.359E-02
6.80E 06	1.069E 01	9.231E 00			

TABLE XXV

RUN 45A+44C PB SLAB AT 64 DEG.

ENERGY	UPPER LIMIT	LOWER LIMIT	ENERGY	UPPER LIMIT	LOWER LIMIT
8.00E 05	1.590E 03	1.502E 03	7.00E 06	3.019E 00	2.271E 00
9.00E 05	1.858E 03	1.762E 03	7.20E 06	2.564E 00	1.859E 00
1.00E 06	1.884E 03	1.809E 03	7.40E 06	2.202E 00	1.575E 00
1.10E 06	1.605E 03	1.551E 03	7.60E 06	1.963E 00	1.387E 00
1.20E 06	1.418E 03	1.375E 03	7.80E 06	1.701E 00	1.155E 00
1.30E 06	1.276E 03	1.241E 03	8.00E 06	1.422E 00	9.135E-01
1.40E 06	1.161E 03	1.130E 03	8.20E 06	1.217E 00	7.376E-01
1.50E 06	1.048E 03	1.020E 03	8.40E 06	1.071E 00	6.135E-01
1.60E 06	9.211E 02	8.977E 02	8.60E 06	9.355E-01	5.095E-01
1.70E 06	7.824E 02	7.636E 02	8.80E 06	8.311E-01	4.253E-01
1.80E 06	6.601E 02	6.445E 02	9.00E 06	7.900E-01	3.854E-01
1.90E 06	5.622E 02	5.496E 02	9.20E 06	7.834E-01	3.933E-01
2.00E 06	4.785E 02	4.679E 02	9.40E 06	7.467E-01	3.955E-01
2.10E 06	4.026E 02	3.937E 02	9.60E 06	6.434E-01	3.233E-01
2.20E 06	3.358E 02	3.281E 02	9.80E 06	4.957E-01	1.700E-01
2.30E 06	2.792E 02	2.724E 02	1.00E 07	3.439E-01	1.631E-02
2.40E 06	2.309E 02	2.248E 02	1.02E 07	2.303E-01	-6.986E-02
2.50E 06	1.914E 02	1.861E 02	1.04E 07	1.876E-01	-9.092E-02
2.60E 06	1.591E 02	1.546E 02	1.06E 07	2.104E-01	-7.136E-02
2.70E 06	1.320E 02	1.276E 02	1.08E 07	2.547E-01	-2.641E-02
2.80E 06	1.094E 02	1.051E 02	1.10E 07	2.803E-01	1.025E-02
2.90E 06	9.055E 01	8.668E 01	1.12E 07	2.763E-01	2.809E-03
3.00E 06	7.489E 01	7.146E 01	1.14E 07	2.485E-01	-2.899E-02
3.20E 06	5.241E 01	4.984E 01	1.16E 07	2.223E-01	-3.628E-02
3.40E 06	3.795E 01	3.564E 01	1.18E 07	2.259E-01	-4.936E-03
3.60E 06	3.016E 01	2.793E 01	1.20E 07	2.446E-01	2.841E-02
3.80E 06	2.489E 01	2.276E 01	1.22E 07	2.447E-01	3.678E-02
4.00E 06	2.027E 01	1.830E 01	1.24E 07	2.150E-01	1.654E-02
4.20E 06	1.654E 01	1.480E 01	1.26E 07	1.699E-01	-1.713E-02
4.40E 06	1.349E 01	1.187E 01	1.28E 07	1.367E-01	-5.191E-02
4.60E 06	1.120E 01	9.731E 00	1.30E 07	1.228E-01	-7.449E-02
4.80E 06	9.785E 00	8.436E 00	1.32E 07	1.122E-01	-7.203E-02
5.00E 06	8.829E 00	7.573E 00	1.34E 07	9.880E-02	-5.444E-02
5.20E 06	7.551E 00	6.315E 00	1.36E 07	9.596E-02	-4.785E-02
5.40E 06	6.061E 00	4.894E 00	1.38E 07	1.056E-01	-5.722E-02
5.60E 06	5.236E 00	4.139E 00	1.40E 07	1.104E-01	-6.177E-02
5.80E 06	5.016E 00	3.945E 00	1.42E 07	1.062E-01	-5.410E-02
6.00E 06	4.827E 00	3.821E 00	1.44E 07	1.016E-01	-4.207E-02
6.20E 06	4.317E 00	3.351E 00	1.46E 07	1.036E-01	-3.519E-02
6.40E 06	3.683E 00	2.788E 00	1.48E 07	1.080E-01	-3.398E-02
6.60E 06	3.390E 00	2.554E 00	1.50E 07	1.053E-01	-3.506E-02
6.80E 06	3.297E 00	2.514E 00			

TABLE XXVI

RUN 73A+73B LAM. SLAB AT 0 DEG.

ENERGY	UPPER LIMIT	LOWER LIMIT	ENERGY	UPPER LIMIT	LOWER LIMIT
8.00E 05	1.012E 04	8.849E 03	7.00E 06	2.475E 03	2.409E 03
9.00E 05	1.109E 04	9.682E 03	7.20E 06	2.210E 03	2.151E 03
1.00E 06	1.185E 04	1.060E 04	7.40E 06	1.932E 03	1.881E 03
1.10E 06	1.332E 04	1.225E 04	7.60E 06	1.688E 03	1.642E 03
1.20E 06	1.508E 04	1.413E 04	7.80E 06	1.512E 03	1.472E 03
1.30E 06	1.674E 04	1.585E 04	8.00E 06	1.402E 03	1.365E 03
1.40E 06	1.814E 04	1.724E 04	8.20E 06	1.324E 03	1.291E 03
1.50E 06	1.898E 04	1.809E 04	8.40E 06	1.247E 03	1.216E 03
1.60E 06	1.898E 04	1.817E 04	8.60E 06	1.159E 03	1.131E 03
1.70E 06	1.817E 04	1.745E 04	8.80E 06	1.058E 03	1.032E 03
1.80E 06	1.699E 04	1.634E 04	9.00E 06	9.487E 02	9.234E 02
1.90E 06	1.572E 04	1.516E 04	9.20E 06	8.424E 02	8.182E 02
2.00E 06	1.452E 04	1.403E 04	9.40E 06	7.517E 02	7.288E 02
2.10E 06	1.339E 04	1.297E 04	9.60E 06	6.762E 02	6.544E 02
2.20E 06	1.235E 04	1.197E 04	9.80E 06	6.070E 02	5.861E 02
2.30E 06	1.132E 04	1.099E 04	1.00E 07	5.400E 02	5.203E 02
2.40E 06	1.025E 04	9.956E 03	1.02E 07	4.784E 02	4.602E 02
2.50E 06	9.075E 03	8.821E 03	1.04E 07	4.256E 02	4.084E 02
2.60E 06	7.875E 03	7.654E 03	1.06E 07	3.803E 02	3.633E 02
2.70E 06	6.752E 03	6.541E 03	1.08E 07	3.393E 02	3.220E 02
2.80E 06	5.773E 03	5.566E 03	1.10E 07	3.007E 02	2.833E 02
2.90E 06	4.929E 03	4.730E 03	1.12E 07	2.638E 02	2.474E 02
3.00E 06	4.173E 03	3.980E 03	1.14E 07	2.296E 02	2.151E 02
3.20E 06	2.938E 03	2.769E 03	1.16E 07	2.000E 02	1.870E 02
3.40E 06	2.276E 03	2.108E 03	1.18E 07	1.753E 02	1.630E 02
3.60E 06	2.177E 03	2.004E 03	1.20E 07	1.538E 02	1.417E 02
3.80E 06	2.358E 03	2.188E 03	1.22E 07	1.352E 02	1.232E 02
4.00E 06	2.544E 03	2.381E 03	1.24E 07	1.199E 02	1.087E 02
4.20E 06	2.615E 03	2.468E 03	1.26E 07	1.076E 02	9.777E 01
4.40E 06	2.623E 03	2.484E 03	1.28E 07	9.681E 01	8.851E 01
4.60E 06	2.561E 03	2.433E 03	1.30E 07	8.662E 01	7.900E 01
4.80E 06	2.466E 03	2.347E 03	1.32E 07	7.650E 01	6.908E 01
5.00E 06	2.421E 03	2.305E 03	1.34E 07	6.659E 01	5.969E 01
5.20E 06	2.468E 03	2.346E 03	1.36E 07	5.760E 01	5.151E 01
5.40E 06	2.553E 03	2.434E 03	1.38E 07	4.998E 01	4.468E 01
5.60E 06	2.623E 03	2.508E 03	1.40E 07	4.358E 01	3.893E 01
5.80E 06	2.715E 03	2.597E 03	1.42E 07	3.796E 01	3.378E 01
6.00E 06	2.834E 03	2.722E 03	1.44E 07	3.272E 01	2.889E 01
6.20E 06	2.930E 03	2.826E 03	1.46E 07	2.777E 01	2.423E 01
6.40E 06	2.950E 03	2.857E 03	1.48E 07	2.331E 01	2.008E 01
6.60E 06	2.874E 03	2.789E 03	1.50E 07	1.964E 01	1.669E 01
6.80E 06	2.704E 03	2.629E 03			

TABLE XXVII

RUN 74D+74E LAM. SLAB AT 13 DEG.

ENERGY	UPPER LIMIT	LOWER LIMIT	ENERGY	UPPER LIMIT	LOWER LIMIT
8.00E 05	1.206E 03	1.116E 03	7.00E 06	1.320E 02	1.265E 02
9.00E 05	1.114E 03	1.014E 03	7.20E 06	1.127E 02	1.075E 02
1.00E 06	1.050E 03	9.675E 02	7.40E 06	9.526E 01	9.036E 01
1.10E 06	1.046E 03	9.785E 02	7.60E 06	8.205E 01	7.745E 01
1.20E 06	1.076E 03	1.017E 03	7.80E 06	7.240E 01	6.804E 01
1.30E 06	1.110E 03	1.055E 03	8.00E 06	6.522E 01	6.111E 01
1.40E 06	1.118E 03	1.061E 03	8.20E 06	5.991E 01	5.606E 01
1.50E 06	1.084E 03	1.029E 03	8.40E 06	5.525E 01	5.151E 01
1.60E 06	1.024E 03	9.734E 02	8.60E 06	4.994E 01	4.638E 01
1.70E 06	9.565E 02	9.101E 02	8.80E 06	4.378E 01	4.043E 01
1.80E 06	8.873E 02	8.434E 02	9.00E 06	3.774E 01	3.455E 01
1.90E 06	8.205E 02	7.817E 02	9.20E 06	3.296E 01	2.990E 01
2.00E 06	7.745E 02	7.402E 02	9.40E 06	2.969E 01	2.678E 01
2.10E 06	7.506E 02	7.198E 02	9.60E 06	2.722E 01	2.443E 01
2.20E 06	7.298E 02	7.019E 02	9.80E 06	2.462E 01	2.193E 01
2.30E 06	6.964E 02	6.717E 02	1.00E 07	2.159E 01	1.905E 01
2.40E 06	6.538E 02	6.312E 02	1.02E 07	1.861E 01	1.624E 01
2.50E 06	6.050E 02	5.850E 02	1.04E 07	1.621E 01	1.397E 01
2.60E 06	5.545E 02	5.369E 02	1.06E 07	1.443E 01	1.220E 01
2.70E 06	5.059E 02	4.888E 02	1.08E 07	1.290E 01	1.061E 01
2.80E 06	4.608E 02	4.438E 02	1.10E 07	1.141E 01	9.072E 00
2.90E 06	4.175E 02	4.011E 02	1.12E 07	1.012E 01	7.901E 00
3.00E 06	3.736E 02	3.578E 02	1.14E 07	9.277E 00	7.289E 00
3.20E 06	2.864E 02	2.727E 02	1.16E 07	8.745E 00	6.908E 00
3.40E 06	2.344E 02	2.211E 02	1.18E 07	8.166E 00	6.370E 00
3.60E 06	2.323E 02	2.189E 02	1.20E 07	7.532E 00	5.792E 00
3.80E 06	2.509E 02	2.381E 02	1.22E 07	7.034E 00	5.377E 00
4.00E 06	2.640E 02	2.520E 02	1.24E 07	6.632E 00	5.071E 00
4.20E 06	2.657E 02	2.550E 02	1.26E 07	6.100E 00	4.695E 00
4.40E 06	2.590E 02	2.491E 02	1.28E 07	5.353E 00	4.136E 00
4.60E 06	2.443E 02	2.351E 02	1.30E 07	4.539E 00	3.421E 00
4.80E 06	2.295E 02	2.209E 02	1.32E 07	3.802E 00	2.716E 00
5.00E 06	2.160E 02	2.077E 02	1.34E 07	3.207E 00	2.179E 00
5.20E 06	2.032E 02	1.949E 02	1.36E 07	2.767E 00	1.842E 00
5.40E 06	1.963E 02	1.882E 02	1.38E 07	2.457E 00	1.649E 00
5.60E 06	1.953E 02	1.875E 02	1.40E 07	2.232E 00	1.509E 00
5.80E 06	1.936E 02	1.859E 02	1.42E 07	2.047E 00	1.359E 00
6.00E 06	1.866E 02	1.794E 02	1.44E 07	1.858E 00	1.194E 00
6.20E 06	1.767E 02	1.698E 02	1.46E 07	1.657E 00	1.033E 00
6.40E 06	1.671E 02	1.606E 02	1.48E 07	1.466E 00	8.898E-01
6.60E 06	1.588E 02	1.525E 02	1.50E 07	1.316E 00	7.779E-01
6.80E 06	1.480E 02	1.421E 02			

TABLE XXVIII

RUN 75E+75F LAM. SLAB AT 30 DEG.

ENERGY	UPPER LIMIT	LOWER LIMIT	ENERGY	UPPER LIMIT	LOWER LIMIT
8.00E 05	9.483E 02	8.838E 02	7.00E 06	3.837E 01	3.574E 01
9.00E 05	9.005E 02	8.289E 02	7.20E 06	3.245E 01	2.999E 01
1.00E 06	8.410E 02	7.835E 02	7.40E 06	2.672E 01	2.447E 01
1.10E 06	8.025E 02	7.570E 02	7.60E 06	2.127E 01	1.920E 01
1.20E 06	8.023E 02	7.633E 02	7.80E 06	1.670E 01	1.477E 01
1.30E 06	8.151E 02	7.792E 02	8.00E 06	1.341E 01	1.159E 01
1.40E 06	8.191E 02	7.832E 02	8.20E 06	1.175E 01	1.008E 01
1.50E 06	7.962E 02	7.615E 02	8.40E 06	1.122E 01	9.629E 00
1.60E 06	7.433E 02	7.119E 02	8.60E 06	1.074E 01	9.204E 00
1.70E 06	6.753E 02	6.472E 02	8.80E 06	9.760E 00	8.319E 00
1.80E 06	6.070E 02	5.810E 02	9.00E 06	8.499E 00	7.150E 00
1.90E 06	5.467E 02	5.240E 02	9.20E 06	7.283E 00	6.010E 00
2.00E 06	5.050E 02	4.852E 02	9.40E 06	6.250E 00	5.047E 00
2.10E 06	4.817E 02	4.640E 02	9.60E 06	5.424E 00	4.286E 00
2.20E 06	4.665E 02	4.506E 02	9.80E 06	4.711E 00	3.643E 00
2.30E 06	4.481E 02	4.341E 02	1.00E 07	3.946E 00	2.934E 00
2.40E 06	4.212E 02	4.085E 02	1.02E 07	3.054E 00	2.095E 00
2.50E 06	3.831E 02	3.719E 02	1.04E 07	2.204E 00	1.291E 00
2.60E 06	3.395E 02	3.299E 02	1.06E 07	1.682E 00	7.773E-01
2.70E 06	2.987E 02	2.894E 02	1.08E 07	1.616E 00	7.165E-01
2.80E 06	2.661E 02	2.568E 02	1.10E 07	1.891E 00	1.025E 00
2.90E 06	2.416E 02	2.326E 02	1.12E 07	2.232E 00	1.394E 00
3.00E 06	2.210E 02	2.126E 02	1.14E 07	2.364E 00	1.527E 00
3.20E 06	1.836E 02	1.764E 02	1.16E 07	2.181E 00	1.366E 00
3.40E 06	1.536E 02	1.466E 02	1.18E 07	1.806E 00	1.053E 00
3.60E 06	1.396E 02	1.325E 02	1.20E 07	1.464E 00	7.692E-01
3.80E 06	1.400E 02	1.330E 02	1.22E 07	1.255E 00	5.886E-01
4.00E 06	1.416E 02	1.348E 02	1.24E 07	1.174E 00	5.362E-01
4.20E 06	1.360E 02	1.298E 02	1.26E 07	1.157E 00	5.838E-01
4.40E 06	1.289E 02	1.230E 02	1.28E 07	1.125E 00	6.180E-01
4.60E 06	1.196E 02	1.142E 02	1.30E 07	1.011E 00	5.226E-01
4.80E 06	1.057E 02	1.006E 02	1.32E 07	7.950E-01	3.145E-01
5.00E 06	9.294E 01	8.811E 01	1.34E 07	5.548E-01	1.088E-01
5.20E 06	8.553E 01	8.081E 01	1.36E 07	4.031E-01	5.625E-03
5.40E 06	8.170E 01	7.717E 01	1.38E 07	3.891E-01	2.366E-02
5.60E 06	7.701E 01	7.271E 01	1.40E 07	4.688E-01	1.188E-01
5.80E 06	7.104E 01	6.688E 01	1.42E 07	5.601E-01	2.267E-01
6.00E 06	6.604E 01	6.218E 01	1.44E 07	6.044E-01	2.932E-01
6.20E 06	6.285E 01	5.926E 01	1.46E 07	5.858E-01	2.899E-01
6.40E 06	5.931E 01	5.597E 01	1.48E 07	5.134E-01	2.218E-01
6.60E 06	5.319E 01	4.999E 01	1.50E 07	4.072E-01	1.208E-01
6.80E 06	4.540E 01	4.250E 01			

TABLE XXIX

RUN 82A+82A8 LAM. SLAB AT 30 DEG.

ENERGY	UPPER LIMIT	LOWER LIMIT	ENERGY	UPPER LIMIT	LOWER LIMIT
8.00E 05	9.675E 02	9.017E 02	7.00E 06	3.807E 01	3.538E 01
9.00E 05	9.281E 02	8.551E 02	7.20E 06	3.286E 01	3.033E 01
1.00E 06	8.678E 02	8.084E 02	7.40E 06	2.776E 01	2.545E 01
1.10E 06	8.383E 02	7.913E 02	7.60E 06	2.349E 01	2.139E 01
1.20E 06	8.469E 02	8.067E 02	7.80E 06	1.991E 01	1.796E 01
1.30E 06	8.640E 02	8.274E 02	8.00E 06	1.682E 01	1.501E 01
1.40E 06	8.559E 02	8.193E 02	8.20E 06	1.434E 01	1.268E 01
1.50E 06	8.127E 02	7.773E 02	8.40E 06	1.246E 01	1.089E 01
1.60E 06	7.499E 02	7.180E 02	8.60E 06	1.076E 01	9.291E 00
1.70E 06	6.836E 02	6.548E 02	8.80E 06	8.910E 00	7.538E 00
1.80E 06	6.196E 02	5.928E 02	9.00E 06	7.095E 00	5.808E 00
1.90E 06	5.633E 02	5.399E 02	9.20E 06	5.713E 00	4.517E 00
2.00E 06	5.221E 02	5.017E 02	9.40E 06	4.808E 00	3.667E 00
2.10E 06	4.939E 02	4.757E 02	9.60E 06	4.051E 00	2.931E 00
2.20E 06	4.704E 02	4.541E 02	9.80E 06	3.257E 00	2.187E 00
2.30E 06	4.458E 02	4.316E 02	1.00E 07	2.645E 00	1.641E 00
2.40E 06	4.202E 02	4.074E 02	1.02E 07	2.500E 00	1.556E 00
2.50E 06	3.926E 02	3.814E 02	1.04E 07	2.820E 00	1.921E 00
2.60E 06	3.614E 02	3.517E 02	1.06E 07	3.278E 00	2.399E 00
2.70E 06	3.274E 02	3.182E 02	1.08E 07	3.444E 00	2.574E 00
2.80E 06	2.925E 02	2.835E 02	1.10E 07	3.111E 00	2.237E 00
2.90E 06	2.602E 02	2.517E 02	1.12E 07	2.430E 00	1.581E 00
3.00E 06	2.316E 02	2.234E 02	1.14E 07	1.774E 00	1.027E 00
3.20E 06	1.840E 02	1.770E 02	1.16E 07	1.412E 00	7.639E-01
3.40E 06	1.527E 02	1.459E 02	1.18E 07	1.282E 00	6.348E-01
3.60E 06	1.448E 02	1.377E 02	1.20E 07	1.149E 00	4.795E-01
3.80E 06	1.479E 02	1.408E 02	1.22E 07	1.002E 00	3.555E-01
4.00E 06	1.445E 02	1.376E 02	1.24E 07	9.266E-01	3.514E-01
4.20E 06	1.355E 02	1.293E 02	1.26E 07	9.257E-01	4.337E-01
4.40E 06	1.279E 02	1.221E 02	1.28E 07	9.363E-01	4.724E-01
4.60E 06	1.201E 02	1.146E 02	1.30E 07	8.938E-01	4.157E-01
4.80E 06	1.091E 02	1.040E 02	1.32E 07	7.839E-01	3.361E-01
5.00E 06	9.643E 01	9.159E 01	1.34E 07	6.658E-01	2.946E-01
5.20E 06	8.553E 01	8.079E 01	1.36E 07	5.933E-01	2.841E-01
5.40E 06	7.977E 01	7.524E 01	1.38E 07	5.598E-01	2.652E-01
5.60E 06	7.850E 01	7.424E 01	1.40E 07	5.146E-01	2.171E-01
5.80E 06	7.684E 01	7.272E 01	1.42E 07	4.255E-01	1.376E-01
6.00E 06	7.024E 01	6.640E 01	1.44E 07	3.023E-01	3.681E-02
6.20E 06	6.060E 01	5.702E 01	1.46E 07	1.797E-01	-6.404E-02
6.40E 06	5.199E 01	4.865E 01	1.48E 07	9.397E-02	-1.398E-01
6.60E 06	4.643E 01	4.324E 01	1.50E 07	6.141E-02	-1.682E-01
6.80E 06	4.245E 01	3.955E 01			

TABLE XXX

RUN 76E+76E8 LAM. SLAB AT 47 DEG.

ENERGY	UPPER LIMIT	LOWER LIMIT	ENERGY	UPPER LIMIT	LOWER LIMIT
8.00E 05	6.067E 02	5.700E 02	7.00E 06	9.658E 00	8.209E 00
9.00E 05	5.746E 02	5.340E 02	7.20E 06	8.850E 00	7.463E 00
1.00E 06	5.258E 02	4.938E 02	7.40E 06	7.795E 00	6.507E 00
1.10E 06	4.744E 02	4.498E 02	7.60E 06	6.675E 00	5.487E 00
1.20E 06	4.630E 02	4.424E 02	7.80E 06	5.612E 00	4.496E 00
1.30E 06	4.737E 02	4.551E 02	8.00E 06	4.642E 00	3.577E 00
1.40E 06	4.669E 02	4.485E 02	8.20E 06	3.952E 00	2.946E 00
1.50E 06	4.381E 02	4.204E 02	8.40E 06	3.657E 00	2.683E 00
1.60E 06	4.001E 02	3.843E 02	8.60E 06	3.570E 00	2.632E 00
1.70E 06	3.593E 02	3.452E 02	8.80E 06	3.449E 00	2.568E 00
1.80E 06	3.208E 02	3.079E 02	9.00E 06	3.213E 00	2.380E 00
1.90E 06	2.894E 02	2.782E 02	9.20E 06	2.894E 00	2.084E 00
2.00E 06	2.670E 02	2.573E 02	9.40E 06	2.526E 00	1.748E 00
2.10E 06	2.520E 02	2.435E 02	9.60E 06	2.146E 00	1.417E 00
2.20E 06	2.408E 02	2.333E 02	9.80E 06	1.770E 00	1.091E 00
2.30E 06	2.294E 02	2.228E 02	1.00E 07	1.365E 00	7.085E-01
2.40E 06	2.155E 02	2.095E 02	1.02E 07	9.064E-01	2.506E-01
2.50E 06	1.978E 02	1.926E 02	1.04E 07	5.046E-01	-1.336E-01
2.60E 06	1.775E 02	1.729E 02	1.06E 07	3.618E-01	-2.416E-01
2.70E 06	1.573E 02	1.528E 02	1.08E 07	5.423E-01	-4.153E-02
2.80E 06	1.393E 02	1.347E 02	1.10E 07	8.796E-01	2.841E-01
2.90E 06	1.244E 02	1.198E 02	1.12E 07	1.141E 00	5.307E-01
3.00E 06	1.114E 02	1.069E 02	1.14E 07	1.229E 00	6.402E-01
3.20E 06	8.873E 01	8.468E 01	1.16E 07	1.206E 00	6.632E-01
3.40E 06	7.206E 01	6.805E 01	1.18E 07	1.150E 00	6.635E-01
3.60E 06	6.565E 01	6.153E 01	1.20E 07	1.082E 00	6.454E-01
3.80E 06	6.524E 01	6.120E 01	1.22E 07	9.854E-01	5.821E-01
4.00E 06	6.112E 01	5.725E 01	1.24E 07	8.398E-01	4.610E-01
4.20E 06	5.263E 01	4.918E 01	1.26E 07	6.512E-01	2.956E-01
4.40E 06	4.560E 01	4.239E 01	1.28E 07	4.499E-01	1.221E-01
4.60E 06	4.005E 01	3.707E 01	1.30E 07	2.789E-01	-1.728E-02
4.80E 06	3.479E 01	3.205E 01	1.32E 07	1.757E-01	-9.226E-02
5.00E 06	3.027E 01	2.769E 01	1.34E 07	1.528E-01	-9.307E-02
5.20E 06	2.697E 01	2.445E 01	1.36E 07	1.932E-01	-3.808E-02
5.40E 06	2.520E 01	2.280E 01	1.38E 07	2.604E-01	3.544E-02
5.60E 06	2.397E 01	2.171E 01	1.40E 07	3.167E-01	9.481E-02
5.80E 06	2.216E 01	1.996E 01	1.42E 07	3.434E-01	1.228E-01
6.00E 06	1.992E 01	1.789E 01	1.44E 07	3.403E-01	1.187E-01
6.20E 06	1.780E 01	1.592E 01	1.46E 07	3.113E-01	9.396E-02
6.40E 06	1.539E 01	1.362E 01	1.48E 07	2.605E-01	5.922E-02
6.60E 06	1.272E 01	1.102E 01	1.50E 07	1.989E-01	1.573E-02
6.80E 06	1.072E 01	9.171E 00			

TABLE XXXI

RUN 76G+76G8 LAM. SLAB AT 64 DEG.

ENERGY	UPPER LIMIT	LOWER LIMIT	ENERGY	UPPER LIMIT	LOWER LIMIT
8.00E 05	3.136E 02	2.960E 02	7.00E 06	3.599E 00	2.753E 00
9.00E 05	2.832E 02	2.638E 02	7.20E 06	3.166E 00	2.361E 00
1.00E 06	2.542E 02	2.390E 02	7.40E 06	2.487E 00	1.758E 00
1.10E 06	2.389E 02	2.273E 02	7.60E 06	1.974E 00	1.283E 00
1.20E 06	2.314E 02	2.217E 02	7.80E 06	1.745E 00	1.111E 00
1.30E 06	2.278E 02	2.192E 02	8.00E 06	1.661E 00	1.069E 00
1.40E 06	2.231E 02	2.147E 02	8.20E 06	1.568E 00	1.005E 00
1.50E 06	2.117E 02	2.037E 02	8.40E 06	1.476E 00	9.346E-01
1.60E 06	1.919E 02	1.849E 02	8.60E 06	1.424E 00	9.195E-01
1.70E 06	1.695E 02	1.631E 02	8.80E 06	1.357E 00	9.016E-01
1.80E 06	1.501E 02	1.441E 02	9.00E 06	1.182E 00	7.316E-01
1.90E 06	1.348E 02	1.297E 02	9.20E 06	8.640E-01	4.023E-01
2.00E 06	1.247E 02	1.202E 02	9.40E 06	5.237E-01	8.054E-02
2.10E 06	1.184E 02	1.143E 02	9.60E 06	3.276E-01	-8.277E-02
2.20E 06	1.127E 02	1.087E 02	9.80E 06	2.962E-01	-9.384E-02
2.30E 06	1.052E 02	1.015E 02	1.00E 07	3.213E-01	-7.342E-02
2.40E 06	9.633E 01	9.291E 01	1.02E 07	3.230E-01	-8.587E-02
2.50E 06	8.671E 01	8.361E 01	1.04E 07	3.218E-01	-7.835E-02
2.60E 06	7.742E 01	7.464E 01	1.06E 07	3.744E-01	-3.979E-03
2.70E 06	6.913E 01	6.635E 01	1.08E 07	4.716E-01	1.085E-01
2.80E 06	6.178E 01	5.893E 01	1.10E 07	5.475E-01	2.079E-01
2.90E 06	5.467E 01	5.186E 01	1.12E 07	5.633E-01	2.588E-01
3.00E 06	4.758E 01	4.481E 01	1.14E 07	5.306E-01	2.358E-01
3.20E 06	3.535E 01	3.290E 01	1.16E 07	4.656E-01	1.539E-01
3.40E 06	2.902E 01	2.663E 01	1.18E 07	3.827E-01	8.023E-02
3.60E 06	2.601E 01	2.355E 01	1.20E 07	3.205E-01	4.654E-02
3.80E 06	2.322E 01	2.081E 01	1.22E 07	2.880E-01	3.425E-02
4.00E 06	2.073E 01	1.845E 01	1.24E 07	2.591E-01	3.083E-02
4.20E 06	1.816E 01	1.612E 01	1.26E 07	2.315E-01	2.591E-02
4.40E 06	1.617E 01	1.427E 01	1.28E 07	2.221E-01	5.360E-03
4.60E 06	1.499E 01	1.326E 01	1.30E 07	2.082E-01	-1.901E-02
4.80E 06	1.332E 01	1.174E 01	1.32E 07	1.641E-01	-3.945E-02
5.00E 06	1.073E 01	9.239E 00	1.34E 07	1.022E-01	-6.662E-02
5.20E 06	8.541E 00	7.106E 00	1.36E 07	5.291E-02	-1.055E-01
5.40E 06	7.883E 00	6.562E 00	1.38E 07	2.524E-02	-1.367E-01
5.60E 06	7.748E 00	6.473E 00	1.40E 07	1.426E-02	-1.437E-01
5.80E 06	7.135E 00	5.904E 00	1.42E 07	1.667E-02	-1.308E-01
6.00E 06	6.232E 00	5.105E 00	1.44E 07	2.871E-02	-1.101E-01
6.20E 06	5.404E 00	4.338E 00	1.46E 07	4.476E-02	-9.048E-02
6.40E 06	4.588E 00	3.569E 00	1.48E 07	5.954E-02	-7.532E-02
6.60E 06	3.969E 00	2.999E 00	1.50E 07	7.066E-02	-6.524E-02
6.80E 06	3.736E 00	2.854E 00			

TABLE XXXII

RUN 165C+165C8 U SLAB AT 0 DEG.

ENERGY	UPPER LIMIT	LOWER LIMIT	ENERGY	UPPER LIMIT	LOWER LIMIT
8.00E 05	1.621E 05	1.500E 05	7.00E 06	7.634E 03	7.336E 03
9.00E 05	1.551E 05	1.417E 05	7.20E 06	6.962E 03	6.677E 03
1.00E 06	1.481E 05	1.372E 05	7.40E 06	6.170E 03	5.903E 03
1.10E 06	1.506E 05	1.420E 05	7.60E 06	5.326E 03	5.075E 03
1.20E 06	1.565E 05	1.491E 05	7.80E 06	4.674E 03	4.437E 03
1.30E 06	1.596E 05	1.528E 05	8.00E 06	4.267E 03	4.045E 03
1.40E 06	1.582E 05	1.515E 05	8.20E 06	3.991E 03	3.784E 03
1.50E 06	1.522E 05	1.457E 05	8.40E 06	3.669E 03	3.468E 03
1.60E 06	1.432E 05	1.374E 05	8.60E 06	3.243E 03	3.050E 03
1.70E 06	1.337E 05	1.286E 05	8.80E 06	2.789E 03	2.613E 03
1.80E 06	1.244E 05	1.198E 05	9.00E 06	2.408E 03	2.242E 03
1.90E 06	1.149E 05	1.109E 05	9.20E 06	2.121E 03	1.961E 03
2.00E 06	1.055E 05	1.020E 05	9.40E 06	1.898E 03	1.746E 03
2.10E 06	9.681E 04	9.374E 04	9.60E 06	1.699E 03	1.555E 03
2.20E 06	8.897E 04	8.627E 04	9.80E 06	1.505E 03	1.367E 03
2.30E 06	8.177E 04	7.949E 04	1.00E 07	1.320E 03	1.192E 03
2.40E 06	7.478E 04	7.278E 04	1.02E 07	1.157E 03	1.038E 03
2.50E 06	6.768E 04	6.594E 04	1.04E 07	1.011E 03	8.979E 02
2.60E 06	6.052E 04	5.902E 04	1.06E 07	8.771E 02	7.651E 02
2.70E 06	5.357E 04	5.215E 04	1.08E 07	7.606E 02	6.483E 02
2.80E 06	4.700E 04	4.564E 04	1.10E 07	6.749E 02	5.654E 02
2.90E 06	4.095E 04	3.968E 04	1.12E 07	6.185E 02	5.160E 02
3.00E 06	3.544E 04	3.425E 04	1.14E 07	5.704E 02	4.766E 02
3.20E 06	2.661E 04	2.563E 04	1.16E 07	5.131E 02	4.264E 02
3.40E 06	2.169E 04	2.078E 04	1.18E 07	4.501E 02	3.682E 02
3.60E 06	2.028E 04	1.938E 04	1.20E 07	3.949E 02	3.163E 02
3.80E 06	2.029E 04	1.943E 04	1.22E 07	3.468E 02	2.705E 02
4.00E 06	2.002E 04	1.924E 04	1.24E 07	2.957E 02	2.231E 02
4.20E 06	1.909E 04	1.841E 04	1.26E 07	2.404E 02	1.752E 02
4.40E 06	1.794E 04	1.732E 04	1.28E 07	1.950E 02	1.382E 02
4.60E 06	1.657E 04	1.602E 04	1.30E 07	1.733E 02	1.207E 02
4.80E 06	1.510E 04	1.460E 04	1.32E 07	1.711E 02	1.211E 02
5.00E 06	1.389E 04	1.343E 04	1.34E 07	1.741E 02	1.277E 02
5.20E 06	1.310E 04	1.264E 04	1.36E 07	1.708E 02	1.292E 02
5.40E 06	1.268E 04	1.224E 04	1.38E 07	1.583E 02	1.218E 02
5.60E 06	1.248E 04	1.206E 04	1.40E 07	1.395E 02	1.077E 02
5.80E 06	1.228E 04	1.185E 04	1.42E 07	1.182E 02	9.051E 01
6.00E 06	1.185E 04	1.145E 04	1.44E 07	9.711E 01	7.221E 01
6.20E 06	1.128E 04	1.091E 04	1.46E 07	7.773E 01	5.446E 01
6.40E 06	1.053E 04	1.018E 04	1.48E 07	6.122E 01	3.945E 01
6.60E 06	9.532E 03	9.188E 03	1.50E 07	4.873E 01	2.903E 01
6.80E 06	8.466E 03	8.146E 03			

TABLE XXXIII

RUN 164A+160B U SLAB AT 13 DEG.

ENERGY	UPPER LIMIT	LOWER LIMIT	ENERGY	UPPER LIMIT	LOWER LIMIT
8.00E 05	7.212E 03	6.917E 03	7.00E 06	1.564E 02	1.466E 02
9.00E 05	5.350E 03	5.056E 03	7.20E 06	1.358E 02	1.265E 02
1.00E 06	4.129E 03	3.917E 03	7.40E 06	1.185E 02	1.098E 02
1.10E 06	3.381E 03	3.234E 03	7.60E 06	1.058E 02	9.765E 01
1.20E 06	2.920E 03	2.800E 03	7.80E 06	9.655E 01	8.885E 01
1.30E 06	2.634E 03	2.525E 03	8.00E 06	8.799E 01	8.073E 01
1.40E 06	2.417E 03	2.308E 03	8.20E 06	7.881E 01	7.203E 01
1.50E 06	2.216E 03	2.111E 03	8.40E 06	7.015E 01	6.366E 01
1.60E 06	2.021E 03	1.925E 03	8.60E 06	6.250E 01	5.641E 01
1.70E 06	1.838E 03	1.751E 03	8.80E 06	5.526E 01	4.954E 01
1.80E 06	1.684E 03	1.602E 03	9.00E 06	4.840E 01	4.295E 01
1.90E 06	1.566E 03	1.494E 03	9.20E 06	4.246E 01	3.734E 01
2.00E 06	1.480E 03	1.416E 03	9.40E 06	3.730E 01	3.247E 01
2.10E 06	1.411E 03	1.353E 03	9.60E 06	3.212E 01	2.750E 01
2.20E 06	1.339E 03	1.286E 03	9.80E 06	2.687E 01	2.244E 01
2.30E 06	1.257E 03	1.210E 03	1.00E 07	2.245E 01	1.828E 01
2.40E 06	1.172E 03	1.130E 03	1.02E 07	1.977E 01	1.592E 01
2.50E 06	1.089E 03	1.052E 03	1.04E 07	1.882E 01	1.520E 01
2.60E 06	1.014E 03	9.813E 02	1.06E 07	1.874E 01	1.514E 01
2.70E 06	9.523E 02	9.204E 02	1.08E 07	1.838E 01	1.478E 01
2.80E 06	9.033E 02	8.718E 02	1.10E 07	1.708E 01	1.358E 01
2.90E 06	8.565E 02	8.263E 02	1.12E 07	1.472E 01	1.141E 01
3.00E 06	8.030E 02	7.743E 02	1.14E 07	1.159E 01	8.500E 00
3.20E 06	6.756E 02	6.516E 02	1.16E 07	8.322E 00	5.419E 00
3.40E 06	5.781E 02	5.553E 02	1.18E 07	5.817E 00	3.063E 00
3.60E 06	5.288E 02	5.056E 02	1.20E 07	4.571E 00	1.935E 00
3.80E 06	5.155E 02	4.931E 02	1.22E 07	4.470E 00	1.909E 00
4.00E 06	5.133E 02	4.918E 02	1.24E 07	5.007E 00	2.549E 00
4.20E 06	4.898E 02	4.703E 02	1.26E 07	5.647E 00	3.425E 00
4.40E 06	4.522E 02	4.335E 02	1.28E 07	6.079E 00	4.131E 00
4.60E 06	4.217E 02	4.042E 02	1.30E 07	6.184E 00	4.391E 00
4.80E 06	3.929E 02	3.766E 02	1.32E 07	5.896E 00	4.214E 00
5.00E 06	3.539E 02	3.381E 02	1.34E 07	5.227E 00	3.719E 00
5.20E 06	3.186E 02	3.031E 02	1.36E 07	4.302E 00	2.962E 00
5.40E 06	3.033E 02	2.884E 02	1.38E 07	3.267E 00	2.038E 00
5.60E 06	2.996E 02	2.854E 02	1.40E 07	2.277E 00	1.141E 00
5.80E 06	2.919E 02	2.780E 02	1.42E 07	1.503E 00	4.762E-01
6.00E 06	2.734E 02	2.604E 02	1.44E 07	1.066E 00	1.500E-01
6.20E 06	2.486E 02	2.362E 02	1.46E 07	9.679E-01	1.449E-01
6.40E 06	2.230E 02	2.114E 02	1.48E 07	1.108E 00	3.478E-01
6.60E 06	2.002E 02	1.889E 02	1.50E 07	1.342E 00	6.143E-01
6.80E 06	1.782E 02	1.677E 02			

TABLE XXXIV

RUN 163B+159C U SLAB AT 30 DEG.

ENERGY	UPPER LIMIT	LOWER LIMIT	ENERGY	UPPER LIMIT	LOWER LIMIT
8.00E 05	6.041E 03	5.819E 03	7.00E 06	6.194E 01	5.840E 01
9.00E 05	4.457E 03	4.237E 03	7.20E 06	5.409E 01	5.076E 01
1.00E 06	3.348E 03	3.194E 03	7.40E 06	4.610E 01	4.307E 01
1.10E 06	2.666E 03	2.565E 03	7.60E 06	3.835E 01	3.557E 01
1.20E 06	2.246E 03	2.165E 03	7.80E 06	3.150E 01	2.892E 01
1.30E 06	1.972E 03	1.901E 03	8.00E 06	2.612E 01	2.372E 01
1.40E 06	1.755E 03	1.685E 03	8.20E 06	2.237E 01	2.015E 01
1.50E 06	1.561E 03	1.494E 03	8.40E 06	1.957E 01	1.745E 01
1.60E 06	1.392E 03	1.332E 03	8.60E 06	1.712E 01	1.513E 01
1.70E 06	1.256E 03	1.202E 03	8.80E 06	1.488E 01	1.306E 01
1.80E 06	1.146E 03	1.095E 03	9.00E 06	1.295E 01	1.122E 01
1.90E 06	1.051E 03	1.007E 03	9.20E 06	1.128E 01	9.621E 00
2.00E 06	9.672E 02	9.283E 02	9.40E 06	9.777E 00	8.213E 00
2.10E 06	8.968E 02	8.619E 02	9.60E 06	8.415E 00	6.959E 00
2.20E 06	8.424E 02	8.109E 02	9.80E 06	7.204E 00	5.836E 00
2.30E 06	8.001E 02	7.726E 02	1.00E 07	6.160E 00	4.870E 00
2.40E 06	7.572E 02	7.323E 02	1.02E 07	5.296E 00	4.103E 00
2.50E 06	7.038E 02	6.817E 02	1.04E 07	4.618E 00	3.494E 00
2.60E 06	6.462E 02	6.269E 02	1.06E 07	4.098E 00	2.981E 00
2.70E 06	5.974E 02	5.790E 02	1.08E 07	3.715E 00	2.613E 00
2.80E 06	5.633E 02	5.455E 02	1.10E 07	3.488E 00	2.441E 00
2.90E 06	5.362E 02	5.194E 02	1.12E 07	3.324E 00	2.338E 00
3.00E 06	5.060E 02	4.903E 02	1.14E 07	2.990E 00	2.039E 00
3.20E 06	4.265E 02	4.138E 02	1.16E 07	2.350E 00	1.427E 00
3.40E 06	3.590E 02	3.473E 02	1.18E 07	1.601E 00	7.169E-01
3.60E 06	3.257E 02	3.143E 02	1.20E 07	1.123E 00	2.902E-01
3.80E 06	3.170E 02	3.063E 02	1.22E 07	1.063E 00	2.951E-01
4.00E 06	3.070E 02	2.971E 02	1.24E 07	1.294E 00	5.855E-01
4.20E 06	2.841E 02	2.754E 02	1.26E 07	1.554E 00	8.993E-01
4.40E 06	2.556E 02	2.476E 02	1.28E 07	1.638E 00	1.044E 00
4.60E 06	2.260E 02	2.185E 02	1.30E 07	1.515E 00	9.615E-01
4.80E 06	1.978E 02	1.909E 02	1.32E 07	1.252E 00	7.307E-01
5.00E 06	1.751E 02	1.687E 02	1.34E 07	9.522E-01	4.737E-01
5.20E 06	1.586E 02	1.523E 02	1.36E 07	7.003E-01	2.720E-01
5.40E 06	1.440E 02	1.379E 02	1.38E 07	5.354E-01	1.499E-01
5.60E 06	1.318E 02	1.261E 02	1.40E 07	4.514E-01	9.839E-02
5.80E 06	1.234E 02	1.179E 02	1.42E 07	4.221E-01	9.637E-02
6.00E 06	1.153E 02	1.102E 02	1.44E 07	4.232E-01	1.195E-01
6.20E 06	1.048E 02	1.001E 02	1.46E 07	4.370E-01	1.478E-01
6.40E 06	9.235E 01	8.790E 01	1.48E 07	4.509E-01	1.704E-01
6.60E 06	8.036E 01	7.613E 01	1.50E 07	4.542E-01	1.876E-01
6.80E 06	7.034E 01	6.649E 01			

TABLE XXXV

RUN 157B+161B U SLAB AT 47 DEG.

ENERGY	UPPER LIMIT	LOWER LIMIT	ENERGY	UPPER LIMIT	LOWER LIMIT
8.00E 05	4.117E 03	3.960E 03	7.00E 06	2.292E 01	1.966E 01
9.00E 05	3.022E 03	2.882E 03	7.20E 06	1.983E 01	1.679E 01
1.00E 06	2.255E 03	2.160E 03	7.40E 06	1.769E 01	1.489E 01
1.10E 06	1.751E 03	1.693E 03	7.60E 06	1.594E 01	1.328E 01
1.20E 06	1.408E 03	1.363E 03	7.80E 06	1.411E 01	1.163E 01
1.30E 06	1.176E 03	1.137E 03	8.00E 06	1.195E 01	9.616E 00
1.40E 06	1.010E 03	9.737E 02	8.20E 06	9.782E 00	7.600E 00
1.50E 06	8.688E 02	8.337E 02	8.40E 06	8.406E 00	6.371E 00
1.60E 06	7.486E 02	7.170E 02	8.60E 06	7.883E 00	5.971E 00
1.70E 06	6.658E 02	6.377E 02	8.80E 06	7.596E 00	5.801E 00
1.80E 06	6.071E 02	5.810E 02	9.00E 06	7.123E 00	5.422E 00
1.90E 06	5.591E 02	5.365E 02	9.20E 06	6.420E 00	4.809E 00
2.00E 06	5.196E 02	4.998E 02	9.40E 06	5.537E 00	4.047E 00
2.10E 06	4.845E 02	4.667E 02	9.60E 06	4.540E 00	3.127E 00
2.20E 06	4.504E 02	4.342E 02	9.80E 06	3.528E 00	2.151E 00
2.30E 06	4.188E 02	4.045E 02	1.00E 07	2.680E 00	1.376E 00
2.40E 06	3.911E 02	3.780E 02	1.02E 07	2.130E 00	9.542E-01
2.50E 06	3.640E 02	3.524E 02	1.04E 07	1.871E 00	7.345E-01
2.60E 06	3.351E 02	3.248E 02	1.06E 07	1.799E 00	6.039E-01
2.70E 06	3.073E 02	2.972E 02	1.08E 07	1.877E 00	7.335E-01
2.80E 06	2.847E 02	2.744E 02	1.10E 07	2.161E 00	1.164E 00
2.90E 06	2.680E 02	2.577E 02	1.12E 07	2.523E 00	1.560E 00
3.00E 06	2.538E 02	2.434E 02	1.14E 07	2.616E 00	1.602E 00
3.20E 06	2.219E 02	2.126E 02	1.16E 07	2.305E 00	1.323E 00
3.40E 06	1.927E 02	1.834E 02	1.18E 07	1.834E 00	1.004E 00
3.60E 06	1.755E 02	1.659E 02	1.20E 07	1.493E 00	8.119E-01
3.80E 06	1.604E 02	1.510E 02	1.22E 07	1.304E 00	6.932E-01
4.00E 06	1.423E 02	1.333E 02	1.24E 07	1.157E 00	5.694E-01
4.20E 06	1.259E 02	1.179E 02	1.26E 07	9.765E-01	4.335E-01
4.40E 06	1.130E 02	1.054E 02	1.28E 07	7.658E-01	3.040E-01
4.60E 06	1.052E 02	9.821E 01	1.30E 07	5.622E-01	1.796E-01
4.80E 06	9.866E 01	9.225E 01	1.32E 07	3.935E-01	5.093E-02
5.00E 06	8.704E 01	8.100E 01	1.34E 07	2.579E-01	-6.243E-02
5.20E 06	7.434E 01	6.853E 01	1.36E 07	1.544E-01	-1.417E-01
5.40E 06	6.652E 01	6.106E 01	1.38E 07	9.655E-02	-1.929E-01
5.60E 06	6.208E 01	5.694E 01	1.40E 07	8.177E-02	-2.144E-01
5.80E 06	5.698E 01	5.201E 01	1.42E 07	9.359E-02	-1.926E-01
6.00E 06	5.038E 01	4.582E 01	1.44E 07	1.301E-01	-1.380E-01
6.20E 06	4.387E 01	3.963E 01	1.46E 07	1.933E-01	-8.293E-02
6.40E 06	3.796E 01	3.399E 01	1.48E 07	2.537E-01	-4.140E-02
6.60E 06	3.247E 01	2.869E 01	1.50E 07	2.770E-01	-1.563E-02
6.80E 06	2.727E 01	2.379E 01			

TABLE XXXVI

RUN 158A+161C U SLAB AT 64 DEG.

ENERGY	UPPER LIMIT	LOWER LIMIT	ENERGY	UPPER LIMIT	LOWER LIMIT
8.00E 05	2.317E 03	2.243E 03	7.00E 06	1.091E 01	9.377E 00
9.00E 05	1.657E 03	1.585E 03	7.20E 06	9.771E 00	8.337E 00
1.00E 06	1.210E 03	1.162E 03	7.40E 06	8.506E 00	7.205E 00
1.10E 06	9.277E 02	8.996E 02	7.60E 06	7.246E 00	6.021E 00
1.20E 06	7.223E 02	7.012E 02	7.80E 06	6.194E 00	5.055E 00
1.30E 06	5.703E 02	5.524E 02	8.00E 06	5.484E 00	4.432E 00
1.40E 06	4.662E 02	4.493E 02	8.20E 06	4.973E 00	4.009E 00
1.50E 06	3.957E 02	3.796E 02	8.40E 06	4.406E 00	3.476E 00
1.60E 06	3.432E 02	3.288E 02	8.60E 06	3.747E 00	2.847E 00
1.70E 06	3.029E 02	2.899E 02	8.80E 06	3.177E 00	2.374E 00
1.80E 06	2.724E 02	2.604E 02	9.00E 06	2.835E 00	2.132E 00
1.90E 06	2.489E 02	2.385E 02	9.20E 06	2.570E 00	1.875E 00
2.00E 06	2.310E 02	2.218E 02	9.40E 06	2.089E 00	1.392E 00
2.10E 06	2.178E 02	2.096E 02	9.60E 06	1.399E 00	7.471E-01
2.20E 06	2.068E 02	1.994E 02	9.80E 06	8.398E-01	2.236E-01
2.30E 06	1.945E 02	1.879E 02	1.00E 07	6.953E-01	1.088E-01
2.40E 06	1.813E 02	1.752E 02	1.02E 07	9.437E-01	4.064E-01
2.50E 06	1.687E 02	1.632E 02	1.04E 07	1.315E 00	7.911E-01
2.60E 06	1.576E 02	1.528E 02	1.06E 07	1.487E 00	9.471E-01
2.70E 06	1.480E 02	1.432E 02	1.08E 07	1.326E 00	8.041E-01
2.80E 06	1.394E 02	1.344E 02	1.10E 07	9.563E-01	4.568E-01
2.90E 06	1.307E 02	1.257E 02	1.12E 07	5.727E-01	6.915E-02
3.00E 06	1.215E 02	1.166E 02	1.14E 07	3.248E-01	-1.892E-01
3.20E 06	1.023E 02	9.791E 01	1.16E 07	2.766E-01	-2.060E-01
3.40E 06	8.691E 01	8.260E 01	1.18E 07	3.833E-01	-2.162E-02
3.60E 06	7.775E 01	7.331E 01	1.20E 07	5.187E-01	1.269E-01
3.80E 06	7.286E 01	6.851E 01	1.22E 07	5.708E-01	1.359E-01
4.00E 06	6.789E 01	6.375E 01	1.24E 07	5.040E-01	7.092E-02
4.20E 06	6.198E 01	5.830E 01	1.26E 07	3.973E-01	4.889E-05
4.40E 06	5.603E 01	5.260E 01	1.28E 07	3.243E-01	-4.949E-02
4.60E 06	4.893E 01	4.579E 01	1.30E 07	2.910E-01	-6.403E-02
4.80E 06	4.109E 01	3.819E 01	1.32E 07	2.823E-01	-4.139E-02
5.00E 06	3.445E 01	3.174E 01	1.34E 07	2.975E-01	3.934E-03
5.20E 06	2.991E 01	2.729E 01	1.36E 07	3.320E-01	5.139E-02
5.40E 06	2.664E 01	2.413E 01	1.38E 07	3.623E-01	8.550E-02
5.60E 06	2.378E 01	2.139E 01	1.40E 07	3.632E-01	9.556E-02
5.80E 06	2.205E 01	1.977E 01	1.42E 07	3.272E-01	7.710E-02
6.00E 06	2.125E 01	1.913E 01	1.44E 07	2.644E-01	3.553E-02
6.20E 06	1.963E 01	1.763E 01	1.46E 07	1.938E-01	-1.829E-02
6.40E 06	1.665E 01	1.478E 01	1.48E 07	1.329E-01	-7.177E-02
6.60E 06	1.384E 01	1.206E 01	1.50E 07	9.096E-02	-1.113E-01
6.80E 06	1.208E 01	1.045E 01			

APPENDIX B

FAST NEUTRON DOSE DATA

Table XXXVII contains dose data for the bare beam taken with the Hurst dosimeter in the spectrometer housing at angles of 0, 4.16, and 8.6°. Three values are given for each measurement. These correspond to the three means of obtaining the dose from the pulse height distribution as described in Chapter V. The dose units are ergs./gm./hr./watt. Table XXXVIII contains similar data for the lead slab. Tables XXXIX and XL contain data for the polyethylene and laminated slabs. On these runs the PHS readings were not recorded. Table XLI contains the dose profile data for the depleted uranium slab. These data were taken with the 1/2-in. diameter by 1/16-in. thick Hornyak button located on a traversing mechanism such that it was one inch from the exit face of the uranium slab. These data are intended for shape comparison only.

TABLE XXXVII

ANGLE DEPENDENCE OF FAST NEUTRON DOSE
FOR THE BARE BEAM

Angle	Integrator	PHS	Analyzer
0°	1.04×10^{-3}	1.12×10^{-3}	1.08×10^{-3}
4.16°	2.96×10^{-4}	3.16×10^{-4}	3.18×10^{-4}
8.6°	2.78×10^{-6}	2.92×10^{-6}	2.92×10^{-6}

TABLE XXXVIII

ANGLE DEPENDENCE OF FAST NEUTRON DOSE
FOR THE LEAD SLAB

Angle	Integrator	PHS	Analyzer
0°	7.58×10^{-6}	9.11×10^{-6}	1.11×10^{-6}
13°	1.07×10^{-6}	1.04×10^{-6}	1.43×10^{-6}
30°	7.87×10^{-7}	8.51×10^{-7}	1.08×10^{-6}
47°	5.20×10^{-7}	6.33×10^{-7}	7.24×10^{-7}
64°	2.69×10^{-7}	3.43×10^{-7}	3.78×10^{-7}

TABLE XXXIX

ANGLE DEPENDENCE OF FAST NEUTRON DOSE
FOR THE POLYETHYLENE SLAB

Angle	Integrator	Analyzer
0°	2.74×10^{-5}	2.88×10^{-5}
13°	4.61×10^{-7}	4.80×10^{-7}
30°	2.73×10^{-7}	2.84×10^{-7}
47°	1.23×10^{-7}	1.31×10^{-7}
64°	4.14×10^{-8}	4.34×10^{-8}

TABLE XL

ANGLE DEPENDENCE OF FAST NEUTRON DOSE
FOR THE LAMINATED SLAB

Angle	Integrator	Analyzer
0°	6.43×10^{-6}	7.05×10^{-6}
13°	5.15×10^{-7}	4.72×10^{-7}
30°	3.04×10^{-7}	2.74×10^{-7}
47°	1.78×10^{-7}	1.49×10^{-7}
64°	1.38×10^{-7}	7.41×10^{-8}

TABLE XLI

FAST NEUTRON DOSE PROFILE BEHIND THE DEPLETED URANIUM SLAB

Radius (in.)	Dose	Radius (in.)	Dose
0	2.92×10^{-2}	11	1.90×10^{-4}
1	2.85×10^{-3}	12	1.42×10^{-4}
2	2.66×10^{-3}	13	1.12×10^{-4}
3	2.28×10^{-3}	14	8.69×10^{-5}
4	1.78×10^{-3}	15	6.40×10^{-5}
5	1.31×10^{-3}	17	4.21×10^{-5}
6	9.01×10^{-4}	19	2.55×10^{-5}
7	6.72×10^{-4}	21	1.86×10^{-5}
8	4.88×10^{-4}	23	1.16×10^{-5}
9	3.63×10^{-4}	27	5.74×10^{-6}
10	2.64×10^{-4}	30	3.77×10^{-6}